

**LATE HOLOCENE GEOLOGIC, OCEANOGRAPHIC AND CLIMATE
HISTORY OF AN ANOXIC FJORD:
EFFINGHAM INLET, WEST COAST, VANCOUVER ISLAND**

By

AUDREY DALLIMORE , M.Sc.

A thesis submitted to the
Faculty of Graduate Studies and Research
in partial fulfillment of the
requirements for the degree of
Doctor of Philosophy

Department of Earth Sciences, Carleton University
and the Ottawa-Carleton Geoscience Centre
Ottawa, Ontario

June 15, 2001



National Library
of Canada

Acquisitions and
Bibliographic Services

395 Wellington Street
Ottawa ON K1A 0N4
Canada

Bibliothèque nationale
du Canada

Acquisitions et
services bibliographiques

395, rue Wellington
Ottawa ON K1A 0N4
Canada

Your file *Votre référence*

Our file *Notre référence*

The author has granted a non-exclusive licence allowing the National Library of Canada to reproduce, loan, distribute or sell copies of this thesis in microform, paper or electronic formats.

The author retains ownership of the copyright in this thesis. Neither the thesis nor substantial extracts from it may be printed or otherwise reproduced without the author's permission.

L'auteur a accordé une licence non exclusive permettant à la Bibliothèque nationale du Canada de reproduire, prêter, distribuer ou vendre des copies de cette thèse sous la forme de microfiche/film, de reproduction sur papier ou sur format électronique.

L'auteur conserve la propriété du droit d'auteur qui protège cette thèse. Ni la thèse ni des extraits substantiels de celle-ci ne doivent être imprimés ou autrement reproduits sans son autorisation.

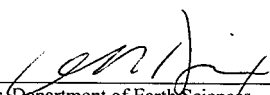
0-612-67015-5

The undersigned hereby recommend to
the Faculty of Graduate Studies and Research
acceptance of the thesis,

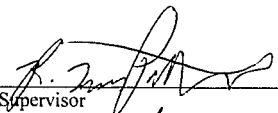
**Late Holocene Geologic, Oceanographic and Climate
History of an Anoxic Fjord: Effingham Inlet,
West Coast, Vancouver Island**

Submitted by
Audrey Dallimore, B.Sc.H., M.Sc.

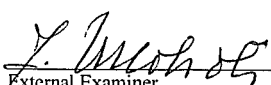
in partial fulfilment of the requirements
for the degree of Doctor of Philosophy



Chair, Department of Earth Sciences



Thesis Supervisor



External Examiner

ABSTRACT

Sediments preserved in the inner basin of anoxic Effingham Inlet on the west coast of Vancouver Island, give a high-resolution record of about 4,000 years of deposition. Changes in productivity and precipitation in the inlet are represented in the sediments by varying thickness of diatom/terrigenous mud varves. Ocean and climate changes affecting the inlet over the late Holocene can be interpreted from upwelling events which oxygenate the bottom waters of the inlet, which are represented by ungraded massive muds intercalated within laminated sediments. Therefore, high rainfall and cooler temperatures are interpreted to have existed about 2,000 to 4,000 y BP, following warmer and drier conditions than today's, prior to about 4,000 y BP.

The depositional record is complicated by graded and massive intervals that are interpreted to be the result of significant ($M > 7$) seismic events, that occurred historically in 1946, and prehistorically about 4,000 y BP, and many other smaller seismic events. A sand bed, is interpreted to be the result of a tsunami traveling up Effingham Inlet about 2,000 y BP, perhaps not surprising along this tectonically active coast.

A total of thirteen oceanographic surveys of the inlet beginning in 1995, confirm the modern anoxic character of the inner basin, and dysoxic character of the outer basin. Upwelled, oxygenated shelf waters can at times flush both the inner and outer basins to varying degrees, with dysoxic/anoxic conditions returning within months. A major

flushing event was recorded in 1999, at the end of the 1997-98 El Niño, and is evidence that Effingham Inlet is being affected by continental scale oceanic processes.

Fish remains, including intact identifiable scales and bones, were retrieved from throughout the sediment record. Ten fish species are represented in the sediments, and the preserved scale counts show a cycling of fish populations in the inlet throughout the past 4,000 years. Although it is unclear what the relationship is between cycling of fish populations and ocean and climate conditions of Effingham Inlet, results of this study show that a low sediment volume record of fish scales, recovered from a small diameter piston core, can give high-resolution information on fish populations and ocean cycles over the late Holocene.

ACKNOWLEDGEMENTS

I am very grateful to have had the opportunity to participate in this project and I can count many new friends among the colleagues I met from across the country during this project, and my graduate work. I am so glad to finally have the opportunity to put your names here all together in this volume permanently. My list of those I would like to acknowledge is long indeed, and my heartfelt thanks to each and every one of you here, for helping in your own unique ways to the successful conclusion of my thesis project and for the way each of you has contributed positively to my work and my life, by sharing your knowledge, expertise and yourselves with me in the past three years.

I would like to acknowledge the Natural Sciences and Engineering Research Council, CORI of Sidney, B.C, Ontario Graduate Scholarship Program and Carleton University for funding my scholarships throughout this work, all very much appreciated.

My gratitude :

Firstly, at Carleton University, to Dr. R.T. Patterson, my supervisor, for your support, unfailing good cheer and constant faith in me to get the job done, when I sometimes hardly had faith in myself; to my colleague and fellow Ph. D. candidate, Alice Chang, you are amazing and thank you for all your help and support, both onboard ship and back in Ottawa; to Pat Lyons and Leslie Taylor, the best lab assistance and computer wizardry I could hope for; to Dr. Sharon Carr and Sheila Thayer, for helping me hang in there throughout my graduate career.

To my colleagues in this project, fellow Ph.D. candidates Murray Hay of Université de Laval, and Trecia Schell of Dalhousie University, for all your companionship, helpful discussions, your hard work onboard and also in the lab at PGC, and for your joie de vie, merci et courage mes amis!

To the members of my examination and defense committees; Dr. André Desrochers, and Dr. Ian Clark of Ottawa University and Drs. Fred Michel, Richard Taylor, John Blenkinsop and Stewart Peck of Carleton University, and a special thanks to Dr. Franco Medioli of Dalhousie University for making the long trek to Ottawa for my defense, and helping to keep me in the game with your encouragement.

To my colleagues at the Pacific Geoscience Center in Sidney, B.C. ; a special thanks to Dr. Rick Thomson for your wonderful support of me right from the very beginning and your generosity in including students in your work and so freely sharing your data, experience and yourself with all of us; to Kim Conway for your many helpful discussions and suggestions during the overwhelming logistical phases of the project and for your never ending patience during all the (very messy) lab work at PGC, and your expert work and guidance onboard; to Bob McDonald for managing the coring with Kim, and manhandling all those heavy cores onboard and at PGC, and being so willing to help whenever I needed it; to Cindy Wright for your tenacity and many helpful discussions; to Dr. Ralph Currie for helping me get the logistics off the ground at PGC and allowing us the use of that wonderful facility; and to Captain Frost of the J.P Tully and his professional and expert crew.

All the expert technical help from the following specialists is very much appreciated ; Janice Baker of the Sidney X-ray clinic, Dr. R. McNeely, GSC Ottawa x-ray facility, Dr. R. Beukens at University of Toronto, Isotracer lab, Dr. Lloyd Snowdon,

GSC Calgary and the staff of Monk's Office Supply in Sidney for all your help in producing this thesis document, the nicest business people anywhere.

Two rare and wonderful people have been my colleagues in science as well as my loyal fellow travelers on the road of life over the past 5 years and are the ones responsible for keeping me at it during my graduate work when the going got rough, which believe it or not was more than once...my dear friends Barbara Mediolini and Patricia Brennan-Alpert; thank you so much. Your unfailing support, joy in your work and zest for life have been my constant inspiration. I am truly blessed with all your help and friendship.

And finally,

I dedicate this thesis with deep gratitude for all your support,
and in awe of your remarkable courage to face so many new challenges during the
completion of this work,
to my family.

My husband Scott Dallimore and our children Brent and Karen, and to the cherished
memory of beautiful B,
without your love and support in my life, nothing is possible.

TABLE OF CONTENTS	Page
Acceptance sheet	ii
Abstract	iii
Acknowledgments	v
Table of Contents	vii
List of Tables	xi
List of Figures	xii
List of Appendices	xv
INTRODUCTION	1
LAMINATED SEDIMENTS	1
LAMINATED SEDIMENT RECORDS OF THE BRITISH COLUMBIA COAST	3
THE FISHERIES RESEARCH PROJECT	11
INTRODUCTION	11
HISTORICAL FISHERIES BACKGROUND	14
FACTORS AFFECTING PELAGIC FISH POPULATION ABUNDANCE	15
BACKGROUND	18
REGIONAL SETTING	18
BEDROCK GEOLOGY	18
TECTONIC SETTING	22
PALEOSEISMIC ACTIVITY	26
QUATERNARY GLACIAL HISTORY	31
POST-GLACIAL SEA LEVELS	36
TERRESTRIAL CLIMATE AND VEGETATION	38
HOLOCENE VEGETATION AND CLIMATE HISTORY	39

OCEANOGRAPHY AND CLIMATE	41
PALEO-FISH POPULATION RESEARCH	49
EFFINGHAM INLET	51
PHYSIOGRAPHY	51
OCEANOGRAPHY	61
MATERIALS AND METHODS	68
OCEANOGRAPHIC CRUISES	68
CORING	68
ONBOARD HANDLING OF CORES	79
OCEANOGRAPHY	
LABORATORY WORK	83
PISTON AND FREEZE CORE HANDLING	83
X-RADIOGRAPHY	83
RADIOCARBON DATING	85
GRAIN SIZE AND ROCK-EVAL ANALYSIS	87
FISH SCALES	
RESULTS	92
PHYSIOGRAPHY OF EFFINGHAM INLET	92
SEISMIC PROFILE	92
DRAINAGE BASIN	
SEDIMENTOLOGY	104
GENERAL	104
<i>INNER BASIN AND OUTER BASIN</i>	104
<i>BARKLEY SOUND</i>	114
<i>FREEZE CORES</i>	114
ROCK-EVAL AND GRAIN SIZE ANALYSES	128
<i>ROCK-EVAL</i>	128
<i>GRAIN SIZE</i>	128
SEDIMENTARY FEATURES	133

X-RADIOGRAPHY	136
<i>LAMINATED SEDIMENTS</i>	136
<i>GRADED AND UNGRADED MASSIVE MUDS</i>	144
<i>DEPOSITIONAL VARIABILITY</i>	145
<i>BIOTURBATION</i>	148
<i>SAND AND SHELL BED</i>	148
<i>LARGE UNGRADED MASSIVE INTERVALS</i>	153
<i>OUTER BASIN CORE FEATURES</i>	163
OTHER SEDIMENTARY FEATURES	170
CALIBRATION OF RESULTS	173
CALIBRATION OF MARINE RADIOCARBON SAMPLES	174
SEDIMENTATION RATES	178
OCEANOGRAPHY	181
FISH SCALES	208
INTERPRETATION AND DISCUSSION	214
SEDIMENTOLOGY	214
LAMINATED SEDIMENTS	214
MASSIVE UNGRADED MUDS	215
GRADED MUDS	217
RADIOCARBON DATES	219
SEDIMENTATION RATES	221
OUTER BASIN SEDIMENTATION RATES	224
PALEOSEISMICITY	227
LARGE UNGRADED MASSIVE INTERVAL	228
SAND AND SHELL GRADED BED	237
CLIMATIC INTERVALS	242
OCEANOGRAPHY	251
BASIN CORRELATION	253
FISH SCALES	258

x

CONCLUSIONS
REFERENCES
APPENDICES

266
274
293

LIST OF TABLES

TABLE	DESCRIPTION	PAGE
1	Piston and freeze cores locations.	73
2	Results of radiocarbon dating.	171
3	Summary of cruise survey data.	182

LIST OF FIGURES

FIGURE	DESCRIPTION	PAGE
1)	Location map of Effingham Inlet.	7
2)	Photograph of the laminated sediments of Effingham Inlet.	9
3)	Geological belts of the Canadian Cordillera.	20
4)	Modern tectonic setting of Vancouver Island.	23
5)	Block diagram of subducting Juan de Fuca Plate.	24
6)	Earthquakes of the past five years in western Canada.	29
7)	Quaternary events and deposits in British Columbia.	34
8)	Position of the Aleutian Low and North Pacific High atmospheric systems.	45
9)	Upwelling on the Vancouver Island Shelf.	47
10)	Photograph of Barkley Sound coastline.	53
11)	Bathymetry and water properties of Effingham Inlet.	55
12)	Aerial photograph of Effingham Inlet, July, 1976.	57
13)	Photograph of Effingham Inlet shoreline.	59
14)	Salinity and water temperature profiles of Effingham Inlet.	64
15)	Oxygen content profiles from Effingham Inlet.	66
16)	Photograph of the CCGS J.P. Tully.	69
17)	Piston coring apparatus aboard the J.P. Tully.	71
18)	Photograph of the onboard handling of freeze cores.	75
19)	Photograph of on deck piston core separation into sections.	77
20)	Photograph of multiple sensor profiling apparatus.	81
21)	Photograph of piston core laboratory work.	90

22) Seismic profile of Effingham Inlet.	93
23) Effingham Inlet drainage basin.	95, 97, 100
24) Aerial photograph of upper drainage basin of Effingham Inlet, July, 1976.	102
25) Photographs of drainage during a heavy rainfall event.	105
26) Inner basin core TUL99A02, descriptions and photographs.	108
27) Outer basin core TUL99A01, descriptions and photographs.	111
28) Barkley Sound core, TUL99A04, descriptions and photographs.	115
29) Photograph of sand and shell bed in Barkley Sound core.	118
30) Photograph of freeze core TUL99B04.	120
31) Rock-Eval data plots.	112, 124, 126
32) Grain size ternary diagram.	129
33) Photographs of inner basin core details.	131
34) Photographs of outer basin core details.	134
35) X-ray of well laminated sediments.	138
36) X-ray of poorly laminated sediments.	140
37) X-ray of anoxic, oxic transitions.	142
38) X-ray of anoxic, dysoxic, oxic transitions.	146
39) X-ray of bioturbation tracks.	149
40) X-ray of sand and shell bed.	151
41) X-ray of large ungraded massive interval.	154
42) X-ray of overturned and folded laminated sediments.	157
43) X-ray of de-watering structures in disturbed laminated sediments.	159
44) X-ray of poorly defined laminations from outer basin core.	161
45) X-ray of outer basin massive sediments.	164
46) X-ray of convoluted bedding and flame structures.	166

47) X-ray of dropstone.	168
48) Depth vs age plots for radiocarbon dates in all cores.	177
49) Sedimentation rates calculated from laminated intervals.	179
50) Location map of CTD rosette, current and tide meters, Barkley Sound core.	183
51) Salinity – depth time series.	185
52) Temperature – depth time series.	187
53) Density – depth time series.	190
54) Dissolved oxygen – depth time series.	192
55) Oxygen – bathymetry profiles.	195
56) Density – bathymetry profiles.	198
57) Alongshore current time series.	204
58) Daily wind stress time series.	206
59) Fish species relative abundances.	209
60) Fish scales and bones of inner basin TUL99B03.	213
61) Correlation of ungraded massive mud, base of piston cores.	233
62) Correlation of sand and shell bed across the inlet.	235
63) Climate intervals in inner basin core TUL99B03.	244
64) Climate intervals in outer basin core TUL99B11.	246
65) Sedimentation rate and climate intervals for inner and outer basin cores.	248
66) Basin correlation.	255
67) Fish scales and climate intervals.	262

POCKET ATTACHMENT

- 1) X-ray composite of freeze core TUL99B04.
- 2) X-ray composite of inner basin core TUL99B03.
- 3) X-ray composite of outer basin core TUL99B11.

LIST OF APPENDICES

APPENDIX	DESCRIPTION	
A	Sediment slabbing “cookie cutter” tool: Design and operation instructions.	293
B	Radiocarbon dating results from Isotrace.	298
C	Photographs and descriptions of TUL99B06.	335
D	Photographs and descriptions of TUL99B09.	352
E	Photographs and descriptions of TUL99B13.	369
F	X-rays and descriptions of TUL99B03.	386
G	X-rays and descriptions of TUL99B11.	422
H	Descriptions of freeze cores.	450
I	ROCK-EVAL and grain-size data.	452
J	Fish scales data.	462

INTRODUCTION

LAMINATED SEDIMENTS

Laminated marine sediments in the geologic record represent the highest resolution, continuous archive of past depositional, oceanic and climatic conditions available. The recent popular and scientific focus on climate change has given impetus to the study of annually laminated sedimentary and biological archives, which can extend the range of our knowledge of climate and ocean conditions beyond historic and instrumental records. Recent studies of tree rings, ice cores, coral records, and laminated marine and lacustrine sediments are refining our knowledge and techniques for the study and interpretation of intra- and inter- annual and decadal records of environmental and depositional conditions (Kemp, 1996; Ware and Thomson, 2000).

In marine environments, where they are preserved, laminated sediments represent a highly detailed record of seasonal variability in their alternating lithic and terrigenous-organic (dark) and biogenic, diatomaceous (light) laminae. A couplet, or in some cases triplet, of these dark and light laminae, when they together represent one year's deposition, are commonly referred to as varves (Kemp, 1996). The dark, terrigenous laminae record annual and seasonal variations in precipitation, while the light, diatomaceous laminae give an indication of annual oceanic productivity, in the form of diatom blooms of the spring and summer seasons. The variability of the diatomaceous

laminac can in turn infer oceanographic and climatic conditions which were conducive to upwelling events, which bring nutrient rich waters to the surface of the coastal ocean (Sancetta, 1996; Kemp, 1996; Grimm et al., 1996 and 1997; Chang et al., 1998; McQuoid and Hobson, 2001).

Long time series of oceanographic and climatic conditions inferred from laminated sediments however, can be interrupted when events departing from the norm occur. These can include; years when rainfall obscures any productive event of the season and/or the complete failure of a primary productivity bloom in a certain year; and obscuring of the annual record by bioturbation, scouring, debris flow and turbidite activity (Sancetta, 1996). Particularly in tectonically active settings, the record can also be obscured or expanded by the erosion or addition of sediment by debris flows and turbidites, which may be the result of sediment disturbance by seismic activity in the area (Anderson, 1996; Blais 1995; Blais- Stevens et al., 1997; Blais Stevens and Claguc, 2001).

However, it is precisely this complicated record of interactive annual variability in climatic, oceanographic, biological, ecological and tectonic conditions that make the studies of laminated sediments so valuable. A wealth of information is contained within their laminac, and the task for the geologist is to decipher the depositional conditions certain sedimentary features within the laminated sediments may represent, and in the

context of the regional setting, reconstruct a plausible depositional scenario to re-create paleo-environmental conditions (Kemp, 1996).

Once individual laminae-forming processes have been identified, using techniques such as digital imagery, resin impregnation, x-radiography, scanning electron and optical microscopy, a knowledge of the present day local atmospheric and water column processes producing the laminae forming flux is required (Kemp, 1996; Pike and Kemp, 1996b). This can be accomplished by oceanographic data time series generated by multiple sensor profiling devices, and moored instrumentation, including sediment traps, tidal, current and meteorological buoys (Kemp, 1996; Patterson et al., 2000).

Concurrent micropaleontological studies also complement the analysis of paleoenvironmental conditions and provide information on cycling ecological conditions (Baumgartner et al., 1992; Blais, 1995; Patterson et al., 2000; Tunnicliffe et al., 2001; O'Connell and Tunnicliffe, 2001; McQuoid and Hobson, 2001; Schell and Dallimore, 2001).

LAMINATED SEDIMENT RECORDS OF THE BRITISH COLUMBIA COAST

It has been known for some years that it may be possible to resolve the depositional history as well as paleoceanographic, paleoclimate and paleoproductivity signals from the preservation of finely laminated sediments in the anoxic (oxygen-free) and dysoxic (low oxygen) bottom waters of inlets and fjords along the coast of British Columbia (Gross et al,

1963; Gucluer and Gross, 1964). This technique was successfully investigated during the Ocean Drilling Program's (ODP) Leg 169S, in Saanich Inlet on southeastern Vancouver Island (Bornhold et al., 1998; Blais-Stevens et al., 1997 and 2001; Blais Stevens and Claguc, 2001). Results of that study give a highly detailed record for the entire Holocene of; sedimentary deposition (Blais, 1995; Blais-Stevens et al., 2001); paleoseismicity (Bornhold et al., 1998; Blais-Stevens, et al, 1997, 2001; Blais-Stevens and Claguc, 2001) ; palco-fish populations (Tunnicliffe et al., 2001, O'Connell and Tunnicliffe, 2001); paleoproductivity (Dean et al., 2001; McQuoid and Hobson, 2001; Hobson and McQuoid, 2001) and paleo-climate in Saanich Inlet (Pellatt et al., 2001). The ODP work in Saanich Inlet expanded upon the techniques developed for a high-resolution paleoenvironmental study of the laminated sediments in the anoxic Santa Barbara, California, ocean basin investigated during ODP Leg 146 (Kennett et al., 1995; Schimmelman and Lange, 1996; Bull and Kemp, 1996; Pike and Kemp, 1996a).

The open ocean signal is somewhat dampened in the sediments of Saanich Inlet however, due to the location of the inlet on the southeastern coast of Vancouver Island near the Fraser River and the Straits of Georgia, which isolate it from the open marine environment of the Pacific Ocean (Figure 1). Consequently, to investigate the possibilities of studying laminated sediments in an open marine setting, in 1995, a research team from the federal Department of Fisheries and Oceans, at the Institute of Ocean Sciences (IOS), Sidney, B.C., began a search for an anoxic inlet on Vancouver Island's west coast.

A reconnaissance oceanographic cruise was undertaken in 1995 to a 17 km long, by 1 km wide fjord open to Barkley Sound, known as Effingham Inlet (Figure 1). Preliminary freeze coring, surficial grab sampling and oceanographic surveys in October 1995, revealed that the inlet exhibits high productivity, stagnant anoxic/dysoxic bottom waters and annually laminated sediments, making it an excellent research target for paleoceanographic research (Patterson et al., 2000; Schell and Dallimore, 2001). The history of fisheries activities in and around Effingham Inlet, in Barkley and Nootka Sounds, also gives an historical context for palco-fish population research.

Fjords such as Effingham Inlet are useful in paleoceanographic research because in many cases, only strong oceanographic events are felt in their inner basins, thus removing most of the background productivity (Timothy and Soon, 2001). Fjords exhibit typical estuarine circulation, whereby a freshwater “wedge” from rivers at the fjord head, flows outwards to the ocean, while saline water flows into the estuary at depth. In highly stratified estuary fjords with shallow sills and weak freshwater input however, the inflow of saline water at depth can be interrupted and the bottom waters become stagnant (Tully, 1949; Syvitski and Shaw, 1996). The resulting dysoxic or anoxic bottom waters aid in the preservation of annually laminated sediments since a thriving benthos cannot become established, and bioturbation, which destroys the laminated structure of sediments, is at a minimum or completely absent (Gross et al., 1963; Kemp, 1996; Anderson, 1996). In highly productive fjords such as Effingham Inlet, the

consumption of oxygen during decomposition processes also contributes to the lack of oxygen, and a rapid consumption of any new influx of oxygen within the water column also occurs. Hence, lengthy packages of undisturbed laminae are easily preserved in the sediment record of anoxic basins and inlets (Kemp, 1996; Patterson et al., 2000).

Preliminary freeze coring and grab sampling in October, 1995, showed that the laminated sediments of Effingham Inlet represent an annual record of deposition. The sediments consist of light colored laminae, deposited under the rain of diatom frustules to the sediment, from annual diatom blooms in spring and summer, which alternate with dark-colored, organic-rich terrigenous and lithic laminae deposited during the rainy seasons of fall and winter (Figure 2): (Patterson et al., 2000). One pair, or couplet, of dark and light laminae represent one years' deposition and therefore can be referred to as varves (Kemp, 1996). Thus, the laminated sediments of Effingham Inlet archive ultra-high resolution information providing valuable data on seasonal scale processes as well as intra- and inter-annual variability under conditions of moderately high marine productivity in the surface waters, as indicated by abundant diatom remains (Patterson et al., 2000).

The findings from the initial October 1995 cruise to Effingham Inlet hinted at the wealth of information about the Holocene depositional, paleoceanic and paleoclimate conditions of coastal Vancouver Island preserved in the laminated sediments. The stage was then set for a concentrated multi-disciplinary study of Effingham Inlet.

Figure 1. Location map of Effingham Inlet, Barkley Sound and Saanich Inlet.

Effingham Inlet Core Locations

Inner Basin Cores

Site 1 :

- Freeze core B01
- Piston core B03
- Piston core A02

Site 2:

- Freeze core B04
- Piston core B06
- Piston core B13

Site 3:

- Freeze core B07
- Piston core B09

Outer Basin cores

Site 4:

- Freeze core B10
- Freeze core B12
- Piston core B11
- Piston core A01

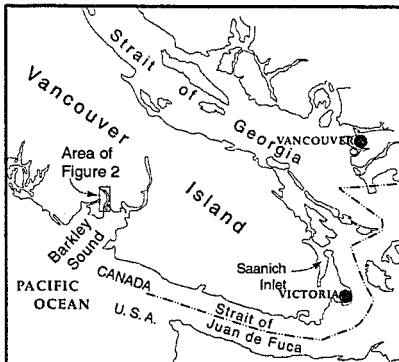
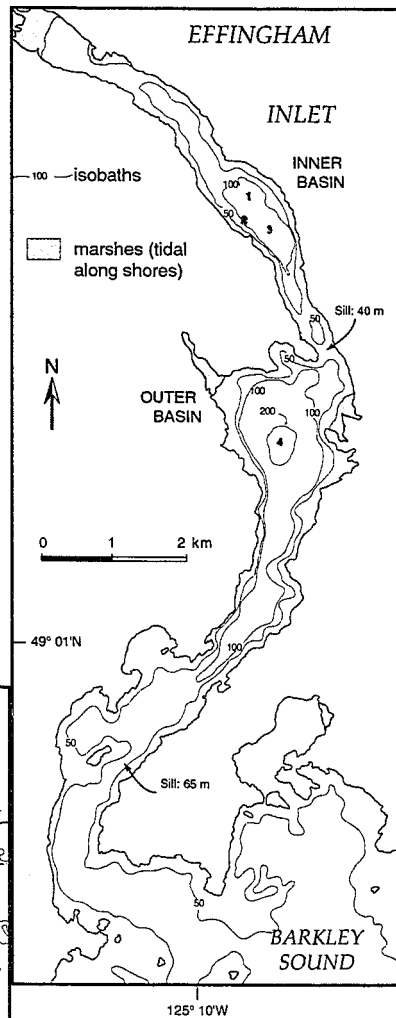
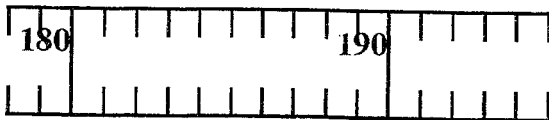
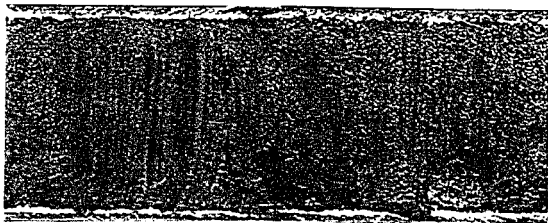


Figure 2. True color photograph of the typically laminated sediments of Effingham Inlet. Lighter colored laminae are diatomaceous-rich , and the darker laminae are terrigenous-rich. Note the variations in thickness of both the diatomaceous and terrigenous laminae throughout this section of core from the inner basin. This represents the high degree of annual variability in both rainfall and productivity which occurred in about 80 years of deposition represented by this section of core. This degree of annual variability is typical throughout the Effingham Inlet depositional record.



TUL97A02/SCT-2 (178-195 cm)

THE FISHERIES RESEARCH PROJECT

INTRODUCTION

My Ph. D. research project is part of the multidisciplinary 1998-2001 NSERC strategic grant study of Effingham Inlet, entitled *Long-term Variability in Pelagic Fish Abundance and Oceanographic Conditions on the British Columbia Shelf*. My supervisor, Dr. R.T. Patterson is the principal scientific investigator for this project. The study is jointly funded by members of the British Columbia fishing industry-sponsored Herring Conservation and Research Society (HCRS) in research partnership with the federal Department of Fisheries and Oceans and NSERC.

The objective of the study is to gather data from oceanographic research cruises aboard the Canadian research vessel the *CCGP J.P. Tully*, to Effingham Inlet on the west coast of Vancouver Island. The data collection is designed to relate variability in oceanographic conditions along the Canadian west coast, to natural fish stock abundance and productivity throughout the late Holocene to the present day. The anoxic conditions of the inlet allow for the preservation of fish scales which are well preserved in the annually laminated sediments (Patterson et al., 2000; Schell and Dallimore, 2001).

To accomplish the study objectives, a large multi-disciplinary team from both the university and government research communities undertook an integrated approach to documenting changes in the oceanographic conditions and fish abundances of the Vancouver

Island upwelling regime over the late Holocene. Our approach collectively includes research in the fields of sedimentology, geochronology, paleoseismicity, micropaleontology, geochemistry, and physical oceanography.

The study results will contribute to the understanding of the natural periodicity of oceanographic processes and marine ecosystems of the northern Pacific throughout the late Holocene, and provide presently unavailable paleoceanographic and paleoclimate interpretations for the study region. The study results could become a predictive tool for the north Pacific fishery, for the conservation and optimal harvesting of west coast fish stocks. Ultimately, the research will provide a new level of understanding of the periodicity of fluctuations in the oceanographic upwelling regime of coastal British Columbia, and the resulting effects on pelagic fish populations, both pre- and post-dating the advent of the west coast commercial fishery in the early 1900's.

My own work specifically, encompasses the sedimentology and geochronology of the inlet and illustrates the modern and geologically recent depositional processes of an anoxic, estuarine fjord in a tectonically active area. A discussion of the results and context of unpublished Effingham Inlet oceanography data of Dr. Richard Thomson of the Department of Fisheries and Oceans, and also the preliminary results of the fish scales micropaleontological laboratory analyses of the Effingham Inlet sediments,

recently completed by contractor Cindy Wright of the Department of Fisheries and Oceans, is also contained in this thesis with the kind permission of these authors.

The results of my own research form a sedimentological and geochronological framework, and an environmental context throughout the late Holocene, for the interpretation of the on-going work of my colleagues participating in this project. A summary of the project and preliminary data analyses can be found at the website

<http://www.earthsci.carleton.ca/Museum/strategicfisheriesproject.html>.

HISTORICAL FISHERIES BACKGROUND

A resurgence of popular interest in the relationship between fish population dynamics and oceanographic processes has occurred since the highly publicized recent collapse of the Pacific salmon industry off the west coast of British Columbia (Glavin, 1999; Finney et al., 2000) and indeed the worldwide realization of fish as a dwindling ocean resource (Parfit, 1995). Commercial fisheries collapses along British Columbia's west coast are not only a recent phenomena however. Although historical fisheries records for the west coast of North America are short, only a century of existing fisheries records are enough to document successive historical collapses of the Pacific sardine fishery all along the coast of North America, beginning in the mid-1940's.

The northern sardine fishery, including the commercial Effingham Inlet fishery, collapsed in the mid-1940's, and was followed by the demise of the central California fishery in the 1950's and subsequently the southern California fishery in the 1960's. This progressive collapse of the Pacific sardine fishery from north to south, was apparently aided by a significant change in the pelagic habitat in the California Current system associated with large-scale climate change in the Pacific during the 1940's (Francis and Hare, 1994; Soutar and Issacs, 1969; Baumgartner et al., 1992; Holmgren-Urbá and Baumgartner, 1993). Thus, there is ample evidence of a tenuous commercial fishery along the west coast of North America, which

has operated for over a century in a poorly understood oceanic regime (Francis and Hare, 1994).

A gradual return of sardine populations to waters off Vancouver Island has been occurring since 1990 however, and is associated with a contemporaneous recuperation of sardine populations off southern California, which may be related to a documented large scale climate shift in the Pacific Ocean in 1977 (Robinson, 1994). Although historical fisheries records are short, they do show that fish populations seem to expand and contract over decadal time scales and over distances which encompass the entire North American Upwelling Zone (Baja California to northern Vancouver Island) (Baumgartner et al., 1992).

FACTORS AFFECTING PELAGIC FISH POPULATION ABUNDANCE

It is known that shifts in the position and intensity of the Aleutian Low atmospheric system over the North Pacific exerts a major control on the stock recruitment of many British Columbian fisheries (Hare and Francis, 1995). Changes in this system influence the stratification and offshore upwelling which can result in increases in plankton abundance. Unfortunately, the nature of the long-term oscillations in this system (decadal to millennial) and the accompanying effects on fish stocks are not well known (Francis and Hare, 1994; Hare and Francis, 1995; Ware and Thomson, 1991).

However, changes in climatic and oceanographic conditions do appear to affect fish populations in several ways (Francis et al., 1998). First, changing climatic conditions lead to

shifts in the surface wind stress and mixed layer depth and stratification, changing the characteristics of the surface layer of the ocean. These circulation changes drive changes in primary productivity including the timing of phytoplankton blooms and phytoplankton assemblage composition. Impacts of these changes appear to cascade through the various trophic levels eventually affecting commercially important pelagic fish populations. Hence the ecosystem may pulse according to climatic changes, especially at lower trophic levels where replacement times are short (Francis et al., 1998; Glavin, 1999).

An underlying assumption of our work is that pelagic fish abundance responds to food availability, which in turn depends on oceanographic parameters that cause fertilization of the surface waters where phytoplankton growth is concentrated (Ware and Thomson, 2001). Off the west coast of British Columbia, upwelling (the flow of water from depths of 100-200 m to the surface caused by wind-driven Ekman transport of surface waters away from the coast) is the principle mechanism driving nutrient supply to the coastal ocean (Thomson, 1981, Patterson et al., 2000). Therefore, an understanding of the pre-historic upwelling regime along this coast is key to the interpretation of evidence of paleo-fish populations found in the sedimentary record.

Although real data are scarce, preliminary research has established a link between changes in the present Pacific stratification and upwelling, climate change and a cycling in fish populations (Robinson, 1994; Finney et al., 2000). Clearly, to interpret paleo-fish populations,

a thorough understanding of the regional oceanographic regime through time is required. The primary objective of the NSERC project of which this research is a part, is to add to the evidence that ocean cycles, which can be interpreted from the sedimentary and paleoecological record of Effingham Inlet, are closely related to fish population cycling in the northern Pacific (Baumgartner et al., 1992).

BACKGROUND

REGIONAL SETTING

BEDROCK GEOLOGY

Effingham Inlet is located on the southwest coast Vancouver Island, which is part of the Canadian Cordillera. The present day Canadian Cordillera was created during Mesozoic and Cenozoic time, as multiple terranes were accreted to the North American craton during an oblique convergence of the North American and Pacific Ocean lithosphere. The strong northwest-southeast structural grain of the present day Canadian Cordillera is a result of this accretion (Clague, 1989e). These ancient terranes were each formed in a unique tectonic setting and have been interpreted as remnants of island arcs, oceanic plateaus and islands, continental margin fragments and complex accretionary terranes (Tipper et al, 1981).

The main terrane underlying Vancouver Island is known as Wrangellia, which extends from Vancouver Island to southern Alaska. It has been interpreted as allochthonous, probably originating far to the south of its present day position. It is characterized by identifiable sequences of Triassic rocks, which are quite distinct from adjacent terranes of different rock sequences, also of Triassic age. Since accretion, the Wrangellia terrane has been fragmented by major horizontal translations and rotations, so

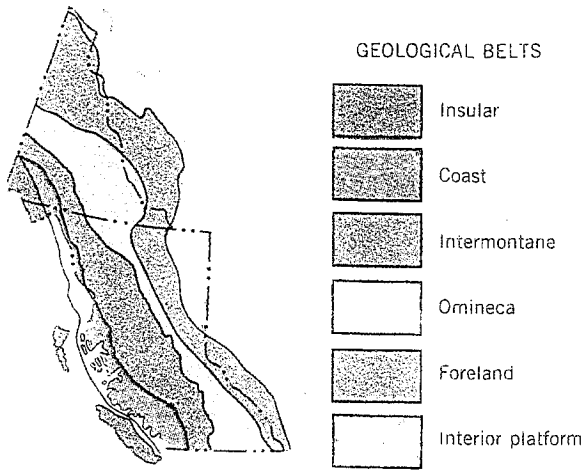
that identifiable pieces can be found from Oregon to Alaska(Jones, 1977; Gabrielese et al., 1991).

The bedrock of Vancouver Island thus consists mainly of; latest Proterozoic to mid-Cretaceous volcanic and sedimentary rock which formed in island-arc or oceanic plateau settings; mid-Cretaceous and younger clastics eroded from uplifting Coast Belt deposits; Paleozoic to Tertiary granitic intrusions; and Late Jurassic to Holocene accretionary complexes (Clague, 1989e).

The Canadian Cordillera has been divided into five major northwest- trending geologic belts (Figure 3)(Gabrielese et al., 1991). Vancouver Island falls within the Insular Belt, which is made up of the Insular mountains, the Saint Elias Ranges, Coastal Depressions, and the continental shelf and slope.

The geologic elements of the Insular Belt were accreted to each other about 200 Ma, during the Middle Jurassic, and collided with other terranes of the Cordillera to the west sometime during the Cretaceous. Accretion of Cordilleran terranes was accompanied by compression which is expressed today in the Vancouver Island area by the great active right-lateral strike-slip fault offshore the Queen Charlotte Islands known as the Queen Charlotte-Fairweather transform fault, which separates the Pacific and North America plates (Clague, 1989e).

Figure 3. Geological belts of the Canadian Cordillera. (from Clague, 1989c)



TECTONIC SETTING

Vancouver Island is located in close proximity to the junction of the Pacific, America and Juan de Fuca plates and 2 smaller lithospheric blocks, the Explorer plate and the Winona Block (Figure 4). Seismic activity in the area is related to the subduction of the oceanic Juan de Fuca Plate beneath the continental North America plate (Figure 5) (Rogers, 1988; Atwater et al., 1995a and b; Hyndman, 1995) and also to displacement along the Queen Charlotte-Fairweather transform fault (Keen and Hyndman, 1979). Present day tectonic movements in the area are; about 40-60 mm/yr of spreading between the Juan de Fuca and Pacific plates; about 50-60 mm/yr of right lateral movement between the Pacific and America plates; and about 40-45 mm/yr, calculated from plate models, of subduction of the Juan de Fuca plate beneath the North America plate (Riddihough and Hyndman, 1991).

However, the amount of subduction of the Juan de Fuca plate occurring at present is the subject of some debate due to the absence of a subduction characteristic marginal trench, the lack of earthquakes in a Benioff zone along the subducting plate, and the quiescence of volcanism in recent geologic times along the mainland Garibaldi and Cascade volcanic belts (Riddihough and Hyndman, 1976). More recently, it has been postulated that the Cascadia subduction zone may now be locked and accumulating strain (Savage et al.,1981) and that great ($M > 8$) subduction earthquakes have occurred in

Cascadia before historic times as a result of the sudden release of sections of a locked subducting plate (Heaton and Hartzell, 1986 and 1987, Rogers, 1988).

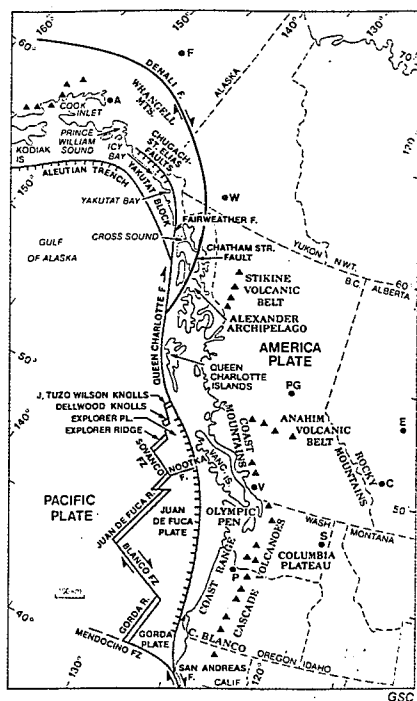
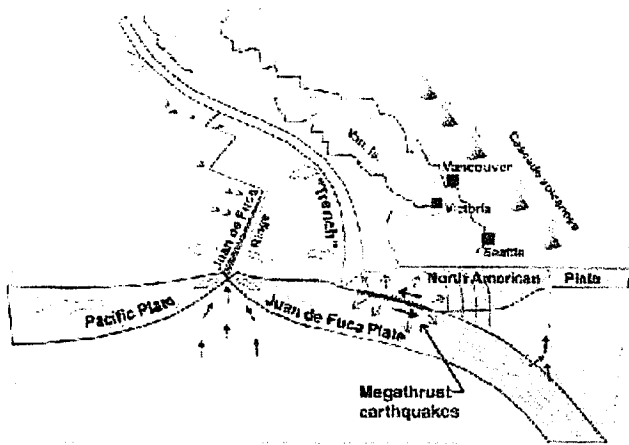


Figure 4. Location map showing modern plate tectonic regime of the northeast Pacific. Triangles represent Miocene and Recent volcanic centers. Place names symbolized as: A, Anchorage; F, Fairbanks; W., Whitehorse; PG, Prince George; V, Vancouver; P, Portland; S., Spokane; C, Calgary; E, Edmonton. (from Riddihough and Hyndman, 1991).

Figure 5. Schematic block diagram showing the subduction of the Juan de Fuca plate beneath North America in the Vancouver Island area.

(from [http:// www.pgc.nrcan.gc.ca/seismo/equinfo/5yr.htm](http://www.pgc.nrcan.gc.ca/seismo/equinfo/5yr.htm))



PALEOSEISMIC ACTIVITY

Southwestern British Columbia is presently very tectonically active (Figure 6) and has experienced four moderate earthquakes during historic times; in 1918 (M=7), in 1946 (M= 7.2), on Vancouver Island and; in 1872 (M=7.4) and in 1949 (M=8.1) in Washington State (Rogers, 1994). The most recent significant earthquake felt in the region, and the largest since the 1949, (M=7.2) quake, recently occurred on February 28, 2001. The epicenter of this M=6.8 quake, was near Olympia, Washington, just to the south of Vancouver Island, and significant damage was sustained in the Puget Sound area of Washington State. No significant damage was reported on Vancouver Island, although significant ground shaking was experienced throughout southern Vancouver Island ([http:// www.pgc.nrcan.gc.ca/scismo/cquinfo/5yr.htm](http://www.pgc.nrcan.gc.ca/scismo/cquinfo/5yr.htm).)

A great, magnitude 9 earthquake occurred in the Vancouver Island area on January 26, 1700 AD, with an inferred epicenter somewhere along the subducting Juan de Fuca plate, just offshore western Vancouver Island. This event is recorded in Japanese historical documents of the resulting tsunami, in oral history of the Pachna Bay native peoples of west coast Vancouver Island, and in coastal tsunami and submergence features on Vancouver Island and in northern Washington State (Atwater et al., 1995a; Clague and Bobrowsky, 1994 a and b). This earthquake has been reconstructed as a subduction earthquake which was the result of a rupture of the entire 900 km length of the thrust fault between the Juan de Fuca and North American plates.

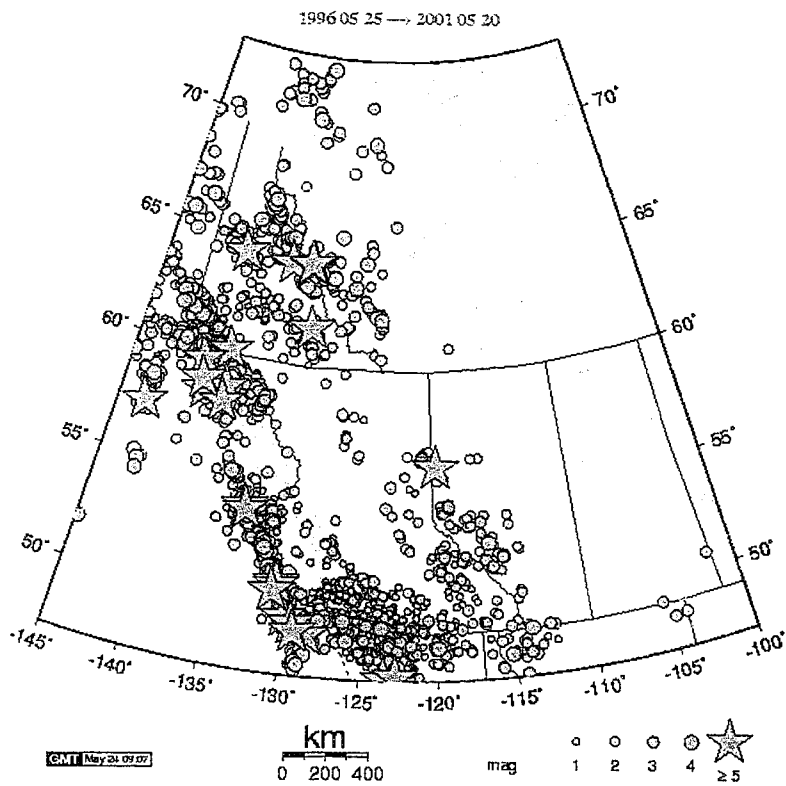
Further evidence for large prehistoric earthquakes has come from (1) studies of massive and laminated sediment packages in anoxic Saanich Inlet on southern Vancouver Island (Blais-Stevens et al., 1997; Blais Stevens and Clague, 2001), (2) stratigraphic evidence of tsunami deposits and associated rapid sea-level change (Atwater, 1987 and 1992; Atwater et al., 1995a; Darienzo and Peterson, 1990; Clague and Bobrowsky 1994a, 1994b; Mathewes and Clague 1994), (3) sand dykes and blows resulting from seismically induced sediment liquefaction (Clague et al., 1992; Obermeier, 1995) and (4) seismically triggered landslides (Adams, 1990; Jacoby et al., 1992; Karlin and Abella 1992 and 1996; Schuster et al., 1992)

Laminated sediments which record seismic events are useful in extending the brief historic seismic record, and particularly in attempting to determine the existence and return periodicity of moderate (M7) to large (M8-9) earthquakes on southern Vancouver Island in the pre-historic past (Blais, 1995; Blais-Stevens et al. 1997; Blais-Stevens and Clague, 2001). In the Saanich Inlet studies, it was concluded that debris flows, expressed as massive muds and silts intercalated within the laminated sediments of the anoxic Saanich Inlet of southeastern Vancouver Island, probably have a seismic origin (Blais, 1995; Blais Stevens et al., 2001, Blais Stevens and Clague, 2001). The seismic events associated with these deposits were postulated to have an average recurrence interval of about 150 years. This value is in fairly close agreement with a modeled return time of

about 100 years for moderate to large earthquakes of southern Vancouver Island (Rogers, 1994).

Figure 6. Locations of earthquakes occurring in the previous five years in Western Canada. (from <http://www.pgc.nrcan.gc.ca/seismo/equinfo/eq-westcan.htm>)

Earthquakes for the Previous 5 Years in Western Canada



QUATERNARY GLACIAL HISTORY

The landscape of British Columbia has been affected by glaciers since 9 Ma (Denton and Armstrong, 1969). A massive ice sheet of interconnected mountain ice sheets and valley and piedmont glaciers, known as the Cordilleran Ice Sheet, has covered the Canadian Cordillera and Vancouver Island several times during the Pleistocene, its most recent advance, during Late Wisconsinan time, is known as the Fraser Glaciation (Clague, 1989c).

The exact history of the advances and retreats of the Cordilleran Ice Sheet however, are largely obscured by the successive glaciations, but it appears that at its maximum extent, the ice sheet covered almost all of British Columbia, the southern Yukon Territory as well as parts of southwestern Alaska and the northwestern United States. Throughout the Pleistocene and early Holocene, glacier advance and retreat was controlled by global climate, and other more local effects such as eustatic sea level lowering, ocean cooling and changes in atmospheric circulation during glacial periods (Clague, 1989c).

Ice in the coastal areas of Vancouver Island covered large areas of the continental shelf after reaching the sea through fjords and valleys (Luternauer and Murray, 1983). The last glacial ice sheet rapidly retreated from Vancouver Island coastal areas about 15k yBP and from higher elevations on the island about 12k yBP (Clague, 1980 and 1981).

Remnants of the last glaciation still exist in the permanent mountain glaciers of the highest Vancouver Island peaks.

Alpine glacial features such as summits, ridges, cirques and horns are common in the mountainous areas of Vancouver Island. The coastline is deeply indented with fjords such as Effingham Inlet, which are located at the oceanward end of glacially carved valleys. Smaller scale sub-alpine and coastal glacial landforms evident on Vancouver Island are for the most part remnants of the retreat of the most recent ice sheets and include glacial fluvial landforms such as meltwater channels, eskers, kames and valley trains, as well as incised depositional plains of glacial lacustrine and glacial marine origin (Mathews, 1989). Outwash deposits from glaciers terminating in the sea or lakes is also common, forming proglacial floodplains and deltas, and subaqueous fans on land, and also offshore on the continental shelf. Glacial till is the most common and extensive surficial material on Vancouver Island and its composition and texture varies widely depending on the type of material from which it is derived. Massive to stratified marine mud with a gravel component of < 5 % gravel-sized material is the most common marine deposit of glacial origin (Clague, 1989b).

During the Fraser Glaciation, present coastal lowlands were submerged due to an isostatically depressed crust. As the Cordilleran Ice Sheet decayed and retreated north east, from coastal areas, marine glacial sedimentation ceased as the crust rebounded isostatically (Luternauer and Murray, 1983; Clague, 1989b).

Quaternary events and deposits are widely variable throughout British Columbia, and are linked to the complicated history of the repetitive local advances and retreats of the ice sheets (Clague, 1989a). This variability is reflected in the stratigraphic nomenclature for British Columbia (Figure 7) (Ryder and Clague, 1989).

Figure 7. Quaternary events and deposits in British Columbia. (from Ryder and Clague, 1989)

POST-GLACIAL SEA LEVELS

The known Quaternary sea level history on Vancouver Island is attributed to a complex interplay of diastrophism, eustasy, isostasy, sediment supply, wave action and tidal current energy (Clague, 1989d; Barrie and Conway, 1999 and 2001). At the onset of the latest Fraser Glaciation about 25 ka BP, sea levels on Vancouver Island initially fell in response to forebulges in the crust and mantle as they isostatically adjusted to the progression of the ice sheet from central British Columbia out towards the western coast of Vancouver Island. Eventually, sea levels rose again as the entire area became isostatically depressed with the progressive growth of the ice sheet.

Sea levels were higher than present day at the climax of the Fraser Glaciation (Clague, 1983). The highest relic shorelines on Vancouver Island are dated to the close of the Pleistocene and were about 50 m above present day levels on the west coast of Vancouver Island, about 150 m above present day on the east coast of the island, and as much as 200 m above present day on mainland British Columbia (Clague, 1981).

Following the most recent deglaciation, about 10,500 yr B.P., a regression occurred and the resulting sea levels on the northwestern coast of Vancouver Island are known to have been 95 m lower than at present due to isostatic rebound following the unloading of the crust with the retreat of the ice sheet (Luternauer et al., 1989). This isostatic uplift, which was greater than eustatic sea level rise at the time, was apparently very rapid at the close of the Pleistocene (Barrie and Conway, 2001), with sea levels

falling more than 100 m in the Courtenay area of east coast Vancouver Island within 2 ka. In an opposite effect sea levels at fjord heads on the British Columbia mainland were about 100 – 200 m higher than today at the same time that shelf areas off Vancouver Island were subaerially exposed. These fjords were still isostatically depressed since they were more recently deglaciated than the outer coast of Vancouver Island (Luternauer et al., 1989). It has been suggested that high sea levels at fjord heads on the mainland and low sea levels on outer Vancouver Island are linked and the consequence of the migration and collapse of a glacial forebulge (Clague, 1989d).

A very rapid transgression occurred after the initial regression following deglaciation of the northern shores of Vancouver Island and the Queen Charlottes however. These areas have a sea level history somewhat different than mainland B.C. and parts of eastern Vancouver Island (Barrie and Conway, 1999 and 2001). The return to present day sea levels in a current regression, on the western shores of Vancouver Island was highly variable over short distances, and depended on the rate of ice retreat in local areas. It is known that present day sea levels were re-established at Victoria on southern Vancouver Island for example about 11.5k yBP (Luternauer et al., 1989), yet it appears that sea level has continued to drop, about 2-4 m, north of Effingham Inlet, in the Tofino area from about 4,000 yBP to the present (Clague et al, 1982). The sea level history in this area is also complicated by well documented sudden sea level changes (up to 4 m) associated with great earthquakes (Clague and Bobrowsky, 1999).

In summary, the west coast of Vancouver Island appears to have experienced an initial regression, then a rapid transgression at the onset of the Fraser Glaciation about 25 k yBP. After deglaciation about 10,500 yBP, a similar regression –transgression cycle related to a mantle forebulge occurred. Present day sea level was re-established on southern Vancouver Island early in deglaciation but a regression appears to be continuing in the Effingham Inlet area to the present day.

TERRESTRIAL CLIMATE AND VEGETATION

Vancouver Island is part of the Pacific Canada broad climatic region defined by Hare and Thomas (1979). In this climate zone, which is cool temperate and very wet, mild and moist Pacific air dominates creating mild, cloudy and wet winters and moderate, relatively dry summers. Precipitation can reach 2500 mm annually, making the area the wettest in Canada. The high levels of precipitation occur mainly in the winter and are the result of both successive frontal systems from the Pacific and an enhancement of the precipitation by local orographic effects, giving higher levels of precipitation with altitude. In the high mountains winter precipitation accumulates in thick snowpacks. In the summer, the cyclonic storms originating in the Gulf of Alaska give way to the influence of a large anticyclone, which brings clear and calm weather (Ryder, 1989).

Air temperatures on Vancouver Island are stable throughout the year on a daily and seasonal basis with variation ranging from only about 1 - 5 °C, decreasing somewhat

inland and with elevation. The mean annual temperature range between summer and winter temperatures is 10-15° C, the lowest in Canada (Ryder, 1989).

Vegetation at low to moderate elevations of the coastal regions of the island is categorized as the Coastal Western Hemlock and Coastal Douglas Fir biogeoclimatic zone. In the moist coastal areas of the island, the dominant trees are western hemlock, Pacific silver fir, Douglas-fir, western red cedar and Sitka spruce. Where coastal areas lie in the rain shadow of the Olympic mainland mountains or the Vancouver Island mountains, Douglas-fir, evergreen shrubs, Garry oak, arbutus and meadow vegetation dominate (Research Branch, 1988).

HOLOCENE VEGETATION AND CLIMATE HISTORY

The climate history of British Columbia unfortunately has not been studied as extensively and methodically as for other provinces (Ritchie, 1987). However, Hebda (1995) has reported his own, and a synthesis of all other paleoclimate work done to date in British Columbia, which gives a general picture of the Holocene climate on Vancouver Island. The Holocene climate record he interprets is inferred from pollen data taken from ten sites on Vancouver Island, including one in Barkley Sound, at the mouth of Effingham Inlet. Temperature projections made from this pollen record however, are complicated by plant migrational and successional factors. In the B.C. pollen record, Hebda interprets increased climate moisture as indicated by an increase in western hemlock, descending lower tree lines, relatively full lakes, and reduced fire frequency.

Hebda (1995) interprets the Holocene climate conditions for west coast

Vancouver Island as; modern climate conditions to 2ky BP, a climate cooler and wetter than today's about 2–4 ky BP, and a climate warmer and drier from 4–10.5 ky BP.

The exact start and end times for these climate trends however, are difficult to precisely determine from region to region, but the cooling at about 4 ky to cooler and wetter conditions than today, from a previous state of warmer and drier conditions than present, has clear indicators along the west coast with observed changes in vegetation and further neoglacial ice advances (Hebda, 1995).

OCEANOGRAPHY AND CLIMATE

The overall ocean-atmosphere climate system of the Pacific Ocean is controlled by relative shifts in the positions of the atmospheric Aleutian Low (AL) and North Pacific High (NPH) pressure systems (Figure 8). The position of these atmospheric systems responds to the location of the Jet Stream, especially in the winter when variability of the Jet Stream is highest (Roden, 1989). The surface currents of the Pacific Ocean are controlled by the position and intensity of the AL and NPH. Strong winds associated with these systems are a major contributor to the three major oceanographic domains that characterize the west coast of North America: the Coastal Upwelling Domain, extending from Baja California to northern Vancouver Island; the Coastal Transition Domain, extending from northern Vancouver Island to Dixon Entrance; and the Coastal Downwelling Domain of the Alaska Coast and Panhandle (Ware and Thomson, 2000).

The position of the AL therefore determines whether there will be costly droughts or flooding on land, and impacts coastal BC fisheries, because changes in the wind system influence mixed layer depth, coastal upwelling, and offshore advection, which can result in modifications to plankton abundance and distribution (Mackas et al., 2001).

Effingham Inlet is located at the apparent, present day northern extreme of the southward-flowing offshore California Current surface current, just at the bifurcation point with the northward flowing offshore Alaska Current. The nearshore currents,

which flow over the Vancouver Island shelf however are strongly seasonally dependent and are of particular significance to periodic upwelling onto the continental shelf of deep (>150 m) slope waters (Thomson, 1981; Patterson et al., 2000).

The southeastward flowing Shelf-Break Current (SBC) dominates in the summer, and reverses in the winter to the northwestward-flowing Northeast Pacific Coastal Current (NEPCC) (Figure 9). The SBC is driven by the prevailing clockwise circulating winds of the North Pacific Atmospheric gyre, while in winter the NEPCC current is driven by the influence of the Aleutian Low pressure gyre (Thomson and Gower, 1998). In summer, the southward flowing SBC is forced seaward by the Ekman transport effect (Figure 8) and creates the conditions for upwelling of deep slope water onto the Vancouver Island continental shelf. These nutrient-rich waters are the source of a dramatic increase in primary productivity in the upper layer of the water column, leading to the diatom blooms, which are common in the spring and summer. This nutrient-rich water is also known to spread on occasion into adjoining inlets, such as Effingham, where it contributes to increased productivity (Thomson, 1981; Patterson et al, 2000).

In the present day oceanic regime off Vancouver Island, air and sea surface temperatures appear to fluctuate on a 2-8 year cycle in response to episodic El Niño and Southern Oscillation oceanic events (ENSO) (Thomson, 1981). These ENSO signals, as well as more periodic oscillations expressed at decadal time scales can also be recognized in the instrumental climate record (Ware, 1995). However, the instrumental record is

barely adequate for analyzing the characteristics of decadal-scale climate variability.

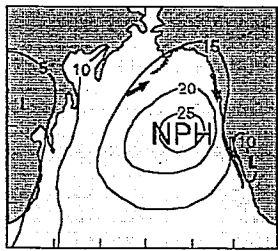
This is particularly true along the west coasts of Canada, where measurement and collection of air and sea surface temperatures only began about 100 years ago. Detailed instrument records of regional oceanic circulation exist for an even shorter time (Ware and Thomson, 2000).

As an example of the utility of high-resolution proxy data in resolving prehistoric ocean and atmosphere variability, a regional 400 year dendrochronological record from the American and southern Canadian Pacific coasts shows clear evidence of the 2-8 year El Niño/Southern Oscillation record, as well as 20-40 year and 60-80 year interdecadal time-scale fluctuations, with the latter cycle frequency dominating air temperature variability along the west coast of north America during this time (Roden, 1989; Ware and Thomson, 2000).

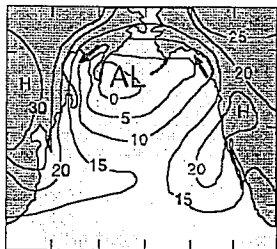
Thus there have been conspicuous temporal modulations of the ENSO and the interdecadal signals. In addition, low-frequency temperature cycles at periods greater than 10 years in the NE Pacific have been significantly coherent and in-phase in all the coastal regions examined so far (Ware and Thomson, 2000). Recent work suggests that the interdecadal oscillation is a worldwide phenomenon that is due to global air-sea interactions (Mann et al., 1995). Additionally, superimposed on this global pattern are regional-scale interactions that force regional variability in climate (Ware and Thomson, 2000).

Clearly, the understanding of present day global and regional, ocean and climate cycles, is key to the interpretation of past geologic, oceanic and climate systems and also for understanding the regimes affecting ecosystems, including fish populations.

Figure 8. Position of the Aleutian Low and North Pacific High atmospheric systems (from Schell and Dallimore, 2001, modified after Thomson, 1981).



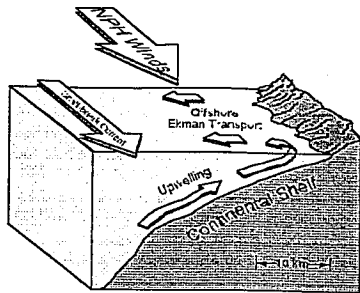
July



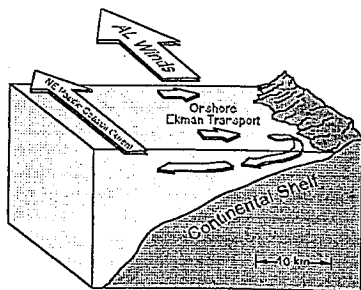
January

Figure 9. Upwelling on the Vancouver Island shelf.

(from Schell and Dallimore, 2001, modified after Thomson, 1981)



A. Summer: North Pacific High influenced coastal circulation off Vancouver Island.



B. Winter: Aleutian Low influenced coastal circulation off Vancouver Island.

PALEO-FISH POPULATION RESEARCH

To date, most paleo-fish population research, based on the counting of fish scales and bones preserved in marine sediments, has been carried out in the Santa Barbara Basin region of Northern California, and the Soledad Basin off southern Baja California. Both of these basins are located in the southern portion of the North American Upwelling Zone (Baja California to northern Vancouver Island). These sites are ideal for paleoenvironmental studies, as they are enclosed coastal basins with strongly anoxic bottom conditions (Soutar and Isaacs, 1969; Baumgartner et al. 1992; Holmgren-Urbá and Baumgartner 1993).

In British Columbia, the first information of prehistoric fish populations came from archaeological sites. Hebda and Frederic (1990) describe diverse fish populations represented in remains of middens dated between 5000 and 6500 yBP. It seems that since that time aboriginal peoples were actively fishing along the British Columbia coast.

In Saanich Inlet on eastern Vancouver Island, researchers involved with analysis of cores spanning the entire Holocene from ODP Site 169S, found remains of hake, herring, flatfish and salmon. That study showed a complete fish population record throughout the Holocene in Saanich Inlet from first appearance of pelagic fish in the record just after de-glaciation about 12,000 yBP. The sediment samples were taken from large volume box core and a longer small volume piston core, and fish population cycles on the order of hundreds of years were resolved from the counting of fish scales and

bones. Fish population cycles appear to occur every 300-400 years in Saanich Inlet (Tunncliffe et al., 2001). A higher resolution of decadal cycles could be resolved from the larger volume box core studies of the last 150 years in Saanich Inlet (O'Connell and Tunncliffe, 2001).

The Saanich studies also presented further refinement and considerations of using fish scales and bones as a paleoenvironmental indicators, such as preferential scale shedding by some species and progressive scale degradation after deposition in the sediments.

EFFINGHAM INLET

PHYSIOGRAPHY

Effingham Inlet is a 17 km long, silled fjord located on the southwest coast of Vancouver Island (Figure 1). On the oceanward side of Vancouver Island, the shoreline is irregular and deeply indented, producing fjords, a coastal configuration which is quite different than the relatively smooth coastline of the United States directly to the south (Figure 10). The inlet is open to the Pacific Ocean through a wide bay, Barkley Sound, and is located in a remote and uninhabited area. The inlet consists of two distinct basins, the “outer basin” which is restricted from open circulation with the Pacific Ocean by a sill rising to 65 m depth and an “inner basin” further restricted from the outer basin and the ocean by a second sill at 40 m depth (Figure 1 and 11). The outer basin is the larger and deeper of the two with a maximum depth of 210 m. The maximum depth of the inner basin is 120 m (Figure 11). A narrow channel extends from the inner basin to a marsh at the head of the inlet fed by the small Effingham River, and tidal marshes are also present on the shores of the outer basin, each fed by small unnamed streams (Figure 12).

The shores of the inlet are steep and rocky, rising abruptly to mountains of 900 to 1200 m on each side of the inlet, comprised mostly of Mesozoic volcanic rocks (Figure 13). Underwater slopes of the inlet nearshore are also steep and rocky, and seem to consist of outcropping volcanic Mesozoic rocks and/or Quaternary glacial gravel (Patterson et al., 2000).

In deeper parts of the basin below about 70 m in depth, sediments are organic-rich, olive-grey mud, with the surface sediment a distinct, black organic-rich mud, a few cm thick. At depths shallower than 70 m in the outer basin and at the head of Barkley Sound, the bottom sediment is a firm grey marine mud and silt, with lower organic content than the olive-grey muds (Patterson et al., 2000).

The shores of the inlet are heavily forested with coniferous trees and logging has occurred since about the 1970's on the upper slopes in the vicinity of the outer basin. Logging scars on the slopes of the outer basin are clearly visible today and on aerial photographs dating to 1976 (Figure 12).

The aerial photograph (Figure 12) also shows the lack of beaches on the shores of the inlet, and that most of the inlet's shorelines are steeply dipping bedrock that plunges directly into the water. It would be very difficult to land or launch even a canoe or kayak anywhere in Effingham Inlet, except at the small marshes located at the head of the Effingham River and the two un-named streams of the outer basin. No roads access the inlet and a handful of isolated fishers' cabins at the mouth of the inlet are the only signs of human habitation.

Figure 10. Photograph of fjord-type coastline, Barkley Sound, Effingham Inlet.



Figure 11. Bathymetry and water properties of Effingham Inlet. (from unpublished data of Patterson et al., 2000)

51

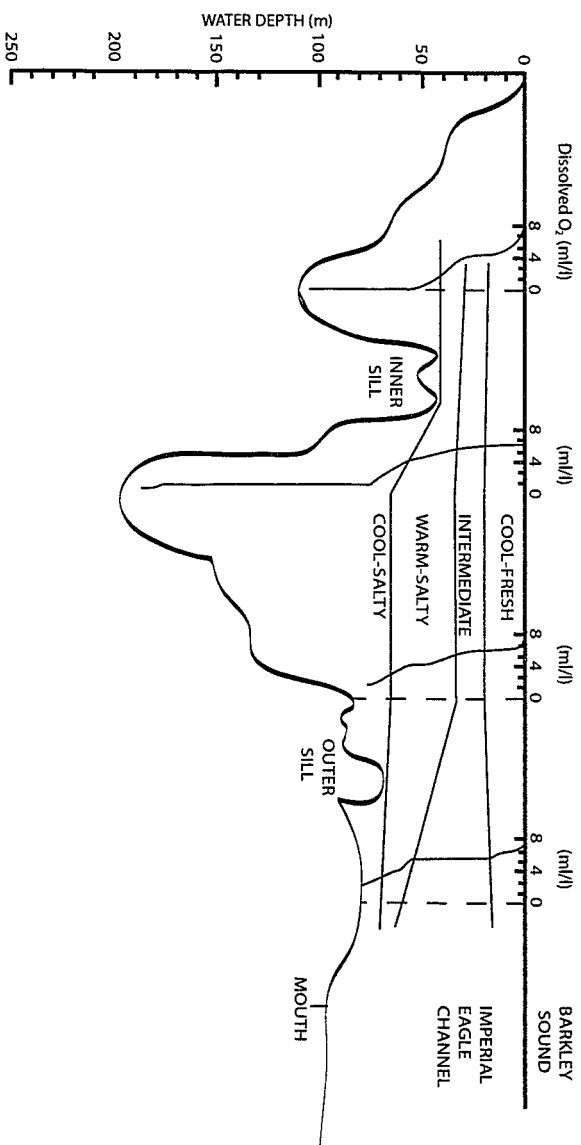


Figure 12. Aerial photograph of Effingham Inlet, 1976. The inner basin is at the top left and Barkley Sound at the bottom right. Notice marshy areas at the head of the inner basin and on both sides of the outer basin where the small Effingham River and two unnamed streams drain into the inlet. Patchy white areas are logging scars, not visible on aerial photographs of the 1930's. What appears to be a sediment-laden plume of ocean water can be seen in Barkley Sound and has crossed the outer sill to reach the outer basin.

SA MAJESTE LA REINE DU CHEF DU CANADA, MINISTERE DE L'ENERGIE, DES MINES ET DES RESSOURCES. T



HER MAJESTY THE QUEEN IN RIGHT OF CANADA, DEPARTMENT OF ENERGY, MINES AND RESOURCES. T

Figure 13. Photograph of steep mountainous shorelines of the outer basin, Effingham Inlet, October, 1999.



OCEANOGRAPHY

The physical oceanography of Effingham Inlet itself was investigated for the first time in October 1995, and again in March 1997, during reconnaissance cruises of the CCGC J.P. Tully (Patterson et al., 2000). Temperature, salinity, oxygen and transmissivity profiles of the inlet were developed along a twenty station transect from Barkley Sound to the inner basin (Figures 11 and 14).

Salinity profiles of the inlet reveal a well-developed, estuarine-type stratification of the water column. Salinities were higher at the bottom of the basins than at the sill depths, indicating a stable, stagnant water column in the basins, conditions conducive to low rates of turnover and subsequent conditions of anoxia and dysoxia in the bottom waters of the inlet (Figure 11 and 15). The salinity profile of the outer basin reveals the movement of basin waters, since the salinity of the bottom waters of the outer basin is higher than at the outer sill, it appears that higher salinity oceanic water occasionally crosses over the sill and enters the outer basin. Additionally, without the periodic addition of higher salinity oceanic waters into the outer basin, one would expect that over time salinity would eventually diminish from heat and salt diffusion (Patterson et al., 2000).

Oxygen profiles of the inlet show a progressive decrease in oxygen with depth in both the outer and inner basins, creating a highly uniform anoxic (no oxygen) / dysoxic

/suboxic (dissolved O₂ < 40 μM/kg)/ low oxic (> 100 μM/kg) water column with depth (Figures 11 and 15).

The sub-oxic/ dysoxic bottom waters are approximately uniform in salinity and temperature, while the overlying waters exhibit a step-like transition zone, in temperature and salinity. In the inner basin, bottom waters of 60 – 70 m depth and greater have oxygen values of zero or near zero, and H₂S appears. Anoxic and dysoxic conditions are also exacerbated by high levels of influx of terrestrial, and, during upwelling-induced diatom blooms of spring and summer, marine organic matter, the decomposition of which rapidly consumes any remaining oxygen in the water column.

Tidal variation in Effingham Inlet is relatively small (< 2m) and tidal currents are weak, except in constricted narrows in the vicinity of the shallow sills.

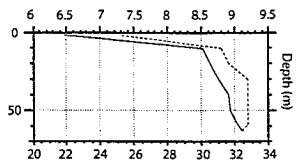
During the January and June, 1999 cruise to Effingham Inlet to monitor the oceanographic transect, an episode of oxygenation (low-oxic) bottom waters in the inner and outer basins was observed, confirming the assumption from salinity data that oxygenated, upwelling waters are able to reach the inner basins of Effingham on occasion. Four months later in October, 1999, oxygen levels had again depleted significantly, suggesting that the characteristic anoxic/dysoxic conditions of the inlet had returned. This significant upwelling event has been attributed to the particularly strong 1997-98 El Niño event in the southern Pacific Ocean, indicating the extent that local oceanographic conditions are affected by global ocean phenomena (R. Thomson, pers.

commun.). Further foraminiferal evidence from the surface sediments, and also sediments at depth in Effingham Inlet, also confirms that even the most isolated and anoxic portions of Effingham Inlet have been periodically oxygenated by upwelling events (Patterson et al., 2000; Schell and Dallimore, 2001).

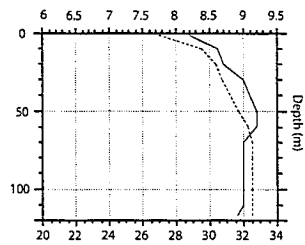
Figure 14. Salinity and water temperature profiles from Effingham Inlet,
(Patterson et al., 2000).

Salinity and Temperature in Effingham Inlet

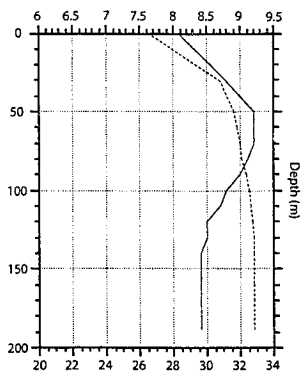
head of inlet



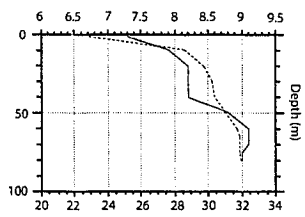
inner basin



outer basin

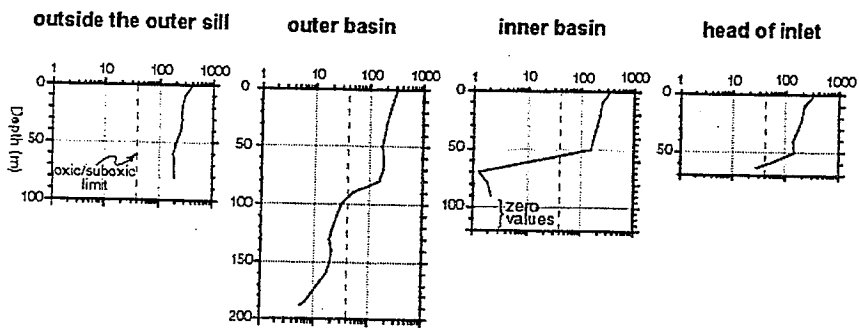


outside the outer sill



— temp (°C)
..... salin (‰)

Figure 15. Oxygen profiles from Effingham Inlet.(from Patterson et al., 2000)



Dissolved oxygen profiles for selected stations in Effingham Inlet
 (μM of O_2 per kg of seawater)

MATERIALS AND METHODS

OCEANOGRAPHIC CRUISE

CORING

The sedimentology of Effingham Inlet was investigated during cruises of the Canadian Coast Guard research vessel, the *CCGC J.P. Tully* (Figure 16) in September, 1997 and October, 1999. A removable A-frame was temporarily secured to the ship for these cruises and was mounted on the starboard aft to facilitate the deployment of a 10 cm diameter piston coring device in 1999, and a 6 cm diameter piston core in 1997 (Figure 17).

The outer and inner basins of the inlets were traversed with a 3.5 kHz air gun seismic system survey during each cruise to locate piston coring sites where sediment packages seemed relatively gas free in the top few meters, and in locations away from particularly steep underwater shore slopes of the basins.

During the 1997 cruise, three 9 m piston cores were recovered, one each from the inner and outer basins (Figure 1), and also a core was taken from the mouth of the inlet in Barkley Sound (Figure 50). During the 1999 cruise, five approximately 11 m piston cores were taken in the inner basin within 500 m of each other, the rationale being to obtain large sediment volumes of the inner basin which were needed for fish scales work on the sediments. One piston core was taken from the outer basin (Table 1, Figure 1).

Figure 16. Photograph of the *CCGS J.P. Tully*, docked alongside the largest oceanographic research vessel in the world, the Japanese *Mirai*, in Victoria, B.C., September, 2001.

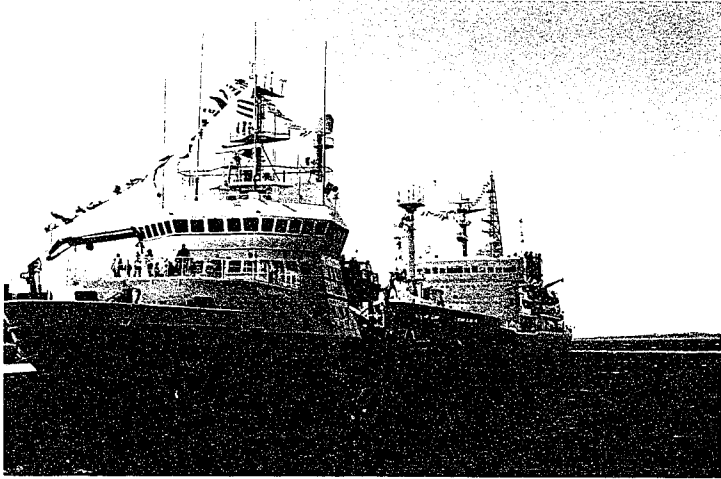


Figure 17. Piston coring apparatus being deployed aboard the J.P. Tully.

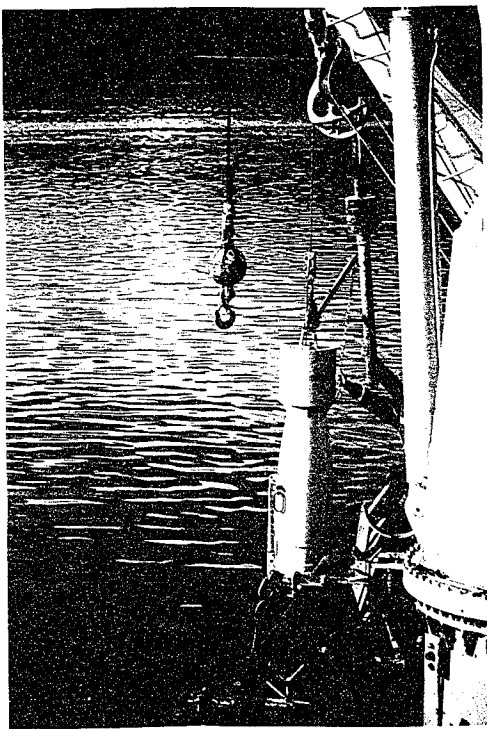


Table 1. Location of piston and freeze cores

Core Identification	Location	Water depth
BARKLEY SOUND		
TUL97A04	48° 57.57 125° 10.39	50 m
OUTER BASIN		
Piston cores		
TUL99B11	49° 02.632 125° 09.23	205 m
TUL97A01	49° 02.550 125° 09.13	200 m
Freeze cores		
TUL99B10	49° 02.642 125° 09.043	205 m
TUL99B12	49° 02.632 125° 09.230	205 m
INNER BASIN		
Piston cores		
TUL97A02	49° 04.360 125° 09.540	100 m
TUL99B03	49° 04.275 125° 09.359	120 m
TUL99B06	49° 04.188 125° 09.337	121 m
TUL99B09	49° 04.173 125° 09.279	122 m
TUL99B13	49° 04.173 125° 09.401	122 m
Freeze cores		
TUL99B01	49° 04.269 125° 09.399	119 m
TUL99B04	49° 02.218 125° 09.429	120 m
TUL99B07	49° 04.145 125° 09.337	121 m

The coring operations during both cruises went well, the only complication was presented by the unconsolidated sediments at the sediment water interface, described by the coring engineer, Mr. Kim Conway of GSC, as a “colloidal soup”. However, during recovery of TUL99B03 in 1999, and also of TUL97A02 in 1997, both located in the inner basin, the ship itself shuddered violently as the piston core fired into the sediments, which meant that the piston core was essentially “free-falling” through the upper unconsolidated sediments and met resistance from the end of the piston core tether and not the upper sediments as intended. These experiences led the ship’s crew to believe that due to the unconsolidated nature of the upper sediments, the piston cores were not sampling the sediment water interface.

In 1999, three “Pederson” freeze cores, of about 2 m in length, were taken from the inner basin and two from the outer basin. The “Pederson” freeze core is essentially a long (3 m) box of about 10 cm², that is filled with lead weights, and then dry ice. The freeze core apparatus was modified by Dr. T. Pederson, from an unpublished design of John Cruisius, based on similar devices described in Huguen et al. (1996) (Figure 18). This apparatus is lowered to the sediment water interface, left for 20 minutes while the surface sediments freeze to its outer face, and then is carefully raised.

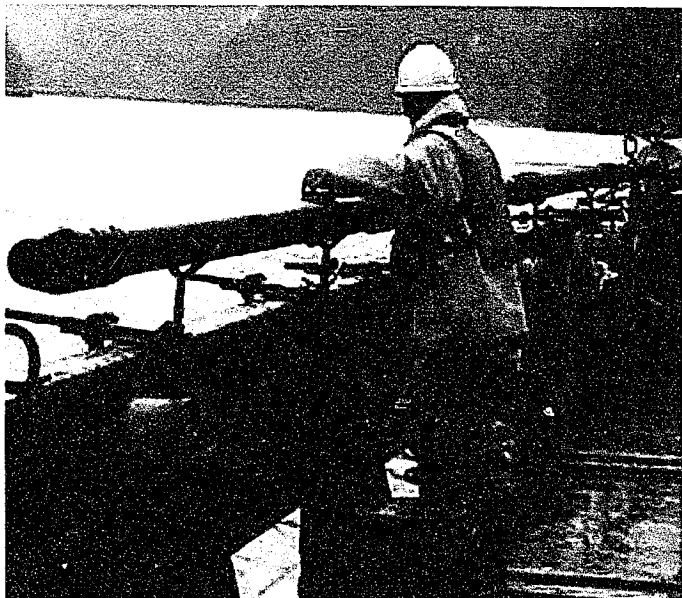
ON-BOARD HANDLING OF CORES

Once on board, the piston cores are separated into eight, 1.5 m sections each, which are encased in a heavy plastic inner liner of the coring device (Figure 19). Core

Figure 18. Photograph of the onboard handling of freeze cores. Dry ice is being loaded into the freeze coring device before deployment.



Figure 19. Separation of piston core sections.



sections are then stood on end, tops up and stored in a 4°C cooler on board the J.P Tully. Upper sections of the core were very wet and sediment convection was occurring in some of the top sections immediately following recovery. Several holes were drilled with a power hand drill, on each recovered section to enable draining of excess water. For the top section, this meant a reduction in cored volume of about half.

The Effingham sediments are quite gas-rich, and in several instances, the piston coring device blew apart forcefully as the sections of the piston core length were being separated on deck. In these cases, up to 20 cm of sediment was lost, which was noted and later accounted for in core descriptions and analyses.

The freeze cores were separated from the Pederson coring device on deck, were placed on plywood, wrapped in plastic film and foil, and then stored in on board chest freezers.

OCEANOGRAPHY

Dr. Richard Thomson of the Canadian Department of Fisheries and Oceans has been monitoring the oceanographic conditions of Effingham Inlet and Barkley Sound, both spatially and temporally, from October, 1995 and on-going through the most recent visit to the inlet in July, 2001. Both moored instrumentation and profile data from shipboard surveys are being utilized.

Moored instrumentation includes pairs of sediment traps and current meters located at the entrance to the inlet and within the inner basin. Sediment trap and current meter records have been kept from May, 1998 to the present.

Profile data are from a multiple-sensor profiling package and a hull-mounted 150 kHz acoustic Doppler current profiler (ADCP). This device measures the current velocity and acoustic backscatter intensity at 8 m depth intervals along the ship track. The profile package consists of a Conductivity-Temperature-Depth (CTD) probe, a 25 cm- pathlength transmissometer, a flurometer, and a 24-Niskin bottle rosette sampler for measuring concentrations of oxygen, nutrients and other dissolved constituents (Figure 20). Profile data has been kept continuously since October, 1995.

Figure 20. Photograph of multiple sensor profiling apparatus.



LABORATORY WORK

PISTON AND FREEZE CORE HANDLING

Piston cores were transferred upright from the ship to a 4° C walk-in cooler at the Pacific Geoscience Center (PGC), at the ship's home port in Sidney, British Columbia. PGC is part of the Geological Survey of Canada (GSC) and, along with the Department of Fisheries and Oceans, occupies part of the research and docking facilities known as the Institute of Ocean Sciences, Sidney (IOS). Freeze cores were transferred to chest freezers in IOS.

Sections four to eight of all the piston cores were sawn lengthwise in half using a small power hand saw, giving an archive and a working half, within 2 weeks of the October, 1999 cruise. Each half was then wrapped in plastic film, and stored flat in sealed plastic containers (D-tubes) containing a wet sponge to maintain humidity. The same procedure was followed for all Sections 1 to 3, two months after the cruise in December, 1999, to allow for continued drainage from the drilled holes in the core liners. Core liner tops were also removed from these sections while in storage to aid in the drying process.

All cores were photographed after splitting with a Nikon 2000 Digital camera and logged, with color descriptions based in the Munsell Color Chart. Freeze cores were also unwrapped from their plastic and foil covering in November 1999, and described. The

freeze cores had oxidized however, and the sediments were uniformly black, leaving few features to describe by eye.

The three piston cores taken in 1997, were handled, split and archived (in 4 °C storage) by Kim Conway of PGC after that cruise. I subsequently described, photographed and sampled them for Rock-Eval and micropaleontology analyses in February, 1999.

When all core description (Figure 21) was complete in December, 1999, the piston core sections were stored flat on racks in their sealed D-tubes in a covered, outdoor hanger at PGC, with an ambient temperature of below 10 °C year-round.

Sampling of the 1997 and 1999 Effingham Inlet cores for radiocarbon dating material, grain size and Rock-Eval analysis and micropaleontology work, including fish scales, was done by myself and others between February 1999 and May, 2000.

X-RADIOGRAPHY

A core sediment slabbing tool, christened the “cookie cutter” was designed to make subsamples suitable for scanning electron microscopy and x-radiography of core sediments. The tool was based on a design first described in Schimmelman et al., (1990) and further refined by Grimm et al., (1996), to aid in the useful technique of x-radiography of laminated sediments (Pike and Kemp, 1996b). Our own tool was further re-designed to meet our needs by my colleague Alice Chang of the Ottawa-Carleton Geoscience Centre, and built in the Science and Technology Center at Carleton

University in Ottawa, Ontario. The cookie cutter was built in two sizes, and its specifications and instructions for use are contained in Appendix A.

In May, 2000, an inner basin core TUL99B03, and an outer basin core TUL99B11, were sampled down their entire lengths using the 20 cm cookie cutter, giving sediment slabs 20 cm in length and 1 cm in thickness. These slabs were wrapped in "Clingwrap" plastic film (due to its unique property, to be x-rayed through) and stored in 4 °C refrigeration.

Subsequently, the cookie cutter slabs were x-rayed, and the films developed in two groups;

- 1) by Alice Chang and Dr. R McNeely of GSC, Ottawa using the GSC, 27-35 kV, 37 Ma belt-feed x-ray machine operating at 1 min, 45 seconds to 3 min and 18 sec. exposure, depending on sediment density, using conventional high-density x-ray film;
- 2) by myself and Janice Baker of the Sidney X-ray Clinic, Sidney, B.C., using a 50 kV, 50 Ma, 40 inch table top x-ray machine operating at 1/5 second exposure and Kodak min-R 2000 single screen mammography film.

The freeze cores were x-rayed intact, in group one.

RADIOCARBON DATING

Suitable organic material for radiocarbon dating was somewhat scarce in the Effingham Inlet and Barkley Sound cores. During core description, however, intact

bivalve shells, an intact fish skeleton preserved on the bedding plane and twigs and sticks were recovered from the cores for conventional and Accelerator Mass Spectrometry (AMS) radiocarbon dating. Material for dating was selected from throughout the cores, in both laminated and massive intervals, and one contemporaneous shell and stick pair were found for dating in the outer basin core TUL99B11, at 939 and 898 cm respectively.

An effort was made to only collect that material which was in-situ and away from the edge of the core barrel to minimize the likelihood that the material had been either picked up from the water column, and/or dragged down the edge of the core barrel during coring, a real possibility due to the wetness of the sediments. Intact shell pairs were recovered where possible to minimize the possibility that the shell had been transported after the organism had died.

A total of 6 radiocarbon dates from the outer basin and 19 radiocarbon dates from the inner basin were calculated by Dr. Ralph Beukens of the Isotracc radiocarbon dating facility at the University of Toronto. Of the inner basin samples, 15 were wood, 4 were intact shell valve pairs and one was an intact fish skeleton. Of the outer basin samples, 2 were wood and 4 were shell (Table 2).

Results are reported in radiocarbon years before present (radiocarbon years BP) and also as calibrated calendar years (cal yBP) using, Dr. R Beukens' own C14Cal program, along with the INTCAL98 dendrochronological database for terrestrial

material, and the MARINE98 reported database for marine material (Stuiver et al., 1998a and b). This calibration program is based on the CALIB and CAL programs of Stuiver and Reimer (1986 and 1993) and Stuiver et al. (1998a and b), widely available for downloading at the internet site <http://depts.washington.edu/qil/calib/manual/>. Dr. Beuken's program, which was used to calculate calendric ages for our samples is identical to the CALIB and CAL programs but has a more accurate treatment of peak overlaps and accompanying errors on calibrations on overlap solutions (R. Beukens pers. commun.). Complete results of the Isotrace radiocarbon dating are contained in Appendix B.

GRAIN-SIZE AND ROCK-EVAL ANALYSIS

Samples for grain-size analyses were taken every ten centimeters from the working half of the inner basin core TUL99B13 and the outer basin core TUL99B11, and analyzed at the Terrain Sciences Division of GSC in Ottawa. Rock-Eval analyses of samples taken every 10 cm along the length of the 1997 cores was performed at the University of Calgary by Dr. Lloyd Snowdon.

FISH SCALES

Sediments for fish scales analysis were sampled in 5 cm pieces from all visibly well-laminated intervals, of the working and archive half of core TUL99B03 (width 10 cm). Each 5 cm sample represents about 21 years of deposition calculated from average laminae counts from core x-rays. A total of 95 samples were obtained, averaging 392

cm³ in volume. Sampling from massive intervals was avoided to insure that any fish remains found were deposited in-situ and not transported from elsewhere, and that the scales and bones found had not been subjected to winnowing or sorting after deposition. Presence of whole, intact gill rakers, which are very fragile bones, in many of the samples from laminated intervals indicated that the fish bones did not undergo any significant amount of mechanical abrasion. Sediments were kept cool at the Institute of Ocean Sciences in Sidney, B.C and the sampling for fish scales work took place 6 months after core recovery.

The following subsequent fish scales laboratory work was performed by Cindy Wright of the Department of Fisheries and Oceans. Sediment samples were gently washed immediately after sampling, through a 250 µm sieve and the residue was stored in alcohol for later observation with a binocular microscope at 100 X power. The residues were picked and counted for total fish scales, and then scales were identified to the species level. Bone fragments with an intact process were also counted, but not identified. The presence or absence of charcoal, ostracods, gastropods, foraminifera, fibre, shell, conifer, sponge and insect fragments were also noted for each sample. The complete results are reported in Appendix J.

Care was taken to insure that scales were counted only once and that the counted scale represented an intact or partially intact scale and not multiple fragments of a single scale. This

was accomplished by counting only those scales that were either 50 % intact, or had an intact scale focus point

Few identification keys or descriptions exist for the identification of fish scales and bone. Most of the identifications for this project were made in comparison to a collection of fish scales begun by the University of British Columbia's Department of Anthropology's Bone Lab, which was kindly made available to this project.

Figure 21. Photograph of piston core laboratory work.



RESULTS

PHYSIOGRAPHY OF EFFINGHAM INLET

SEISMIC PROFILE

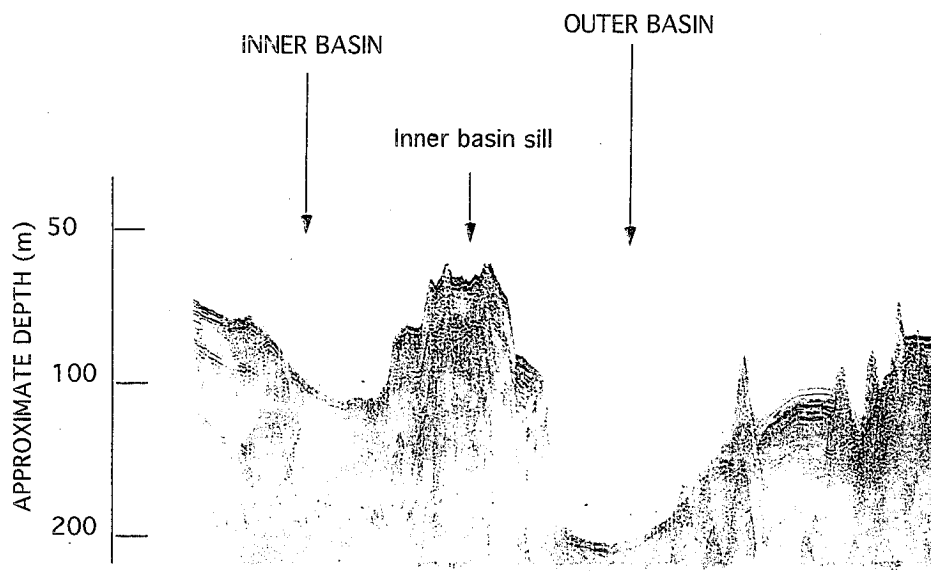
A 3.5 kHz airgun seismic traverse of Effingham Inlet from Barkley Sound to the inner basin (Figure 22) shows the bathymetry of the inlet and clearly indicates how the location of the sills restricts oceanic water masses from entering the inner basin. The floor of the inlet is well draped with sediment, and the brightening and shadowing effect of the sediment beds is probably evidence of gas content in the sediments (K. Conway, pers. commun.). Gas bubbles in the upper piston core sections on recovery are also evidence of high gas content in the sediments.

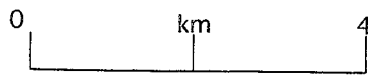
Sediments appear to drape undisturbed along the inlet floor. However, upon close examination, the sediments of the deepest parts of the basins appear to slump slightly in a step-like manner towards the center of the basins. This effect is less pronounced in the outer basin. This probably means that slumping and creeping of the sediment package has occurred in both basins, and possibly even overturning of sediments nearest the steepest basin slopes, which is faintly discernable at the north side of the outer basin.

DRAINAGE BASIN

A schematic figure derived from topographic maps, shows the Effingham Inlet drainage basin, with the drainage divide connecting points of highest elevation

Figure 22. Seismic profile of Effingham Inlet from 3.5 kHz airgun seismic traverse, vertical exaggeration about 50 X).





OUTER BASIN



Outer basin sill



BARKLEY SOUND

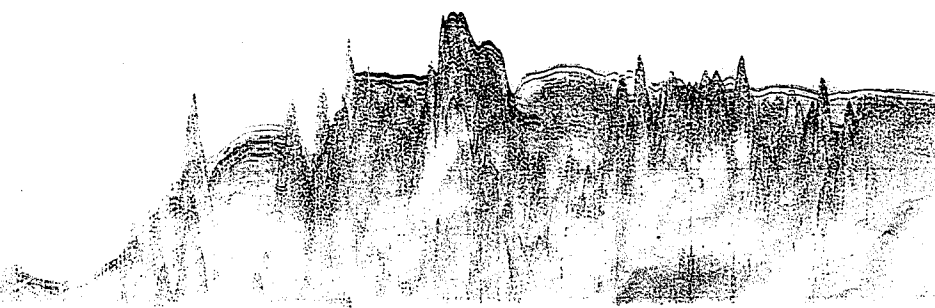
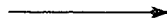
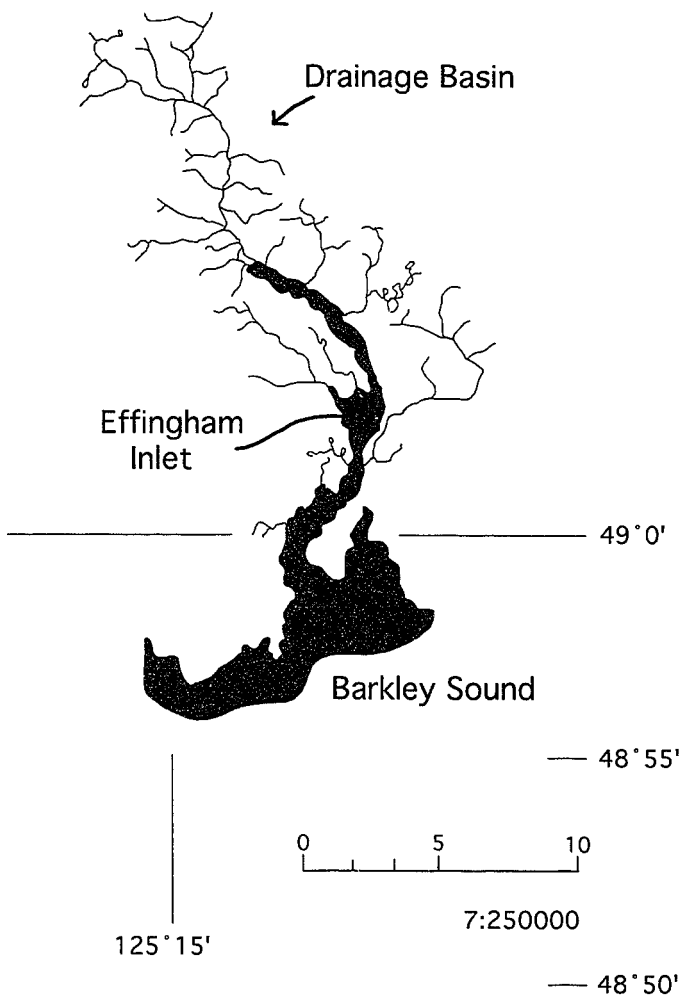
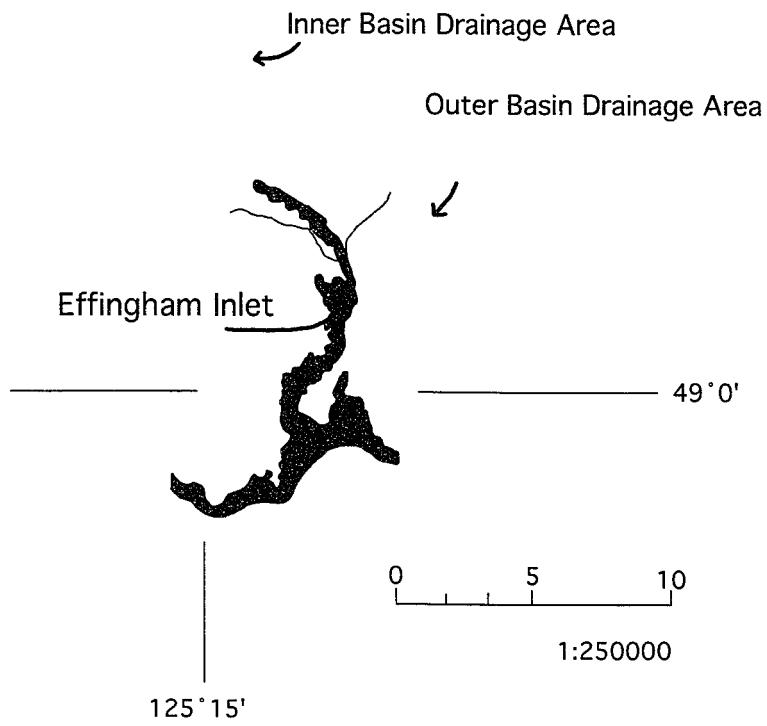


Figure 23 a. Effingham Inlet drainage basin.



Effingham Inlet Drainage Basin

Figure 23b. Inner and outer drainage basin areas of Effingham Inlet.



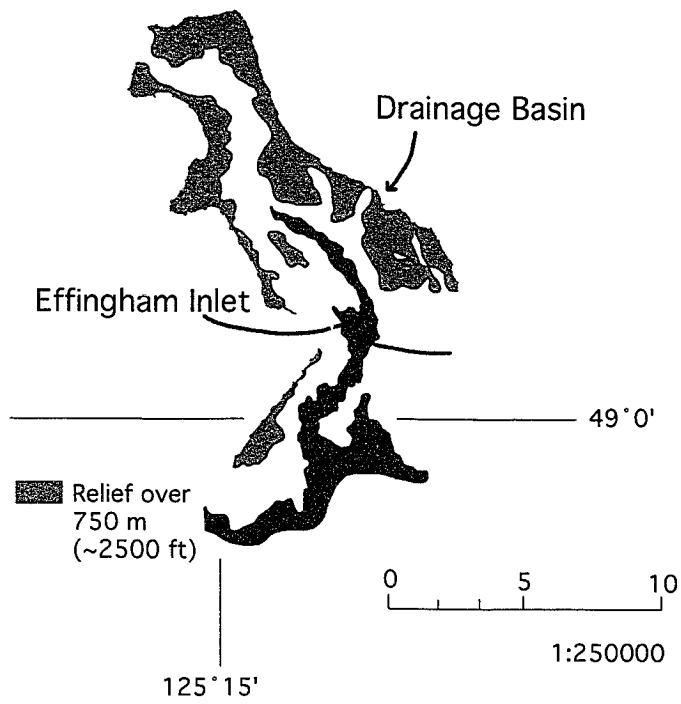
Inner and Outer Basins at Effingham Inlet: drainage basin areas

surrounding the inlet (Figure 23a). The drainage basin of the inner basin, is about 52 km² and the drainage basin of the outer basin is about 27 km² (Figure 23b) giving a total drainage area to Effingham Inlet of about 79 km².

Run-off enters the inlet through the small Effingham River at the head of the inner basin, a small un-named stream in the inner basin, and through two un-named streams on either side of the outer basin. Most of the inner basin drainage area is comprised of mountainous relief over 750 m, giving a steep stream gradient, and hence high erosive power to the tributaries of the Effingham River (Figure 23c). An aerial photograph from July, 1976, of Effingham Inlet and the inner basin drainage area (Figure 24) clearly shows the mountainous terrain drained by the Effingham River, which is a braided stream in its upper reaches, and in comparison, the much smaller and less well developed drainage systems of streams entering the outer basin. In the river valley floor directly to the north of Effingham Inlet, where the stream gradient of the Effingham River is low, the river meanders across a small flood plain where the coarsest sediment is deposited, and the river finally terminates in a small marshy delta at the head of the inlet.

The two smaller streams entering the outer basin have less developed drainage systems and also terminate in small deltas colonized by tidal marsh vegetation (Figures 12 and 24). An examination of aerial photographs of the inlet from the 1930's, before logging of the inlet shores occurred, indicates that the small delta on the eastern side of the inner basin has expanded somewhat. This is perhaps due to the more recent logging

Figure 23c. Relief within the Effingham Inlet drainage basin.



Relief within Effingham Inlet
Drainage Basin

Figure 24. Aerial photograph of Effingham Inlet and the upper reaches of the drainage basin of the Effingham River, July, 1976. Note the glacial cirques and arêtes in the mountains to the west of the inlets, and the snow cover persisting well into the summer season.

© SA MAJESTE LA REINE DU CHEF DU CA © SA MAJESTE LA REINE DU CHEF DU CANADA, MINIST



209

A24503 - 199

A24503 - 200

© HER MAJESTY THE QUEEN IN RIGHT OF © HER MAJESTY THE QUEEN IN RIGHT OF CANADA,

MAJESTE LA REINE DU CHEF DU CANADA, MINISTERE DE L'ENERGIE, DES MINES ET DES RESSOURCES. T



24503 — 200

HER MAJESTY THE QUEEN IN RIGHT OF CANADA, DEPARTMENT OF ENERGY, MINES AND RESOURCES. T

activity in the upper reaches of its drainage basin, which is evident in the aerial photographs of July, 1976 as white patches on the forested slopes surrounding the inlet. During the cruise to the inlet of October, 1999, heavy rainfall occurred and almost immediately after the rain began, it was observed that waterfalls appeared on all sides of the inlet and rainwater cascaded into the inlet in a chaotic fashion from all directions, directly from the slopes surrounding the inlet (Figure 25). This continued for some hours after the rain ceased, when the surface of the inlet remained covered with pieces of bark, twigs and soil. Clearly, sediment and fresh rainwater enter the inlet not only from the established drainage courses, but also directly from the steep, soil-poor shores of the inlet itself.

SEDIMENTOLOGY

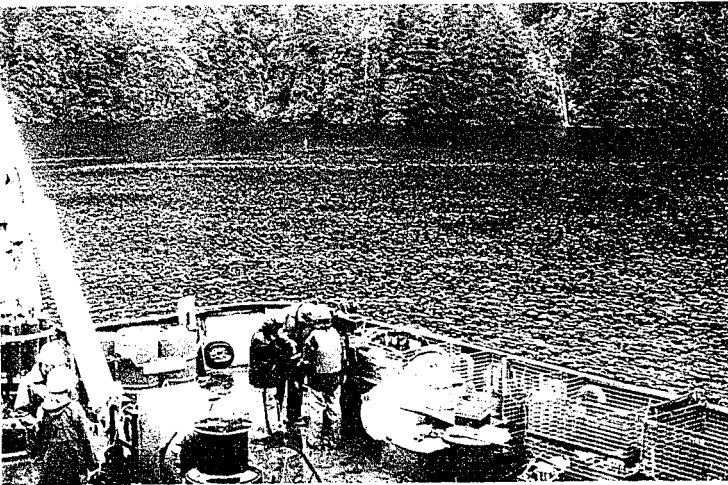
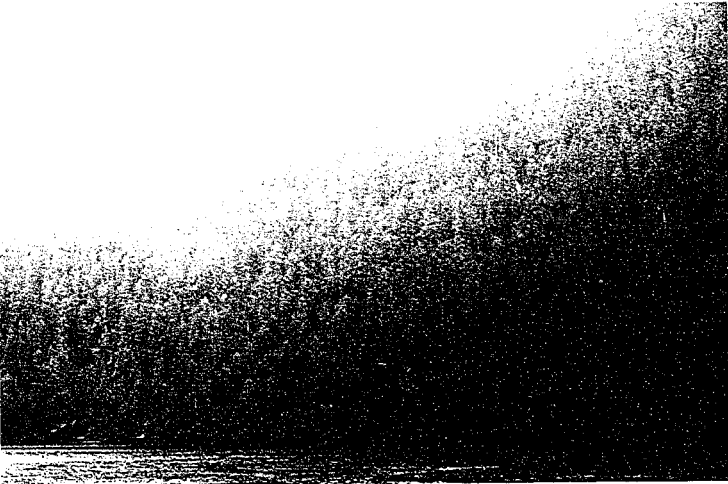
GENERAL

Inner and outer basin cores

The sediments of the inner and outer basins of Effingham Inlet are comprised of the following.

- 1) Laminated sediments, which consist of alternating laminae of, olive to dark olive grey diatomaceous (M. Hay, pers. commun.) mud laminae and dark olive grey to black mud and silt laminae (Figure 2). Laminae thickness is highly variable, especially within the diatomaceous laminae and ranges from 1 mm to 1.5 cm. Sections of laminated muds are not commonly greater than 20 cm in length.

Figure 25. Photographs of the shores of Effingham Inlet in heavy rain, October, 1999. In the top photograph, notice flashes of white on the heavily treed slopes, which are cascades of water entering the inlet in waterfalls such as the one in the lower photograph.

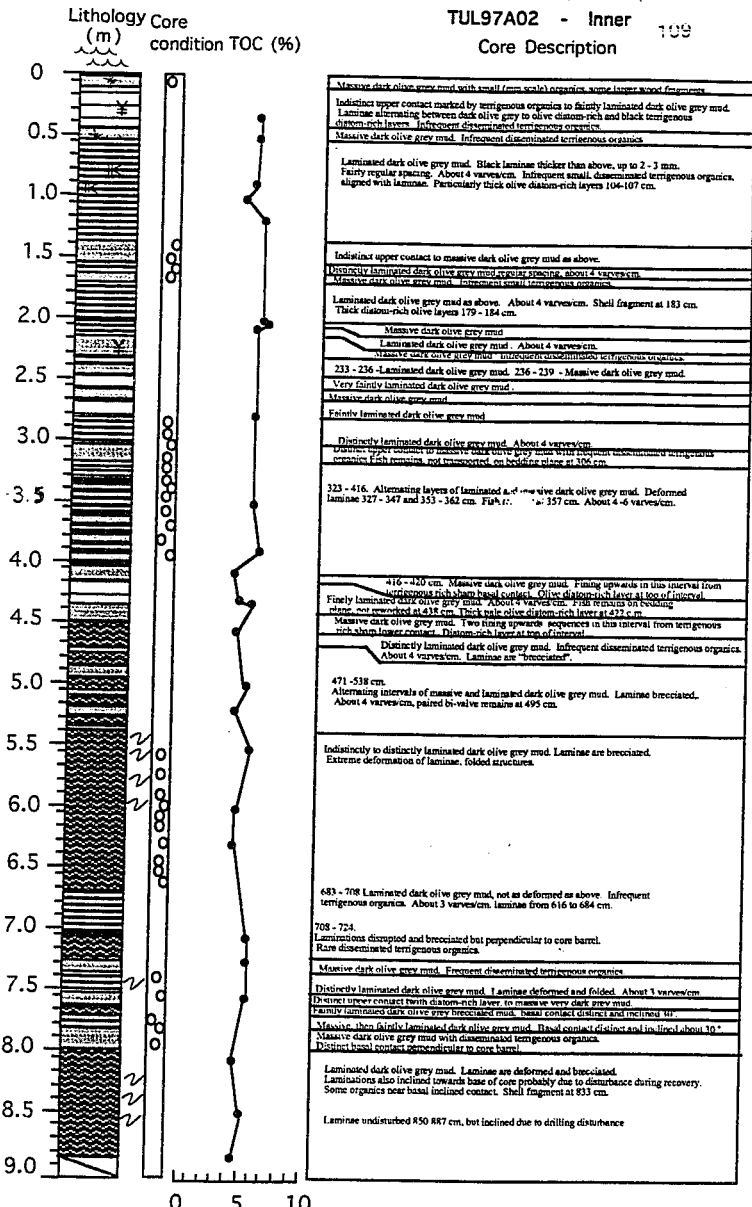


- 2) Massive muds and silts are intercalated within the laminated sediments at irregular intervals, dark olive grey to black in color. To the eye, many of these massive beds have no structure but under x-radiography some appear to have a very subtle fining upwards grading defined by either grain size or small terrigenous organic fragments of what appears to be humus-like material. Terrigenous organic fragments can also consist of small pieces of twigs and bark up to several centimeters in length. These beds are commonly less than 10 cm in thickness.
- 3) Graded muds and silts, dark olive grey to black in color, with sharp basal contacts, intercalated within the laminated sediments at irregular intervals. Fining upwards from a fine to coarse sand, and occasionally shell fragments and gravel, at the base is defined by grain size, and also by fine terrigenous organic fragments. These beds commonly exhibit a light grey mud bed of 1 to 2 cm in thickness near or at the top of the bed. These beds are commonly less than 10 cm in length
- 4) Rare sand beds of several centimeters thickness are the coarsest sediments found in the cores of the inner and outer basin.

In the inner basin cores, the laminated beds are more numerous and well defined, and terrigenous fragments are common. Ungraded massive beds are more common in the outer basin core. All sediments are wet and unconsolidated in the top 2 sections of the piston cores. The inner basin cores also contain deformed wavy varves, and "brecciated" varves where the laminae have been broken and disturbed on a

Figure 26. Photographs and core description for inner basin core TUL97A02.

TUL97A02 - Inner
Core Description 109



- Legend**
- Organic fragments
 - Massive mud
 - Laminated mud
 - Faintly laminated mud
 - Brecciated laminae
 - Folded laminae
 - Gas disturbance

Core description by Audrey Dalimore, Ottawa-Carleton Geoscience Centre, 06/99, after collection, field descriptions and archiving by Kim Conway, Pacific Geoscience Centre and Richard Thomson, Institute of Ocean Sciences, 03/97.

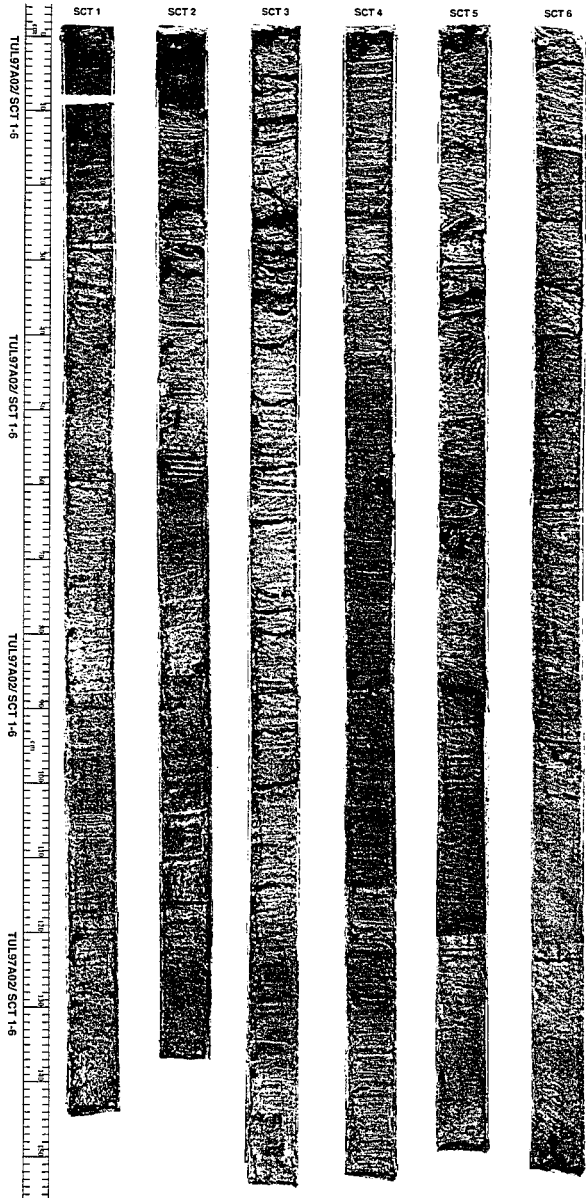
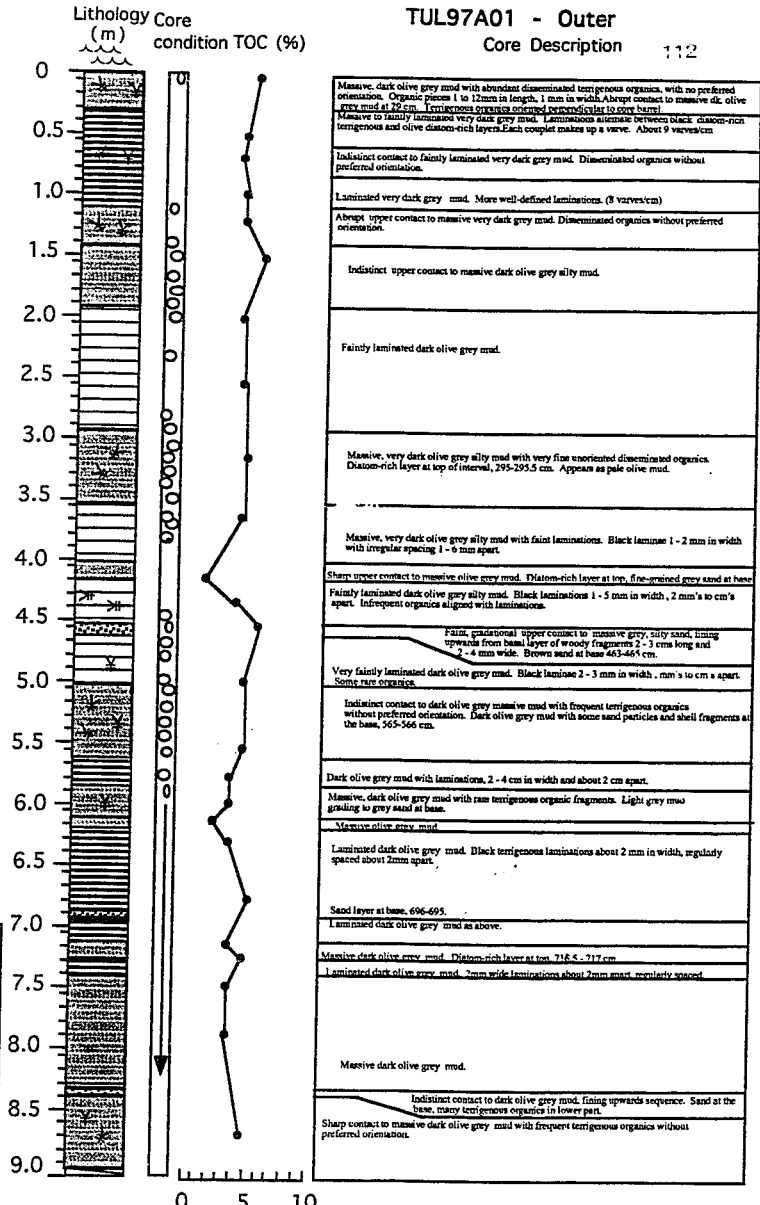


Figure 27. Photographs and description of outer basin core TUL97A01.

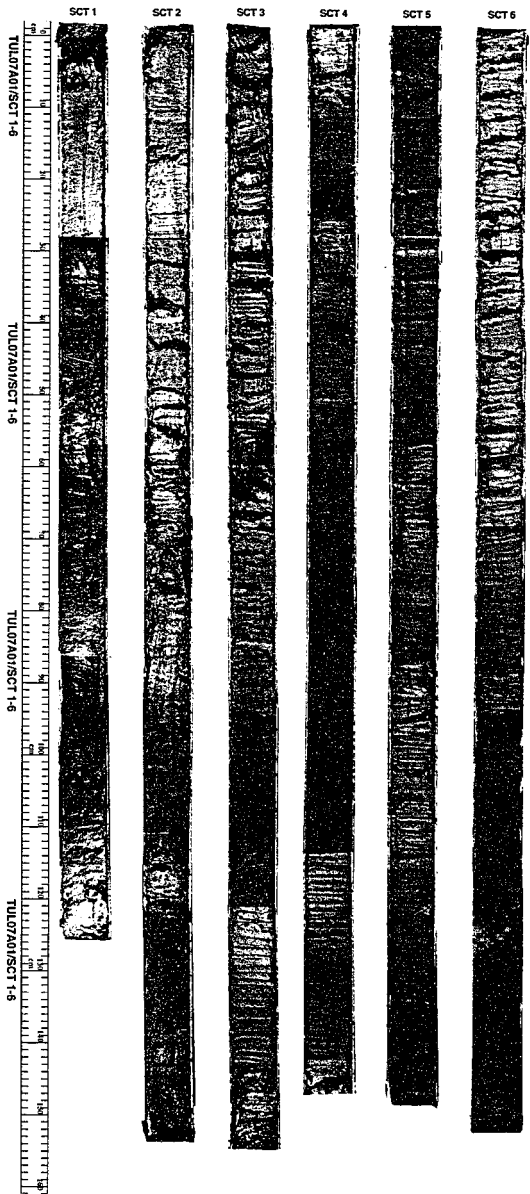
TUL97A01 - Outer
Core Description 112



- Legend**
- ☒ Organic fragments
 - ▒ Massive mud
 - ▒ Laminated mud
 - ▒ Faintly laminated mud
 - ▒ Sand
 - Gas disturbance

0.0 - 0.5	Massive, dark olive grey mud with abundant disseminated terrigenous organics, with no preferred orientation. Organic pieces 1 to 12mm in length, 1 mm in width. Abrupt contact to massive dk. olive grey mud at 49 cm. Terrigenous organics oriented perpendicular to core barrel.
0.5 - 1.0	Massive to faintly laminated very dark grey mud. Laminations alternate between black chaoon-rich terrigenous and olive chaoon-rich layers. Each couplet makes up a wave. About 9 waves/cm.
1.0 - 1.5	Indistinct contact to faintly laminated very dark grey mud. Disseminated organics without preferred orientation.
1.5 - 2.0	Laminated very dark grey mud. More well-defined laminations. (8 waves/cm)
2.0 - 2.5	Abrupt upper contact to massive very dark grey mud. Disseminated organics without preferred orientation.
2.5 - 3.0	Indistinct upper contact to massive dark olive grey silty mud.
3.0 - 3.5	Faintly laminated dark olive grey mud.
3.5 - 4.0	Massive, very dark olive grey silty mud with very fine unoriented disseminated organics. Chaoon-rich layer at top of interval, 295-295.5 cm. Appear as pale olive mud.
4.0 - 4.5	Massive, very dark olive grey silty mud with faint laminations. Black laminae 1 - 2 mm in width with irregular spacing 1 - 6 mm apart.
4.5 - 5.0	Sharp upper contact to massive olive grey mud. Diatom-rich layer at top, fine-grained grey sand at base. Faintly laminated dark olive grey silty mud. Black laminations 1 - 5 mm in width, 2 mm's to cm's apart. Infrequent organics aligned with laminations.
5.0 - 5.5	Faint, gradational upper contact to massive grey, silty sand, lining upwards from basal layer of woody fragments 2 - 3 cm long and 2 - 4 mm wide. Brown sand at base 463-465 cm.
5.5 - 6.0	Very faintly laminated dark olive grey mud. Black laminae 2 - 3 mm in width, .mm's to cm's apart. Some rare organics.
6.0 - 6.5	Indistinct contact to dark olive grey massive mud with frequent terrigenous organics without preferred orientation. Dark olive grey mud with some sand particles and shell fragments at the base, 565-566 cm.
6.5 - 7.0	Dark olive grey mud with laminations, 2 - 4 cm in width and about 2 cm apart.
7.0 - 7.5	Massive, dark olive grey mud with rare terrigenous organic fragments. Light grey mud grading to grey sand at base. Massive olive grey mud.
7.5 - 8.0	Laminated dark olive grey mud. Black terrigenous laminations about 2 mm in width, irregularly spaced about 2mm apart.
8.0 - 8.5	Sand layer at base, 696-695. Laminated dark olive grey mud as above.
8.5 - 9.0	Massive dark olive grey mud. Diatom-rich layer at top 716 & 717 cm. Laminated dark olive grey mud, 2mm wide laminations about 2mm apart, regularly spaced. Massive dark olive grey mud. Indistinct contact to dark olive grey mud, fining upwards sequence. Sand at the base, many terrigenous organics in lower part. Sharp contact to massive dark olive grey mud with frequent terrigenous organics without preferred orientation.

Core description by Audrey Dallimore, Ottawa-Carleton Geoscience Centre, 06/99, after collection, field descriptions and archiving by Kim Conway, Pacific Geoscience Centre and Richard Thomson, Institute of Ocean Sciences, 03/97.



millimeter and centimeter scale (Figure 26, section 5 and 6) (Blais Stevens et al., 1997).

Photographs of an inner basin (TUL97A02), and an outer basin core (TUL97A01) along with core descriptions are shown in Figures 26 and 27. The photographed piston cores were all retrieved during the 1997 cruise and 2 years of drying before core logging allows their features to be more visible under conventional photography. Breaks in these cores are due to drying and are not present in the 1999 piston cores.

Photographs, x-radiographs and descriptions of the 1999 piston cores are found in Appendices C to G.

Barkley Sound Core

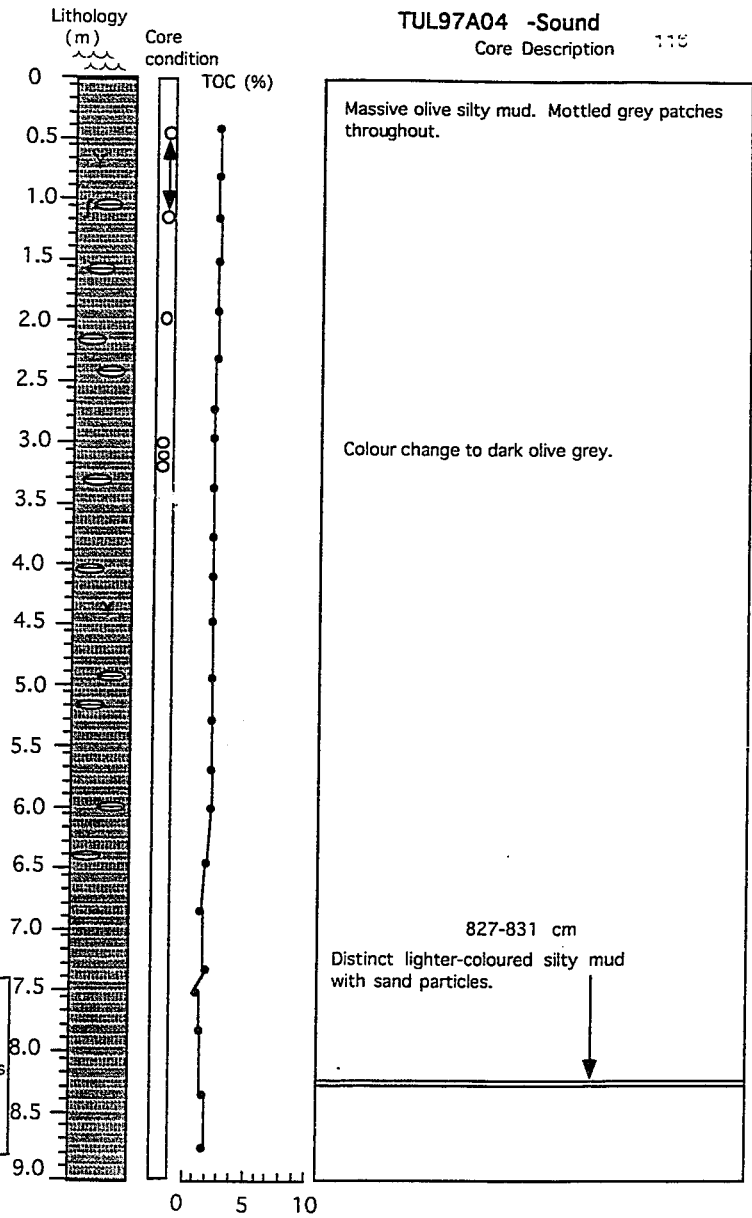
Sediments of the Barkley Sound core are comprised of a uniform, well-compacted and featureless olive to dark olive grey silt (Figure 28). The only change in lithology in this core is a 4 cm thick coarse sand bed, which contains many shell fragments, at 827 cm (Figure 29).

Freeze cores

Sediments of all the inner basin freeze cores consist of 18 to 30 cm of well defined laminated sediments, exhibiting thick (~ 1 – 1.5. cm) varves, above an olive grey to black massive mud bed containing large terrigenous organic pieces and fragments (Figure 30). The outer basin freeze core TUL99B10 has this same

Figure 28. Photographs and description of Barkley Sound core TUL97A04.

TUL97A04 -Sound
Core Description 115



TUL97A04/SCT 1-6
TUL97A04/SCT 1-6
TUL97A04/SCT 1-6



SCT 1



SCT 2



SCT 3



SCT 4

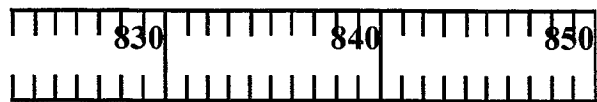


SCT 5



SCT 6

Figure 29. Photograph of sand and shell bed in the Barkley Sound core.



TUL97A04/SCT6 (823-850 cm)

Figure 30. Photograph of freeze core TUL99B04, photographed on deck immediately after recovery. Note the well defined laminations in the top of the core underlain by a massive mud interval. Lens cap for scale.

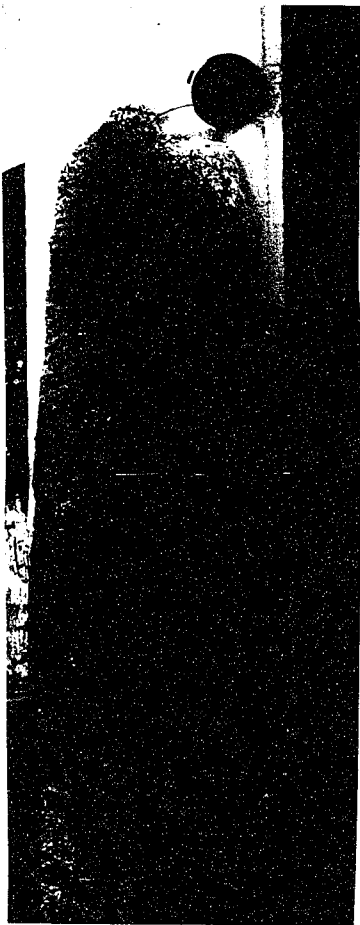


Figure 31a. Rock-Eval plot for inner basin core TUL97A02.

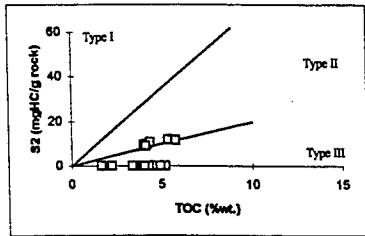
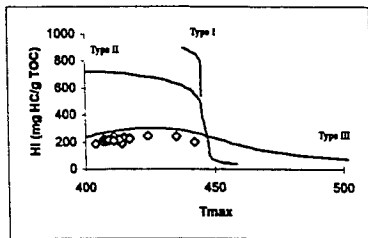
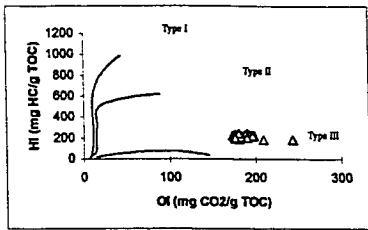


Figure 31b. Rock-Eval plot of outer basin core TUL97A01.

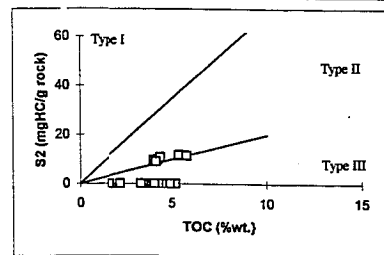
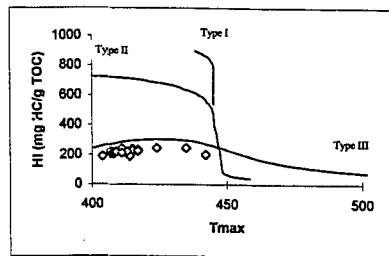
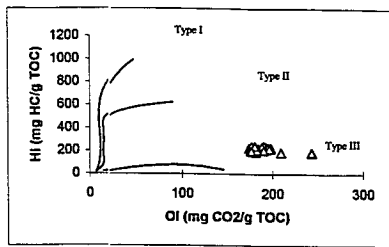
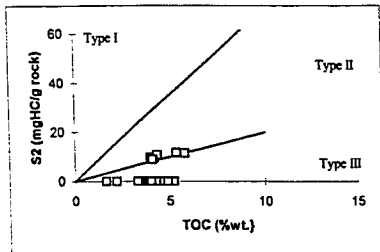
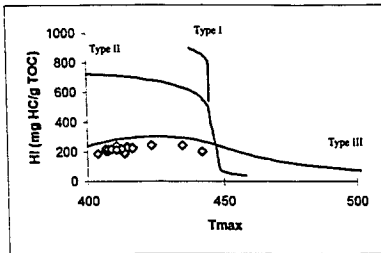
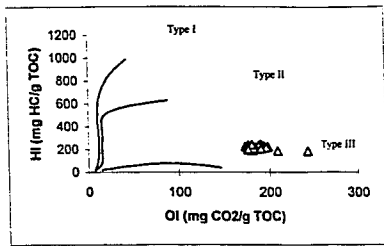


Figure 31c. Rock-Eval plot of Barkley Sound core TUL97A04.



lithology while the other outer basin freeze core TUL99B12 contains no laminated sediments and only the massive mud bed (Appendix H, pocket attachment).

ROCK-EVAL AND GRAIN SIZE ANALYSES

Rock-Eval

The total organic carbon (TOC) contents of the 1997 core sediments, were part of the Rock-Eval analyses and are shown graphically in Figures 27, 28 and 29, and are also contained in Appendix I. The average TOC content of the sediments is about 5 %, with slightly higher TOC in the inner basin and decreasing oceanwards towards Barkley Sound.

Rock-Eval analyses of the 1997 cores, when plotted (Figure 31), falls within Type III organic matter origin which means that the organic matter present in all cores is :

- 1) fresh and immature (i.e. not thermally altered),
- 2) terrestrially derived and therefore has a very low Hydrogen Index and a very high Oxygen Index value, in comparison with published results for dysoxic/anoxic Holocene lake sediments (Medioli, in press), as well as Cretaceous shallow anoxic marine sediments. (Medioli,1998).

Rock-Eval analysis is not usually performed on unconsolidated Holocene sediments (Espitalié et al., 1977; Macauley et al., 1995; Peters et al., 1996) so a complete analysis of this data is somewhat speculative (L. Snowdon, pers. commun).

However, the results do show that

Figure 32. Ternary diagram of grain size analyses for inner basin core TUL99B13 and outer basin core TUL99B11.

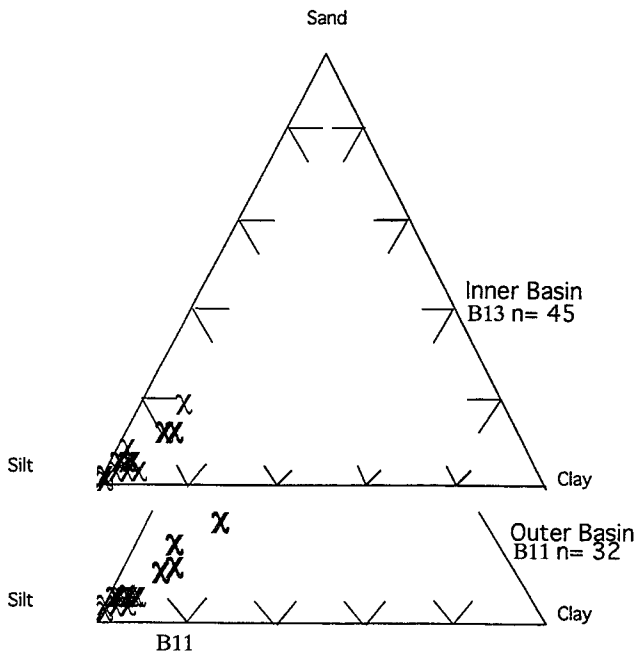
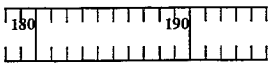
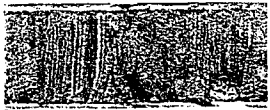
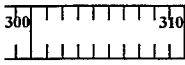


Figure 33. Details from core photographs of inner basin core TUL97A02.

- a) Well laminated sediments.
- b) Fish skeleton on the bedding plane.
- c) Brecciated laminated mud.
- d) Laminated interval with small massive units intercalated between laminated sections.
- e) Disturbed and brecciated laminated mud.
- f) Overturned laminations.
- g) Massive interval intercalated within laminated sediments with characteristic light grey mud at the top.



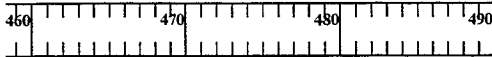
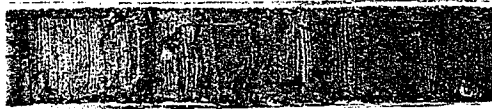
TUL97A02/SCT-2 (178-195 cm)



TUL97A02/SCT3 (300-310 cm)



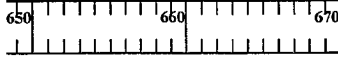
TUL97A02/SCT3 (338-350 cm)



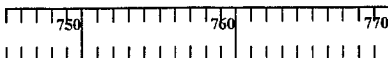
TUL97A02/SCT-4 (460-490 cm)



TUL97A02/SCT5 (605-620 cm)



TUL97A02/SCT-5 (650-670 cm)



TUL97A02/SCT-6 (745-770 cm)

the organic matter within the Effingham Inlet sediments is strongly terrigenous as opposed to marine or algal in origin, despite the high diatom content of the varves.

Grain size analysis

Grain size analyses of an inner basin core (TUL99B13) and an outer basin core (TUL99B11) show that all sediments fall within the silt particle size range with only a few samples containing some very fine sand. Outer basin sediments are very marginally coarser, with more samples falling within a very fine sand range (Figure 32, Appendix I).

SEDIMENTARY FEATURES

Sedimentary features are well preserved in the inner basin cores, particularly in sections 4 and below where sediments are drier (Figure 33a). Laminae within laminated intervals are highly variable in thickness, and laminated sections are rarely greater than 20 cm in length, before being interrupted by a massive or graded mud interval (Figure 33 c and h). In sections 7 and 8 of the inner basin cores, laminations can appear disturbed and are smeared, brecciated, folded and overturned (Figure 33c).

Graded massive intervals commonly have a sharp basal contact and are sometimes capped by a thin (~1 cm) bed of light grey mud (Figure 33 h). A distinct 2-4 cm sand, gravel and shell fragment bed is found in all the inner basin cores except for TUL97A02.

Intact fish skeletons are not uncommon on bedding planes in the inner and outer basin cores (Figure 33c). Large (1-10 cm) pieces of wood, intact and fragmented

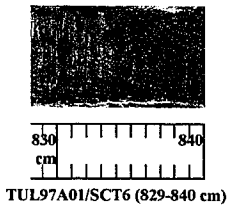
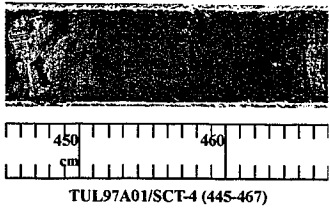
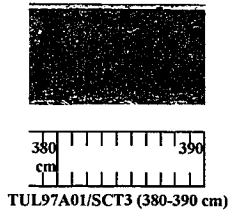
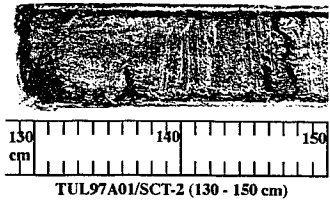
Figure 34 . Photographs of details from the outer basin core TUL99B01.

- a) Massive and poorly laminated sediments.

- b) Massive and poorly laminated sediments.

- c) Sand and shell bed.

- d) Sand and shell bed.



bivalve shells, stones and in one case a piece of tree stump colonized by barnacles (Appendix C, B06S7C, 962 cm), are also commonly found in the inner basin cores, in both laminated, massive and graded intervals.

Sedimentary details in the outer basin core are less visible to the eye, with most laminated intervals very faintly laminated (Figure 34 a,b). Two distinct sand, gravel and shell fragment beds, 3 – 4cm thick appear in each of the outer basin cores at (Figure 34 c,d).

X-RADIOGRAPHY

The x-rays taken of the sediment slabbed with the “cookie cutter” tool, of the inner basin core TUL99B03 and the outer basin core TUL99B11, are very useful in discerning sedimentary features not visible by eye in the piston core sediments.

Again, x-rays show that sedimentary features are more numerous and well defined in the inner basin core than the outer basin core.

Laminated sediments

A section of very well laminated sediments from the inner basin core TUL99B03, from 894-914 cm, is shown in Figure 35. The undisturbed, well preserved annual laminae indicate anoxic bottom water conditions during the deposition of the sediments in this slab since they are undisturbed by bioturbation. Note the distinct alternating laminations of light colored diatom layers with the darker terrigenous-rich layers in the bottom two-thirds of the slab. At 906 and 907.5 cm, the diatom layers are darker, and

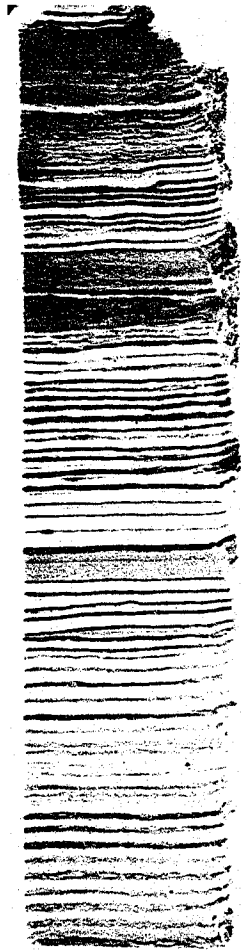
these represent a different diatom species than in the lighter colored diatom laminae (A. Chang and M. Hay, pers. commun.). Another obvious feature of this slab is the variability in thickness of the diatom laminae, which represents changes in the primary productivity from year to year (Sancetta, 1996).

The bottom half of the slab represents about 33 years of deposition during which winter rainfall was about the same in each year. Conditions conducive to bringing nutrient-rich waters to the surface of the ocean just offshore Effingham Inlet remained constant, promoting a yearly diatom bloom in spring and summer.

The top third of the slab however represents a more complex period of annual conditions in the inlet. Between 894 and 901 cm, the light colored diatomaceous laminae are obscured by the darker colored terrigenous-rich laminae. This probably represents a period of high rainfall and oceanic conditions not conducive to the annual diatom bloom (Sancetta, 1996). The number of years represented by these terrigenous-rich laminae sections, is about 10 years of deposition per cm, compared to about 4 to 5 years per cm in the lower two thirds of the slab. Not all sections of laminated sediments are as well preserved as those in Figure 35 however, which come from section 8 of inner basin core TUL99B03. More poorly defined laminations, probably due to wetness of the sediments higher in the piston core, are more typical of the whole sediment column in the inner basin. An example of poorly laminated, wet sediments from section 1 of TUL99B03 is illustrated in the x-ray of Figure 36.

Figure 35. X-ray of well laminated sediments from section 8 of inner basin core
TUL99B03.

Interval III
894-914 cm



Typical well laminated
interval III sediments.

Differing diatom
species

Figure 36. X-ray of poorly laminated sediments from section 1 of inner basin core

TUL99B03.

Interval I
104-124 cm



Typical poorly defined laminations

Figure 37. X-ray of transitions from anoxic to oxic conditions.

Interval I
164-177 cm



Oxic conditions

Transition

Anoxic conditions

Sharp basal contact,
fining upwards massive
interval

Graded and ungraded massive beds

Two general types of unlaminated sediments are found in the Effingham Inlet cores (Figure 37).

- 1) A graded mud deposit with sand grains at the base, which appear black on the x-ray, with a sharp basal contact and fining upwards defined by grain size, in the bottom half of the slab. This deposit lies above well laminated sediments indicating anoxic conditions, and at the top of the deposit, a rapid return to anoxic conditions is indicated by the sharp contact with laminated sediments above. The sharp basal and top contacts infer that this deposit was emplaced instantaneously, with possible erosion of existing underlying laminated sediments occurring (Blais-Stevens et al., 2001).

An ungraded massive mud deposit lies above the graded deposit in the top half of the slab, with conspicuously absent grading. On close observation, the laminated sediments at the base become more and more indistinct until the laminations disappear altogether. Bioturbation tracks are not clearly evident, however, this ungraded deposit in a normally anoxic environment, is interpreted to mean a transition to dysoxic and/or oxygenated conditions (Blais Stevens et al, 2001). If this interpretation is correct, and previously deposited laminated sediments have been destroyed by bioturbating benthos organisms which have established themselves in

dysoxic or oxic conditions, it is not immediately possible to interpret how many years of deposition this interval represents.

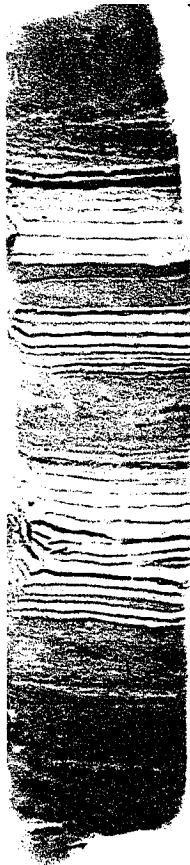
Depositional variability

Another slab from section 4 of inner basin core TUL99B03, shows the typical variability of depositional conditions found in the inner basin piston cores (Figure 38). Well defined laminated sediments in this slab, which were deposited under anoxic conditions, are interrupted by numerous periods of oxic and/or dysoxic conditions and also periods of high rainfall, which alone or in combination, destroy or obscure the annual diatom bloom, if and when it occurs.

A particularly interesting variability in depositional conditions occurs from 475 cm to the top of the slab. For 6 years, very thick (~ 0.5 cm) diatom laminae represent a healthy spring and summer phytoplankton bloom in the inlet, followed by fall and winter conditions of very low rainfall, as exhibited by the thin (< 1 mm) terrigenous-rich dark colored laminae. Immediately following these years however, is a very heavy rainfall year, represented by a particularly thick (2 mm) terrigenous-rich laminae. This is followed by a number of years of high rainfall and low primary productivity represented by thick and numerous terrigenous-rich laminae and thin or absent diatomaceous laminae. Finally at about 471 cm at the top of the slab, the laminations are obscured by possible bioturbation under oxic conditions. This sediment sequence clearly indicates the high

Figure 38. X-rays of transitions from oxic to dysoxic to anoxic conditions from inner basin core TUL99B03.

Interval II
469-489 cm



Transition to oxic conditions

Biorturbation ?

Anoxic

Oxic

Dysoxic/ high rainfall

Anoxic

Dysoxic/ high rainfall

variability in ocean and climate conditions in Effingham Inlet over the short span of a decade.

Bioturbation

The evidence for the existence of bioturbation in the Effingham Inlet piston cores is very weak, however, poorly defined bioturbation tracks can occasionally be deciphered in ungraded massive units of the inner basin core, on the X-ray negatives, if viewed with strong backlighting. An example of these faint tracks are shown in Figure 38 at about 471 to 472 cm, and in Figure 39, at about 255-257 cm. (Please note that the dark dots throughout the slab in Figure 39 are contained in the Clingwrap covering of the slab and are not features within the sediments). However, these possible bioturbation tracks are quite difficult to see on a hard copy print of the x-ray. Note the lengthy ungraded mud interval, greater than 10 cm, in Figure 39, which is interpreted as representing oxic and/or dysoxic conditions of the bottom waters.

Sand and shell bed

A distinctive sand, gravel and shell deposit is found at about mid-core in all the inner, outer basin and Barkley Sound piston cores and is shown on x-ray in Figure 40. Coarse and fragmented shell material is in black while white fragments in the coarse interval are terrigenous organic fragments such as tree bark pieces and twigs. Numerous shell fragments were observed in this deposit in the piston core sediments themselves. Of note are the sharp basal contact and the 8 cm massive interval above the sandy base, with

Figure 39. X-ray of bioturbation tracks in massive mud from inner basin core

TUL99B03.

Interval I
245-265 cm



Transition from anoxic
to oxic conditions, with
poorly defined bioturbation
tracks.

Figure 40. X-ray of sand and shell bed from inner basin core TUL99B03.

interval II
345-365 cm



Poorly defined laminations

Typical interval II
variability

Fining upward massive
interval

Sharp basal contact

Sand and gravel

Indistinct transition
to oxic conditions

laminations slowly re-developing in the top of the slab. The ungraded mud just beneath the sandy layer may also be associated with this depositional event, as it appears that the laminations at about 385 cm may have been eroded and slightly disturbed by the ungraded mud above.

Large ungraded massive interval

Two very large (>50 cm) massive mud intervals exhibiting a chaotic fabric of sand, mud, gravel and large (2-5 cm) terrigenous organics, are contained in the Effingham Inlet piston and freeze cores.

- 1) At the base of the inner basin piston cores, for example, 920-970 cm in section 7 of inner basin core TUL99B03 (Appendix F), shown in the x-ray of Figure 41.
- 2) In all of the freeze cores, with the exception of TUL99B12 of the outer basin, beneath an uninterrupted well laminated interval from the sediment-water interface, to the massive deposit. An x-ray of this deposit in freeze core TUL99B04 is shown in the pocket attachment and described for all freeze cores in Appendix H.

Note the similarity in size and fabric of these two large massive intervals. The white fragments on these x-rays are pieces of terrigenous organic fragments, such as pieces of bark, wood and twigs.

Figure 41. X-ray of large ungraded massive interval from section 7 of inner basin core TUL99B03.

Interval III
933-953 cm

Large ungraded massive
interval with chaotic fabric



Disturbed laminated sediments

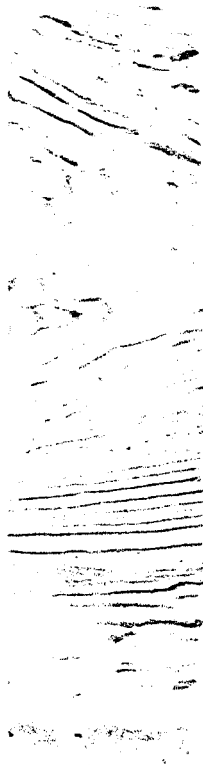
Inner basin core TUL99B03 penetrated deep enough into the sediments to reveal highly disturbed laminations beneath the large massive interval found in section 7. The freeze cores do not extend beyond the massive interval preserved in them however, to indicate what is below it in the sediment column.

The disturbance in the sediments located just beneath the massive interval of section 7, core TUL99B03, is in the form of folding and overturning of consolidated laminations (Figure 42). The disturbed laminations immediately beneath these folded laminations, illustrate a different type of deformation, with apparently “smearcd” laminations possibly representing de-watering structures that occur after the sediment column has been shaken to the point of overcoming consolidation of the sediments (Figure 43) (Atwater et al., 1995a and b; Clague et al., 1992).

The disturbed sediments continue from just beneath the base of the large massive interval at 972 cm, in TUL99B03, for 118 cm (from 972 to 1090 cm);(Appendix F). Below the deformed laminae are well laminated sediments representing about 30 years of deposition, which are underlain by another fairly large, graded massive interval of 18 cm in length, again containing large terrigenous organic fragments (1098 to 1116 cm); (Appendix F). This massive interval however is underlain by undisturbed, well laminated mud to the base of the core.

Figure 42. X-ray of overturned and folded disturbed laminated sediments from inner basin core TUL99B03.

Interval III
974-990 cm



Distorted laminations
beneath large massive
interval.

Figure 43. X-ray of de-watering structures in laminated sediments of inner basin core

TUL99B03.

Interval III
1009 -1029 cm

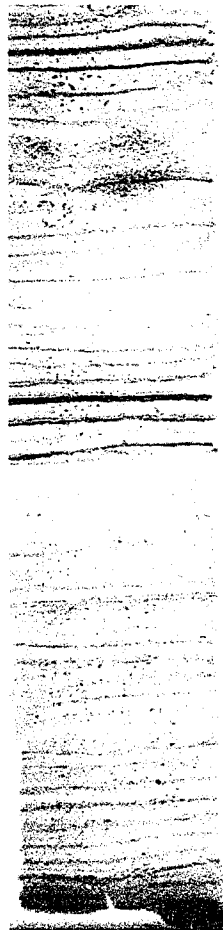


Distorted laminations
beneath large massive
interval.

Possible de-watering
structures.

Figure 44. X-ray of poorly defined laminations from outer basin core TUL99B11.

Outer Basin core B11
789-808 cm



Typical poorly defined laminations, diatom laminae less distinct than in inner basin cores.

Outer basin core sedimentary features

The x-rays of the outer basin core TUL99B11 (Appendix G) reveal the same sedimentary features as the inner basin cores, but more muted. The top two sections of TUL99B11 were too wet to slab for x-rays, and wetness of sections 3 and 4 indicate that the sediments of the inner basin are less consolidated than those of the outer basin. The laminations, where present, are typically poorly defined. However, throughout the outer basin cores the diatom laminae are generally darker in color, coarser grained and, thicker than those observed in the inner basin cores (Figure 44) (Please note that the dark spotting on this x-ray is part of the Clingwrap covering of the slab and not a sedimentary feature). This may indicate that diatom laminae in the outer basin may contain more lithic material than the diatom laminae of the inner basin (Sancetta, 1996).

Well laminated sediments in the outer basin core are unusual, possibly due to the wetness of the sediments, since the most well defined laminations only occur in sections 7 and 8. The majority of the outer basin sediments are either poorly laminated (Figure 44), or are ungraded massive muds (Figure 45).

The sand, gravel and shell bed found in the other inner and outer basin cores is present in TUL99B11 at 740 cm, and another similar bed is present at 863 cm (Appendix G).

Figure 45. X-ray of massive sediments from outer basin core TUL99B11.

Outer basin
641-701 cm

Typical ungraded massive muds and poorly
defined laminations

165

641 cm

661 cm

681 cm

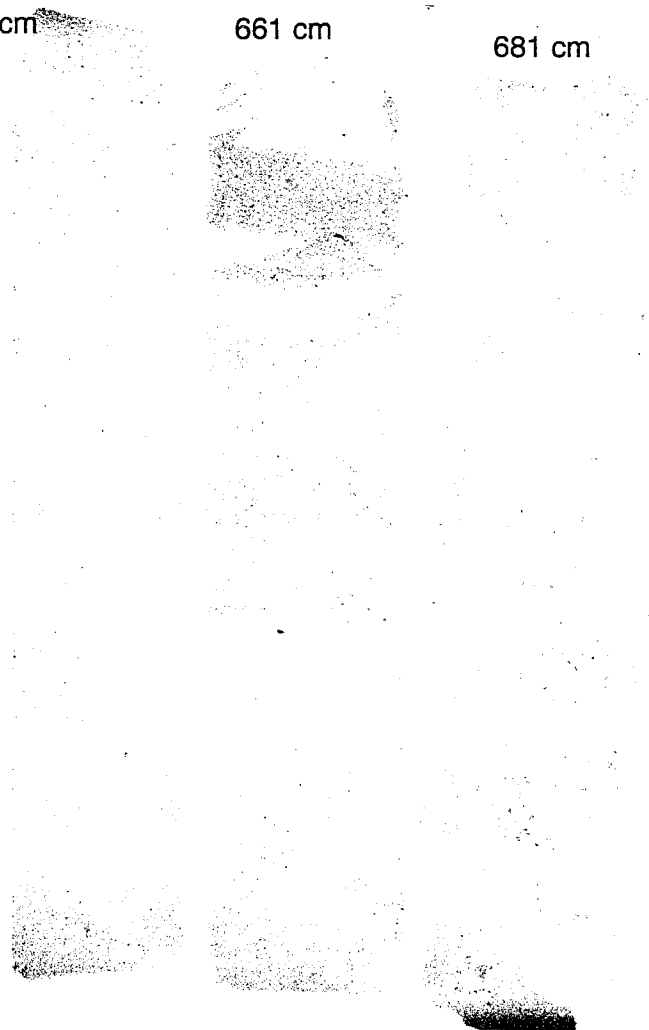
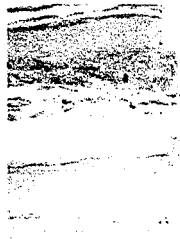


Figure 46. X-ray of convoluted bedding and tiny flame structures from inner basin core

TUL99B03.

Interval II
452 -457 cm



Convoluted laminae and
tiny flame structures.

Figure 47. X-ray of dropstone in the sediments of inner basin core TUL99B03.

Interval III
910-915 cm



Dropstones

Other sedimentary features

Convolute laminae and tiny flame structures (O'Brien, 1996) are evident in the laminated sediments of section 4 of inner basin core TUL99B03, at 454 cm (Figure 46) (Appendix F). Although subtle, these structures are interpreted as indicating a change in flow of the bottom currents and very low energy bottom scouring (O'Brien, 1996).

Large rounded stones and pebbles are found in the Effingham Inlet cores in both laminated and non-laminated intervals, and are not associated with graded deposits containing coarse sand and gravel or large terrigenous organics (Figure 47). Their appearance in the sediment column seems to be the result of the stones and pebbles falling independently through the water column, not associated with the deposition of other coarse grained sediments, and these stones and pebbles are therefore interpreted as dropstones (Hewitt, 1996).

Intact shells show up clearly on the x-rays throughout the cores in both laminated and massive sediments. Examples are from the outer basin core TUL99B11 at 716 cm (Appendix H) and from the inner basin core TUL99B03 at 587 cm (Appendix F).

RADIOCARBON AGE DATING

Suitable organic material for dating was somewhat scarce in the Effingham Inlet cores. A further radiocarbon sampling complication was finding radiocarbon dating material within the laminated sections. Organic material was easily found in the massive intervals however, but could possibly be out of stratigraphic sequence if the

Table 2. Results of radiocarbon dates and calibration from Effingham Inlet cores.

deposit is graded and the sample has been re-worked and re-deposited. In total, 20 samples were collected from the inner basin cores for radiocarbon dating (Table 2).

The chronological control on the outer basin is much less accurate than for the inner basin. Only six radiocarbon dates are available and four of these must be taken with caution since they are from shell material (see discussion below). One of these six dates is the only date for the inlet that seems to be out of stratigraphic sequence. TO-8686, from outer basin core TUL99B11 at 969 cm, is a shell date which is younger than the overlying dates. The shell material was sampled from the base of a sandy massive interval from an intact bi-valve shell. The interpretation of this date is problematic.

Only one radiocarbon date was obtained from a shell fragment found in the Barkley Sound core (TUL97A04) due to the scarcity of dateable material in that core.

CALIBRATION OF RESULTS

Results are reported in years before present (BP), as well as calibrated years BP (cal yBP), in both BC/AD and yBP nomenclature (Table 2). As can be expected, the calibrated results increase the uncertainty of the date by several hundred years in most cases. Calibration results vary widely and the range of possible accepted ages in comparison to the INTCAL98 data set for terrestrial material, were presented at both the 68.3% (1 σ) and 95.5 % (2 σ) confidence intervals for each radiocarbon date by the Isotracc Lab at University of Toronto and are contained in Appendix B.

It should be noted that the youngest date, TO- 8671 from TUL99B03 at 97 cm, has a wide range of possible ages and a complicated probability plot (Appendix B). This is because the calibration curve is relatively flat for the last 500 years when anthropogenically produced ^{14}C -free CO_2 from fossil fuel burning has diluted the ^{14}C in the atmosphere, making the amount of remaining radiocarbon in the sample difficult to match precisely to the INTCAL98 dendrochronologically derived calibration curve. This date therefore has to be interpreted with caution (R. Beukens, pers. commun.)

CALIBRATION OF MARINE RADIOCARBON DATING SAMPLES

Further complications exist when calibrating the marine shell and fish bone material. The calibration of the marine samples is dependent on the model of the marine CO_2 in the oceans used in the chosen calibration dataset, which is quite different than the atmospheric CO_2 reservoir which has been calibrated by ^{14}C analysis of dendrochronologically dated wood. The currently accepted model is that of Stuiver and Braziunas (1993).

The oceanic reservoir of CO_2 is not in equilibrium, and unlike the atmospheric pool where mixing is rapid, complete oceanic mixing is dependent on CO_2 exchange with the atmosphere, vertical diffusion and ocean currents and can take approximately 2,000 years between the surface layers and the abyssal plains waters (R. Beukens, pers. commun.). The Stuiver and Braziunas (1993) model produces a reservoir correction R assuming that CO_2 exchange with the atmosphere and vertical diffusion of CO_2 in the

ocean are location independent, but are age dependent with respect to the atmospheric exchange. Their reservoir correction R , is a function of age and depth and is part of the INTCAL98 database. The range of R is approximately 200 to 400 years.

However, local CO_2 reservoir effects can modify the R for example in the case of older, upwelled waters which will contain significantly less CO_2 than surface waters which have more CO_2 due to atmospheric exchange. The local effect has been measured for several locations by measuring the ^{14}C in marine shells and contemporaneous terrestrial material which gives a local correction factor, ΔR (Stuiver et al., 1998a and b). The local ΔR however assumes that the ocean current regime in place at the time of the shell-terrestrial pair, has been the same throughout time. Fjords and inlets can also complicate this picture since their gradation from fresh to marine waters and various flushing profiles over time can create distinct micro-environments quite separate from the local oceanic waters.

The shell material of our study was calibrated using the marine data set MARINE98 (Stuiver et al., 1998b) which gives a local reservoir correction, ΔR , of $+390 \pm 25$ years for the ocean waters west of Vancouver Island. This figure yields a rough correction of -801 ± 23 years "too old" for marine samples for this location. Since this correction is very large, it is preferable to try and calculate a local reservoir correction for the specific study area from as many marine/terrestrial contemporaneous sample pairs as possible. In our study only one such pair was found from the outer basin

core TUL99B11 (T0-8685, wood from 939 cm and TO-8684, shell from a paired bi-valve from 898 cm) (Appendix B). This yielded a Delta-R of - 120 +/- 45 years for Effingham Inlet, which is very different from the Delta-R of + 390 years currently accepted for the waters west of Vancouver Island.

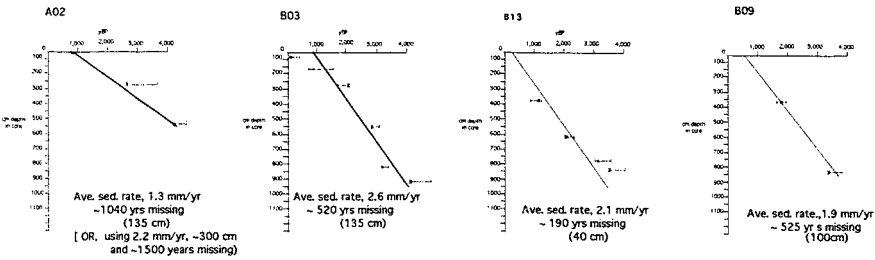
Table 2 gives calibrated age ranges for all the marine material calculated using both the accepted Delta-R for oceanic areas of west Vancouver Island (+390 years) and the calculated Delta-R for Effingham Inlet (- 120 years). The calculated calibrated age range is further extended using the calculated Effingham Delta-R, casting some doubt on the general utility of calibrated shell dates from Effingham Inlet. However, it should be noted that whichever method of calibration is used the dates for the inner basin are in stratigraphic sequence to each other, when radiocarbon age is plotted against depth in the core (Figure 48) indicating that even the shell dates are giving an approximate age to the sediments they are found in.

A fish skeleton found intact on the bedding plane at 285 cm from the inner basin core TUL97A02 has an estimated radiocarbon age of 3410 +/- 50, again, a date which is in stratigraphic sequence (Figure 48). However, for an accurate evaluation of the utility of this date, the following should be considered. To date, only shells have been used in marine/terrestrial contemporaneous specimen pairs to determine published Delta-R values. To have an accurate idea of where the ^{14}C in the fish's body came from, we must

Radiocarbon dates and sedimentation rates

Sediment age (yBP) vs Depth (cm)

Inner basin cores - Ave. sed. rate 2.2 mm/yr



Outer basin - Ave. sed. rate, 5.5 mm/yr

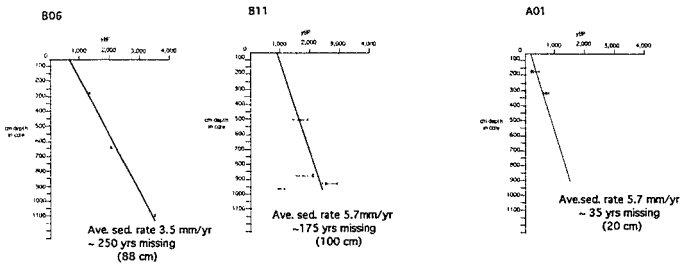


Fig.48 Radiocarbon dates, in years before present, are plotted for each core against depth in core.

Shell dates are plotted in red. Lines are drawn as best fit, and an average sedimentation rate is calculated for each core. Data points also show error bars which represent the maximum calendar year age range calculated for each radiocarbon years date (see Table 2).

An average sedimentation rate for the inner basin is derived from the cores with the best date control, B03, B09, and B13. The dating control of both outer basin cores gives the same sedimentation rate.

An estimate of the amount of sediment missing from over penetration during coring is made by a simple linear transformation to bring the graphed data points for each core through the origin, i.e. extending the average calculated sedimentation rate through time to the present. These estimates are in close agreement with core tops age estimates derived from radiocarbon dates and laminae counting.

have an idea of what species the fish is, where, how deep and on what the fish feeds and what its migratory range is. If the fish feeds in the inlet, then the marine/terrestrial pair should apply. If it feeds in the ocean at relatively shallow depths and stays mainly in the cold current off Vancouver Island, then Delta-R of +/- 390 years should apply.

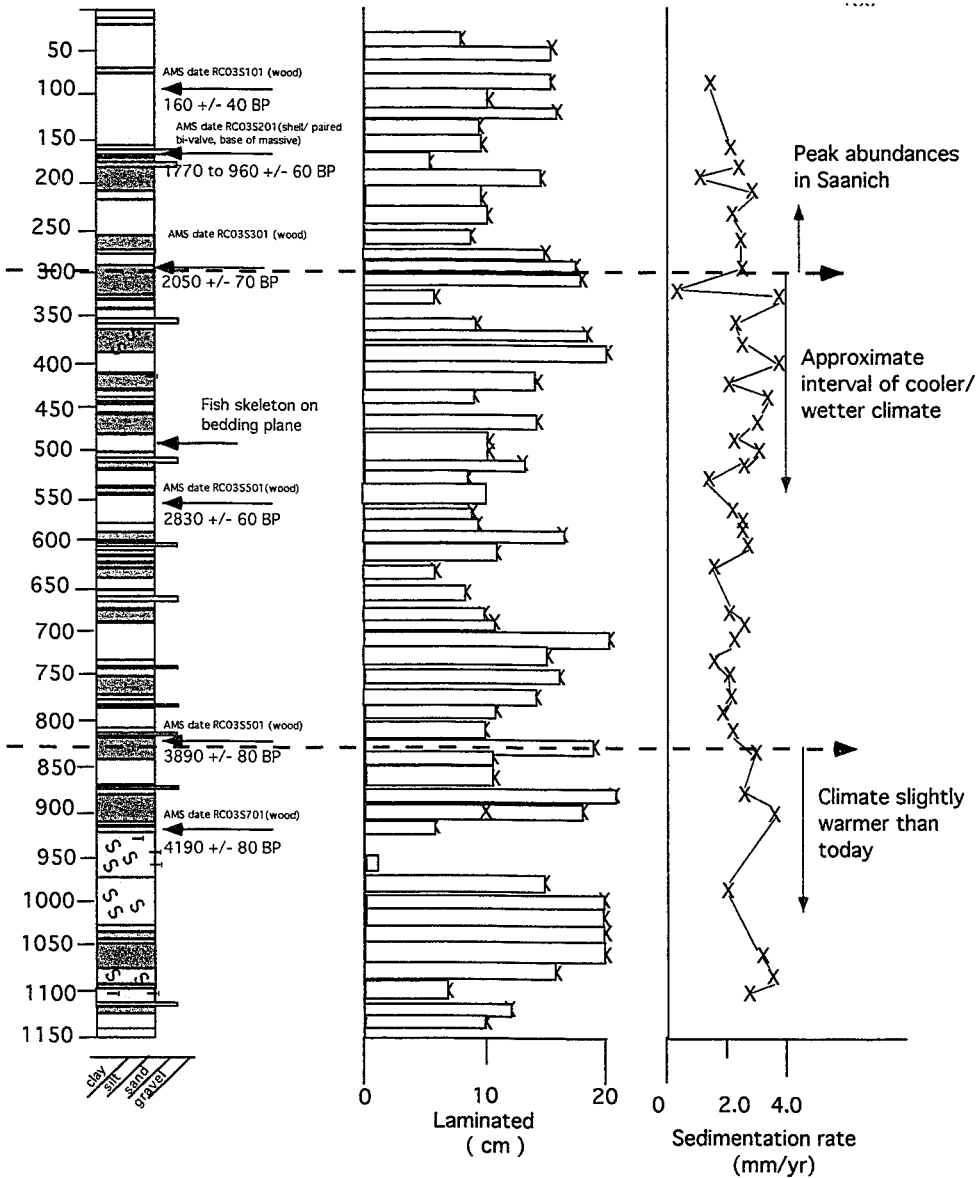
SEDIMENTATION RATES

The radiocarbon dates for the inner and outer basin piston cores are plotted with their complete error ranges from all methods of radiocarbon date calibration, reported in Table 2, as Figure 48. Lines on these graphs are drawn as best fit to the eye, since each point has variable error bars associated with it. In our case, when terrestrial and marine dating samples are being dealt with together, and particularly when the calibrated dates for the marine material are somewhat in question, "best fit by eye" is an accepted data plotting method within the radiocarbon dating research community (R. Beukens, pers. commun.) to see if calculated radiocarbon dates are in stratigraphic sequence, and for estimating sedimentation rates.

Sedimentation rates can also be calculated as the slope of the depth vs age plots, resulting in 1.3 to 3.5 mm/yr in the inner basin and 5.7 mm/yr in the outer basin (Figure 48). Varves of the inner basin core TUL99B03 were also counted from the core x-ray, and an average sedimentation rate based on these counts for each uninterrupted laminated interval of the core is plotted in Figure 49. The estimated average sedimentation rate for the inner basin cores determined from the counted laminated intervals, is approximately

Figure 49. Sedimentation rates calculated from laminated intervals in TUL99B03. Red represents well laminated intervals, salmon represents poorly laminated intervals and grey represents massive muds. Column 2 shows the length of interval of laminated sediments used to count varves.

?? Depth to sediment-water interface ??



2.4 mm. This is in close agreement with an average sedimentation rate in the inner basin cores of 2.2 mm/year as calculated from the depth vs age plots (Figure 48).

OCEANOGRAPHY

A full discussion of the unpublished results of the on-going physical oceanography surveys of Effingham Inlet begun in 1995, is beyond the scope of this thesis. However, with the permission of Dr. R. Thomson of the Department of Fisheries and Oceans, I will present selected time series oceanography data that is integral to the interpretation of the depositional record of Effingham Inlet. The data were presented by Dr. Thomson during a project workshop at PGC in May, 2001, and the following interpretation of the results is based on fruitful conversations with he and Dr. D. Ware, C. Wright, Dr. B. Burd and Dr. R.T. Patterson who were in attendance.

The time series data from Effingham Inlet continues to confirm that the along channel water property structure of the inlet undergoes marked variability over time, associated with seasonal changes in wind-induced mixing, surface heating and cooling, local runoff and coastal upwelling. Table 3 gives a summary of the 13 along channel cruise surveys to Effingham Inlet between December, 1999 and October, 2000, and reveals anomalously oxygenated bottom waters during 1999. The location of the CTD/rosette stations (EF) in the inlet and Barkley Sound, and the location of the current meter and tidal height data stations (CTC) are shown in Figure 50.

Table 3.

Effingham Inlet: Summary of Cruise Survey Data for the Central and Inner Basins

Year	Jan	Feb	Mar	Apr	May	Jun	July	Aug	Sept	Oct	Nov	Dec
1995												X
1996												
1997			X									
1998					X				X			
1999	O				X	O			O	O		
2000			X		X		X			X		

X = No Oxygen in bottom waters

O = Oxygen present in bottom waters

Figure 50. Location map of CTD rosette stations (EF), current and tide meters (CTC) and location of Barkley Sound core TUL97A04.

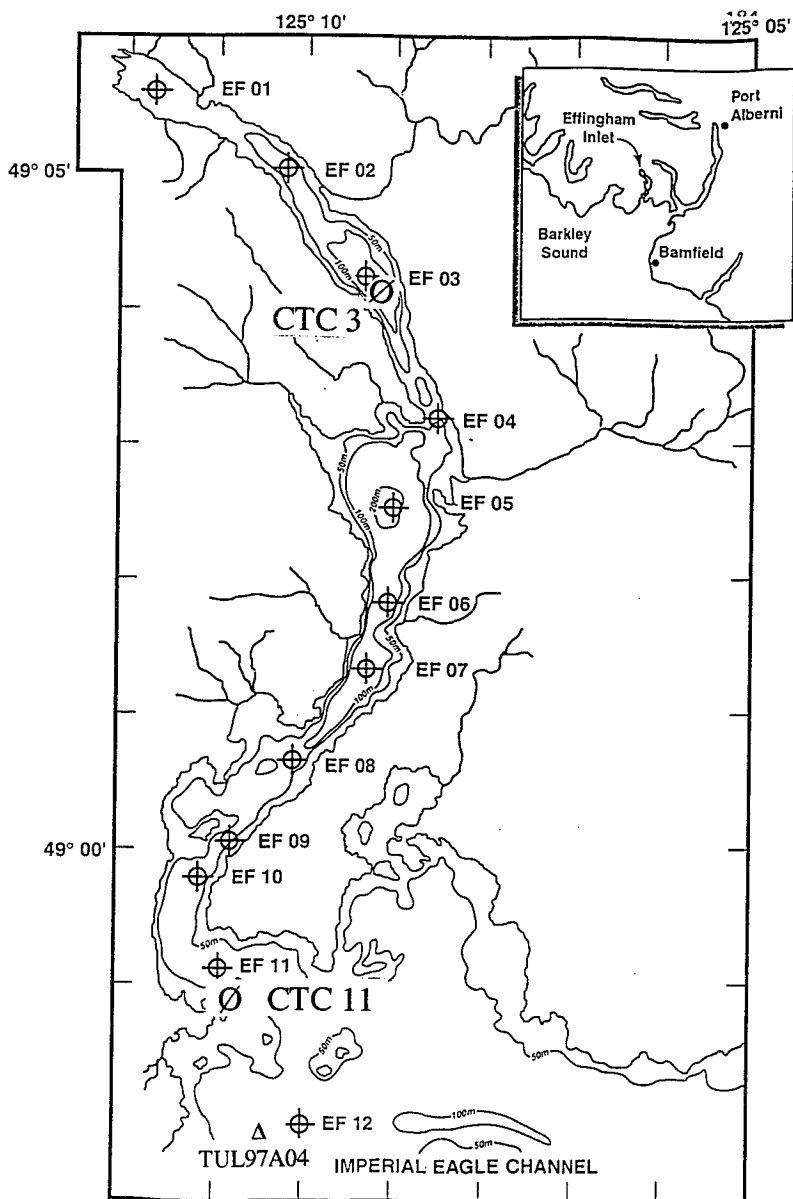
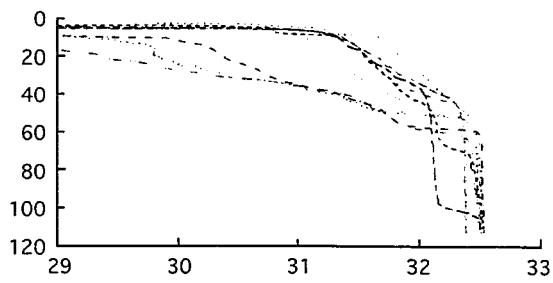
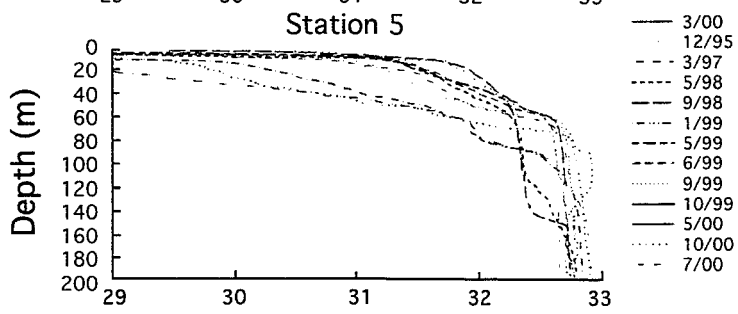


Figure 51. Salinity - depth time series plots.

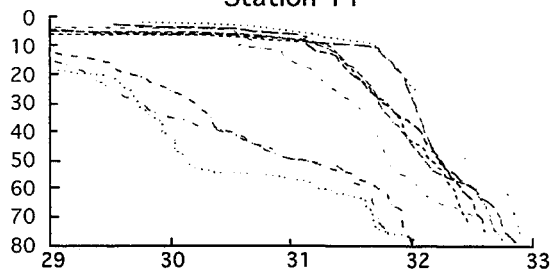
Station 3



Station 5



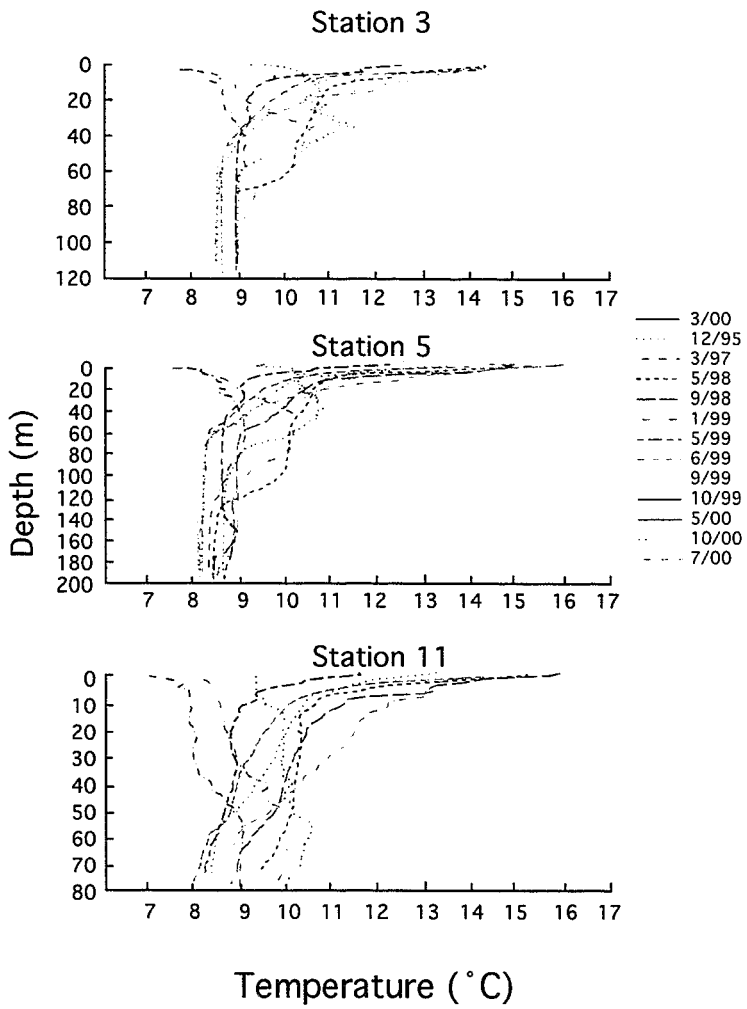
Station 11



Salinity (ppt)

- 3/00
- 12/95
- - 3/97
- - 5/98
- - 9/98
- - 1/99
- - 5/99
- - 6/99
- 9/99
- 10/99
- 5/00
- 10/00
- - 7/00

Figure 52. Temperature – depth time series plots.



Time series salinity profiles of the inlet reveal the characteristic estuarine-type stratification of the water column in the inlet over time (Figure 51). The bottom waters of the inner and outer basins are approximately uniform in salinity and temperature (Figure 52) and the overlying waters exhibit a step-like transition zone to the surface. Notice the anomalous increase in depth of the surface freshwater wedge, on salinity profile Figure 51, for the month of January, 1999 (i.e. low salinity values ,< 31 ‰ normally ~ 32‰, up to 40 m in depth). Other thick freshwater wedges of low salinity, indicating high rainfall and/or strong stream and river discharge events, occur in December 1995 and March 1997 (Figure 51).

In the northeast Pacific, salinity drives the density profiles (R. Thomson, pers. commun.). In Effingham Inlet, the low salinity of fresh surface waters, combined with weak tidal current energy, results in a stable stratified water column which inhibits mixing. The density profiles of Figure 53 reveal this characteristic water column stratification in the inner basin. Deep, cold and uniformly saline waters make up water mass IV, less saline cold water overlying is bottom water mass III, which itself is overlain by the warmer and progressively less saline, step-like transition of water mass II, and finally the upper warmer fresh water mass I.

Time series dissolved oxygen profiles show the characteristic decrease in oxygen in the inner and outer basins with depth (Figure 54). The January, 1999 anomalous event, is obvious in the dissolved oxygen data as well. The sampling in January, 1999

Figure 53. Density – depth time series plots.

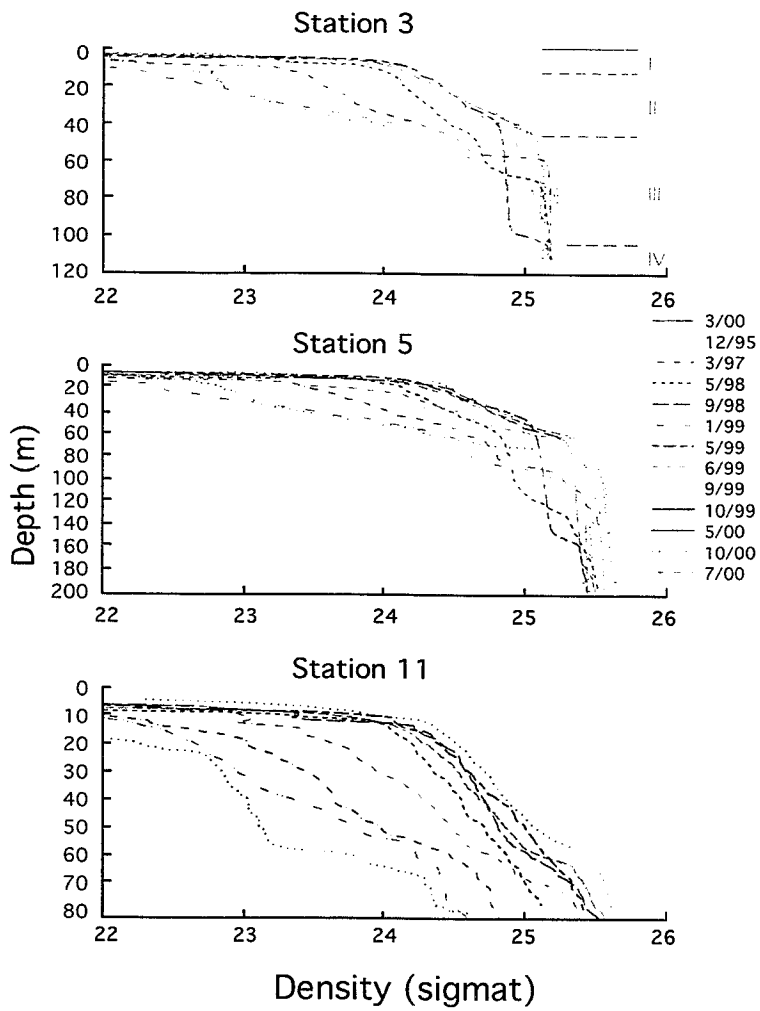
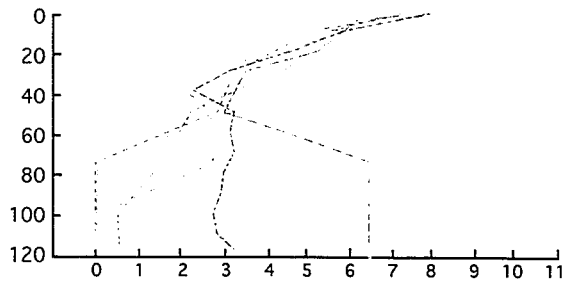
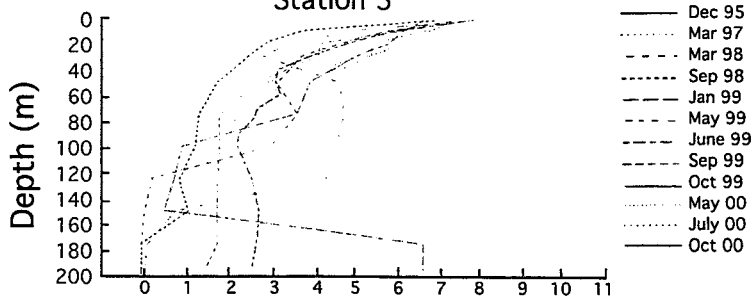


Figure 54. Dissolved oxygen-depth time series plots.

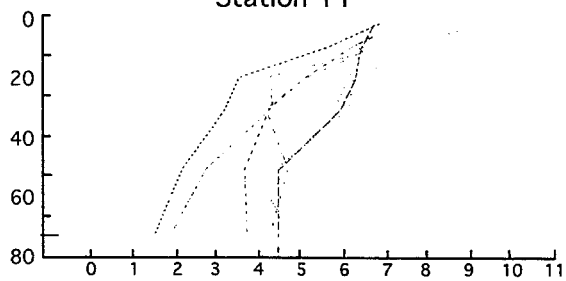
Station 3



Station 5



Station 11



Dissolved Oxygen (mg/L)

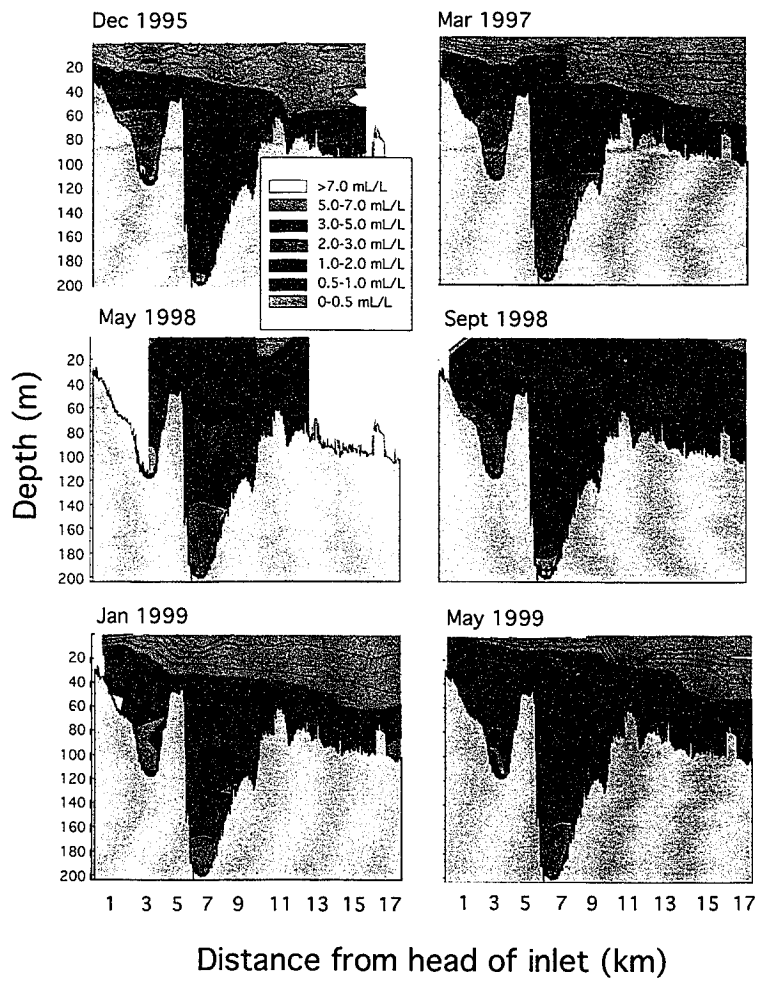
revealed high oxygen levels in the bottom water and low (1-2 mg/L) oxygen levels at mid-depth in the inner and outer basins, suggesting that flushing of the basin with oxygenated waters had already occurred. This is consistent with deep-water intrusions, known as upwelling events, that advect moderately low oxygen water over the sills into the inner and outer basins. The cold ocean waters dissipate the anoxic bottom waters of the inlet, without appearing to raise the overall oxygen content of the waters above (Figure 54), indicating that the upwelled waters are entering the inlet along the bottom and not sinking to the bottom from above as would occur during an overturning of the water column.

By May, 1999, bottom water stagnation had again occurred resulting in anoxic bottom conditions, despite the high mid-depth oxygen levels which penetrated part-way down the water column in the outer deep basin. By June, 1999, oxygen levels were generally lower throughout the water column, but anoxia in the deep inner and outer basins was gone. These moderate oxygen levels are evidence of additional flushing events occurring sometime between May and June, 1999.

Oxygen levels decreased in both basins from September through October 1999 and once again had become fully anoxic by March 2000. Stagnation of the bottom waters therefore seems to recur after flushing by oxygenated upwelled waters within four to six months.

Figure 55. Oxygen-bathymetry profiles.

Oxygen profiles: Effingham Inlet



Oxygen Profiles: Effingham Inlet

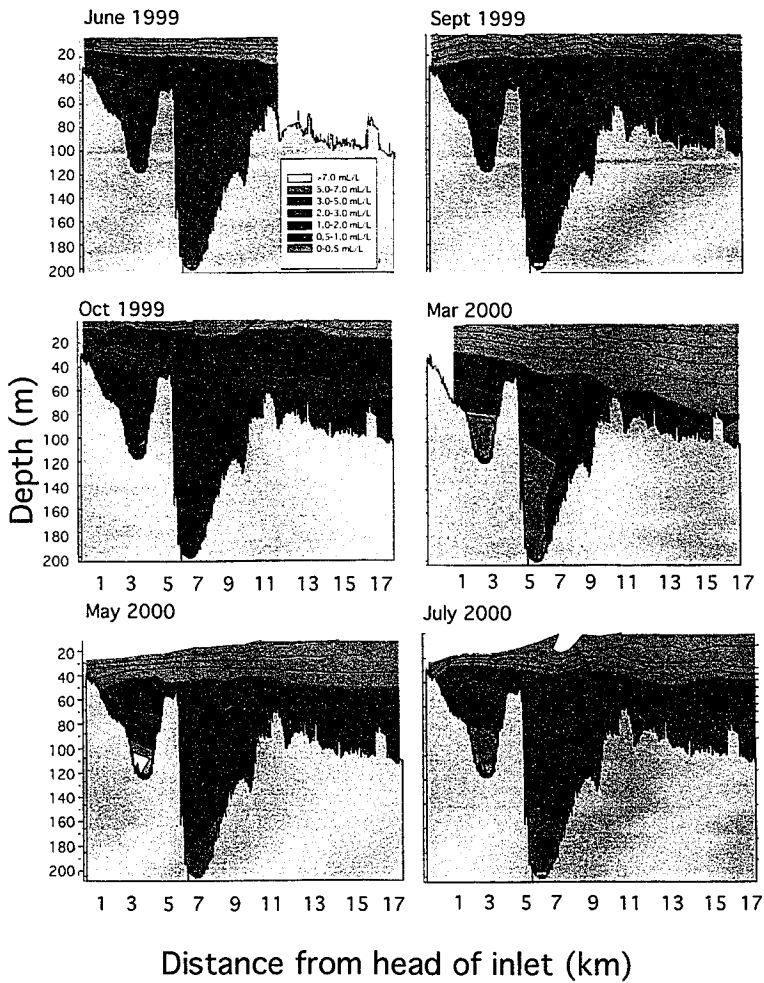
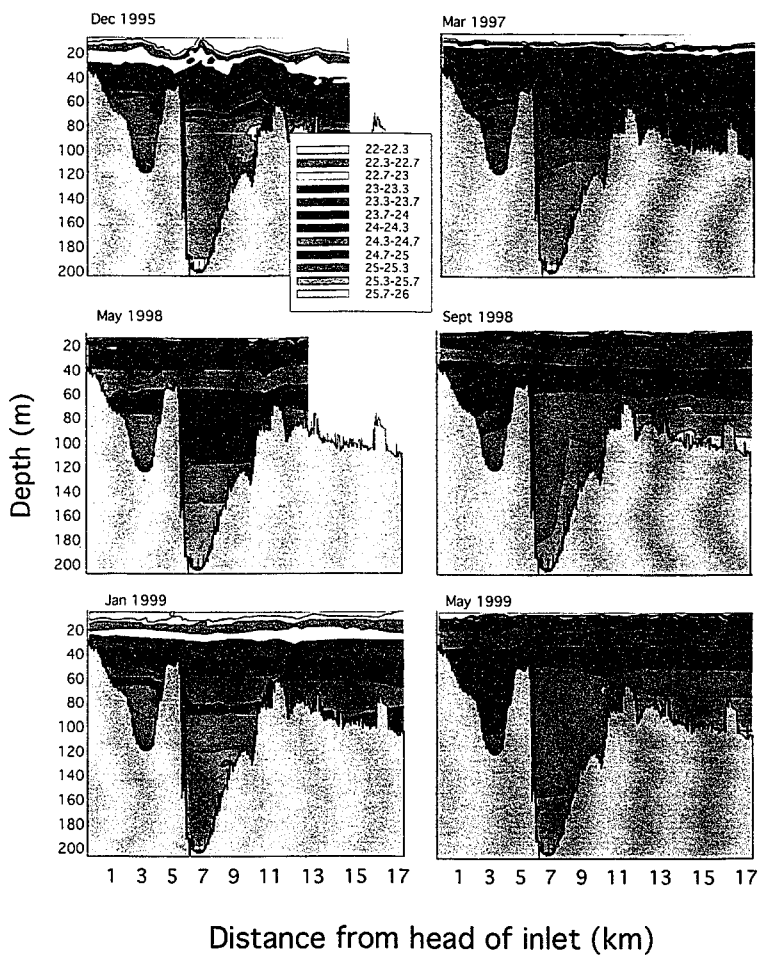
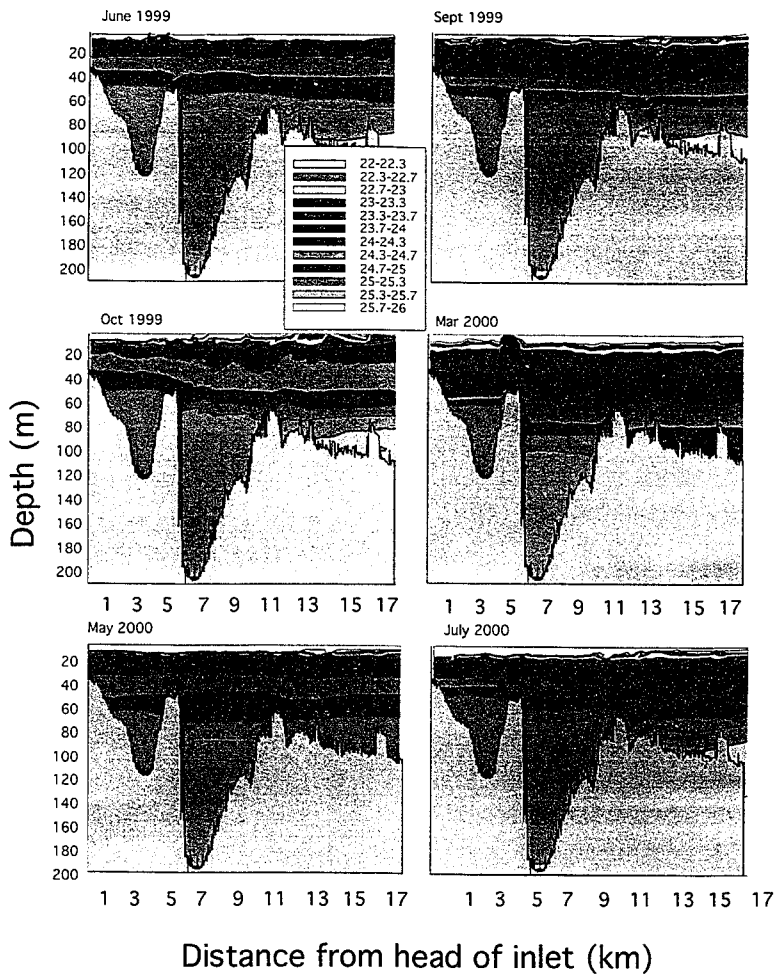


Figure 56. Density – bathymetry profiles.

Density profiles: Effingham Inlet



Density profiles: Effingham Inlet



When plotted with the bathymetry of the inlet, the oxygen and density profiles clearly illustrate the flushing events of 1999 (Figures 55 and 56). Note that in January 1999, the bottom waters of both the inner and outer basins have been oxygenated (waters in red in Figure 55 for January 1999), but lower oxygen content waters still overlie the oxygenated bottom waters. This once again indicates that the inlet is still stratified with respect to density during flushing as a result of upwelling events, and the mechanism by which the ocean waters enter the inlet is by “sliding” along the bottom and overtopping the sills, beneath the stable, stratified water column.

The increased fresh water run-off and precipitation, which enters Effingham Inlet in the winter months, is clearly illustrated by the large fresh (high oxygen content 5 –7 mL/L) water wedge (Figure 55), shown in red, at the surface in December 1995, January 1999 and March, 2000. Also note that the oxygen conditions of the inner and outer basins are generally the same over time, indicating that both the inner and outer basins are affected by the same flushing events.

The density profiles plotted against bathymetry in Figure 56, show as could be expected, that the inlet waters are highly stratified, even during the flushing event of January 1999. The high density bottom water mass (25 – 25.3 σ_t) of May 1999, shown in red, almost completely fills the outer basin, but in June 1999, it has overtopped the inner basin sill and now fills most of the inner basin, illustrating the mechanics of dense cold and saline bottom waters overtopping the sill to the inner basin. Although the vertical

exaggeration in these profiles is about 50 X, it is conceivable that as water masses “slide” over the sills, they accelerate somewhat down the slopes of the inner and outer basins after overtopping the sills.

It should be noted for clarity here, that although the upwelled waters are originally deep and cold ocean waters, they have been replenished with oxygen by reaching the surface along the coast during the upwelling process. Surface waters move seaward due to the Ekman transport effect at the beginning of upwelling events, and the resulting physical “space” at the surface along the coast, is filled by the upwelling deep and cold oceanic waters which are then oxygenated and enter the inlet where they can, which is beneath the highly stable stratified water columns of the inner and outer basins (Thomson, 1981; Pickard and Emery, 1990).

During the December 1995 cruise, a surface lens of anomalously cool, fresh water ($< 10.0\text{ }^{\circ}\text{C}$, $< 27.0\text{ }‰$) was observed in the outer basin. Waters of the surface freshwater wedge are usually about 12 to 15 $^{\circ}\text{C}$. This lens is thought to have originated from the main drainage discharge zone of the outer basin along its eastern shore. Similarly, a tongue of warmer, slightly more saline water was observed in the outer basin during the summer 1995 cruise, moving down the slope of the outside wall of the outer basin. This water had mixed to a depth of 120 m in the outer basin but apparently was not dense enough to mix to the seafloor at 20 m. This illustrates the apparently freshwater drainage

discharge into the outer basin, and the very weak estuarine circulation in the inlet due to the lack of year-round discharge from the Effingham River.

Waters of Effingham Inlet are quite murky, with transmissivity values of only 66 % compared to the open ocean transmissivity of 95 %. This is probably due to the many fine organics suspended in the water column.

Mean alongshore current and temperature time series from 1995 to 2001, from 35 m depth at the mouth of Effingham Inlet are shown in Figure 57. Note the relatively warm surface water at the end of 1998, about 14° C which quickly decreases to about 8 ° C in January 1999, coinciding with the upwelling event into the inlet. Water temperatures do not recover until later in 2000. Additionally, the alongshore current is particularly weak in January 1999 (< 0 m/s) coinciding with the upwelling event, and is also weak (< 0.2 m/s) in May 2000, which coincides with the weaker, spring upwelling event of 1999. Waters remain cold in May 2000 at 8 ° C.

Daily mean wind stress in Barkley Sound is shown in Figure 58. Just before the January 1999 upwelling event, the wind stress is fairly high at ~ 0.2 N/m², and is weaker prior to the spring 1999 flushing events at < 0.1 N/m².

Figure 57. Alongshore current time series.

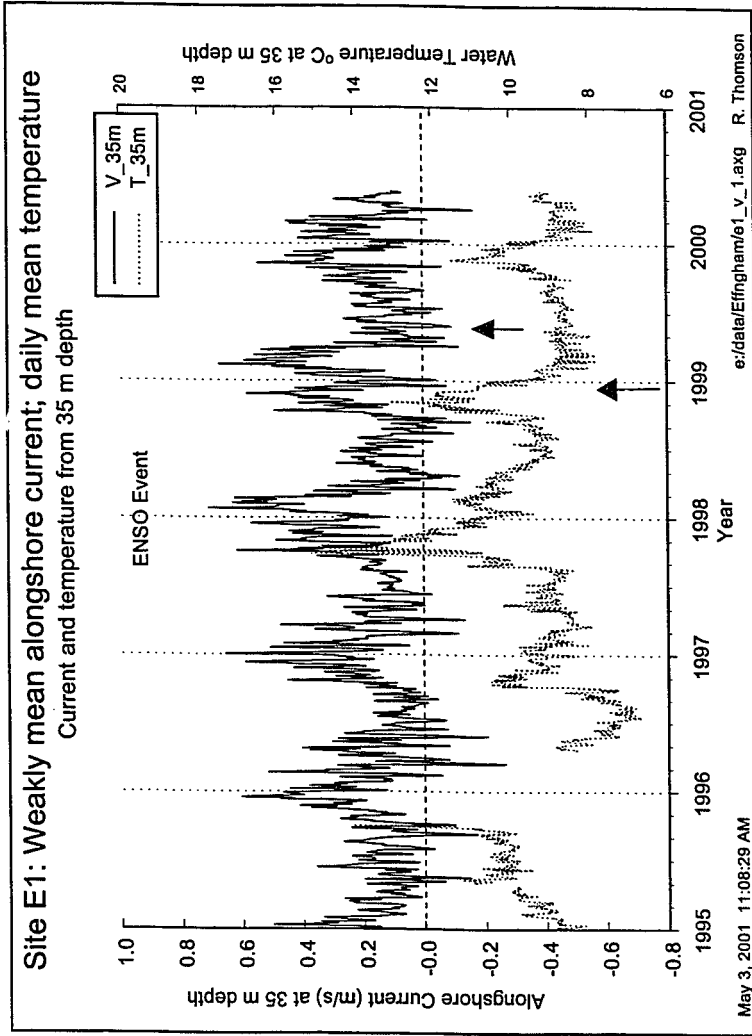
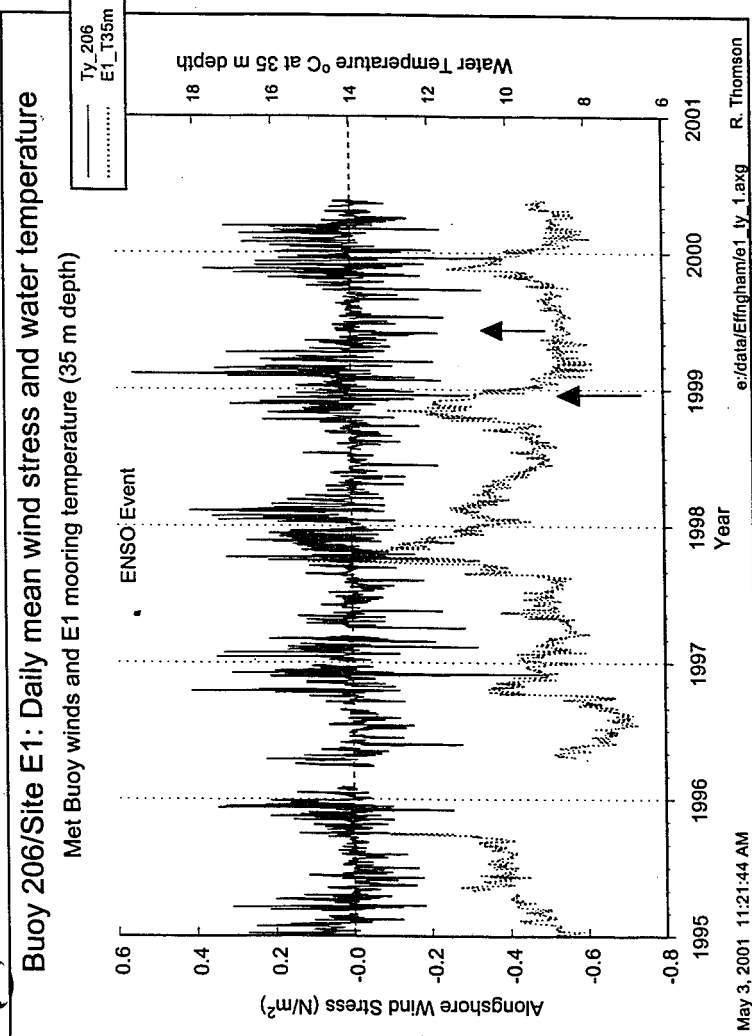


Figure 58. Daily wind stress time series.

0



FISH SCALES

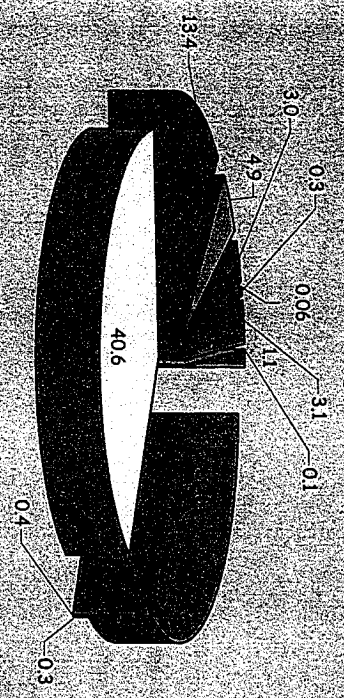
The following fish scales data, by C. Wright, was also presented at the May, 2001 project workshop and the basic interpretation of the preliminary results presented here is the result of many fruitful discussions with C. Wright, and also with the participants of the workshop.

This is the first study of such a long record of fish scales from a small volume piston core (Baumgartner et al., 1992; Tunnicliffe et al., 2001). Fish scales in the Saanich Inlet study had disintegrated appreciably down core and therefore bones were the only reliable record of paleo-fish populations left in the Saanich sedimentary record (Tunnicliffe et al., 2001). Plots of total fish scales and bones with depth in the Effingham sediments, revealed that there is no appreciable down core loss of either, giving a complete record (C. Wright, pers. commun.). The total number of fish scales, bones, ostracods, forams, charcoal fragments and anhydrite crystals, found in each sample of Effingham Inlet sediment from the inner basin piston core TUL99B03, each representing about 21 years of deposition, is presented in Appendix J.

A total of 4,236 scales were counted from 95 samples of 392.7 cm³ (~ 21 years of deposition) over the length of the identified laminated sections of core TUL99B03. Scales were identified, in order of total abundance, from the following fish taxa; anchovy (1,827), herring (1,328 total, 407 adult, 921 juvenile), rockfish (511), hake (209), surfperch (122), shark and skate (110) sardine (10), cod (13), jack mackerel (2) and

Figure 59. Fish species relative abundances.

Percent Abundances from Core 3B (Inner Basin)



- Herring Total
- Herring/Sardine
- Sardine
- Anchovy
- Rockfish
- Hake
- Surfperch
- Greenling
- Cod
- Shark/Skate
- Jack Mackerel
- Unidentified

greenling (2) (Figure 59). Dogfish scales were not identified, but several dogfish teeth were found in the upper core. Ten scales were categorized as either herring or sardine, but overall, only forty-six scales were unidentifiable, giving a 99 % success rate of scale identification for scales greater than 50 % intact (C. Wright pers. commun.).

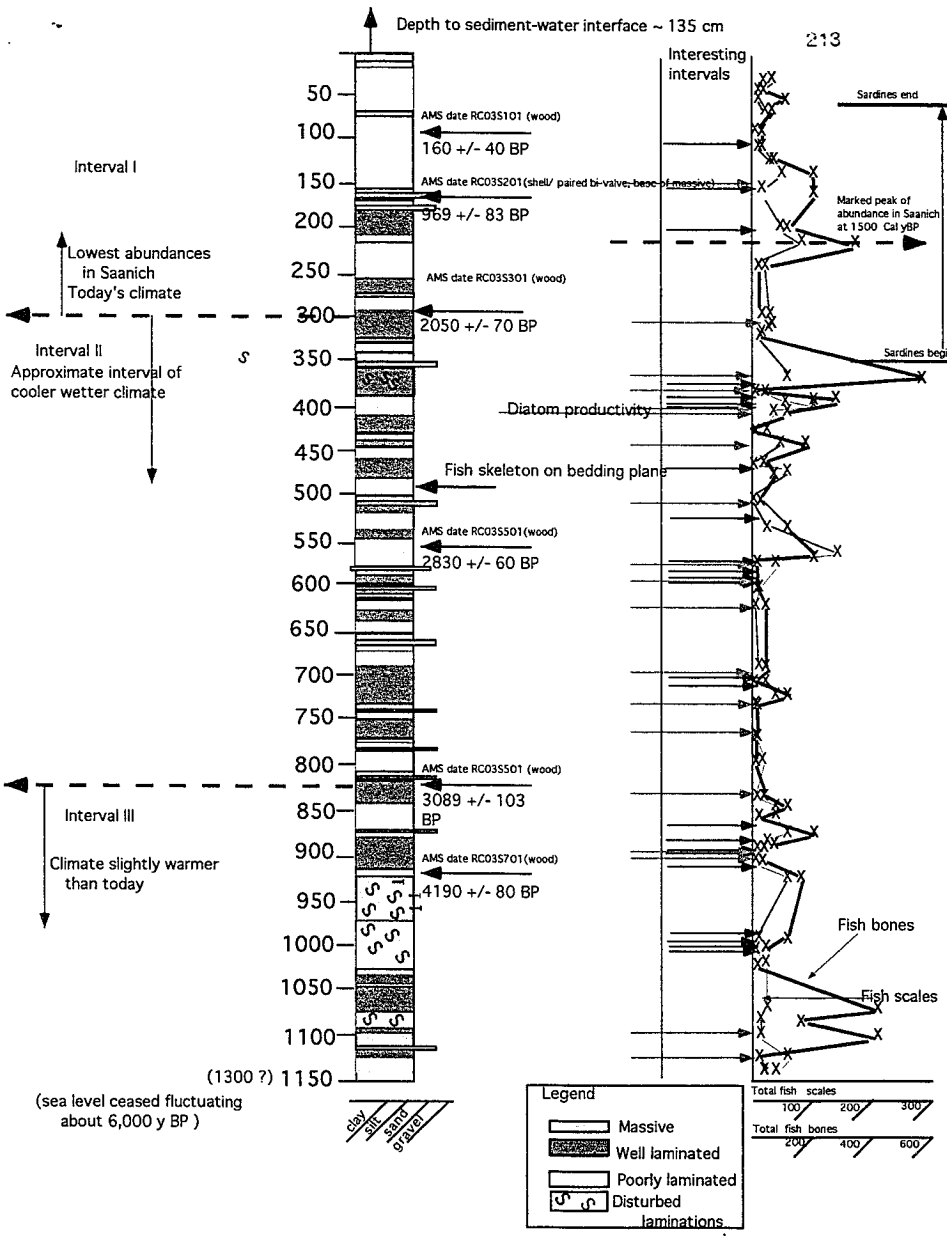
A total of 9,128 fish bones and bone fragments were also counted from the 95 samples over the length of the core. Most bone material appears to belong to smaller fish. Of these bones and fragments, approximately 10 % were identifiable vertebrac. The majority of recovered bones were identified as various small body bones, head bones, rays and many gill rakers.

In general, the ten fish species found represented in the fish scale record of Effingham Inlet are found throughout the core, with two notable exceptions. Sardine scales appear at 145 cm and disappear below 512 cm. Jack mackerel has only two appearances in the core, at 680 cm and at 721 cm. In the case of sardines, their disappearance in the record is particularly of note since sardine scales are quite robust and therefore resistant to degradation over time. Although each of these species represents less than 1 % of the scales found in Effingham Inlet, their clustered appearance is perhaps significant (C. Wright, pers. commun.). Herring are preferentially found near the top of the core. An increase in hake is accompanied by an increase in anchovy at 1010 to 1015 cm, however the relationship is the reverse elsewhere in the core.

A particularly strong signal in the fish scales data of this study, is the lowest ebb of abundance of the record, in the last 1,000 years, a pattern also found in the Saanich Inlet studies (Tunncliffe et al, 2001; O'Connell and Tunncliffe, 2001) and in the fish scales studies of Santa Barbara Basin (Baumgartner et al., 1992). However, a marked abundance peak was recorded in Saanich Inlet about 1,500 yBP, which seems to coincide with a moderate abundance peak in the Effingham record at about the same time (Figure 60).

The total numbers of fish scales and bones found in sampled laminated sediments only, are plotted next to the inner basin core TUL99B03 sediment column (Figure 60). Times of high productivity, as represented by particularly thick diatom laminae in the sediments, are indicated with red arrows, and samples with particularly unique assemblages of detritus are indicated with black arrows, as a first look at the data for trends and associations. Figure 60 shows that fish scales and bones are cycling, mostly in tandem, throughout the sediment record of TUL99B03, but there appears to be no appreciable relationship between sedimentology and/or high productivity, and an increase in either fish scales or bones.

On-going cyclostratigraphy and wavelet analyses on the inner basin sediments may reveal if fish population cycles are in phase with cycles in the climate/ocean regime.



INTERPRETATION AND DISCUSSION

SEDIMENTOLOGY

LAMINATED SEDIMENTS

The laminated sediments of Effingham Inlet show remarkable variability in the thickness of both the diatom and terrigenous laminae, and indicate the high annual variability in both diatom productivity and precipitation that can occur even in the span of a decade (Figure 38). Preliminary results of light and SEM microscopy studies by my colleague Alice Chang, performed on the diatom laminae in thin sections made from resin peels, indicate that the varves are more complex than can be seen with the eye. The common sequence of events within an annual varve is:

- 1) a silty/terrigenous winter laminae,
- 2) a sublaminae of centric diatoms (*Thalassiosira* and *Skeletonema*) in a spring laminae,
- 3) a layer of *Chaetoceros* resting spores and,
- 4) a sublamina of mixed diatoms or silty and fragmented diatoms in a late summer laminae.

These “quadruplets” do not occur in all years and extremely thick laminae of monospecific *Skeletonema* are also commonly present throughout the core (A. Chang, pers. commun.). This preliminary work indicates that the intra- seasonal variability can be just as complex as the inter-seasonal variability in both rainfall and productivity.

Preliminary results of a micropaleontology study by my colleague Murray Hay shows that diatoms from Effingham Inlet sediments can be categorized into four distinct assemblages. These assemblages confirm that oceanic conditions are affecting the outer basin more than the more isolated inner basin (M. Hay, pers. commun.)

MASSIVE UNGRADED MUDS

The massive ungraded muds are generally interpreted to represent years of oxygenation of bottom waters by upwelling events, when a bioturbating benthos can become established and destroy evidence of the laminations. The lack of evidence for bioturbation tracks is somewhat problematic to this interpretation however. Either there is poor preservation of bioturbation tracks in the unconsolidated sediments and/or a different mechanism is responsible for destroying laminated sediments.

Several lines of evidence lead to weak density currents, associated with advecting upwelled and oxygenated water masses advecting over the sills and into the inlet, as a possible mechanism of erosion, re-suspension and re-deposition of basin sediments, possibly resulting in the ungraded massive muds. For example, in some ungraded massive intervals, laminae appear to “fade” away into the upper unlaminated interval (Figure 37) without any evident bioturbation tracks. Secondly, the convoluted laminae and flame structures immediately beneath an ungraded massive interval in Figure 46, may show evidence of very gentle erosion, re-suspension and re-deposition of unconsolidated laminated sediments by an incoming density current. This could explain

the existence of lengthy (>10 cm) ungraded massive intervals that appear to represent decades of oxygenation of the basin waters (Figure 39), which appears to be an unlikely scenario in light of the modern oceanography data showing a very rapid return to anoxic conditions within a matter of months after rare oxygenation events.

Graded mud intervals also appear to have been aerated upon deposition in some cases, which may increase the opportunity to establish a bioturbating benthos, if only for a few seasons. For example in the outer basin, frequent color changes from dark olive grey sediments (dysoxic/anoxic depositional conditions) to black ungraded massive and graded mud intervals (dysoxic/oxic depositional conditions) (Kemp, 1996; Sancetta, 1996), indicate that some debris flows are transporting sediments from a shallower, aerated zone of the inlet. However, an example of an immediate transition to anoxic conditions after deposition of a graded mud interval representing a debris flow in Figure 37, is further evidence that anoxia is the normal state of the inner basin waters. High rates of sedimentation combined with high organic influx, appear to return the bottom waters quickly to anoxia, after deposition of oxygen-containing sediments in debris flow deposits.

Sediment deposited from suspension in a density current, as a process to explain the ungraded massive mud deposits, does not discount the possible existence of bioturbating organisms at times, and most likely it is a combination of these two processes that creates the ungraded muds. In laminated marine sediments, the burrowing

habits of benthic organisms can leave traces of disturbance in recently deposited sediments of from several millimeters to several decimeters by deep burrowers (Anderson, 1996). Studies from oceanographic surveys where bioturbation tracks are well preserved, give an indication of the dissolved oxygen content of the bottom waters from the concentration of bioturbation tracks per unit area (Anderson et al., 1989). Vertical borings are characteristic of an oxic to low oxic environment while horizontal burrows are more common as oxygen content decreases.

The lack of preservation of bioturbation tracks in Effingham Inlet sediments does not allow for this type of analysis. However, the faint horizontal tracks visible beneath lengthy sections of ungraded muds (>10 cm) (Figure 39) perhaps represent successive seasons of oxygenation events allowing a bioturbating benthos to establish and survive from one season to the next, and destroy laminated structure in the sediments.

GRADED MUDS

In marine and freshwater environments, slumping of poorly consolidated sediments results in sediment gravity flows, which in turn are categorized with respect to the type of mechanism whereby sedimentary particles are supported within the flows (Collinson and Thompson, 1989). "Fluid" flows, demonstrating viscous behavior result in turbidity currents and concentrated suspensions, and "debris" flows, which exhibit plastic behavior, result in grain flows and mudflows. The resulting deposits each have

specific sedimentary features (Middleton and Hampton, 1973 and 1976; Middleton and Southard, 1984).

Sedimentary deposits which are the result of debris flows are characterized as having massive structure or weakly defined fining upwards grading, and often have evidence of shearing at the base resulting in some erosion of the underlying sediments (Middleton and Southard, 1984). This description would fit most of the graded massive intervals in Effingham Inlet. In Saanich Inlet, massive intervals were also interpreted as debris flows and attributed to paleoseismic disturbances as the triggering mechanism of the initiating sediment slump (Blais Stevens et al., 1997 and 2001).

The debris flows in Effingham Inlet are somewhat coarser grained than in Saanich Inlet however. For those intervals in the Effingham cores where a pronounced fining upwards from a coarse-grained sandy base of a graded bed is evident, it could perhaps be argued that this deposit is the result of a turbidity flow of sediments running the length of the inlet from, for example, a discharge event of the Effingham River, in a suspended sediment plume. However, the complete turbidite sediment package characterized by Bouma (1962) is not evident in these intervals. In particular, the parallel laminae, and sand and silt ripples of Bouma units B,C, and D are absent. Therefore it is unlikely that the coarser grained, graded massive intervals are complete turbidity flows originating from the small Effingham River and traveling the length of the inlet.

More likely the graded massive intervals represent slumps from different parts of the basin, initiating debris flows. Coarser grained deposits may originate from the slumping of the glacial gravel shoulders of the inlet, creating incomplete turbidite deposits. Finer-grained graded muds, containing only terrigenous fragments are perhaps deposits from lower energy debris flows originating from more minor slumping of the basin sediments.

RADIOCARBON DATES

One of the main questions raised by the data in this study, is the interpretation of the radiocarbon dates, and therefore the chronological and/or relative ages of depositional events recorded in the sediments of the cores. Radiocarbon dating control of the Effingham Inlet material is complicated by a number of factors.

- 1) Using pieces of wood for radiocarbon dating, that have been on land and in the water column for an indeterminate length of time after the tree has died. This would tend to make the dates too old.
- 2) Using shell and fish material for radiocarbon dating, from organisms that lived in an undetermined marine CO₂ pool, as discussed in the results. The margin of uncertainty in using shell and fish material for dating in Effingham Inlet is further complicated since the one terrestrial and shell contemporaneous pair found, did not yield a Delta-R reservoir correction within the range expected for the northeastern part of the Pacific. It should be

noted however that the shell and wood samples of the contemporaneous pair were 41 cm apart in the core, and therefore not precisely at the same age datum in the sediments. The main complication in interpreting the Delta-R from Effingham Inlet, may be the character of the inlet itself, which has several micro-environments with respect to the biota that are quite different from open marine conditions.

- 3) The radiocarbon dates are in stratigraphic sequence in all cores however, with the exception of TO-8686 from 969 cm of TUL99B11. This date is more than a thousand years younger than TO-8685, located just above it at 939 cm in the sediment column (Table 2, Figure 48). The interpretation of this date is somewhat problematic, since it is out of stratigraphic sequence and also because it is from a shell. However, it is possible that this represents older sediments which have been deposited on younger during sediment gravity flows, which is entirely possible in this basin. However, the fact that this is the only instance of a radiocarbon date out of stratigraphic sequence throughout the cores, would suggest that in general, sediment gravity flows are not complicating the chronological picture, particularly in the inner basin, but may be the explanation for the anomalously young date, TO - 8686.

SEDIMENTATION RATES

An advantage of a laminated sediment package is the chronological control provided in annually laminated sections, which can provide a check for the calculated radiocarbon dates. When average sedimentation rates estimated from laminated sections of TUL99B03, are multiplied with the length of the cores and compared to radiocarbon ages in the cores, in general, there is good agreement. Conversely, a date of 4,190 radiocarbon yBP at 937 cm in core TUL99B03 (TO- 8676) agrees well with the average sedimentation rate of 2.5 mm/year for the inner basin, estimated from laminated sediments (Figure 49) (i.e. $937 \text{ cm} \div 4,190 \text{ years} = 2.2 \text{ mm/year}$).

However, when using a date higher up in this core, from 169 cm, of 969 radiocarbon years (TO- 8672), the agreement is not as good, giving a sedimentation rate of 4.4 mm/year which is too high. By "adding" material missing from the top of this core however (Figure 48) the sedimentation rate would then be a little closer to the average calculated from the laminated sediments.

In general, there is very little compaction of sediments in the cores, and sedimentation rates are actually somewhat higher at the base of TUL99B03 than at the top (Figure 49). Compaction of sediments with depth therefore does not seem to be a factor in interpreting the radiocarbon dates. Therefore in general it appears that the radiocarbon age agreement with sedimentation rates calculated from the laminated intervals is only true if there is sediment missing from the tops of the cores. The

difficulty in coring the sediment-water interface, and the depth vs age plots of Figure 48, not passing through the origin, illustrate that this is probably true. Difficulty in sampling the sediment-water interface in the unconsolidated laminated sediments was also encountered in Saanich Inlet where up to 2 m of sediment was missing from piston core tops (Bornhold et al., 1998; Blais Stevens et al., 2001).

By transforming the depth vs age plot lines (Figure 48) to pass through the origin, the amount of sediment missing from each core can be estimated, and by applying the average sedimentation rate for each core, the time interval represented by the missing sediments can also be estimated. By using this method, between about 40 and 135 cm of sediment appears to be missing from the tops of the inner basin cores, and between about 20 and 100 cm of sediment is missing from the tops of the outer basin cores. These results appear on each plot in Figure 48.

By using the assumption that some sediment is missing off the tops of the piston cores, and applying the average sedimentation rates to the total lengths of the cores, then comparing the result to the radiocarbon dates, it is also clear that little sediment has been eroded and re-deposited outside of the basins by the sediment gravity flows. In the example above from 937 cm in TUL99B03 (TO- 8676), even at the base of the core, the radiocarbon age is in good agreement with sedimentation rates from the laminated intervals, indicating that even though the sedimentology of the cores tells us that

sediment gravity flows are occurring in the basin, they appear to be eroding and re-depositing material within the basins instead of transporting it elsewhere.

Removal of sediment by sediment gravity flows and density currents has no doubt happened at intervals throughout the cores however, particularly where it is difficult to “best fit” the depth vs age plot lines to a straight line (Figure 48, TUL99B13). However in general, the sediment gravity flows do not appear to have removed a substantial amount of sediment from the inner and outer basins. Conversely, any large amounts of sediment added to the basin, for example in the large massive intervals in the tops of the freeze cores and at the base of the piston cores has occurred infrequently enough that with variability in laminae deposition, over time, the sedimentation rate is about the same on average.

It should be noted that the depth vs age plot for the inner basin core TUL97A02 is somewhat anomalous compared to the other inner basin cores. By assuming a different best fit line however, not passing through the youngest date TO-8130, an average sedimentation rate equal to the inner basin average, 2.2 mm/year is the result. If this new line is used, it appears that about 300 cm of sediment may be missing from this core which would represent about 1500 years of deposition. The lithologies in this core also give evidence that TUL97A02 passed well into the sediment column and is sampling sediments older than those found in the other piston cores, since over a meter of distinctly deformed and overturned laminae occur in this core below about 750 cm (Figure 26).

This is a lengthy and distinctive sediment package, that is not recognized in any of the other piston cores, with the exception of in TUL99B03, beneath the large ungraded massive interval at the base of the core (Figure 26).

An explanation therefore for the TO-8130 date from TUL97A02, which appears to be “too young”, may be that because it was sampled from a piece of wood in the disrupted sediments near the top of the core barrel in section 1, it is possible that during coring, the wood may have been picked up from higher up in the sediment column and dragged down the side of the core barrel.

OUTER BASIN SEDIMENTATION RATE

It seems somewhat counter intuitive that the sedimentation rate for the outer basin is much higher than for the inner basin (average of 5.5 mm/year in the outer basin and 2.2 mm/year in the inner basin) since the largest drainage course, the Effingham River, empties into the inner basin (Figures 23 and 24). Rock-Eval plots show that the high organic content of the sediment (ave. TOC > 5 %), is mostly terrigenous in origin, which would suggest that sediment is entering the inlet directly from the land without being winnowed out along a river course. The steep sides of the inlet in the outer basin may therefore contribute somewhat to the higher amount of sediment entering the outer basin during frequent heavy rainfall events in the fall and winter, than might be expected from the two small un-named streams alone (Figures 12 and 23c). However, this does not

seem to fully explain a sedimentation rate in the outer basin more than twice that for the inner basin.

The braided channels of the Effingham River seem to indicate that the coarsest bedload has been deposited in the river's small flood plain before reaching the inner basin, indicating that the Effingham River, although its drainage basin is much larger than for the two un-named streams of the outer basin, is probably dropping most of its coarse sediment load on its flood plain during high discharge events and not into the inner and outer basins.

A larger fluvial influence than is evident in the Effingham Inlet sediments, was recorded in the Saanich Inlet sediments. The varves in Saanich Inlet were actually triplets, which included a clay layer of varying thickness attributed to flooding events of the nearby Cowichan River (Blais Stevens et al., 1997 and 2001). This type of lithic laminae associated with deposition of fluvial sediments is not evident in Effingham Inlet sediments. Although it is possible that some of the graded sediment gravity flows may represent major discharge events from the Effingham River, particularly those with sand at the base indicating a modified turbidity deposit, it is unlikely that the two un-named streams entering the outer basin would contribute more sediment than the Effingham River does to either the inner or outer basins.

The grain size analyses for both basins shows a fairly uniform silt grain size in the sediments (Figure 32), indicating that neither basin is receiving appreciably more coarse

lithic sediment than the other, which would be expected if one of the three drainage courses was contributing a greater proportion of sediment preferentially to either the inner or outer basin. If this is the case, the increased sediment load found in the outer basin is passing through the inner basin in suspension and settling in the outer basin. This is probably occurring somewhat for a very fine sediment fraction during high discharge events of the Effingham River.

An alternative explanation may be that sediment is entering the outer basin through Barkley Sound from the ocean. Evidence for an oceanward source of increased sediment in the outer basin comes from on-going sediment trap work in Jervis Inlet, B.C., on the west coast of Vancouver Island (Timothy, 2001). That study showed that increased settling fluxes of sediment were recorded in a trap positioned 50 m above the sea floor (in water depths of 600-700 m) which coincided with deep-water renewal events, as indicated by marked increases in dissolved oxygen in the bottom waters. It is speculated that these observations imply that renewal events (oxygenation events which occur in that inlet on a 2-4 year time-scale) are sufficiently turbulent to re-suspend bottom sediment up to 50 m above the bottom, or to carry sediment as a plume up-inlet and away from the sill, which is 240 m deep in Jervis Inlet (S. Calvert, pers. commun.); (Timothy, 2001).

Therefore, the most likely explanation for the much higher sedimentation rate in the outer basin is the re-suspension, transport and deposition of sediment by upwelled

ocean waters entering the inlet. The poorly laminated sediments of the outer basin, and evidence from the diatoms (M. Hay pers. commun.) and foraminifera found in the outer basin sediments (Schell and Dallimore, 2001) all indicate that the outer basin is usually dysoxic, or oxic as opposed to the normal condition of anoxia for the inner basin. The higher level of oxygen in the outer basin waters is also an indication of the higher incidence of oxygenated upwelled waters reaching the outer basin than the inner basin.

Although the velocity of these "density" currents entering the inlet appears to be very weak (R. Thomson, pers. commun), particularly in the inner basin where bottom currents traveling above 1 cm/sec have not been recorded, the convoluted laminae and flame structures evident in the inner basin sediment x-ray of Figure 46, show that upwelled dense water masses have erosive power even in the inner basin. The greater frequency of upwelling waters creating density currents along the bottom, in the outer basin, could then account for the higher sedimentation rate there.

PALEOSEISMICITY

The unlaminated massive muds of Saanich Inlet were interpreted as evidence of the periodicity of seismic activity in the area, and a return time of major seismic events for the area was thus posulated to be about 150 to 570 years (Blais Stevens et al., 1997 and 2001). The paleoseismic record in Effingham Inlet is somewhat more complicated however, since massive and graded muds can originate from either upwelling events or from sediment debris flows, possibly triggered by seismic shaking. The Effingham

record therefore does not show a consistent record of debris flows resulting in either graded or massive mud deposits, which are clearly the result of seismic shaking, on the return periodicity as seen in Saanich Inlet.

LARGE UNGRADED MASSIVE INTERVALS

The large ungraded, massive unit in the freeze cores however, gives us a modern analog for the expression in the sediments of a large seismic event affecting the Effingham Inlet area. On June 23, 1946, a large ($M=7.2$) earthquake, with an epicenter in east-central Vancouver Island, 75 kms to the northeast of Effingham Inlet (Rogers, 1980), shook Vancouver Island. Liquefaction of sediments, resulting in terrestrial as well as submarine landslides, was initiated on both coasts of Vancouver Island by the seismic shaking associated with this earthquake. The freeze core x-ray of TUL99B04 (pocket attachment) shows that the massive unit occurred about 50 years ago, by varve counting, and therefore, is probably the result of a large debris flow triggered by the 1946 earthquake.

It is known that the degree of sediment deformation observed can be related mathematically to earthquake magnitude and distance from the earthquake epicenter. It was observed for the 1946 earthquake, that sediment disturbance, including liquefaction and loss of strength in both terrestrial and submarine sediments, occurred within a 100 km radius of the epicenter, which is consistent with the empirical relationship between maximum epicentral distance of liquefied sediments and earthquake magnitude

(Kuribayashi and Tatsouka, 1975). According to this relationship, liquefaction of sediments can be expected within 110 km of the epicenter of a large ($M > 7$) earthquake, and Effingham Inlet is within this range at 75 km from the epicenter of the 1946 earthquake (Rogers, 1980). Therefore, we know what type of a sedimentary signature a large, $M > 7$, earthquake, occurring within the calculated maximum sediment liquefaction range from the epicenter of Effingham Inlet (110 km), will leave.

It would be interesting to take another freeze core in Effingham Inlet today after the recent February 2001, $M=6.8$ earthquake centered ~ 50 km from Effingham Inlet in Olympia, Washington, and observe any resulting disturbance to the upper laminated sediments of the freeze core. Although strong ground shaking was felt throughout Vancouver Island, landslides and submarine slumps were not reported, in contrast to their widespread occurrence across Vancouver Island after the 1946 earthquake.

An interesting observation by a bystander on a mountain overlooking Shawnigan Lake on Vancouver Island after the February 28, 2001 earthquake, was reported that day on CBC radio. The bystander reported that his attention was first drawn by concentric ripples in the central part of the lake, which spread outwards to the shore and which preceded perceptible ground shaking. This observation may mean that sediments in the center of deep basins may be more affected by seismic shaking than nearshore sediments, as they are affected sooner by the approaching seismic waves. Thus in the moderate to

large earthquake range ($M > 7$), the degree of disturbance in the sediments may depend not only on the distance from the epicenter but also on location in the basin.

Additionally, in the high rainfall zone of Vancouver Island, wet years or high rainfall events can lead to landslides and sediment instability. This might contribute to a degree of sediment slumping in a wet year or years, during which a moderate earthquake event occurs, which may not occur with the same magnitude of earthquake at the same epicentral distance in a drier year, or in a drier climate period (Evans and Gardner, 1989).

The second large massive interval in the cores, (Appendix F, 810 cm in TUL99B03), can also be interpreted as representing a large earthquake with an epicenter within 110 km of Effingham Inlet, since it is almost identical to the massive unit of the 1946 earthquake preserved in the freeze cores. The severely disturbed and “brecciated” laminations found beneath this interval also point to a significant ground shaking event which is not evident above in the sediment column, further evidence of a large seismic event in the vicinity of Effingham Inlet associated with this deposit. Water saturated silt can be transformed from a solid to a liquid with strong seismic shaking when pore pressure increases to the point that sediment grains do not support each other (Clague and Bobrowsky, 1999). The observed “smeared” appearance of varves in the base of TUL99B03 (Figure 43), and also in the lower sections of TUL97A02 (Figure 26), may be the result of liquefaction in the sediments, which would also attest to strong seismic shaking associated with deposition of the large massive interval at the base of the cores.

The many large pieces of wood within this debris flow probably indicate that sediment was also falling into the inlet from the surrounding steep shorelines during the seismic shaking. Commonly, terrigenous fragments are found in both the graded massive intervals and are very evident in the large massive intervals from the freeze cores and from the base of the piston cores. These sediments therefore probably come from either slumps from the land surrounding the slopes of the basin, and/or from sediment slumps of surface sediments in shallower parts of the basin. The deposits containing terrigenous fragments are often black in color indicating that their origin is either from the land or from oxygenated surface sediments in shallower areas of the basin. Landslides in general are probably not a significant source of terrigenous material in these large massive units, since landslide scars are not clearly evident on the shores of Effingham Inlet (Figures 12 and 24).

A characteristic thin (1 – 2 cm) light grey bed at the top of the large massive interval in both the freeze cores (Figure 30) and the piston cores (Appendix F, S7C4, ~ 924 cm) may also be associated with a particularly vigorous debris flow, resulting in their deposition. A similar light colored clay bed was often observed at the top of massive intervals in Saanich Inlet (Blais Stevens et al., 1997 and 2001) and was interpreted there to represent the settling of the finest particles out of suspension, after sediment disturbance by the deposition of a debris flow. It is probably from the same origin in Effingham and possibly contains very fine grained clays and diatoms resuspended by a

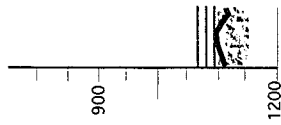
high energy debris flow. The characteristic waviness of the light grey bed may imply a current moving across the recently deposited sediments (O'Brien, 1996), which could also possibly be associated with disturbance of the normally tranquil water column of the inner basin, during and immediately following, the deposition of this unit. Disturbance in the basin waters may be a result of their oscillation in response to seismic shaking, an effect that was observed after the 1946 earthquake in inlets around Vancouver Island (Rogers, 1989).

The radiocarbon dates of the piston cores show that the event responsible for the deposition of the large massive interval at the base of the piston cores, occurred about 4,000 years ago. The buried peats of the estuaries in southwestern Washington record seven earthquakes over the last 3500 years, which is not a long enough record to see a signature of the interpreted seismic event of 4,000 years ago in Effingham Inlet. The precise paleoseismic record in Saanich Inlet also extends back only to about 3,000 y BP (Blais Stevens, et al., 2001). Therefore, the $M > 7.2$ earthquake of about 4,000 yBP recorded in the Effingham Inlet sediments (Figure 61), has perhaps not yet been detected in other paleoseismic proxy records of the west coast.

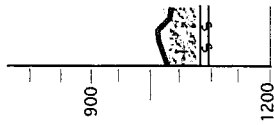
The great $M=9$ subduction earthquake that occurred on January 26, 1700AD with a modeled epicenter within about 100 km from Effingham Inlet, no doubt left its signature in the sediments, since the magnitude and epicentral distance put this earthquake well within the range of expected sediment liquefaction. A massive mud unit

Figure 61. Correlation of the large ungraded massive mud at the bottom of the piston cores of the inner basin.

B06



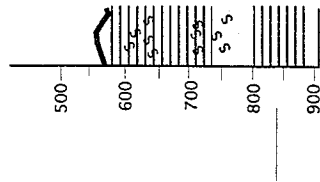
B13



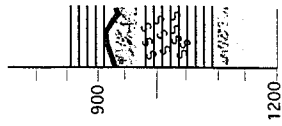
B03



A02



B03

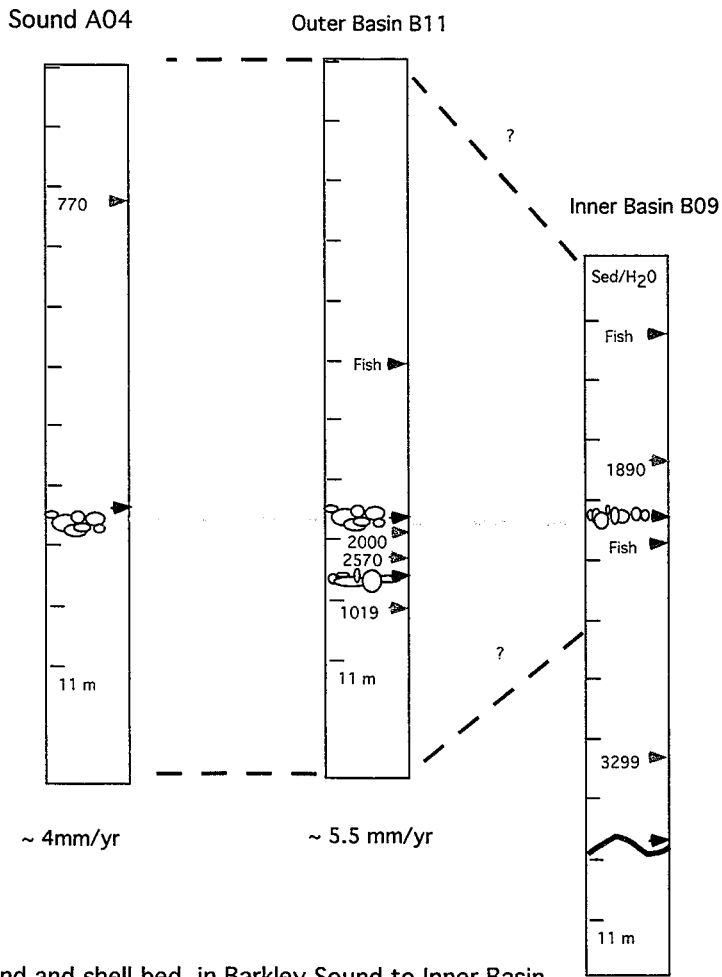


Legend

- Well laminated intervals of at least 20 cm.
- Poorly laminated intervals and small massive intervals.
- Massive interval > 20 cm.
- Disturbed laminations.
- Distinctive lt grey wavy mud layer.

Large massive interval capped by lt grey wavy mud layer at base of cores.

Figure 62. Correlation of the sand and shell bed from Barkley Sound to the inner basin.



Sand and shell bed in Barkley Sound to Inner Basin

~ 2.2 mm/yr

which could be associated with this event, does not appear at the top of the piston cores however. The amount of sediment calculated to be missing from the top of the piston cores, would explain its absence however. It does not appear as if sediments of 300 years in age have been sampled by any of the piston cores, except for possibly TUL99B13 (Figure 48). The piston core TUL99B13 may have sampled the sediments of this age, however, the wetness of the sediments in this core created convection in the core liner upon recovery, in both sections 1 and 2, and as a result any sediment structure in the top two sections of this core have been destroyed (Appendix E).

SAND AND SHELL BED

The sand and shell bed in about mid-core is found in all inner and outer basin cores except for TUL99A02, and also found in the Barkley Sound core (Figure 29 and 62). The bed is about 2 to 4 cm thick and consists of sand and some gravel as well as many shell fragments (Figure 40). However, instead of the gradual fining upwards defined by particle size, over 5 to 10 cm, as is common in the other graded beds of the cores, this bed consists of only a massive sand and is overlain by massive mud. The massive fabric of the sand bed is characteristic of rapid aggradation under a pervasive sand load which is settling out of suspension in a turbidity current traveling at high rates of speed (Arnott and Hand, 1989). This deposition mechanism is characteristic of a Bouma A division of a turbidite deposit, but the upper laminated and rippled sediments of the Bouma B,C, and D units are not present. The many shell fragments of the sand and

shell bed indicate that its origin is probably seaward (Clague and Bobrowsky, 1994b) as opposed to a turbidity flow from a flood event of the Effingham River.

It is possible that the basinwide distribution of this massive sand bed, its appearance as well in the Barkley Sound core and the shell content of the bed, indicate that it was deposited as the result of a tsunami. The tsunami wave possibly broke with its characteristic extremely high energy, along the shores of Barkley Sound, and/or traveled up the inlet with a sediment load of coastal glacial sand and gravel, to break at the head of the inlet in the marsh of the Effingham River. Tsunami deposits are common all along the western coasts of Vancouver Island and western Washington State, and are usually found landward in coastal areas as deposits of sheet sand. The distinctive tsunami deposit in coastal areas of western North America, consists of a massive sand, gravel and flotsam, and is sometimes deposited far inland (Clague and Bobrowsky 1994a and b; Atwater et al., 1995a and b, Benson et al., 1997).

The massive ($M = 9.2$) subduction earthquake which occurred in Alaska on March 28, 1964 (Plafker, 1969) sent a series of destructive tsunami waves up nearby Alberni Inlet, B.C., which also opens to the ocean on Barkley Sound, to the town of Port Alberni (Clague et al., 1994). Three main waves struck Port Alberni that night, resulting in waves up to 4.3 m in height and the sea surging onto the land for over a kilometer, at a velocity of about 50 km/hour. Parts of the town were completely destroyed, even though damage of this magnitude was not reported from other locations along the west coast of

Vancouver Island. It is speculated that the energy of the incoming tsunami wave was somehow oriented just at the right angle to travel up the narrowing Alberni Inlet, probably amplifying its energy in the process.

It has been calculated that the period of oscillation of the 1964 tsunami wave arriving at the mouth of Effingham Inlet, perfectly matched the natural period of oscillation for the inlet. In effect, the length and depth of the inlet were such as to set up a "1/4 wave resonator", so that a resonance condition took place, which greatly amplified the waves (Murty ,1997).

Upon examining the laminae in the x-ray of freeze core TUL99B04, no disturbance of the laminae occurring about 1964, or indeed in any time period between 1946 and the present day, is evident (pocket attachment). The tsunami of the great earthquake of 1700AD also left behind a sheet of sand in Port Alberni, even more widespread than the 1964 tsunami sand deposit, suggesting the massive size of the 1700AD earthquake. Thus it appears that although tsunami can affect this seismically active coast on a regular basis, the orientation to the sea of each coastal inlet, and the physical configuration of the inlet itself, will dictate which inlets receive the brunt of the wave energy.

It is therefore possible that the sand and shell bed found throughout Effingham Inlet, which is dated about 2,000 years ago is the result of a tsunami, probably coming from the southwest, since the 1962 tsunami originating in Alaska approached from the

northwest and did not appear to affect Effingham Inlet. If the Effingham sand and shell bed does represent a tsunami deposit, it could be associated either with a seismic event along the tectonically active North American coast, or to a seismic event across the Pacific in the seismically active areas of the southwestern Pacific Ocean.

We know from Japanese historical documents, and modelling, that a tsunami resulting from the June 1700AD great M~9 Cascadia subduction zone earthquake just offshore Vancouver Island, took only 10 hours to cross the Pacific and pile up on the Pacific shores of Japan. According to North American native oral traditions, coastal villages of aboriginal peoples from California to the west coast of Vancouver Island in North America were also devastated by this tsunami, and it appears that waves of 20 m in height were experienced in some North American bays and inlets as the result of the seismic disturbance associated with that earthquake (Clague and Bobrowsky, 1999).

Clague and Bobrowsky (1999) speculate that a large (M>7) earthquake occurred in the Vancouver Island area between 2800 and 2400 years ago and Blais-Stevens et al. (2001) speculate that large earthquakes maybe responsible for debris flows in Saanich Inlet dated at 1,800, 2,200 and 2,220 y BP. Any of these interpreted events could be associated with the Effingham sand and shell bed, when the error ranges of the radiocarbon dates are taken into consideration.

Return times for large (M>7) earthquakes have been speculated at anywhere between 100 to 570 years (Blais-Stevens et al., 1997 and 2001; Clague and Bobrowsky,

1999). The return time of massive $M > 9$ subduction plate earthquakes, such as the one in 1700AD, has been speculated as recurring on average every 500 years, but with a range of anywhere between 200 years to 1300 years (Clague and Bobrowsky, 1999). If this is true, the Effingham sediments should contain evidence of more than two great earthquake events in the last 4,000 years. If the 1700AD earthquake is expressed in the Effingham Inlet sediments, but is missing in the piston core tops due to overpenetration, then it appears that a return time for a large $M > 7$ earthquake with an epicenter within 110 km (to affect soil and sediment disturbance and liquefaction) is about twice every 4,000 years. A similar large seismic event also occurred elsewhere at about 2,000 y BP however, if the sand and shell bed is representative of a tsunami, yet far enough away from the inlet to leave sediments undisturbed.

This does not mean that the return time of large earthquakes is disproved by the Effingham Inlet sediment record however. The Effingham paleoseismic record is obscured and/or masked by the massive intervals representing oxic conditions resulting from strong upwelling events. It is also possible that large earthquakes occurred somewhere along the Cascadia subduction zone during the last 4,000 years, but outside of the 110 km epicentral distance of sediment liquefaction, and therefore did not leave a signature in the Effingham Inlet sediments.

CLIMATIC INTERVALS

Upon first examinations of the x-rays of the Effingham Inlet cores, it was immediately apparent that below about 820 cm of inner basin core TUL99B03, the laminations are remarkably uninterrupted by massive intervals, with the particular exception of the large massive interval, which we have interpreted as related to a single event in time, and a smaller graded massive unit just below it (Appendix F, S8C6,C7, ~ 1100 cm) which also probably represents an instantaneous debris flow event. There is no evidence of ungraded massive muds representing periods of oxygenation of the inlet below ~ 820 cm in TUL99B03 (Appendix F, S6C7) which represents a radiocarbon time of about 4,000 years ago.

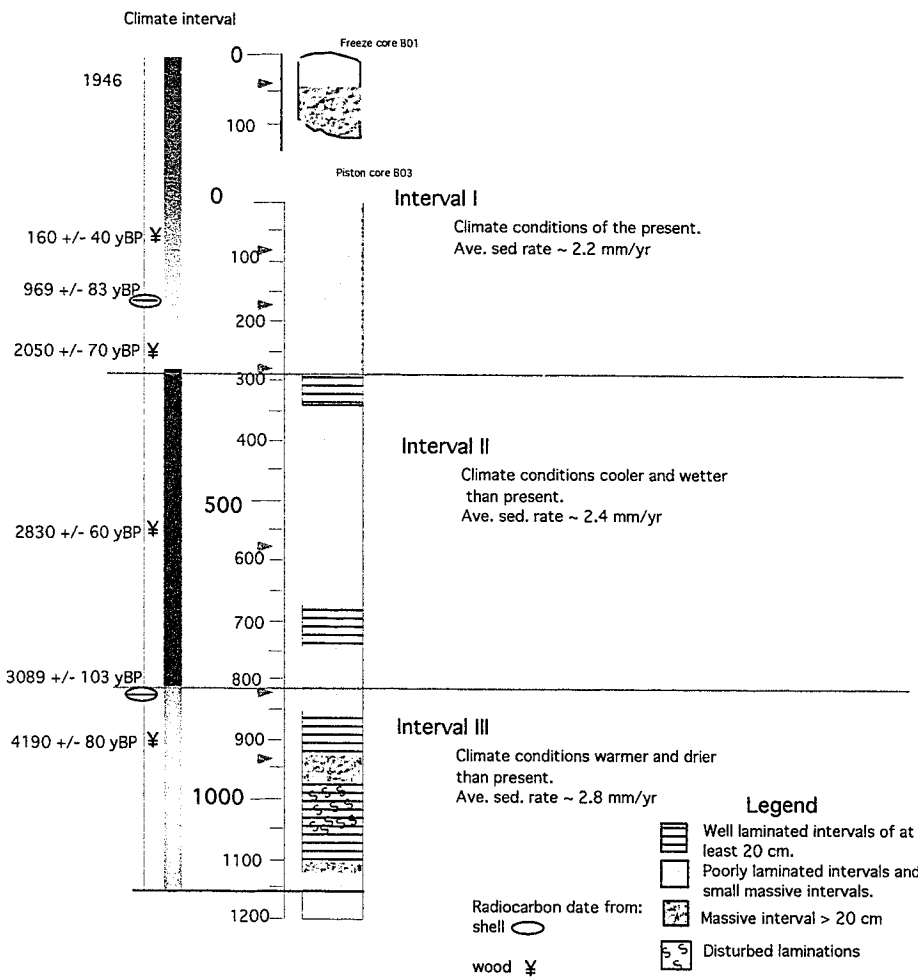
A climate interval warmer and drier than today's is well defined in the pollen record of western Vancouver Island, and occurred about 4,000 years ago (Hebda, 1995). Similarly, a less distinct, qualitative change in the lithological character of TUL99B03, easily seen in an x-ray composite of that core (pocket attachment) occurs at about 300 cm, which represents about 2,000 radiocarbon years before present. This time coincides with another shift in climate state defined from the pollen record, from a period much cooler and wetter than today's from about 4,000 to 2,000 y BP, to today's climatic conditions. The inner basin core TUL99B03 sediments therefore can generally be qualitatively matched to Hebda's (1995) western Vancouver Island climate states interpreted from the pollen record as follows (Figure 63).

- 1) Interval I: Present day to ~2,000 y BP, present climate conditions. Poorly to well laminated muds. Anoxic/dysoxic conditions, infrequent oxic conditions.
- 2) Interval II: ~ 2,000 y BP to ~4,000 y BP, cooler and wetter climate conditions than today. Frequent massive, ungraded and graded mud intervals, poorly to well defined laminations, usually less than 10 cm in length. Frequent oxic conditions alternating with anoxic/dysoxic conditions.
- 3) Interval III: ~ 4,000 y BP and older, warmer and drier climate than today. Well laminated sediments, no short graded or ungraded massive mud intervals, interrupted only by one large massive interval and a moderately sized graded mud just beneath it. Anoxic conditions.

The sedimentation rate in the outer basin is more than twice the sedimentation rate for the inner basin and therefore these climate intervals, and qualitative lithological divisions, are not clearly evident in the sediments of the outer basin core TUL99B11 (Figure 64 and pocket attachment). The outer basin core sediments were probably all deposited within the interpreted climate Interval I (Figure 65).

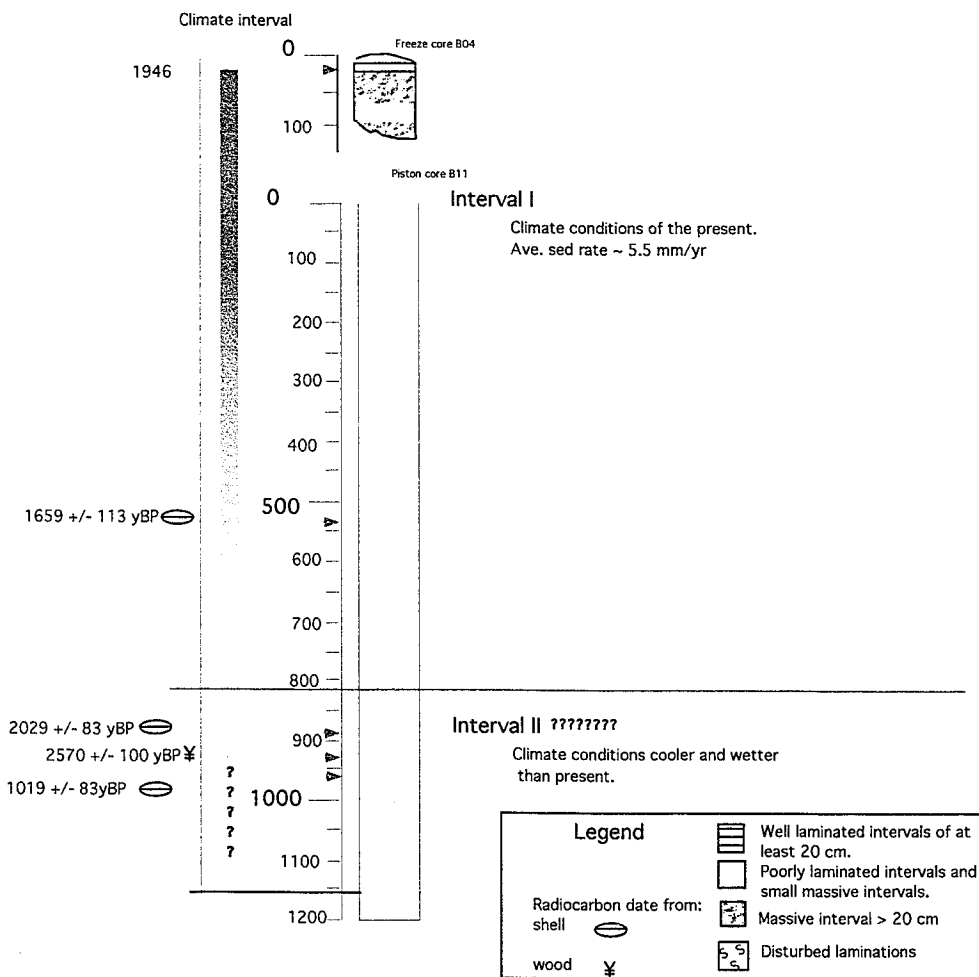
These three climate intervals, which appear to be represented in the sediments of the inner basin, would offer an explanation for the observed pattern of lithologies.

Figure 63. Climate intervals in inner basin core TUL99B03.



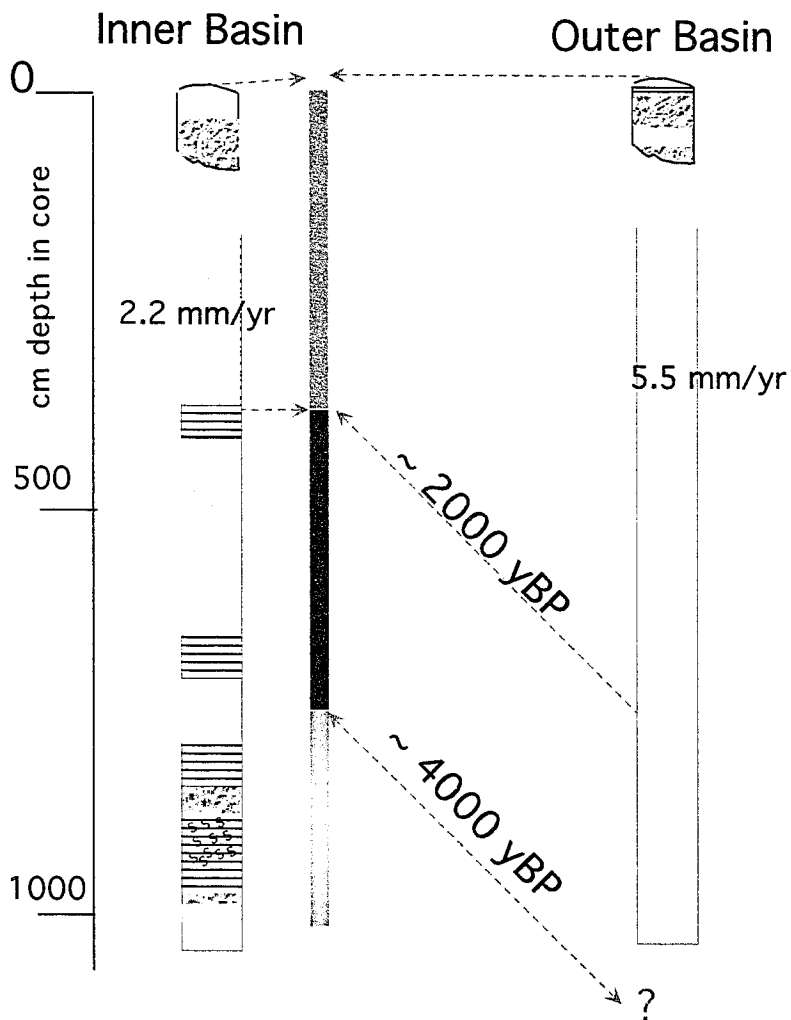
Inner basin sedimentation, from piston core B03 and freeze core B01.
Sedimentation rates calculated from laminated sections only

Figure 64. Climate intervals in outer basin core TUL99B11.



Outer basin sedimentation, from piston core B11 and freeze core B04.
Sedimentation rates calculated from laminated sections only

Figure 65. Sedimentation rates and climate intervals for inner and outer basins.



Comparitive sedimentation rates, inner and outer basins.

Frequent oxygenation events in Interval II for example, interpreted from ungraded massive intervals, would be expected with higher precipitation during the cooler and wetter climate conditions of that interval. Increased precipitation and run-off, would create a thick freshwater wedge in the upper water column of the inlet, which in turn would increase the stability of the water column, allowing dense upwelled waters to enter the basin. This apparent expression in the sediments of subtle changes in the local climate, gives an indication of the utility of the Effingham Inlet sediments for high-resolution palaeoenvironmental studies.

It should also be noted that an alternative explanation for the apparent persistent anoxia of the inner basin after about 4,000 yBP, could also be a physical isolation of the inlet during a lower sea-level stand. The inner basin sill is only 40 m depth and post-glacial sea levels on Vancouver Island have fluctuated rapidly, by as much as 85 m in less than 1,000 years during deglaciation (Clague, 1989d). It is therefore not impossible that at about, 4,000 y BP, the inner basin was isolated by an exposed, or nearly exposed sill during a lower sea level stand than today's. This scenario is not likely however according to the poorly known sea level history of this area. The evidence from the nearby Tofino area just to the northwest of Effingham Inlet, is that sea level has been dropping from a higher stand since about 4,000 y BP to present sea levels (Clague et al., 1982). The sea level history of this coastline however is very complex and poorly understood, so a physical isolation of the inner basin from the ocean cannot be discounted

as an explanation for the persistent anoxic conditions prior to 4,000 y BP, and would weaken the hypothesis that climate conditions before about 4,000 yBP were warmer and drier than today's, creating conditions of persistent anoxia in the bottom waters of the inlet.

OCEANOGRAPHY

The most outstanding feature of the time series Effingham Inlet oceanography data is the profound effect on the physical characteristics of the inlet waters of the oxygenation event by upwelled waters in 1999. This disruption of normal anoxic/dysoxic conditions to colder, oxygenated bottom waters in the inner and outer basins is attributed to a very strong El Niño event in the southern Pacific which took place from February, 1997 to about March, 1998, and resulted in oxygenation of the bottom waters of Effingham Inlet sometime in the late fall of 1998. This Pacific-wide disruption has been referred to as the Pacific event of the century (. Thomson, pers. commun.), and indeed, the undisturbed laminations of the freeze core indicate that oxygenation events of the inlet have been extremely brief, or absent since at least 1946.

The mechanisms affecting the upwelling events creating deepwater oxygenation in Effingham Inlet appear to be the following.

- 1) Strong coastal winds: The major upwelling events of January and June 1999 were preceded by strong ($> 0.2 \text{ N/m}^2$) persistent NW wind events along the coast (Figure 57).

- 2) A stratified water column in the inlet: High precipitation and runoff stratifies the upper layer of the water column (Figure 55), inhibiting vertical turbulent mixing and allowing deep water masses to advect into the basins along the bottom, under a stable stratified water column. In contrast, weak stratification permits turbulent mixing which acts as a barrier preventing deep water intrusions at the sills.
- 3) Weak (neap) tidal currents. Shear-induced mixing is minimal during weak neap tidal currents which allows cold, saline and therefore dense upwelled water to slide over the sills beneath a highly stratified water column. During strong (spring) tides, mixing is more intense and the mean density of the intruding bottom water is decreased, inhibiting flushing of the basins.
- 4) "Preconditioning": Vertical diffusion over time and weak turbulent mixing (highly stratified waters) within silled basins gradually lowers the density of deep and intermediate waters, preparing, i.e. "preconditioning" basin waters for flushing by more dense intrusive water from the open ocean.

These conditions, which combine during the occurrence of an upwelling event, which oxygenates the bottom waters of the inner basin, seem to be in delicate balance. It is probably a subtle interplay of these conditions, combined with a very strong oceanic event such as the El Niño of 1997-98, that allows oxygenated waters into the inlet in the present day. However, as the numerous oxygenation events interpreted from the sediments of Interval II in core TUL99B03 (Figure 63) would indicate, the high levels of

precipitation during an interpreted cooler and wetter climate interval, may have been the driving force for oxygenation of the inlet from 2,000 to 4,000 years ago, due to the increased stability of the water column during high rainfall years. This annual high precipitation probably somewhat masks the 2 to 8 year ENSO event more evident perhaps in Interval I and Interval III of the cores, where laminated sections are less frequently interrupted by years of high rainfall and/or ungraded massive muds representing periods of oxygenation. The higher frequency of graded muds in the Interval II of the cores also indicates that sediment instability is greater during years of high rainfall in Effingham Inlet.

A high-resolution cyclostratigraphy study of the digitized x-rays of sediments of the inner basin piston core TUL99B03, is on-going and the results of that study will contribute to the interpretation of the ocean and climate conditions such as the ENSO signal, that are cyclically affecting Effingham Inlet over time.

BASIN CORRELATION

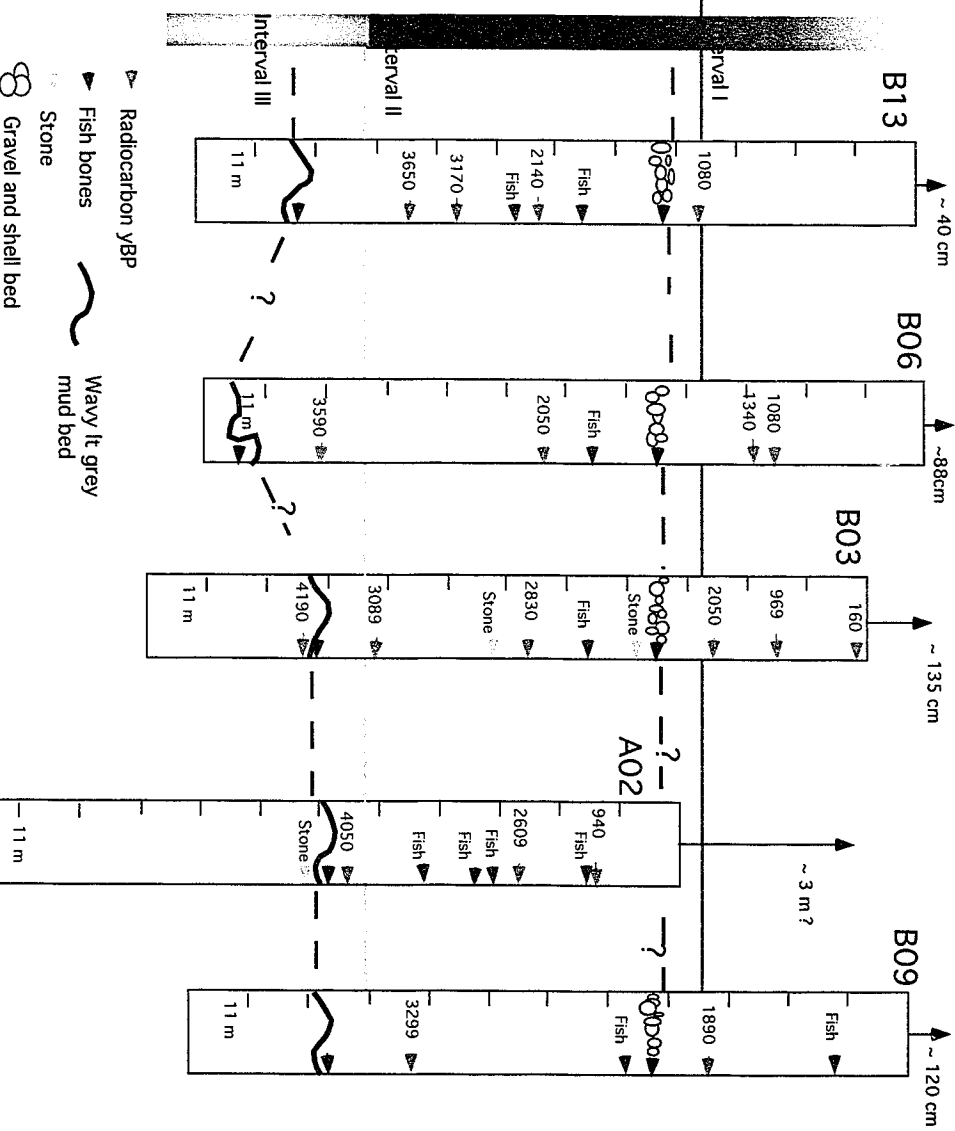
Stratigraphic markers are scarce in the cores of Effingham Inlet complicating core correlation across the inner and outer basins. The large massive interval at the base of the cores, which is capped by the wavy light grey mud bed, is evident in all of the inner basin piston cores, with the exception of TUL97A02, which contains the wavy bed but not the large massive interval. Sediments beneath this wavy marker in TUL97A02 however, are severely disturbed, for a meter or more, as they are in TUL99B03 beneath the large

massive interval, indicating that this wavy light grey bed is probably the same one found in the other cores, and can be used as a stratigraphic marker in core TUL97A02.

A second basin-wide recognizable stratigraphic marker is the shell and sand bed which is also found in all the cores including the Barkley Sound core, except for the inner basin core TUL97A02. However, if TUL97A02 is correlated to the other cores by the wavy light grey mud layer, it appears that TUL97A02 is so deep in the sediment column that it has overshot the sand and shell bed, explaining its absence in this core even though it is evident in the cores on either side of it in the same basin. Difficulty in retrieving this core (see Results) and also the presence of highly deformed laminations in the bottom of this core for several meters in section 5 of the core (Figure 26), the top of which are also evident below the large massive interval in TUL99B03, also seem to suggest that sediments older than the other piston cores have been penetrated by TUL97A02. As previously suggested, by reconstructing the depth vs age line in Figure 48 (by discounting TO- 8130 which seems to be “too young”) to match an average sedimentation rate of 2.2 mm/year in the inner basin, it could be calculated that about 300 cm of sediments are missing from the top of TUL97A02, which would place it in stratigraphic position below the sand and shell bed, thus explaining its absence in this core.

By hanging a cross section from a datum of the sand and shell bed in the inner basin, which may represent a moment in time, (Figure 66) a picture of the depositional history of the basin from the lithologies of the piston cores begins to emerge. The cross-

Figure 66. Basin correlation of inner basin cores.



section seems to work fairly well stratigraphically, however, the radiocarbon dates, particularly for TUL97A02 are not as neatly in co-ordination across the basin. This could be explained however, by the discounting of date TO-8130 from TUL97A02, as discussed above(Radiocarbon, Results), and by taking into account the difficulty in using radiocarbon dating for an accurate geochronology of the sediments in Effingham Inlet. As previously discussed, some of the dates from Effingham Inlet have error ranges of up to several hundred years associated with them (Table 2).

The fish skeletons found on the bedding planes and the dropstones found in the cores seem to fall within the climate Interval II (drawn from core depths in TUL99B03, determined from x-rays), on the cross section of the inner basin cores (Figure 66). This would appear to make sense since the fish skeletons may represent fish kill events, when the inlet floor would be littered with fish skeletons, increasing the chances that the core barrel will pass through one of them. Interval II is during the time that frequent upwelling events are advecting oxygenated waters into the inlet on a regular basis, forcing the anoxic waters upwards into the biotic zone, possibly resulting in the higher incidence of the fish skeletons in Interval II of the cores.

The few dropstones found in the cores also fall within Interval II(Figure 66) which would mean that the incidence of a thick freshwater wedge freezing over during particularly cold winters was higher in Interval II. Higher precipitation and a climate somewhat colder than today's, during Interval II, would explain the dropstones in this

interval of the core since these conditions would be conducive to freezing over of at least the inner basin. Freezing of inlets of Vancouver Island today is uncommon, although not completely unheard of (D. Ware, pers. commun).

The correlation of Figure 66 is somewhat satisfying when all the evidence is taken into consideration, but does not completely explain stratigraphic relationships and radiocarbon dates. This is perhaps to be expected in an inlet where lateral variability in deposition is affected by bathymetry, character of the surrounding and nearby sediments and radiocarbon dates are taken from floating wood and marine material. This same difficulty in lateral correlation was experienced in Saanich Inlet as well, even though a clear datum of the Mazama ash was evident as a distinct stratigraphic and chronological marker. In Saanich Inlet, sedimentation rates and incidence of massive units was dependent on location in the inlet as well (Matis Stevens, et al., 1997 and 2001).

For our purposes however, the cross section of the inner basin does illustrate once again the complex and detailed depositional history of Effingham Inlet, which is closely related to variability in climate, ocean and also tectonic conditions.

FISH SCALES

At a 25 year sampling interval from a composite of three, 6.5 cm diameter piston cores, Tunnicliffe et al. (2001) were able to define centennial scale changes in the fish population of Saanich Inlet from the sedimentary fish bone record. O'Connell and Tunnicliffe (2001) were able to further refine the Saanich fish populations analysis to a

40 to 60 year scale based on the sedimentary fish scale record sampled on a 2 year interval, from a large volume box core representing deposition of the last 150 years. Our data seem to show some variability on a centennial and millennial time scale (Figure 60). However, due to our 21 year average time interval represented by the volume of sediments in each sample which was required to obtain a sedimentary fish scales record from the piston core, we are not able to resolve decadal or annual variability in the paleo-fish populations of Effingham Inlet. Our small volume piston core study does however, seem adequate to discern broad variability in paleo-fish populations on a centennial and millennial scale.

For example, a simple statistical treatment of determining means for the total fish scales counts for the three climate Intervals I,II and III, defined from the sediments in Effingham Inlet, shows that there may be a relationship to fish population cycling and climate/ ocean cycles in Effingham Inlet (Figure 67).

Fish scales and bones are not as reliable for paleoenvironmental, and species population studies, as for example foraminifera are in the marine environment (Patterson,1993, Patterson et al., 1998 and 2000) and thecamoebians (arcellaccans) are in the freshwater environment (Medioli and Scott, 1988; Dallimore et al., 2000). Testate protozoa such as foraminifera and thecamoebians, leave a substantial number of remains in very small volumes of sediments, are cosmopolitan and can be linked with specific environmental conditions. The same level of interpretive accuracy cannot be obtained

using fish scales and bones as proxies for either paleoenvironments or an accurate idea of paleofish populations, due to the following considerations.

- 1) Scale shedding (highly deciduous) species such as herring and hake, give a taxonomic bias in the record towards these cartilaginous fish (O'Connell and Tunnicliffe, 2001).
- 2) Schooling behavior may be responsible for an over-representation in the record of schooling fish. We see this in our data, with more than twice as many juvenile herring found, as adult herring. Herring school in the juvenile and not the adult phase, creating this over-representation in the data of juvenile herring scales (C. Wright, pers. commun.).
- 3) The sedimentary fish scale record must also be interpreted in light of trophic relationships. For example, dogfish prey on herring, which in turn prey on hake. It would therefore be expected that these fish would be represented together in the record, yet at relative abundances that reflect their positions in the food chain. This factor may be complicated however by the habits of each species, whether they are resident in the inlet, or if they merely feed there (C. Wright, pers. commun.).
- 4) Scale shedding behavior must also be considered. In fact some taxa actually use scale shedding as a defense mechanism. An entire school of herring for example

may shed scales when they are under attack to confuse the attacker (O'Connell and Tunnicliffe, 2001).

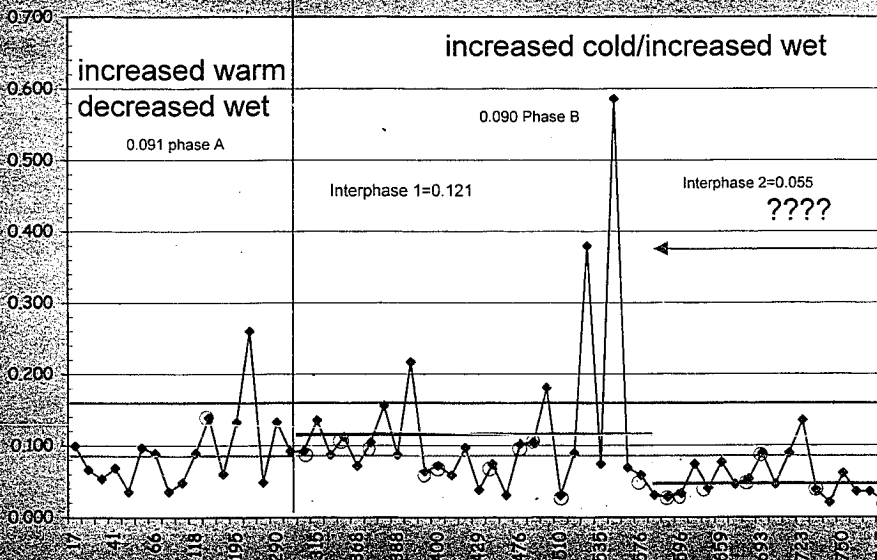
- 5) Fish kills and individual fish skeletons may confuse the record. This is especially true in an anoxic inlet such as Effingham, when advecting of upwelled waters into the inlet along the bottom, can displace low-oxygen bottom waters upward into the biotic zone, initiating catastrophic fish kills, which send many fish skeletons into the record at an instantaneous moment in time (Pickard and Emery, 1990).
- 6) The chemical composition of scales varies from species to species, which affects the thickness and structure of scales. For example, hake scales are thicker than herring and therefore may show enhanced preservation in the record (O'Connell and Tunnicliffe, 2001).
- 7) It is not yet known how accurately a sedimentary fish scale assemblage represents a living fish population (Tunnicliffe et al., 2001).
- 8) It is not well known what the mechanism of transfer of primary productivity is through the marine food chain, to fish. Hence it is difficult to directly infer what the effects of variable climate, ocean, upwelling and paleo-productivity conditions are on fish populations (Ware and Thomson, 1991).

All of the above notwithstanding however, this study shows a cycling of fish populations over broad century and millennial time scales. Additionally, the data shows important presence or absence of certain species, such as the sardines, over time, even

Figure 67. Fish scales and climate intervals with depth, from inner basin core

TUL99B03.

#scales/cm3



increased warm
decreased wet

increased cold/increased wet

0.091 phase A

0.090 Phase B

Interphase 1=0.121

Interphase 2=0.055

????



#scales/cm3

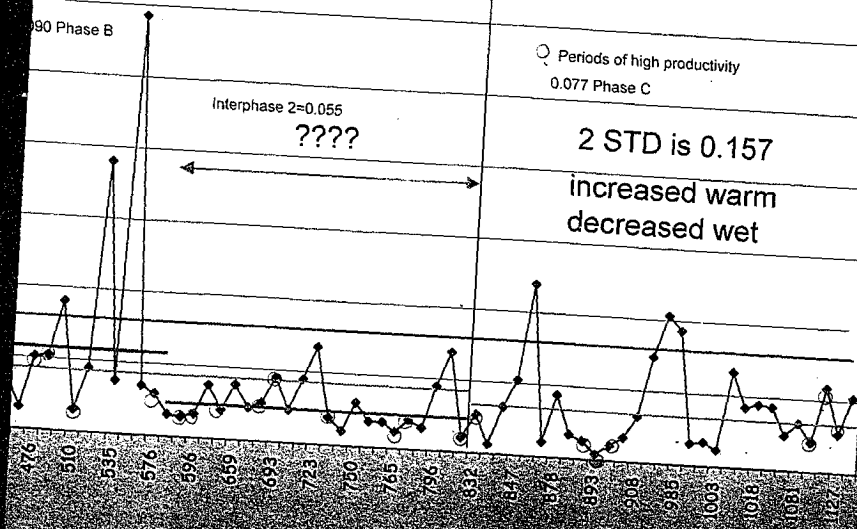
Increased cold/increased wet

90 Phase B

○ Periods of high productivity
0.077 Phase C

Interphase 2=0.055
????

2 STD is 0.157
increased warm
decreased wet



before commercial fishing occurred in the Effingham Inlet area. The cycling of sardine populations before humans were fishing commercially along this coast also gives a natural context to the progressive commercial sardine fishery collapses and recoveries of the last sixty years (Francis and Hare, 1994) along the west coast of North America.

Although it is the collapse of the lucrative salmon fishery that receives the most popular media attention, salmon are not well represented in the sediment record, which is illustrated by the absence of salmon scales in the Effingham Inlet sediments. This is because salmon scales are not deciduous and their scales biodegrade quickly once they reach the sediments (C. Wright, pers. commun.). The studies from Saanich Inlet of O'Connell and Tunnicliffe, (2001) and Tunnicliffe et al. (2001), also noted the almost complete lack of salmon scales and bones in the record even though salmon populations inhabit Saanich Inlet. Therefore, fluctuations in salmon populations have to be inferred from climate and ocean records (Glavin 1999; Finney et al., 2000), as well as from the pelagic fish populations whose scales preserve in the record.

The marked decrease in the sedimentary fish record in the last 1,000 years reported here from Effingham Inlet (Figure 60), and also from Saanich Inlet (Tunnicliffe et al., 2001) and Santa Barbara Basin (Baumgartner et al., 1992) gives an indication that oceanic conditions are affecting fish populations over the entire North American upwelling regime, and that a basin-scale oceanic signal affecting marine ecosystems is strong enough to transcend the limitations of sedimentary fish scale techniques.

A longer and larger volume piston core, as well as future studies in adjacent inlets, would contribute to the refinement of techniques for using sedimentary fish scales and bones to reconstruct past fish populations of the northeastern Pacific throughout the Holocene. Although our study resulted in a detailed description of the climate and oceanographic history of Effingham Inlet throughout the late Holocene, we were not able to directly link the sedimentary fish scales records to ocean and climate conditions. Clearly however, fish populations as well as ocean and climate conditions are cycling on local and regional scales spatially, and centennial and millennial scales temporally, in Effingham Inlet and also along the entire North American coastal upwelling regime (Baumgartner et al., 1992; Thomson and Gower, 1998; Tunnicliffe et al., 2000).

To further our knowledge of paleo-fish populations, we must now look towards a refinement in the understanding of the chain of events leading from a change in climate and ocean conditions, to changes in populations over time of the fish species that preserve in the sedimentary record of anoxic basins. Understanding this apparently complex link between marine environments and pelagic fish populations, will help us to relate our knowledge of the climate and ocean conditions of the past, interpreted from the detailed sedimentary records found in anoxic basins such as Effingham Inlet, to the sedimentary record of paleo-fish populations.

CONCLUSIONS

The detailed sediment record of Effingham Inlet, Vancouver Island, B.C., gives a high-resolution account of the geologic, oceanographic and climate history of both the inlet and the southwest coast of Vancouver Island, throughout the Late Holocene. It would be impossible to interpret the sediment record preserved in Effingham Inlet without considering the combined effect that geologic, tectonic, oceanographic and climatic processes have on depositional conditions. The fish scales data further shows us that ecosystems of the inlet also respond to the changing interplay between these processes, which operate on time scales from seasonal to millennial. Although some of the cause and effect links between these processes remain somewhat mysterious, the following conclusions can be reached from this study.

GEOLOGIC

- 1) The laminated diatomaceous muds are preserved free of destructive bioturbation under anoxic depositional conditions. Variable thickness of the diatomaceous laminae represents the remarkable variability in intra- and inter-annual phyto-plankton productivity.
- 2) Massive muds are interpreted to be the result of the re-suspension and re-deposition of laminated muds by low velocity density currents entering the inlet from the ocean; and/or are the result of bioturbation under low oxic or oxic conditions. In either scenario, the ungraded muds represent oxygenation

(flushing) of the bottom waters of the inlet by upwelled cold, saline and therefore dense oxygenated ocean waters advecting over the sills and into the inlet.

- 3) The graded mud deposits which may contain fine sand, are interpreted to be the result of debris flows initiated by sediment slumping of the sides of the inlet, and possibly also of small turbidity flows generated by higher energy debris flows from major sediment slumps. Turbidity flows carrying sediment loads from discharge events of the Effingham River are unlikely. Sediment slumps are probably initiated by seismic shaking, and/or sediment instability which appears to be more pronounced during climate intervals of high precipitation.
- 4) Sediment of the inlet reaches the bottom mostly through suspension settling through the water column, of diatom frustules and organic rich terrigenous fragments and fine lithic particles. Sedimentation rates are on average 2.2 mm/year in the inner basin and 5.5 mm/year in the outer basin. Most of the organic content of the sediment comes from terrestrial sources, despite the high marine phytoplankton sediment content. Much of the terrigenous sediment appears to enter the inlet directly from the sides of the basin, and the four small drainage courses during heavy rainfall events. However, a substantial amount of sediment, representing a doubling of the annual

sediment load to the inner basin, reaches the outer basin suspended in water masses traveling up the inlet from Barkley Sound.

- 5) Two lengthy (> 40 cm) ungraded massive mud deposits containing many terrigenous fragments, are interpreted as the result of debris flows resulting from submarine sediment slumping, and perhaps minor landslides, initiated by; the June, 1946, M=7.2 earthquake, and ; another earthquake of similar magnitude with an epicenter within a 110 km radius of Effingham Inlet, about 4,000 years ago. Apparently, no other major seismic event (discounting the 1700 AD earthquake not recorded in the sediments due to overpenetration of piston coring) has disturbed the sediments within that time, within a 110 km radius, which is the maximum epicentral distance for sediment liquefaction for an M=7 earthquake, determined empirically. However, it is probable, according to the known periodicity of major earthquakes in this region, that many major seismic events have occurred nearby during the last 4,000 years, initiating slumping in Effingham Inlet that resulted in smaller deposits of graded muds, yet they occurred outside of the 110 km epicentral radius of sediment liquefaction, and therefore significant sediment disturbance, for a major (M>7) earthquake.
- 6) An ungraded sand deposit which appears in the cores from Barkley Sound to the inner basin, was deposited about 2,000 y BP, and is interpreted to be the

result of a tsunami traveling up the inlet. The tsunami may have been initiated by a major earthquake, occurring outside of the 110 km sediment liquefaction radius, or perhaps anywhere along the seismically active Pacific Rim. An historical tsunami affecting Barkley Sound and nearby Alberni Inlet in March, 1964, did not disturb the sediments in Effingham Inlet and therefore it appears that orientation to the coast, of the mouth of a coastal inlet, and the physical configuration of the inlet itself, determines the effect an in-coming tsunami will have on the inlet.

- 7) Sea level history of the area is poorly known but the continuously laminated sediments older than 4,000 years may indicate a lower sea level, effectively isolating the inner basin from ocean waters at that time.

OCEANOGRAPHIC

- 1) In the present day, the inner basin is normally anoxic at depth and the outer basin is normally anoxic/dysoxic at depth.
- 2) In rare circumstances upwelled, oxygenated, cold and saline waters can enter the inner and outer basins if the following conditions exist together; an ENSO event strong enough to affect the northeastern Pacific Ocean, strong and sustained coastal winds from the northwest, a stratified water column intensified by run-off and precipitation, weak (neap) tidal currents and decreases in the density of deep and intermediate inlet waters by vertical diffusion over time.

- 3) A strong upwelling or "flushing" event, which oxygenated the waters of the inlet, was recorded in 1999 following a strong El Niño event of 1997-1998. No other strong or sustained flushing event is recorded in the sediments of the inlet from the present day to 1946, when the record is obscured by a debris flow deposit. After a flushing event, high sedimentation rates and organic decomposition return the basins to their normal anoxic/dysoxic conditions within a matter of months.
- 4) A higher incidence of flushing events between about 2,000 and 4,000 years ago may mean that freshwater run-off, effectively intensifying the water column stratification, may have been the determining factor allowing ocean waters into the inlet more frequently, during a climate interval of higher precipitation than today. An increased frequency of sustained northeast winds offshore during a colder climate interval may also have prevailed during that time.
- 5) The complete absence of flushing events prior to 4,000 y BP may mean either that the climate was substantially drier than today's and/or that changes in coastal winds, driven by changes in the Pacific Aleutian Low and North Pacific High atmospheric systems, altered the coastal current regime, preventing upwelled ocean waters from entering the inlet. Due to the shallow (40 m) inner basin sill however, more information about the sea level at that time is needed to conclusively interpret oceanic conditions prior to 4,000 years ago.

CLIMATIC

- 1) The variability in the deposition of laminated sediments, and the frequency of massive intervals intercalated within the laminated sediments, allows a qualitative climatic division of the sediments, which corresponds to the pollen record for this area. In climate Interval I, mostly laminated sediments were deposited from the present to about 2,000 y BP, indicating stable climatic conditions and brief, infrequent flushing events. In climate Interval II, laminated sediments are interrupted frequently (every 20 years or less) by massive and graded muds, deposited from about 2,000 to 4,000 y BP, indicating common flushing events and sediment instability, representing a climate interval cooler and wetter than today's. In climate interval III, well laminated sediments deposited prior to about 4,000 y BP, are only interrupted twice, by two debris flows associated with seismic shaking, and indicate a climate warmer and drier than today's.
- 2) The presence of dropstones in climate Interval II indicates that the inlet can freeze over during high precipitation seasons, which were common in that climate interval.
- 3) The presence of fish skeletons in the sediments of climate Interval II, may represent vigorous flushing events that displace anoxic waters upwards into the

biotic zone and initiating fish kills, once again indicating a climate interval of high precipitation leading to more frequent flushing events during that time.

PALEO-FISH POPULATIONS

- 1) Fish scales and bones are well preserved throughout the Effingham Inlet cores.
- 2) The use of sedimentary fish scales to interpret paleo-fish populations has a number of limitations, due to an incomplete understanding of, fish ecology, how a sedimentary fish scale assemblage directly relates to a living population and the mechanism of transfer of primary productivity through the marine food chain.
- 3) Sardine populations appear to have been cycling prior to commercial sardine fishing.
- 4) Total pelagic fish populations appear to have been cycling throughout the 4,000 years represented in the Effingham Inlet cores, however, how the fish population cycles relate to climate and ocean conditions is as yet, unclear.

This study has shown that complex, dynamic and subtle interactions between depositional, tectonic, oceanographic and climatic conditions, combine to form the rich geologic record preserved in the sediments of Effingham Inlet. We have barely opened the door on the library of information preserved in them. Hopefully the study results presented in this thesis, will form a foundation for on-going and future studies of these

sediments, which will reveal ever more detailed information about the evolution of the

Pacific North American coast, marine ecosystems, ocean and climate.

REFERENCES

- Adams, J., 1990. Paleoseismicity of the Cascadia subduction zone, evidence from turbidites off the Oregon-Washington margin. *Tectonics*, 9: 569-583.
- Anderson, R.Y., 1996. Seasonal sedimentation: a framework for reconstructing climatic and environmental change. *In* *Palaeoclimatology and Palaeoceanography from Laminated Sediments*, Kemp, A.E.S. (ed.), Geological Society Special Publication, No. 116: 1-17.
- Anderson, R.Y., Gardner, J.V and Hemphill-Haley, E., 1989. Variability of the late Pleistocene-early Holocene oxygen minimum zone off northern California. *In* Peterson, D.H. (ed.), *Aspects of climate variability in the Pacific and western America*, American Geophysical Union, Geophysical Monograph, 55: 75-84.
- Amott, R.W.C., and Hand, B.M., 1989. Bedforms, primary structures and grain fabric in the presence of suspended sediment rain. *Journal of Sedimentary Petrology*. 59: 1062-1069.
- Atwater, B.F., 1987. Evidence for great Holocene earthquakes along the outer coast of Washington State. *Science*, 236: 942-944.
- Atwater, B.F., 1992. Geologic evidence for earthquakes during that past 2000 years along Copalis River, southern coast Washington. *Journal of Geophysical Research*, 97: 1901-1919.

- Atwater, B.F., Nelson, A.R. and Clague, J.J., 1995a. Summary of coastal geologic evidence for past great earthquakes at the Cascadia subduction zone. *Earthquake Spectra*, 11: 1-18.
- Atwater, B.F., Nelson, A.R., Clague, J.J., Carver, G.A., Yamaguchi, D.K., Bobrowsky, P.T., Bourgeois, J., Darienzo, M.E., Grant, W.C., Hemphill-Haley, E., Kelsey, H.M., Jacoby, G.C., Nishenko, S.P., Palmer, S.P., Peterson, C.D. and Reinhart, M.A., 1995b. Summary of coastal geologic evidence for past great earthquakes at the Cascadia subduction zone. *Earthquake Spectra*, 11: 1-18.
- Barrie, J.V. and Conway, K.W., 1999. Late Quaternary glaciation and postglacial stratigraphy of the northern Pacific margin of Canada. *Quaternary Research*, 51: 113- 123.
- Barrie, J.V. and Conway, K.W. ,2001. Rapid sea level change and coastal evolution on the Pacific margin of Canada. *Journal of Sedimentary Geology, Decadal to Millennial Variability of Interglacial Sea Levels and Shoreline*, Fletcher, C. and Murray-Wallace, C.,(eds). In press.
- Baumgartner, T.R., Soutar, A. and Ferreira-Bartina, V., 1992. Reconstruction of the history of Pacific sardine and Northern anchovy populations over the past two millennia from sediments of the Santa Barbara basin, California Cooperative Fisheries Investigations Report, 33: 22-40.

- Benson, B.E., Grimm, K.A. and Clague J.J., 1997. Tsunami deposits beneath tidal marshes on northwestern Vancouver Island, British Columbia. *Quaternary Research*, 48: 192-204.
- Blais, A. 1995. Foraminiferal biofacies and Holocene sediments from Saanich Inlet, B.C.: implications for environmental and neotectonic research. Ph.D. thesis, Carleton University, Ottawa, Ontario, Canada, 275 p.
- Blais-Stevens, A. and Clague, J.J., Bobrowsky, P.T., and Patterson, R.T., 1997. Late Holocene sedimentation in Saanich Inlet, British Columbia, and its paleoseismic implications. *Canadian Journal of Earth Sciences*, 34:1345-1357.
- Blais-Stevens, A. and Clague, J.J., 2001. Paleoseismic signature in late Holocene sediment cores from Saanich Inlet, British Columbia. *Marine Geology*, 174:3-26.
- Blais-Stevens, A., Bornhold, B.D., Kemp, A.E.S., Dean, J.M., and Vaan, A.A., 2001. Overview of late Quaternary stratigraphy in Saanich Inlet, British Columbia: results of Ocean Drilling Program Leg 169S. *Marine Geology*, in press.
- Bornhold, B.D., Firth, J.V., Adamson, L.M., Baldauf, J.G., Blais, A., Elvert, M., Fox, P.J., Hebda, R., Kemp, A.E.S., Moran, K., Morford, J.H., Mosher, D.C., Prairie, Y.T., Russell, A.D., Schulteiss, and P., Whiticar, M.J., 1998. *Proceedings of the Ocean Drilling Program, volume 169S, Sites 1033 and 1034, Initial Reports, Saanich Inlet, Victoria, B.C.*, 138 p.

- Bouma, A.H., 1962. Sedimentology of some flysch deposits. Elsevier, Amsterdam, 168 p.
- Bull, D. and Kemp, A.E.S., 1996. Composition and origins of laminae in late Quaternary and Holocene sediments from the Santa Barbara Basin. *In* Palaeoclimatology and Palaeoceanography from Laminated Sediments, Kemp, A.E.S. (ed.), Geological Society Special Publication, No. 116. 263p.
- Chang, A.S., Grimm, K.A., and White, L.D., 1998. Diatomaceous sediments from the Miocene Monterey Formation, California: A lamina-scale investigation of biological, ecological and sedimentary processes. *Palaios* 13: 439-458.
- Clague, J.J., 1980. Late Quaternary geology and geochronology of British Columbia. Part 1: radiocarbon dates; Geological Survey of Canada, paper 80-13, 28 p.
- Clague, J.J., 1981. Late Quaternary geology and geochronology of British Columbia. Part 2: summary and discussion of radiocarbon-dated Quaternary history; Geological Survey of Canada, paper 80-35, 41 p.
- Clague, J.J., 1983. Glacio-isostatic effects of the Cordilleran Ice Sheet, British Columbia Canada. *In* Shorelines and isostasy, Smith, D.E. and Dawson, A.G., (eds.), Academic Press, London, England, p. 321-343.
- Clague, J.J. (compiler), 1989a. Quaternary geology of the Canadian Cordillera. *In* Quaternary Geology of Canada and Greenland, Fulton, R.J. (ed.), Geological Survey of Canada, no. 1:17-22.

- Clague, J.J., 1989b. Character and distribution of Quaternary deposits (Canadian Cordillera). *In* Quaternary Geology of Canada and Greenland, Fulton, R.J. (ed.), Geological Survey of Canada, no. 1: 34-38.
- Clague, J.J., 1989c. Cordilleran Ice Sheet. *In* Quaternary Geology of Canada and Greenland, Fulton, R.J. (ed), Geological Survey of Canada, no. 1, 34-38.
- Clague, J.J., 1989d. Quaternary sea levels (Canadian Cordillera). *In* Quaternary Geology of Canada and Greenland, Fulton, R.J. (ed). Geological Survey of Canada, no.1, 43- 47.
- Clague, J.J., 1989e. Bedrock geology (Canadian Cordillera). *In* Quaternary Geology of Canada and Greenland, Fulton, R.J. (ed). Geological Survey of Canada, no.1, 2-24.
- Clague J.J. and Bobrowsky, P.T., 1994a. Evidence for a large earthquake and tsunami 100 –400 years ago on western Vancouver Island, British Columbia. *Quaternary Research*, 41: 176-184.
- Clague ,J.J. and Bobrowsky, P.T., 1994b. Tsunami deposits beneath tidal marshes on Vancouver Island, British Columbia. *Quaternary Research*, 41: 176-184.
- Clague, J.J. and Bobrowsky, P.T. and Hamilton, T.S., 1994. A sand sheet deposited by the 1964 Alaska tsunami at Port Alberni, British Columbia. *Estuarine, Coastal and Shelf Science*. 38: 413-421.

- Clague, J.J. and Bobrowsky, P.T., 1999. The geological signature of great earthquakes off Canada's West Coast. *Geoscience Canada*, 26: 1–15.
- Clague, J.J., Harper, J.R., Hebda, R.J. and Howe, D.E., 1982. Late Quaternary sea levels and crustal movements, coastal British Columbia. *Canadian Journal of Earth Sciences*, 19: 597-618.
- Clague, J.J., Naesgaard, E. and Sy, A. 1992. Liquefaction features on the Fraser Delta: evidence for prehistoric earthquakes? *Canadian Journal of Earth Sciences*, 29: 1734-1745.
- Collinson, J.D. and Thompson, D.B., 1989. *Sedimentary Structures*. Chapman and Hall, Cambridge, 207 p.
- Dallimore, A., Schröder-Adams, C.J. and Dallimore, S.R., 2000. Holocene environmental history of thermokarst lakes on Richards Island, Northwest Territories, Canada. *Journal of Paleolimnology*, 69: 980-993.
- Darlenzo, M.E. and Peterson, C.D., 1990. Episodic tectonic subsidence of late Holocene salt marshes, northern Oregon, central Cascadia margin. *Tectonics*, 9: 1-22.
- Dean, J.M., Kemp, A.E.S. and Pearce, R.B., 2001. Paleo-flux records from electron microscope studies of laminated sediments, Saanich Inlet, British Columbia. *Marine Geology*, 174: 139-158.
- Denton, G.H. and Armstrong, R.L., 1969. Miocene-Pliocene glaciations in southern Alaska. *American Journal of Science*, 267: 1121-1142.

- Espitalié, J., Laporte, J.L., Madec, M., Marquis, F., Leplat, P., Paulet, J. et
Boutefeu, A. 1977. Méthode rapide de caractérisation des roches de mères de
leur potentiel pétrolier et de leur degré d'évolution. *Revue de l'Institut
Français, Pétrolier*, v.32:23-42.
- Evans, S.G. and Gardner, J.J., 1989. Geological hazards in the Canadian Cordillera. . In
Chapter 12 of *Quaternary Geology of Canada and Greenland*, Fulton, R.J.
(ed.), Geological Survey of Canada, no. 1:699-739.
- Finney, B.P., Gregory-Eaves, I., Sweetman, J., Douglas, M.S.V. and Smol, J.P., 2000.
Impacts of climatic change and fishing on Pacific Salmon abundance over the
past 300 years. *Science*, 290: 795-799.
- Francis, R.C. and Hare, S.R., 1994. Decadal-scale regime shifts in the large marine
ecosystems of the Northeast Pacific; a case for historical science. *Fisheries
Oceanography*, 3(4):279-291.
- Francis, R.C., Hare, S.R., Hollowed, A.B. and Wooster, W.S., 1998. Effects of
interdecadal climate variability on the oceanic ecosystems of the Northeast
Pacific. *Fisheries Oceanography*, 7(1): 1–21.
- Gabrielese, H., Monger, J.W.H., Wheeler, J.O. and Yorath, C.J., 1991. Part a.
Morphogeological belts, tectonic assemblages and terranes. In Chapter 2 of
Geology of the Cordilleran Orogen in Canada, H. Gabrielelese and C.J. Yorath
(eds.), Geological Survey of Canada, *Geology of Canada*, 4: 15-28.

- Glavin, T., 1999. Ocean of turmoil: probing the North Pacific's puzzling cycles of change. *Canadian Geographic*, 119(4): 38-52.
- Grimm, K.A., Lange, C.M. and Gill, A.S., 1996. The biological forcing of hemipelagic sedimentary laminae: Evidence from ODP Site 893, Santa Barbara basin, California. *Journal of Sedimentary Research*, 66(3): 613-624.
- Grimm, K.A., Lange, C.M. and Gill, A.S., 1997. Self-sedimentation of phytoplankton blooms in the geologic record. *Sedimentary Geology (Expressed)*, 110(3-4): 151-161.
- Gross, M.G., Gucluer, S.M., Creager, J.S. and Dawson, W.A., 1963. Varved marine sediments in a stagnant fjord. *Science* 141 : 918-919.
- Gucluer, S.M and Gross, M.G., 1964. Recent marine sediments in Saanich Inlet, a stagnant marine basin. *Limnology and Oceanography* 9: 359-376.
- Hare, F.K. and Thomas, M.K., 1979. *Climate Canada*. Wiley Publishers of Canada, Toronto, Ontario, 256 p.
- Hare, S. and Francis, R.C., 1995. Climate change and salmon production in the Northeast Pacific Ocean. In Beamish, R.J. (ed), *Climate Change and Northern Fish Populations*. Canadian Special Publication of Fisheries and Aquatic Sciences, 121 : 357-372.

- Heaton, T.H. and Hartzell, S.H., 1986. Source characteristics of hypothetical subduction zone earthquakes in the northwestern United States. *Seismological Society of America . Bulletin*, 76: 675-703.
- Heaton, T.H. and Hartzell, S.H., 1987. Earthquake hazards on the Cascadia subduction zone. *Science*, 236: 162-168.
- Hebda, R.J. and Frederick, S.G., 1990. History of marine resources of the northeast Pacific since the last glaciation. *Transcripts of the Royal Society of Canada, I*: 319-342.
- Hebda, R.J., 1995. British Columbia vegetation and climate history with focus on 6 ka BP. *Géographie Physique et Quaternaire*, 49 (1) : 55-79.
- Hewitt, A.T., 1996. A high resolution record of ice-rafting from the Northeast Pacific. Unpublished Master's Thesis, University of Victoria, Victoria, B.C., 105 p.
- Hobson, L.A. and McQuoid, M.R., 2001. Pelagic diatom assemblages are good indicators of mixed water intrusions into Saanich Inlet, a stratified fjord in Vancouver Island. *Marine Geology*, 174: 125-138.
- Holmgren-Urbá, D., and Baumgartner, T.R., 1993. A 250-year history of pelagic fish abundances from the anaerobic sediments of the central Gulf of California: *CALCOFI Reports*, 34: 60-68.
- Hughen, K.A., Overpeck, J.T., Peterson, L.C. and Anderson, R.F., 1996. The nature of varved sedimentation in the Cariaco Basin, Venezuela, *In* *Palaeoclimatology*

and Palaeoceanography from Laminated Sediments, Kemp, A.E.S. (ed.),
Geological Society Special Publication, No. 116. 263p.

Hyndman, R.D., 1995. Giant earthquakes of the Pacific Northwest. *Scientific American*,
276(6): 1621-1623.

Jacoby, G.C., Williams, P.L., and Buckley, B.M., 1992. Tree ring correlation between
prehistoric landslides and abrupt tectonic events in Seattle Washington.
Science, 258: 1621 – 1623.

Johnson, A.M and Rodine, J.R., 1984. Debris flow. *In* Slope stability. D. Brunsden and
D.B. Prior (eds.), John Wiley and Sons, New York, pp. 257-361.

Jones, D.L., Silberling, N.J. and Hillhouse, J., 1977. Wrangellia- A displaced terrane in
northwestern North America. *Canadian Journal of Earth Sciences*, 14: 2565-
2577.

Karlin, R.E. and Abella, S.E.B., 1992. Paleoearthquakes in the Puget Sound region
recorded in sediments from Lake Washington, U.S.A. *Science*, 258: 1617 –
1619.

Karlin, R.E., and Abella, S.E.B., 1996. A history of Pacific Northwest earthquakes
recorded in Holocene sediments from Lake Washington. *Journal of*
Geophysical Research, 101: 6137 – 6150.

Keen, C.E. and Hyndman, R.D., 1979. Geophysical review of the continental margins of
eastern and western Canada. *Canadian Journal of Earth Sciences*, 16: 712-747.

- Kemp, A.E.S., 1996. Laminated sediments as paleo-indicators. In *Palaeoclimatology and Palaeoceanography from Laminated Sediments*. Kemp, A.E.S. (ed.), Geological Society Special Publication, No. 116. p 263.
- Kennett, J.P., Baldauf, J.G. and Lyle, M. (Eds), 1995. *Proceedings of the Ocean Drilling Program, Scientific Results, 146 (Part 2)*. College Station, Texas, 360 p.
- Kuribayashi, E. and Tatsouka, F., 1975. Brief review of liquefaction during earthquakes in Japan. *Soils and Foundations*, 15: 81-92.
- Luternauer, J.L. and Murray, J.W., 1983. Late Quaternary morphologic development and sedimentation, central British Columbia continental shelf. Geological Survey of Canada, paper 83-21, 38 p.
- Luternauer, J.L., Clague, J.J., Conway, K.W., Barrie, J.V., Blasié, B. and Mathewes, R.W., 1989. Late Pleistocene terrestrial deposits on the continental shelf of western Canada: Evidence for rapid sea-level change at the end of the last glaciation. *Geology*, 17: 357-360.
- Mackas, D.L., et al., 2001. GLOBEC CANADA: Response of marine ecosystems to environmental variability *Canadian Journal of Fisheries and Aquatic Sciences*. 58: 685-702.
- Mann, M.E., Park, J. and Bradley, R.S., 1995. Global interdecadal and century-scale climate oscillations during the past five centuries. *Nature*, 378: 266-270.

- Mathewes, R.W. and Clague, J.J., 1994. Detection of large prehistoric earthquakes in the Pacific Northwest by microfossil analysis. *Science*, 264: 688-91.
- Mathews, W.H., 1989. Development of Cordilleran landscapes during the Quaternary. In *Quaternary Geology of Canada and Greenland*, Fulton, R.J. (ed.), Geological Survey of Canada, no. 1: 32-34.
- Macauley, G., Snowden, L.R. and Ball, F.D., 1985. Geochemistry and geological factors governing exploitation of selected Canadian oil shale deposits. *Geological Survey of Canada Paper 85-13*, 65 p.
- McQuoid, M.R. and Hobson, L.A., 2001. A Holocene record of diatom and silicoflagellate microfossils in sediments of Saanich Inlet, ODP Leg 169S. *Marine Geology*, 174: 111-124.
- Medioli, B. E., 2001. Geochemical, grain size, mineralogical and chronological data from three shallow cores in the Red River Valley (Horseshoe Lake, Lake Louise, Manitoba and Salt Lake, North Dakota) GSC Open File #4025, 80 p.
- Medioli, B.E. 1998. Cenomanian to Santonian sea-level history from a proximal setting in the Western Canada sedimentary basin, southern Rocky Mountain foothills, Alberta. Unpublished Master's thesis, Carleton University Ottawa., 183 p.

- Medioli, F.S. and Scott, D.B., 1988. Lacustrine thecamoebians (mainly arcellaceans) as potential tools for paleolimnological interpretations. *Palaeogeography, Palaeoclimatology, Palaeoecology*, 62: 361-386.
- Middleton, G.V. and Hampton, M.A., 1973. Sediment gravity flows: mechanics and deposition, *In* Turbidites and deepwater sedimentation. Middleton, G.V. and Bouma, A.H. (eds.), Los Angeles, Pacific Section, SEPM. p. 1-35.
- Middleton, G.V. and Hampton, M.A., 1976. Subaqueous sediment transport and deposition of sediment gravity flows. *In* Marine transport and environmental management, D.J. Stanley and D.J.P. Swift (eds.), Swift Wiley and Sons, Toronto, pp. 197-218.
- Middleton, G.V. and Southard, J.B., 1984. Mechanics of sediment movement. Short course notes No. 3. Providence, Eastern Section, SEPM.
- Murty, T.S., 1977. Seismic sea waves and tsunamis. *Bulletin, Fisheries Research Board of Canada*, 397 p.
- Obermeier, S.F., 1995. Preliminary estimates of the strength of prehistoric shaking in the Columbia River valley and the southern half of coastal Washington, with emphasis for a Cascadia subduction zone earthquake of about 300 years ago. United States Geological Survey, Open-file Report 94-589.

- O'Brien, N.R., 1996. Shale lamination and sedimentary processes. *In* *Palaeoclimatology and Palaeoceanography from Laminated Sediments*. Kemp, A.E.S. (ed.), Geological Society Special Publication, No. 116. 263p.
- O'Connell, J.M. and Tunnicliffe, V., 2001. The use of sedimentary fish remains for interpretation of long term fish population fluctuations. *Marine Geology*, 174: 177-196.
- Parfit, M., 1995. Diminishing returns. *National Geographic*, November.
- Patterson, R.T. 1993. Late Quaternary benthic foraminiferal biofacies and palaeoceanography of Queen Charlotte Sound and southern Hecate Strait, British Columbia. *Journal of Foraminiferal Research*, 23:1-18.
- Patterson, R.T., Burbidge, S.M and Luternauer, J.L., 1998. Atlas of common benthic foraminiferal species for Quaternary shelf environments of western Canada. Geological Survey of Canada, Bulletin 503, 91 p.
- Patterson, R.T., Guilbault, J-P., and Thomson, R.E., 2000. Oxygen level control on foraminiferal distribution in Effingham Inlet, Vancouver Island, British Columbia. *Journal of Foraminiferal Research*, 30(4): 321-335.
- Pellatt, M.G., Hebda, R.J., and Mathewes, R.W., 2001. High resolution Holocene vegetation history and climate from Hole 1034B, ODP Leg 169S, Saanich Inlet, Canada. *Marine Geology*, 174: 211-226.

- Peters, E., 1986. Guidelines for evaluating petroleum source rock using programmed pyrolysis. *American Association of Petroleum Geologists, Bulletin* 70: 318-329.
- Pickard, G.L. and Emery, W.J., 1990. *Descriptive physical oceanography*. Butterworth-Heinmann, Oxford,, p 281 – 286.
- Pike, J. and Kemp, A.E.S., 1996a. Records of seasonal flux in Holocene laminated sediments, Gulf of California. *In Palaeoclimatology and Palaeoceanography from Laminated Sediments*, Kemp, A.E.S. (ed.), Geological Society Special Publication, No. 116. 263p.
- Pike, J. and Kemp, A.E.S., 1996b. Preparation and analysis techniques for studies of laminated sediments. *In Palaeoclimatology and Palaeoceanography from Laminated Sediments*, Kemp, A.E.S. (ed.), Geological Society Special Publication, No. 116. 263p.
- Plafker, G., 1969. Tectonics of the March 27, 1964 , Alaska earthquake. United States Geological Survey, Professional Paper 543-1, 74 p.
- Research Branch, 1988. Biogeoclimatic zones of British Columbia. Map 1: 2,000,000. Ministry of Forests, British Columbia, Victoria.
- Riddihough, R.P. and Hyndman, R.D., 1976. Canada's active western margin – the case for subduction. *Geoscience Canada*, 3: 269-278.

- Riddihough, R.P and Hyndman, R.D., 1991. Modern plate tectonic regime of the continental margin of western Canada, Chapter 13. *In* Geology of the Cordilleran Orogen in Canada, H. Gabrielse and C.J. Yorath (eds), Geological Survey of Canada, Geology of Canada, 4: 435- 455.
- Ritchie, J.C., 1987. Postglacial Vegetation of Canada. Cambridge University Press, 178 p.
- Robinson, C.L.K. 1994. The influence of ocean climate on coastal plankton and fish production. *Fisheries Oceanography*, 3: 159-171.
- Robinson, S.N. and Thomson, G., 1981. Radiocarbon corrections for marine shell dates with application to southern Pacific northwest coast prehistory. *Syesis*, 14: 45-57.
- Roden, G.I., 1989. Analysis and interpretation of long-term climate variability along the west coast of North America. *Geophysical Monographs*, 1: 55: 93-111.
- Rogers, G.C., 1980. A documentation of soil failure during the British Columbia earthquake of 23 June, 1946. *Canadian Geotechnical Journal*, 17: 122-127.
- Rogers, G.C., 1988. An assessment of the megathrust earthquake potential of the Cascadia subduction zone. *Canadian Journal of Earth Sciences*, 25: 844-852.
- Rogers, G.C., 1994. Earthquakes in Vancouver. *In* Monger, J.W.H. (ed), *Geology and geological hazards of the Vancouver region, southwestern British Columbia*. Geological Survey of Canada, Bulletin 481: 221-229.

- Ryder, J.M., 1989. Climate (Canadian Cordillera). *In* Quaternary Geology of Canada and Greenland, Fulton, R.J. (ed.), Geological Survey of Canada, no. 1: 26-31.
- Ryder, J.M and Clague, J.J., 1989. British Columbia (Quaternary stratigraphy and history, Cordilleran Ice Sheet). *In* Chapter 1 of Quaternary Geology of Canada and Greenland, R.J. Fulton (ed), Geological Survey of Canada, Geology of Canada, no. 1: 48-58.
- Sancetta, C., 1996. Laminated diatomaceous sediments: controls on formation and strategies for analysis. *In* Palaeoclimatology and Palaeoceanography from Laminated Sediments, Kemp, A.E.S. (ed.), Geological Society Special Publication, No. 11: 17-23.
- Schell, T., and Dallimore, A., 2001. Holocene paleoproductivity in the Northeastern Pacific determined by foraminiferal assemblages in a fjord of western Vancouver Island, British Columbia. *Palaeogeography, Palaeoclimatology, Palaeoecology*, (in press).
- Schimmelmann, A. and Lange, C.B., 1996. Tales of 1001 varves: a review of Santa Barbara Basin sediment studies. *In* Palaeoclimatology and Palaeoceanography from Laminated Sediments, Kemp, A.E.S. (ed.), Geological Society Special Publication, No. 116. 263p.
- Schuster, R.L., Logan, R.L. and Pringle, P.T., 1992. Prehistoric rock avalanches in the Olympic mountains, Washington. *Science*, 258: 1620-1621.

- Soutar, A., and Issacs, J.D., 1969. History of fish populations inferred from fish scales and anaerobic sediments off California: CALCOFI Reports, 13: 63-70.
- Stuiver, M. and Reimer, P.J., 1986. A computer program for radiocarbon age calibration. Radiocarbon, 28: 1022-1030.
- Stuiver, M. and Reimer, P.J., 1993. Extended ^{14}C database and revised CALIB radiocarbon calibration program. Radiocarbon, 35: 215-230.
- Stuiver, M. and Braziunas, T.F., 1993. Radiocarbon and ^{14}C ages of marine samples to 10,000 B.C. Radiocarbon 35(1): 137-189.
- Stuiver, M., Reimer, P.J., Bard, E., Beck, J.W., Burr, G.S., Hughen, K.A., Kromer, B., McCormac, F.G., Plicht, J., and Spurk, M., 1998a. INTCAL 98 Radiocarbon age calibration 24,000 – 0 cal BP. Radiocarbon, 40: 1041-1083.
- Stuiver, M., Reimer, P.J., and Braziunas, T.F. 1998b. High-precision radiocarbon age calibration for terrestrial and marine samples. Radiocarbon 40: 1127-1151.
- Syvitski, J.P.M. and Shaw, J., 1996. Sedimentology and geomorphology of fjords. Chapter 5, In Geomorphology and Sedimentology of Estuaries, Perillo, G.M.E. (ed), Developments on Sedimentology 53. Elsevier.
- Thomson, R.E., 1981. Oceanography of the British Columbia coast. Canadian Special Publication of Fisheries and Aquatic Sciences 56, 219p.
- Thomson, R.E. and Gower, J.F.R., 1998. A basin-scale instability event in the Gulf of Alaska. Journal of Geophysical Research, 103: 3033-3040.

- Timothy, D.A., 2001. Primary production and settling flux in two fjords of B.C., Canada.
Unpublished Ph.D. thesis, University of British Columbia, Vancouver, B.C.
- Timothy, D.A. and Soon, M.S., 2001. Primary production and deep-water oxygen content of two British Columbia fjords. *Marine Chemistry*, 73: 37-51.
- Tipper, H.W., Woodsworth, G.J. and Gabrielse, H., 1981. Tectonic assemblage map of the Canadian Cordillera and adjacent parts of the United States of America.
Geological Survey of Canada, Map 1505A.
- Tully, J.P., 1949. Oceanography and prediction of pulp-mill pollution in Alberni Inlet.
Fisheries Research Board of Canada, Bulletin 83, p. 169.
- Tunnicliffe, V., O'Connell, J.M and McQuoid, M.R., 2001. A Holocene record of fish remains from the Northeastern Pacific. *Marine Geology*, 174: 197-210.
- Ware, D.M., 1995. A century and a half of change in the climate of the NE Pacific Ocean. *Canadian Journal of Fisheries and Aquatic Sciences*, 48: 2296- 2306.
- Ware, D.M. and Thomson, R.E., 1991. Link between long-term variability in upwelling and fish production in the northeast Pacific Ocean. *Canadian Journal of Fisheries and Aquatic Sciences*. 48: 2296-2306.
- Ware, D.M. and Thomson, R.E., 2000. Interannual to multidecadal timescale climate variations in the Northeast Pacific. *Journal of Climate*, 13: 3209-3220.

APPENDIX A

Sediment slabbing “cookie cutter” tool: design and operation instructions

COOKIE CUTTER SEDIMENT SLAB SAMPLING DEVICE

ALICE S. CHANG

Department of Earth Sciences, Carleton University, Ottawa, Ontario,
K1S 5B6
Achang2@chat.carleton.ca

April 2000

INTRODUCTION

The "cookie cutter" device is useful for producing sediment slabs of constant thickness. This is perfect for x-raying, making subsamples for scanning electron microscopy, etc (see Schimmelman et al., 1990; Grimm et al., 1996). The cutter works best on moist samples as suction of the water causes the sediments to adhere to the inner walls of the cutter and remains in the core. However, with a bit of patience, the wet slab can still be extracted. The cutter is not recommended for use in dry sediments.

MATERIALS

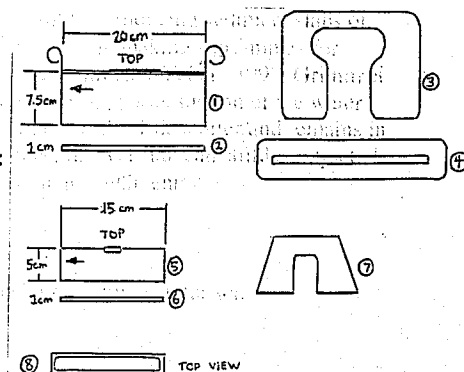
There are a total of eight pieces in the cookie cutter set.

The 20-cm cookie cutter consists of :

1. metal cutter
2. 20 cm long acrylic bar
3. handle
4. acrylic sleeve

The 15-cm cookie cutter consists of:

5. metal cutter
6. 15 cm long acrylic bar
7. handle
8. one Deltrin tray



PROCEDURES

Using the 20 cm cookie cutter

A. Pre-sampling preparation

1. Have a piece of plastic film (Note, "Clingwrap" can be x-rayed through, "Saran Wrap" cannot) on the table top ready to receive sediment slab.
2. Insert the acrylic bar into metal cutter; push the bar all the way to the top of the cutter using the handle. *** Always make sure that the acrylic bar is inside the cutter before you sample, otherwise you will have a difficult time extracting the sediment slab.
3. You may also wish to use the acrylic sleeve as a guide. The sleeve allows some stability to the surface of the core so that the slot covers the interval you want to sample at.**** This step is optional, if you do not wish to use the sleeve, go on to Step B1.

B. Sampling

1. Make sure the "up" arrow on the cutter is pointing towards the stratigraphic "up" direction of your core. This makes it easier to remember the up direction of your slab once it has been extracted from the core. If you are using the sleeve, insert the cutter through the slot.
2. Samples should be extracted from the center of the core, so that the maximum depth can be sampled. Place the cutter lightly in position at the interval of where you want to take the sample. Adjust position if desired.
3. Press the cutter firmly into the core, applying pressure evenly on both ends of the cutter.***Make sure you are pushing the cutter perpendicular to the sediment bedding (if the bedding is horizontal) and not at an angle. If bedding is not apparent, try to keep the cutter as upright as possible so that you are not sampling at an angle.

C. Extraction

1. Extract the cutter carefully and slowly. You may want to gently rock the cutter back and forth to free the cutter, since the surrounding sediment in the core may stick to the outside walls of the cutter. The cutter will now feel heavy because it contains sediment. If you are using the sleeve, you can firmly hold down the sleeve as you are pulling out the cutter so that the surrounding sediments won't get pulled up as well.
2. Bring the cutter over to where you have prepared the plastic film.
3. Hold the cutter out flat, a few cm over the film. Insert the acrylic handle into the top of the cutter and push slowly. I like to hold onto the cutter's rings with both hands, use my stomach as a barrier and pull the cutter towards me.*** Make sure that even pressure is applied so that the sediments pushed out evenly; otherwise, if pressure is pushed on one end, the sediment might get skewed.
4. Make sure the slab is over the film when the slab is fully pushed out. The slab will pop down gently onto the film. Sometimes the acrylic bar gets stuck to the slab. Carefully remove the bar from the slab.

D. Post-Sampling Procedures

1. Wrap the sample securely with the film to maintain moisture. Label the sample.
2. Thoroughly wash the cutter, the bar and the handle before sampling again to prevent cross contamination. Let the tools dry for a bit. (Excess water inside the cutter may prevent sediment from adhering to cutter walls).

Using the 15 cm cookie cutter

This device is used in a similar fashion to the 20 cm long cutter, except for some minor differences as outlined below:

1. Follow steps A1-2 (Pre-sampling preparation), B1-3 (Sampling) and C1-2 and 4 (Extraction) from the previous section.
2. Extraction. Insert the handle into the top of the cutter. Because there are no rings on the cutter to hang on to, I like to firmly hold the metal cutter at the ends with both hands and once again

use my stomach to butt the handle and pull the cutter towards me.

3. Finish off the sampling procedures by following Steps D1-2 (Post-sampling procedures) from the previous section.

REFERENCES

Grimm, K.A., Lange, C.B. and Gill, A.S., 1996. Biological forcing of hemipelagic sedimentary laminae: Evidence from ODP Site 893, Santa Barbara Basin, California. *Journal of Sedimentary Research*, V.66: 613-624.

Schimmelman, A., Lange, C.B. and Berger, W.H., 1990. Climatically controlled marker layers in Santa Barbara sediments, and fine-scale core-to-core correlation. *Limnology and Oceanography*, v. 35: 165-173.

APPENDIX B

Radiocarbon dating results from Isotracer

IsoTrace Radiocarbon Laboratory

Accelerator Mass Spectrometry Facility
at the University of Toronto

299
60 St. George Street
Toronto (Ont) Canada M5S 1A7
Telephone: (416) 978-4628
Fax: (416) 978-4711
Email: roelf.beukens@utoronto.ca

Radiocarbon Analysis Report

June 4, 1999

Submitter: A.Dallimore, Dept of Earth Sciences, Carleton Univ, Ottawa ON

These results are the average of 2 separate analyses (normal precision) and are corrected for natural and sputtering fractionation to a base of $\delta^{13}\text{C} = -25\%$. The sample ages are quoted as uncalibrated conventional radiocarbon dates in years before present (BP), using the Libby ^{14}C meanlife of 8033 years. The errors represent 68.3% confidence limits.

Before hydrolysis, the outer 15% of the shell samples was removed by HCl leaching to ensure that clean, unaltered carbonate material was used. No marine reservoir corrections have been included in the results for these samples. The "Weight used" for the wood samples signifies the wet weights.

Sample Identification	Description	Weight used (mg)	IsoTrace Lab number	Age (years BP)
TUL97A01-340cm	wood frag	2400	TO-8127	730 \pm 50
TUL97A01-205cm	shell frag	89	TO-8128	990 \pm 40
TUL97A04-249cm	shell frags	432	TO-8129	1580 \pm 50
TUL97A02-14cm	wood frag	328	TO-8130	940 \pm 50
TUL97A02-306cm	fish bones	145	TO-8131	3410 \pm 50
TUL97A02-588cm	wood frag	2500	TO-8132	4050 \pm 50

I would like to hear your comments on these results. If these results are used in a publication, I would appreciate it if you could send me a reprint.



Dr. R. P. Beukens

ISOTRACE RADIOCARBON CALIBRATION REPORT
Output by calibration program CL4CAL
Copyright (c) R.P.Beukens

300

04-Jun-99

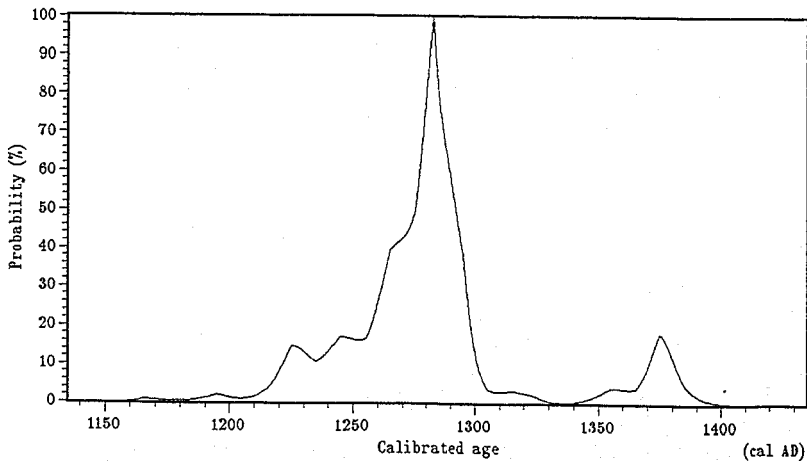
TO-8127 TUL97A01-340cm wood frag

Radiocarbon date : 730 ± 50 BP

All solutions, with a probability of 50% or greater for the calibrated age of this radiocarbon date, have been calculated from the dendro calibration data. The 68% and 95% confidence intervals, which are the 1σ and 2σ limits for a normal distribution, are also given. A probability of 100% means the radiocarbon date intersects the dendro calibration curve at this age. All results are rounded to the nearest multiple of 5 years.

Probability	cal Age	68.3 % c.i.	95.5 % c.i.
100 %	1280 cal AD	1260 AD - 1295 AD	1215 AD - 1300 AD

Calibrated with the standard data set INTCAL98 from:
M.Stuiver et al.; Radiocarbon 40#3 (1998) p1041



04-Jun-99

TO-8128 TUL97A01-205cm shell frag

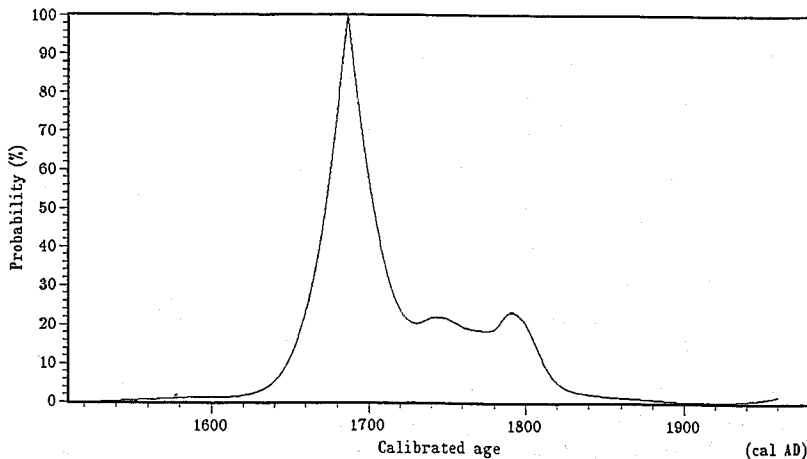
Radiocarbon date : 990 ± 40 BP

All solutions, with a probability of 50% or greater for the calibrated age of this radiocarbon date, have been calculated from the dendro calibration data. The 68% and 95% confidence intervals, which are the 1σ and 2σ limits for a normal distribution, are also given. A probability of 100% means the radiocarbon date intersects the dendro calibration curve at this age. All results are rounded to the nearest multiple of 5 years.

Probability	cal Age	68.3 % c.i.	95.5 % c.i.
100 %	1685 cal AD	1665 AD - 1710 AD	1635 AD - 1820 AD

Calibrated with the marine data set MARINE98 from:
M.Stuiver, P.J.Reimer, and Th.F.Braziunas; Radiocarbon 40#3 (1998) p1127

Delta R reservoir correction = 390 ± 25 years
from M.Stuiver and T.F.Braziunas; Radiocarbon 35#1 (1993) p156



04-Jun-99

TO-8129 TUL97A04-249cm shell frags

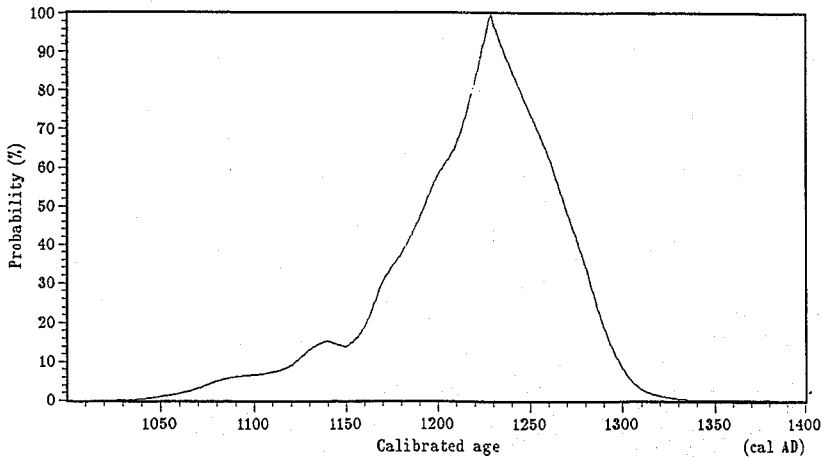
Radiocarbon date : 1580 ± 50 BP

All solutions, with a probability of 50% or greater for the calibrated age of this radiocarbon date, have been calculated from the dendro calibration data. The 68% and 95% confidence intervals, which are the 1σ and 2σ limits for a normal distribution, are also given. A probability of 100% means the radiocarbon date intersects the dendro calibration curve at this age. All results are rounded to the nearest multiple of 5 years.

Probability	cal Age	68.3 % c.i.	95.5 % c.i.
100 %	1225 cal AD	1170 AD - 1280 AD	1075 AD - 1305 AD

Calibrated with the marine data set MARINE98 from:
M.Stuiver, P.J.Reimer, and Th.F.Braziunas; Radiocarbon 40#3 (1998) p1127

Delta R reservoir correction = 390 ± 25 years
from M.Stuiver and T.F.Braziunas; Radiocarbon 35#1 (1993) p156



04-Jun-99

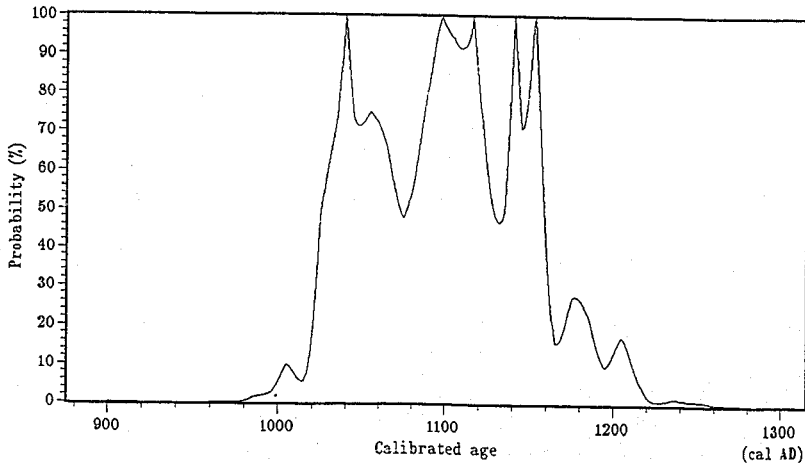
TO-8130 TUL97A02-14cm wood frag

Radiocarbon date : 940 ± 50 BP

All solutions, with a probability of 50% or greater for the calibrated age of this radiocarbon date, have been calculated from the dendro calibration data. The 68% and 95% confidence intervals, which are the 1σ and 2σ limits for a normal distribution, are also given. A probability of 100% means the radiocarbon date intersects the dendro calibration curve at this age. All results are rounded to the nearest multiple of 5 years.

Probability	cal Age	68.3 % c.i.	95.5 % c.i.
100 %	1040 cal AD	1020 AD - 1160 AD	995 AD - 1215 AD
100 %	1095 cal AD	1020 AD - 1160 AD	995 AD - 1215 AD
100 %	1115 cal AD	1020 AD - 1160 AD	995 AD - 1215 AD
100 %	1140 cal AD	1020 AD - 1160 AD	995 AD - 1215 AD
100 %	1150 cal AD	1020 AD - 1160 AD	995 AD - 1215 AD

Calibrated with the standard data set INTCAL98 from:
 M.Stuiver et al.; Radiocarbon 40#3 (1998) p1041



06-Mar-01

TO-8131 TUL97A02-306cm fish bones

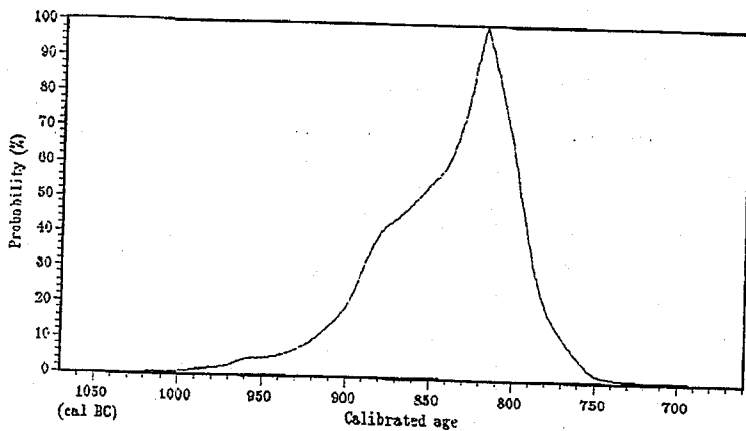
Radiocarbon date : 3410 ± 50 BP

All solutions, with a probability of 50% or greater for the calibrated age of this radiocarbon date, have been calculated from the dendro calibration data. The 68% and 95% confidence intervals, which are the 1σ and 2σ limits for a normal distribution, are also given. A probability of 100% means the radiocarbon date intersects the dendro calibration curve at this age. All results are rounded to the nearest multiple of 5 years.

Probability	cal Age	68.3 % c.i.	95.5 % c.i.
100 %	815 cal BC	885 BC - 785 BC	960 BC - 755 BC

Calibrated with the marine data set MARINE98 from:
 M.Stuiver, P.J.Reimer, and Th.F.Braziunas; Radiocarbon 40#3 (1998) p1127

Delta R reservoir correction = 390 ± 25 years
 from M.Stuiver and T.F.Braziunas; Radiocarbon 35#1 (1993) p156



ISOTRACE RADIOCARBON CALIBRATION REPORT
 Output by calibration program C14CAL
 Copyright (c) R.P.Beukens

305

*-see appendix
 scale of Nov 06/01*

04-Jun-99

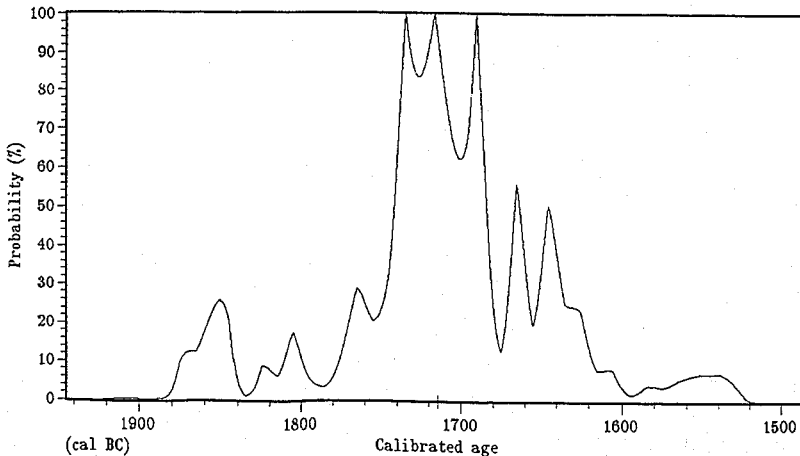
TO-8131 TUL97A02-306cm fish bones

Radiocarbon date : 3410 ± 50 BP

All solutions, with a probability of 50% or greater for the calibrated age of this radiocarbon date, have been calculated from the dendro calibration data. The 68% and 95% confidence intervals, which are the 1σ and 2σ limits for a normal distribution, are also given. A probability of 100% means the radiocarbon date intersects the dendro calibration curve at this age. All results are rounded to the nearest multiple of 5 years.

Probability	cal Age	68.3 % c.i.	95.5 % c.i.
100 %	1735 cal BC	1745 BC - 1680 BC	1780 BC - 1600 BC
100 %	1715 cal BC	1745 BC - 1680 BC	1780 BC - 1600 BC
100 %	1690 cal BC	1745 BC - 1680 BC	1780 BC - 1600 BC
56 %	1665 cal BC	1670 BC - 1655 BC	1780 BC - 1600 BC
50 %	1645 cal BC	1650 BC - 1625 BC	1785 BC - 1600 BC

Calibrated with the standard data set INTCAL98 from:
 M.Stuiver et al.; Radiocarbon 40#3 (1998) p1041



ISOTRACE RADIOCARBON CALIBRATION REPORT
 Output by calibration program C14CAL
 Copyright (c) R.P.Beukens

306

04-Jun-99

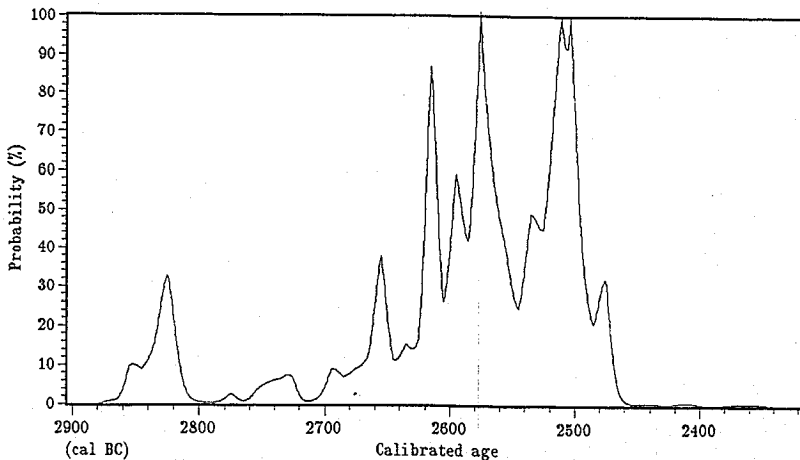
TO-8132 TUL97A02-588cm wood frag

Radiocarbon date : 4050 ± 50 BP

All solutions, with a probability of 50% or greater for the calibrated age of this radiocarbon date, have been calculated from the dendro calibration data. The 68% and 95% confidence intervals, which are the 1σ and 2σ limits for a normal distribution, are also given. A probability of 100% means the radiocarbon date intersects the dendro calibration curve at this age. All results are rounded to the nearest multiple of 5 years.

Probability	cal Age	68.3 % c.i.	95.5 % c.i.
87 %	2615 cal BC	2620 BC - 2605 BC	2700 BC - 2465 BC
100 %	2575 cal BC	2600 BC - 2550 BC	2700 BC - 2465 BC
100 %	2510 cal BC	2540 BC - 2490 BC	2700 BC - 2465 BC
100 %	2500 cal BC	2540 BC - 2490 BC	2700 BC - 2465 BC

Calibrated with the standard data set INTCAL98 from:
 M.Stuiver et al.; Radiocarbon 40#3 (1998) p1041



IsoTrace Radiocarbon Laboratory

Accelerator Mass Spectrometry Facility
at the University of Toronto

307
60 St. George Street
Toronto (Ont) Canada M5S 1A7

Telephone: (416) 978-4628
Fax: (416) 978-4711
Email: roelf.beukens@utoronto.ca

Radiocarbon Analysis Report

October 21, 2000

COPY

Submitter: R.T.Patterson, Dept of Earth Sciences, Carleton Univ, Ottawa ON

These results are the average of 2 separate analyses (normal precision) and are corrected for natural and sputtering fractionation to a base of $\delta^{13}\text{C} = -25\text{‰}$. The sample ages are quoted as uncalibrated conventional radiocarbon dates in years before present (BP), using the Libby ^{14}C meanlife of 8033 years. The errors represent 68.3 % confidence limits.

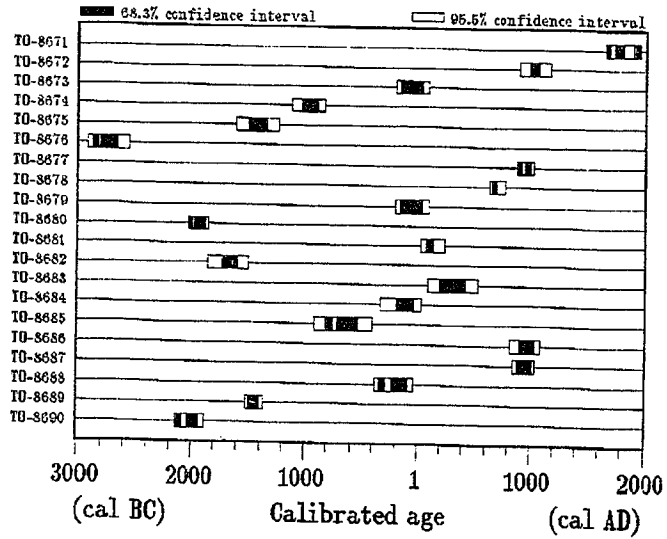
Before hydrolysis, the outer 50-75 % of shell samples TO-8672, TO-8675, and TO-8687 was removed by HCl leaching to ensure that clean, unaltered carbonate material was used. The remaining shell samples were too small for a preleach. Marine reservoir corrections have not been applied to the results for these shell samples.

Sample Identification	Description	Weight used (mg)	IsoTrace Lab number	Age (years BP)
RC03S101	wood frags	476	TO-8671	160 ± 40
RC03S201	shell valves	88	TO-8672	1770 ± 60
RC03S301	wood frags	135	TO-8673	2050 ± 70
RC03S501	wood frag	545	TO-8674	2830 ± 60
RC03S601	shell valves	355	TO-8675	3890 ± 80
RC03S701	wood frag	562	TO-8676	4190 ± 80
RC06S301	wood twig	184	TO-8677	1080 ± 50
RC06S302	wood frag	498	TO-8678	1340 ± 50
RC06S502	wood twigs	380	TO-8679	2050 ± 80
RC06S801	wood twig	147	TO-8680	3590 ± 50
RC09S302	wood frag	430	TO-8681	1890 ± 50
RC09S601	shell valves	40	TO-8682	4100 ± 60
RC11S501	shell valve frag	46	TO-8683	2460 ± 90
RC11S801A	shell frag	24	TO-8684	2830 ± 60
RC11S801	wood frag	291	TO-8685	2570 ± 100
RC11S802	shell frags	82	TO-8686	1820 ± 60
RC13S401	wood twig	506	TO-8687	1080 ± 60
RC13S502	wood twig	441	TO-8688	2140 ± 60
RC13S603	wood frag	627	TO-8689	3170 ± 50
RC13S701	wood frags	600	TO-8690	3640 ± 50

I would like to hear your comments on these results. If these results are used in a publication, I would appreciate it if you could send me a reprint.

ISOTRACE RADIOCARBON CALIBRATION SUMMARY 308
Output by calibration program C14CAL98
Copyright (c) R.P.Beukens

06-Feb-01



ISOTRACE RADIOCARBON CALIBRATION REPORT 309
 Output by calibration program C14CAL98
 Copyright (c) E. P. Beukens

06-Feb-01

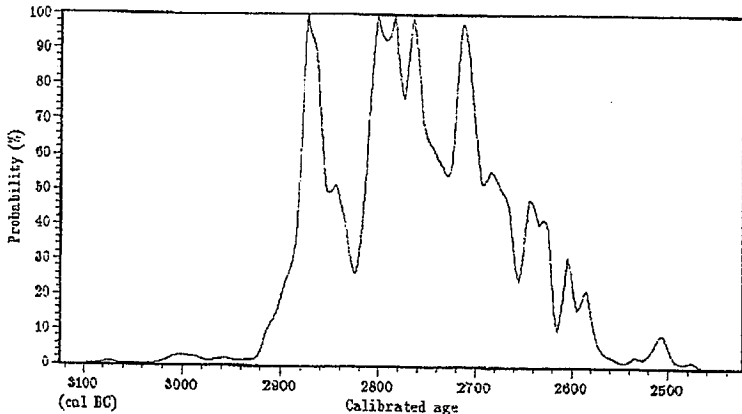
TC-2676 RC035701 wood frag

Radiocarbon date : 4190 ± 80 BP

All solutions, with a probability of 50% or greater for the calibrated age of this radiocarbon date, have been calculated from the dendro calibration data. The 68% and 95% confidence intervals, which are the 1σ and 2σ limits for a normal distribution, are also given. A probability of 100% means the radiocarbon date intersects the dendro calibration curve at this age. All results are rounded to the nearest multiple of 5 years.

Probability	cal Age	68.3 % c.i.	95.5 % c.i.
100 %	2870 cal BC	2885 BC - 2830 BC	2920 BC - 2565 BC
100 %	2800 cal BC	2820 BC - 2660 BC	2920 BC - 2565 BC
100 %	2785 cal BC	2820 BC - 2660 BC	2920 BC - 2565 BC
99 %	2765 cal BC	2820 BC - 2660 BC	2920 BC - 2565 BC

Calibrated with the standard data set INTCAL98 from:
 M. Stuiver et al.; Radiocarbon 40#3 (1998) p1041



ISOTRACE RADIOCARBON CALIBRATION REPORT
 Output by calibration program C14CAL98
 Copyright (c) R.P.Beukens

06-Feb-01

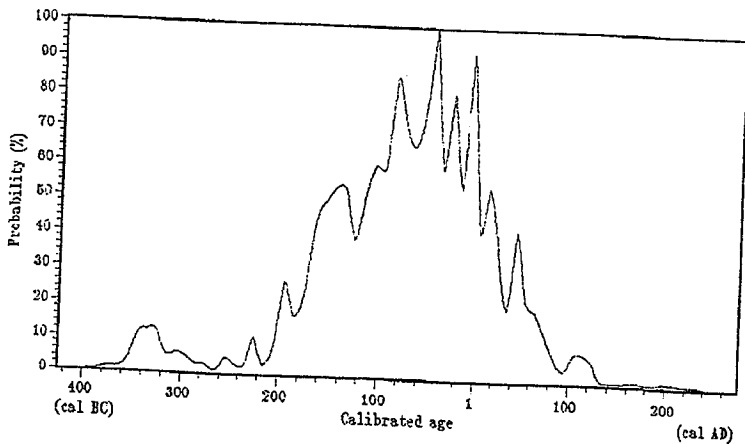
TO-8679 RC06S502 wood twigs

Radiocarbon date : 2050 ± 80 BP

All solutions, with a probability of 50% or greater for the calibrated age of this radiocarbon date, have been calculated from the dendro calibration data. The 68% and 95% confidence intervals, which are the 1 σ and 2 σ limits for a normal distribution, are also given. A probability of 100% means the radiocarbon date intersects the dendro calibration curve at this age. All results are rounded to the nearest multiple of 5 years.

Probability	cal Age	68.5 % c.i.	95.5 % c.i.
100 %	45 cal BC	170 BC - 25 AD	205 BC - 90 AD

Calibrated with the standard data set INTCAL98 from:
 M.Stuiver et al.; Radiocarbon 40#3 (1998) p1041



ISOTRACE RADIOCARBON CALIBRATION REPORT
Output by calibration program C14CAL98
Copyright (c) R.F. Beuclens

311

06-Feb-01

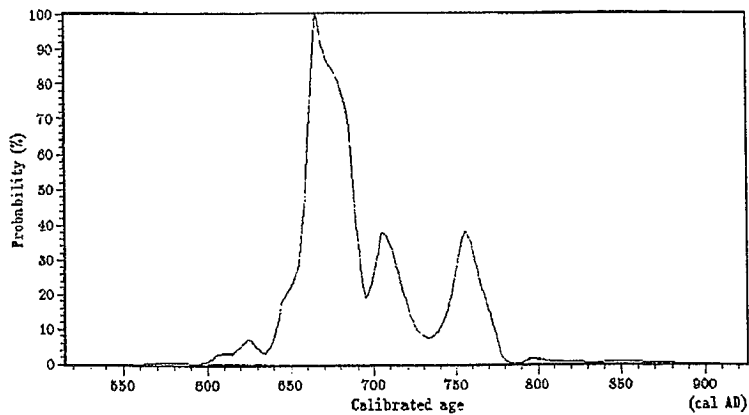
TC-8678 RC06S332 wood frag

Radiocarbon date : 1340 ± 50 BP

All solutions, with a probability of 50% or greater for the calibrated age of this radiocarbon date, have been calculated from the dendro calibration data. The 68% and 95% confidence intervals, which are the 1σ and 2σ limits for a normal distribution, are also given. A probability of 100% means the radiocarbon date intersects the dendro calibration curve at this age. All results are rounded to the nearest multiple of 5 years.

Probability	cal Age	68.3 % c.i.	95.5 % c.i.
100 %	665 cal AD	655 AD - 690 AD	635 AD - 775 AD

Calibrated with the standard data set INTCAL98 from:
M. Stuiver et al.; Radiocarbon 40#3 (1998) p1041



ISOTRACE RADIOCARBON CALIBRATION REPORT 312
Output by calibration program C14CAL98
Copyright (c) R.P.Beukens

06-Feb-01

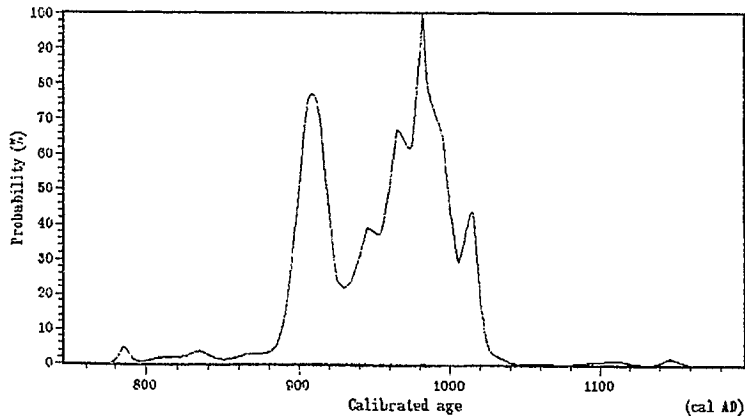
TD-9677 RC06S301 wood twig

Radiocarbon date : 1050 ± 50 BP

All solutions, with a probability of 50% or greater for the calibrated age of this radiocarbon date, have been calculated from the dendro calibration data. The 68% and 95% confidence intervals, which are the 1 σ and 2 σ limits for a normal distribution, are also given. A probability of 100% means the radiocarbon date intersects the dendro calibration curve at this age. All results are rounded to the nearest multiple of 5 years.

Probability	cal Age	68.3 % c.i.	95.5 % c.i.
77 %	905 cal AD	895 AD - 920 AD	880 AD - 1025 AD
100 %	980 cal AD	940 AD - 1000 AD	880 AD - 1025 AD

Calibrated with the standard data set INTCAL98 from:
M.Stuiver et al.; Radiocarbon 40#3 (1998) p1041



ISOTRACE RADIOCARBON CALIBRATION REPORT
Output by calibration program C14CAL98
Copyright (c) R.P.Beukens

313

06-Feb-01

TO-8675 RC03S601 shell valves

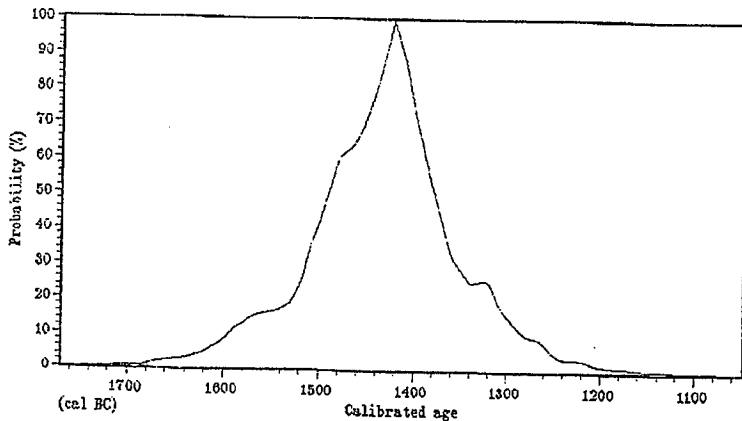
Radiocarbon date : 3890 ± 80 BP

All solutions, with a probability of 50% or greater for the calibrated age of this radiocarbon date, have been calculated from the dendro calibration data. The 68% and 95% confidence intervals, which are the 1 σ and 2 σ limits for a normal distribution, are also given. A probability of 100% means the radiocarbon date intersects the dendro calibration curve at this age. All results are rounded to the nearest multiple of 5 years.

Probability	cal Age	68.3 % c.i.	95.5 % c.i.
100 %	1420 cal BC	1510 BC - 1355 BC	1620 BC - 1245 BC

Calibrated with the marine data set MARINE98 from:
M.Stuiver, P.J.Reimer, and Th.P.Braziunas; Radiocarbon 40#3 (1998) p1137

Delta R reservoir correction = 390 ± 25 years
from M.Stuiver and T.F.Braziunas; Radiocarbon 35#4 (1993) p156



ISOTRACE RADIOCARBON CALIBRATION REPORT
 Output by calibration program C14CAL98
 Copyright (c) R.P.Beukens

06-Feb-01

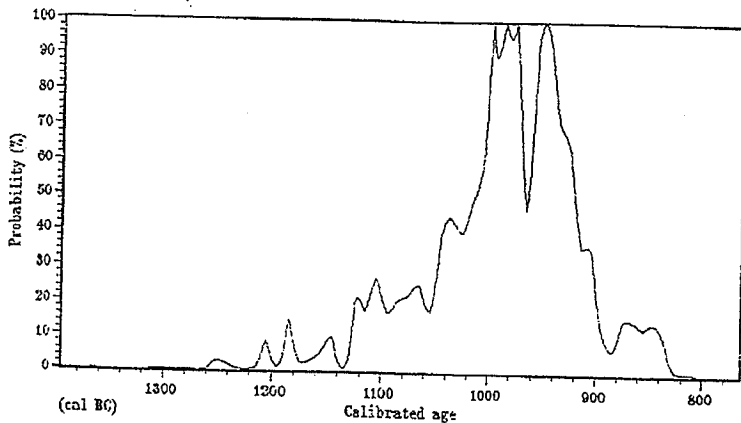
TC-8574 RC038501 wood frag

Radiocarbon date : 2830 ± 60 BP

All solutions, with a probability of 50% or greater for the calibrated age of this radiocarbon date, have been calculated from the dendro calibration data. The 68% and 95% confidence intervals, which are the 1σ and 2σ limits for a normal distribution, are also given. A probability of 100% means the radiocarbon date intersects the dendro calibration curve at this age. All results are rounded to the nearest multiple of 5 years.

Probability	cal Age	68.3 % c.i.	95.5 % c.i.
100 %	995 cal BC	1045 BC - 900 BC	1130 BC - 830 BC
100 %	985 cal BC	1045 BC - 900 BC	1130 BC - 830 BC
100 %	975 cal BC	1045 BC - 900 BC	1130 BC - 830 BC
100 %	945 cal BC	1045 BC - 900 BC	1130 BC - 830 BC

Calibrated with the standard data set INTCAL98 from:
 M.Stuiver et al.; Radiocarbon 40:3 (1998) p1041



ISOTRACE RADIOCARBON CALIBRATION REPORT
Output by calibration program C14CAL98
Copyright (c) R.P.Baukens

315

06-Feb-01

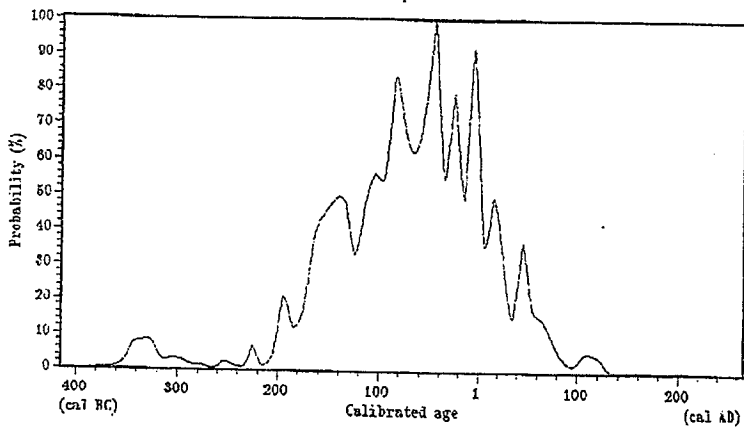
TO-8673 RC038301 wood frags

Radiocarbon date : 2050 ± 70 BP

All solutions, with a probability of 50% or greater for the calibrated age of this radiocarbon date, have been calculated from the dendro calibration data. The 68% and 95% confidence intervals, which are the 1σ and 2σ limits for a normal distribution, are also given. A probability of 100% means the radiocarbon date intersects the dendro calibration curve at this age. All results are rounded to the nearest multiple of 5 years.

Probability	cal Age	68.3 % c.i.	95.5 % c.i.
100 %	45 cal BC	165 BC - 25 AD	205 BC - 80 AD

Calibrated with the standard data set INTCAL98 from:
M.Stuiver et al.; Radiocarbon 40#3 (1998) p1041



06-Feb-01

TO-8672 RC03S201 shell valves

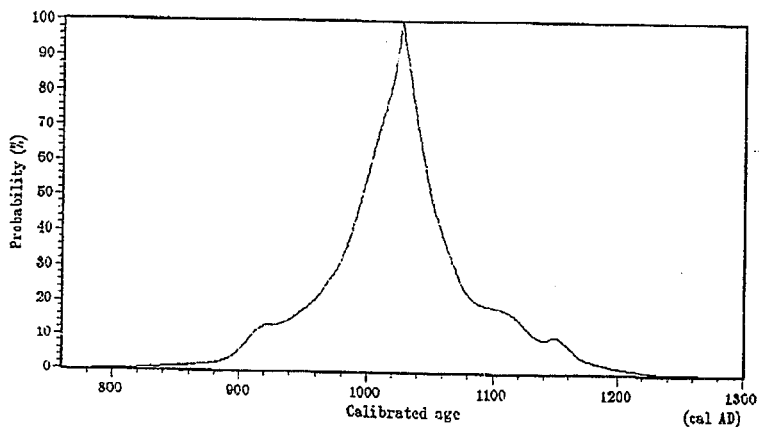
Radiocarbon date : 1770 ± 50 BP

All solutions, with a probability of 50% or greater for the calibrated age of this radiocarbon date, have been calculated from the dendro calibration data. The 68% and 95% confidence intervals, which are the 1σ and 2σ limits for a normal distribution, are also given. A probability of 100% means the radiocarbon date intersects the dendro calibration curve at this age. All results are rounded to the nearest multiple of 5 years.

Probability	cal Age	68.3 % c.i.	95.5 % c.i.
100 %	1025 cal AD	975 AD - 1065 AD	895 AD - 1165 AD

Calibrated with the marine data set MARINE98 from:
M.Stuiver, F.J.Reimer, and T.F.Braziunas; Radiocarbon 40#3 (1998) p1127

Delta R reservoir correction = 390 ± 25 years
from M.Stuiver and T.F.Braziunas; Radiocarbon 35#1 (1993) p156



ISOTRACE RADIOCARBON CALIBRATION REPORT 317
 Output by calibration program CL4CAL98
 Copyright (c) R.P.Beukens

06-Feb-01

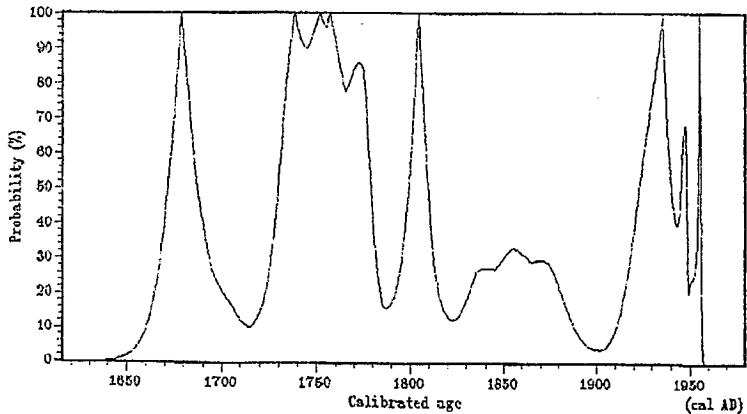
TO-8671 RC03S101 wood frags

Radiocarbon date : 160 ± 40 BP

All solutions, with a probability of 50% or greater for the calibrated age of this radiocarbon date, have been calculated from the dendro calibration data. The 68% and 95% confidence intervals, which are the 1σ and 2σ limits for a normal distribution, are also given. A probability of 100% means the radiocarbon date intersects the dendro calibration curve at this age. All results are rounded to the nearest multiple of 5 years.

Probability	cal Age	68.3 % c.i.	95.5 % c.i.
100 %	1675 cal AD	1665 AD - 1690 AD	1655 AD - 1895 AD
100 %	1735 cal AD	1725 AD - 1780 AD	1655 AD - 1895 AD
100 %	1750 cal AD	1725 AD - 1780 AD	1655 AD - 1895 AD
100 %	1755 cal AD	1725 AD - 1780 AD	1655 AD - 1895 AD
100 %	1805 cal AD	1795 AD - 1810 AD	1655 AD - 1895 AD
100 %	1935 cal AD	1915 AD - 1945 AD	1905 AD - 1955 AD
100 %	1955 cal AD	1950 AD - 1955 AD	1905 AD - 1955 AD

Calibrated with the standard data set INTCAL98 from:
 M.Stuiver et al.; Radiocarbon 40#3 (1998) p1041



ISOTRACE RADIOCARBON CALIBRATION REPORT
 Output by calibration program CALCAL96
 Copyright (c) R.P.Beukens

05-Feb-01

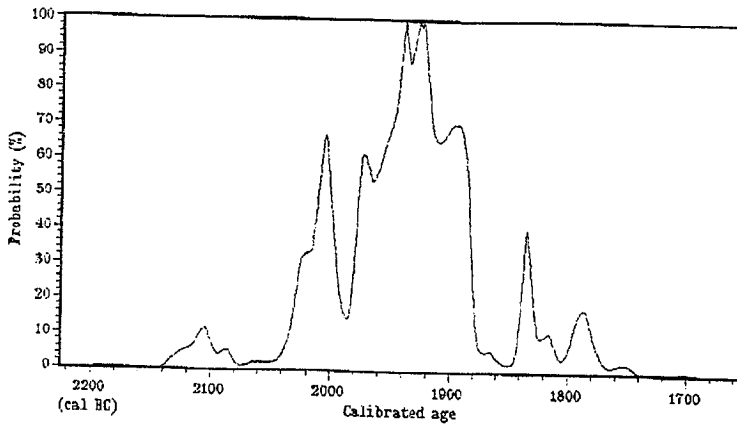
TC-8680 RC058601 wood twig

Radiocarbon date : 3590 ± 50 BP

All solutions, with a probability of 50% or greater for the calibrated age of this radiocarbon date, have been calculated from the dendro calibration data. The 68% and 95% confidence intervals, which are the 1σ and 2σ limits for a normal distribution, are also given. A probability of 100% means the radiocarbon date intersects the dendro calibration curve at this age. All results are rounded to the nearest multiple of 5 years.

Probability	cal Age	68.3 % c.i.	95.5 % c.i.
67 %	2005 cal BC	2025 BC - 1995 BC	2040 BC - 1860 BC
100 %	1935 cal BC	1920 BC - 1880 BC	2040 BC - 1860 BC
100 %	1925 cal BC	1950 BC - 1890 BC	2040 BC - 1860 BC
100 %	1920 cal BC	1980 BC - 1860 BC	2040 BC - 1860 BC

Calibrated with the standard data set INTCAL96 from:
 M.Stuiver et al.; Radiocarbon 40#3 (1998) p1041



ISOTRACE RADIOCARBON CALIBRATION REPORT
 Output by calibration program C14CAL98
 Copyright (c) R.P.Beukens

05-Feb-01

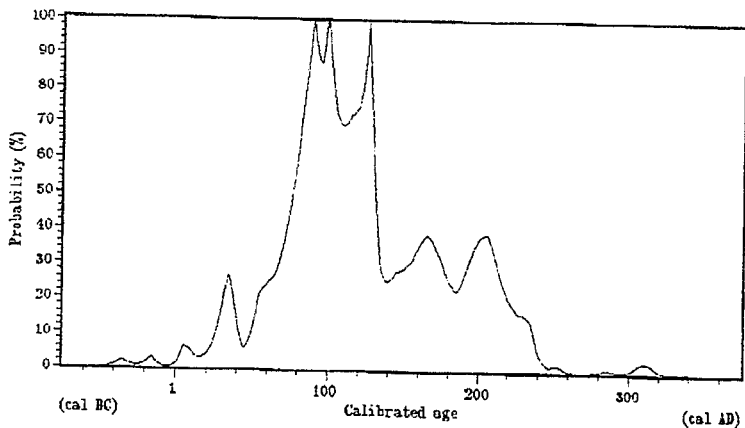
TC-8681 RC09S302 wood frag

Radiocarbon date : 1890 ± 50 BP

All solutions, with a probability of 50% or greater for the calibrated age of this radiocarbon date, have been calculated from the dendro calibration data. The 68% and 95% confidence intervals, which are the 1σ and 2σ limits for a normal distribution, are also given. A probability of 100% means the radiocarbon date intersects the dendro calibration curve at this age. All results are rounded to the nearest multiple of 5 years.

Probability	cal Age	68.3 % c.i.	95.5 % c.i.
100 %	90 cal AD	65 AD - 130 AD	20 AD - 240 AD
100 %	95 cal AD	65 AD - 130 AD	20 AD - 240 AD
100 %	125 cal AD	65 AD - 130 AD	20 AD - 240 AD

Calibrated with the standard data set INTCAL98 from:
 M.Stuiver et al.: Radiocarbon 40#3 (1998) p1041



ISOTRACE RADIOCARBON CALIBRATION REPORT
Output by calibration program C14CAL98
Copyright (c) R.P.Beukens

320

06-Feb-01

TO-8692 R009S601 shell valves

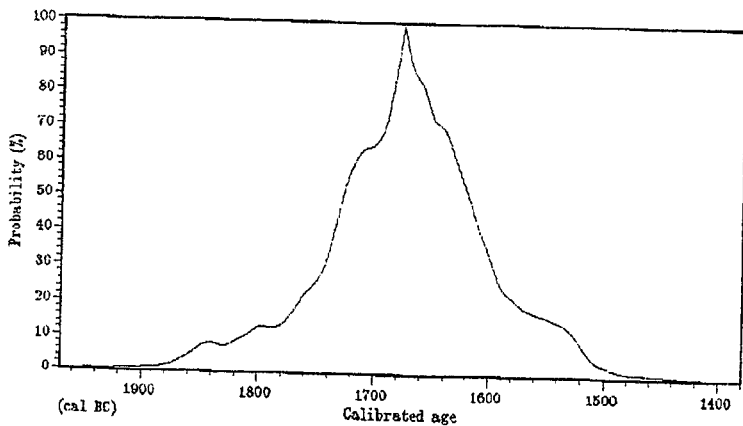
Radiocarbon date : 4100 ± 60 BP

All solutions, with a probability of 50% or greater for the calibrated age of this radiocarbon date, have been calculated from the dendro calibration data. The 68% and 95% confidence intervals, which are the 1 σ and 2 σ limits for a normal distribution, are also given. A probability of 100% means the radiocarbon date intersects the dendro calibration curve at this age. All results are rounded to the nearest multiple of 5 years.

Probability	cal Age	68.3 % c.i.	95.5 % c.i.
100 %	1675 cal BC	1740 BC - 1595 BC	1860 BC - 1505 BC

Calibrated with the marine data set MARINESS from:
M.Stuiver, P.J.Reimer, and Th.F.Braziunas; Radiocarbon 40#3 (1998) p1127

Delta R reservoir correction = 390 ± 25 years
from M.Stuiver and T.F.Braziunas; Radiocarbon 35#1 (1993) p156



ISOTRACE RADIOCARBON CALIBRATION REPORT
Output by calibration program C14CAL93
Copyright (c) R.F.Beukens

321

06-Feb-01

TO-8663 RC115501 shell valve frag

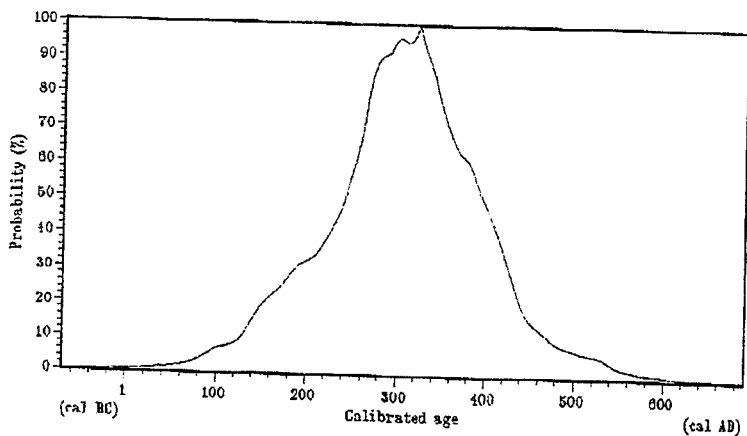
Radiocarbon date : 2460 ± 90 BP

All solutions, with a probability of 50% or greater for the calibrated age of this radiocarbon date, have been calculated from the dendro calibration data. The 58% and 95% confidence intervals, which are the 1σ and 2σ limits for a normal distribution, are also given. A probability of 100% means the radiocarbon date intersects the dendro calibration curve at this age. All results are rounded to the nearest multiple of 5 years.

Probability	cal Age	68.3 % c.i.	95.5 % c.i.
100 %	320 cal AD	195 AD - 425 AD	85 AD - 535 AD

Calibrated with the marine data set MARINE98 from:
M.Stuiver, P.J.Reimer, and Th.F.Braziunas; Radiocarbon 40#3 (1998) p1127

Delta R reservoir correction = 390 ± 25 years
from M.Stuiver and T.F.Braziunas; Radiocarbon 35#1 (1993) p156



ISOFRACE RADIOCARBON CALIBRATION REPORT
Output by calibration program CL4CAL98
Copyright (c) R.P.Beukens

322

06-Feb-01

TO-2684 RC118801A shell frag

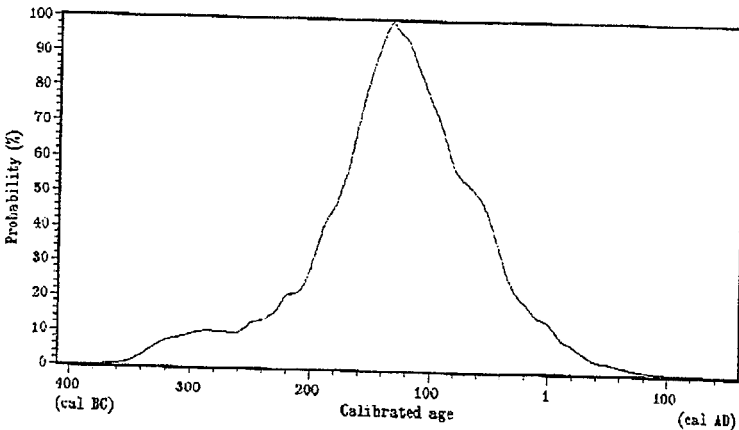
Radiocarbon date : 2630 ± 60 BP

All solutions, with a probability of 30% or greater for the calibrated age of this radiocarbon date, have been calculated from the dendro calibration data. The 68% and 95% confidence intervals, which are the 1σ and 2σ limits for a normal distribution, are also given. A probability of 100% means the radiocarbon date intersects the dendro calibration curve at this age. All results are rounded to the nearest multiple of 5 years.

Probability	cal Age	68.3 % c.i.	95.5 % c.i.
100 %	130 cal BC	195 BC - 35 BC	335 BC - 30 AD

Calibrated with the marine data set MARINE98 from:
M.Stuiver, P.J.Reimer, and Th.F.Braziunas; Radiocarbon 40#3 (1998) p1127

Delta R reservoir correction = 390 ± 25 years
from M.Stuiver and T.F.Braziunas; Radiocarbon 35#1 (1993) p156



ISOTRACE RADIOCARBON CALIBRATION REPORT 323
 Output by calibration program C14CAL98
 Copyright (c) R.F.Benkens

06-Feb-01

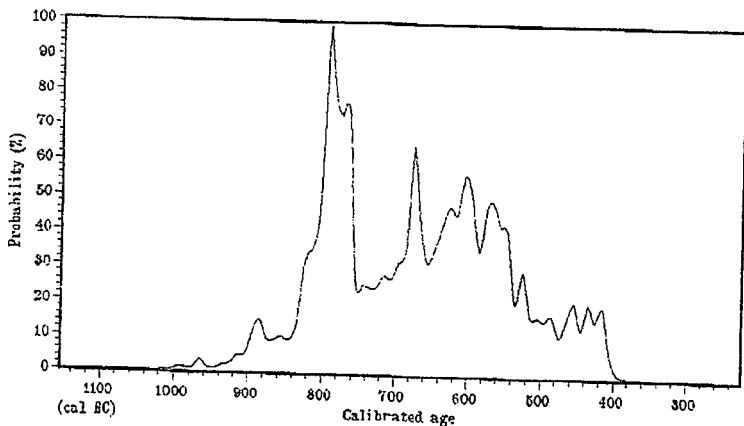
TD-9685 RC118801 wood frag

Radiocarbon date : 2570 ± 100 BP

All solutions, with a probability of 50% or greater for the calibrated age of this radiocarbon date, have been calculated from the dendro calibration data. The 68% and 95% confidence intervals, which are the 1σ and 2σ limits for a normal distribution, are also given. A probability of 100% means the radiocarbon date intersects the dendro calibration curve at this age. All results are rounded to the nearest multiple of 5 years.

Probability	cal Age	68.3 % c.i.	95.5 % c.i.
100 %	790 cal BC	620 BC - 755 BC	915 BC - 400 BC
65 %	675 cal BC	715 BC - 535 BC	915 BC - 400 BC

Calibrated with the standard data set INTCAL98 from:
 M. Stuiver et al.; Radiocarbon 40#3 (1998) p1041



ISOTRACE RADIOCARBON CALIBRATION REPORT
 Output by calibration program C14CAL98
 Copyright (c) R.P.Beukens

06-Feb-01

TO-8686 RC118802 shell frags

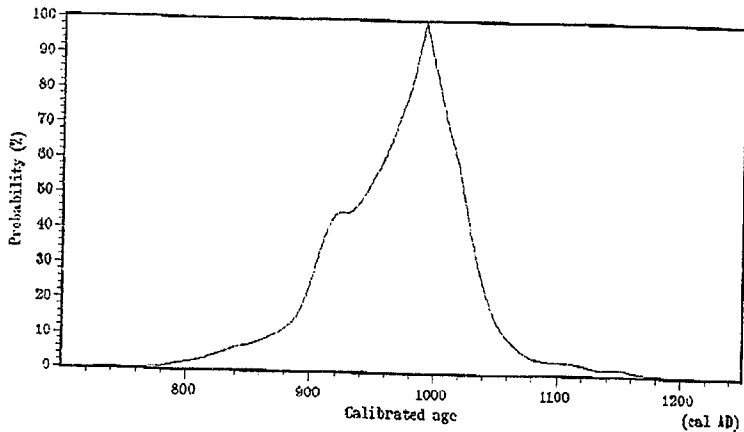
Radiocarbon date : 1820 ± 60 BP

All solutions, with a probability of 50% or greater for the calibrated age of this radiocarbon date, have been calculated from the dendro calibration data. The 68% and 95% confidence intervals, which are the 1σ and 2σ limits for a normal distribution, are also given. A probability of 100% means the radiocarbon date intersects the dendro calibration curve at this age. All results are rounded to the nearest multiple of 5 years.

Probability	cal Age	68.3 % c.i.	95.5 % c.i.
100 %	990 cal AD	905 AD - 1035 AD	825 AD - 1080 AD

Calibrated with the marine data set MARINE98 from:
 M.Stuiver, P.J.Reimer, and Th.F.Braziunas; Radiocarbon 40#3 (1998) p1127

Delta R reservoir correction = 390 ± 25 years
 from M.Stuiver and T.F.Braziunas; Radiocarbon 35#1 (1993) p156



ISOTRACE RADIOCARBON CALIBRATION REPORT 325
 Output by calibration program CL4CAL98
 Copyright (c) R.P.Beukens

06-Feb-01

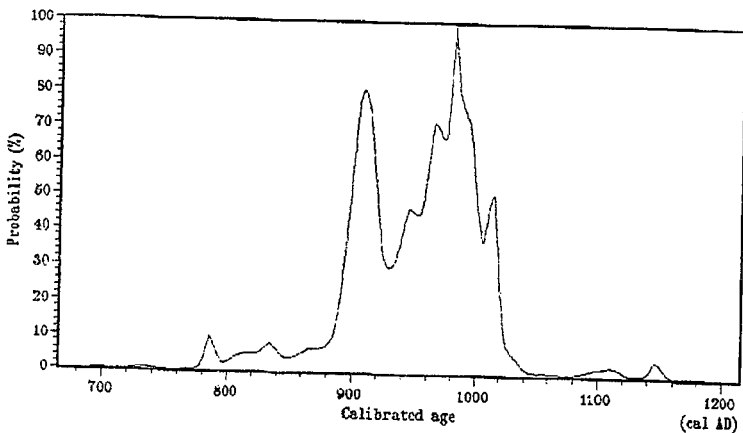
TO-8687 RC138401 wood twig

Radiocarbon date : 1080 ± 60 BP

All solutions, with a probability of 50% or greater for the calibrated age of this radiocarbon date, have been calculated from the dendro calibration data. The 68% and 95% confidence intervals, which are the 1σ and 2σ limits for a normal distribution, are also given. A probability of 100% means the radiocarbon date intersects the dendro calibration curve at this age. All results are rounded to the nearest multiple of 5 years.

Probability	cal Age	68.3 % c.i.	95.5 % c.i.
81 %	965 cal AD	890 AD - 925 AD	850 AD - 1035 AD
100 %	980 cal AD	930 AD - 1015 AD	855 AD - 1030 AD

Calibrated with the standard data set INTCAL98 from:
 M.Stuiver et al.; Radiocarbon 40#3 (1998) p1041



FEB-05-2001 14:38 FROM 412 978 4711 TO 91613222568 P.09

ISOTRACE RADIOCARBON CALIBRATION REPORT
Output by calibration program C14CAL98
Copyright (c) R.F. Beukens

326

06-Feb-01

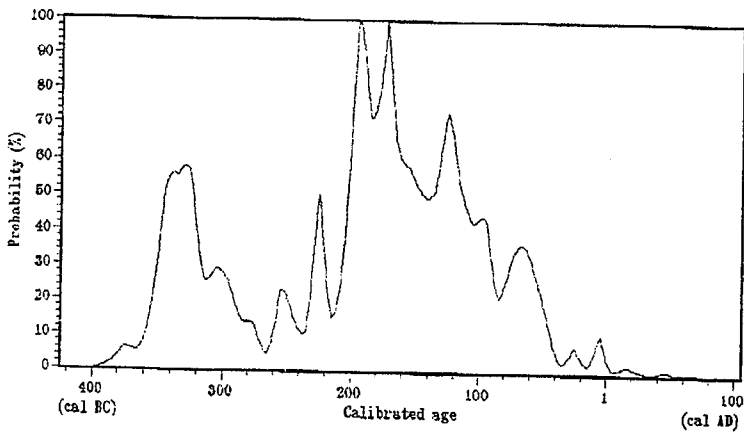
TC-8688 RC135502 wood twig

Radiocarbon date : 2140 ± 60 BP

All solutions, with a probability of 50% or greater for the calibrated age of this radiocarbon date, have been calculated from the dendro calibration data. The 68% and 95% confidence intervals, which are the 1 σ and 2 σ limits for a normal distribution, are also given. A probability of 100% means the radiocarbon date intersects the dendro calibration curve at this age. All results are rounded to the nearest multiple of 5 years.

Probability	cal Age	68.3 % c.i.	95.5 % c.i.
55 %	235 cal BC	350 BC - 295 BC	360 BC - 25 BC
58 %	220 cal BC	350 BC - 295 BC	380 BC - 35 BC
50 %	225 cal BC	230 BC - 215 BC	380 BC - 35 BC
100 %	195 cal BC	205 BC - 90 BC	375 BC - 35 BC
100 %	170 cal BC	295 BC - 90 BC	375 BC - 35 BC

Calibrated with the standard data set INTCAL98 from:
M. Stuiver et al.; Radiocarbon 40#3 (1998) p1041



ISOTRACE RADIOCARBON CALIBRATION REPORT
Output by calibration program C14CAL98
Copyright (c) P.P.Beukens

327

06-Feb-01

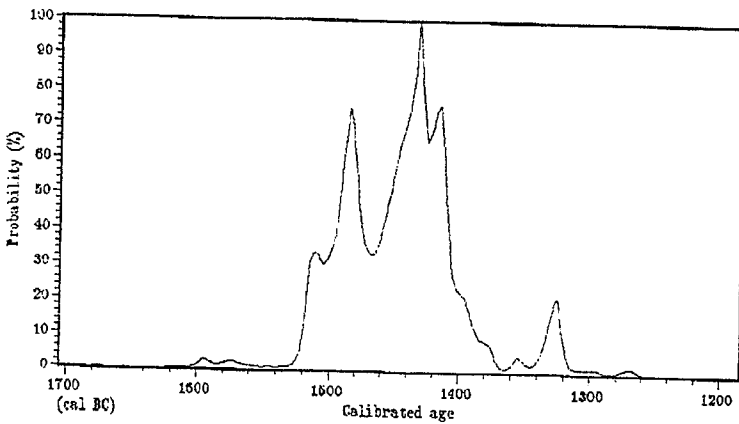
TO-8689 RC133603 wood frag

Radiocarbon date : 3170 ± 50 BP

All solutions, with a probability of 50% or greater for the calibrated age of this radiocarbon date, have been calculated from the dendro calibration data. The 68% and 95% confidence intervals, which are the 1 σ and 2 σ limits for a normal distribution, are also given. A probability of 100% means the radiocarbon date intersects the dendro calibration curve at this age. All results are rounded to the nearest multiple of 5 years.

Probability	cal Age	68.3 % c.i.	95.5 % c.i.
100 %	1430 cal BC	1500 BC - 1405 BC	1520 BC - 1370 BC

Calibrated with the standard data set INICAL98 from:
M.Stuiver et al.; Radiocarbon 40#3 (1998) p1041



ISOTRACE RADIOCARBON CALIBRATION REPORT 328
 Output by calibration program CL4CAL98
 Copyright (c) R.P.Beukens

06-Feb-01

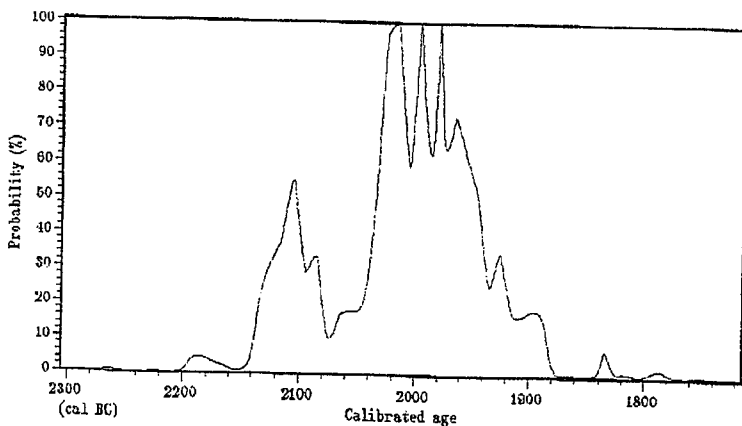
TO-5690 RC138761 wood fragment

Radiocarbon date . 3640 ± 50 BP

All solutions, with a probability of 50% or greater for the calibrated age of this radiocarbon date, have been calculated from the dendro calibration data. The 68% and 95% confidence intervals, which are the 1 σ and 2 σ limits for a normal distribution, are also given. A probability of 100% means the radiocarbon date intersects the dendro calibration curve at this age. All results are rounded to the nearest multiple of 5 years.

Probability	cal Age	68.3 % c.i.	95.5 % c.i.
5% ±	2105 cal BC	2130 BC - 2080 BC	2140 BC - 1880 BC
100 ±	2015 cal BC	2035 BC - 1935 BC	2140 BC - 1880 BC
100 ±	1995 cal BC	2035 BC - 1935 BC	2140 BC - 1880 BC
100 ±	1980 cal BC	2035 BC - 1935 BC	2140 BC - 1880 BC

Calibrated with the standard data set INTCAL98 from:
 M.Stuiver et al.: Radiocarbon 40#3 (1998) p1041



ISOTRACS RADIOCARBON CALIBRATION REPORT
 Output by calibration program C14CAL98
 Copyright (c) R.P.Beukens

329 7

06-Feb-01

TO-8672 RC03S201 shell valves

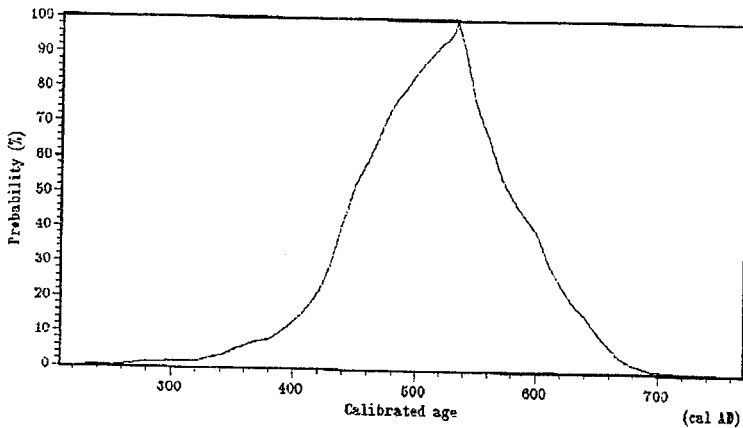
Radiocarbon date : 1770 ± 60 BP

All solutions, with a probability of 50% or greater for the calibrated age of this radiocarbon date, have been calculated from the dendro calibration data. The 68% and 95% confidence intervals, which are the 1σ and 2σ limits for a normal distribution, are also given. A probability of 100% means the radiocarbon date intersects the dendro calibration curve at this age. All results are rounded to the nearest multiple of 5 years.

Probability	cal Age	68.3 % c.i.	95.5 % c.i.
100 %	530 cal AD	430 AD - 605 AD	345 AD - 665 AD

Calibrated with the marine data set MARINE98 from:
 M.Stuiver, P.J.Reimer, and Th.F.Braziunas; Radiocarbon 40#3 (1998) p1127

Delta R reservoir correction = -120 ± 45 years
 Based on results for RC11S801A and RC11S801



ISOTRACE RADIOCARBON CALIBRATION REPORT
 Output by calibration program C14CAL98
 Copyright (c) R.P.Seukens

06-Feb-01

TO-8675 RC039601 shell valves

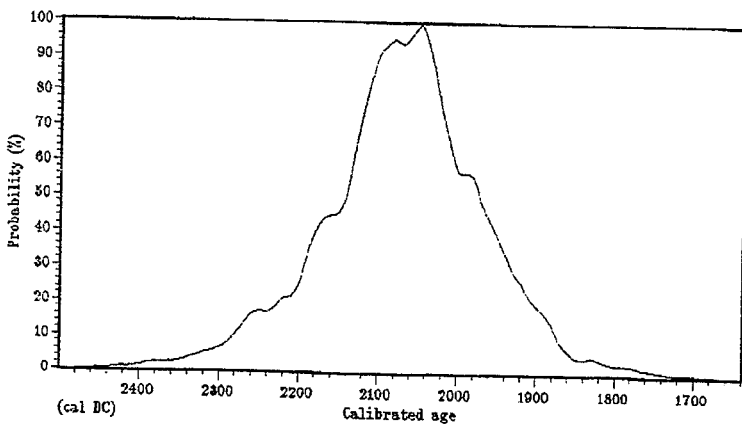
Radiocarbon date : 3890 ± 80 BP

All solutions, with a probability of 50% or greater for the calibrated age of this radiocarbon date, have been calculated from the dendro calibration data. The 68% and 95% confidence intervals, which are the 1σ and 2σ limits for a normal distribution, are also given. A probability of 100% means the radiocarbon date intersects the dendro calibration curve at this age. All results are rounded to the nearest multiple of 5 years.

Probability	cal Age	68.5 % c.i.	95.5 % c.i.
100 %	2045 cal BC	2190 BC - 1935 BC	2330 BC - 1840 BC

Calibrated with the marine data set MARINE98 from:
 M.Stuiver, P.J.Reimer, and Th.F.Braziunas; Radiocarbon 40#3 (1998) p1127

Delta R reservoir correction = -120 ± 45 years
 Based on results for RC118801A and RC118801



ISOTRACE RADIOCARBON CALIBRATION REPORT
 Output by calibration program C14CAL98
 Copyright (c) R.P.Euikens

06-Feb-01

TD-2682 RC09S601 shell valves

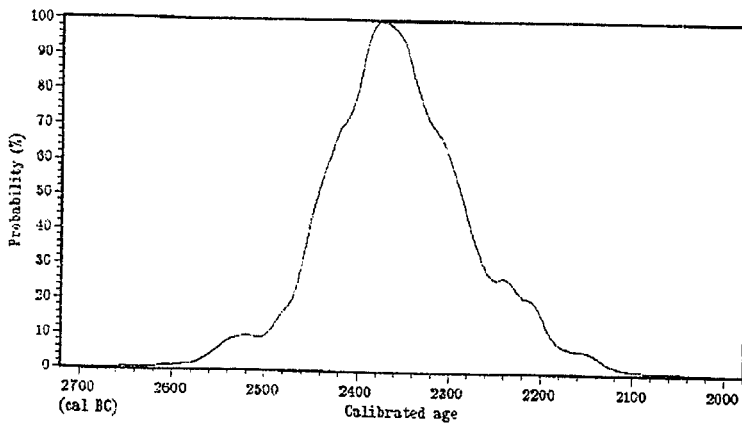
Radiocarbon date : 4100 ± 60 BP

All solutions, with a probability of 50% or greater for the calibrated age of this radiocarbon date, have been calculated from the dendro calibration data. The 68% and 95% confidence intervals, which are the 1σ and 2σ limits for a normal distribution, are also given. A probability of 100% means the radiocarbon date intersects the dendro calibration curve at this age. All results are rounded to the nearest multiple of 5 years.

Probability	cal Age	68.3 % c.i.	95.5 % c.i.
100 %	2375 cal BC	2455 BC - 2265 BC	2555 BC - 2135 BC

Calibrated with the marine data set MARINE98 from:
 M.Stuiver, P.J.Reimer, and Th.F.Braziunas; Radiocarbon 40#3 (1998) p1127

Delta R reservoir correction = -120 ± 45 years
 Based on results for RC11S801A and RC11S801



ISOTRACE RADIOCARBON CALIBRATION REPORT 332
 Output by calibration program C14CAL98
 Copyright (c) R.P.Beukens

06-Feb-01

TD-8683 RC11S501 shell valve frag

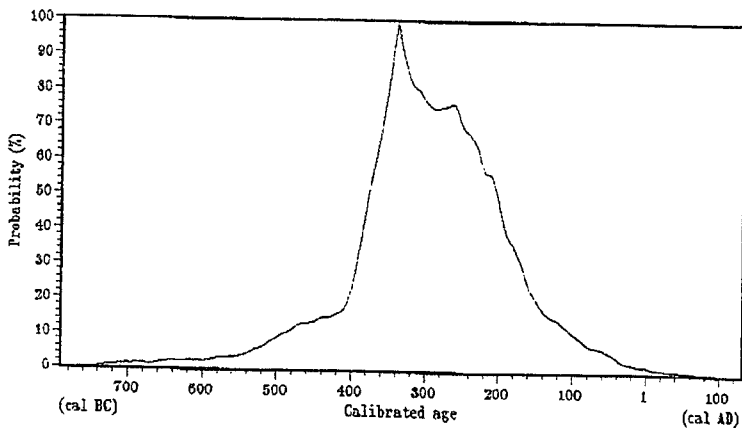
Radiocarbon date : 2460 ± 90 BP

All solutions, with a probability of 50% or greater for the calibrated age of this radiocarbon date, have been calculated from the dendro calibration data. The 68% and 95% confidence intervals, which are the 1σ and 2σ limits for a normal distribution, are also given. A probability of 100% means the radiocarbon date intersects the dendro calibration curve at this age. All results are rounded to the nearest multiple of 5 years.

Probability	cal Age	68.3 % c.i.	95.5 % c.i.
100 %	340 cal BC	390 BC - 170 BC	535 BC - 40 BC

Calibrated with the marine data set MARINE98 from:
 M.Suivver, P.J.Reimer, and Th.F.Braziunas; Radiocarbon 40#3 (1998) p1127

Delta R reservoir correction = -120 ± 45 years
 Based on results for RC11S801A and RC11S801



ISOTRACE RADIOCARBON CALIBRATION REPORT 333
Output by calibration program C14CAL98
Copyright (c) R.P.Beukens

06-Feb-01

TC-5684 RC11S801A shell frag

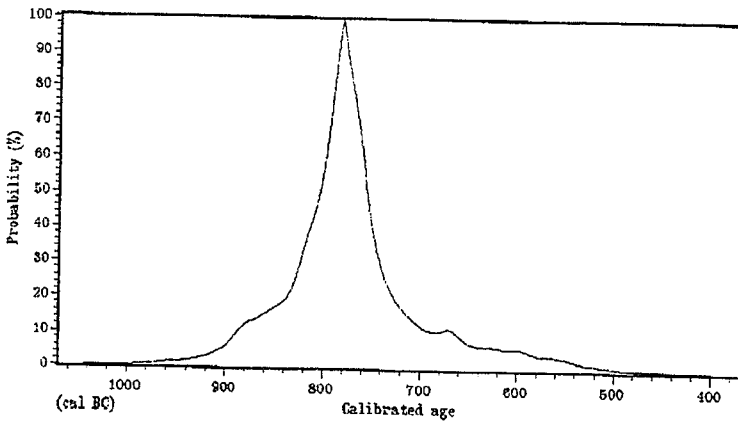
Radiocarbon date : 2830 ± 60 BP

All solutions, with a probability of 50% or greater for the calibrated age of this radiocarbon date, have been calculated from the dendro calibration data. The 68% and 95% confidence intervals, which are the 1σ and 2σ limits for a normal distribution, are also given. A probability of 100% means the radiocarbon date intersects the dendro calibration curve at this age. All results are rounded to the nearest multiple of 5 years.

Probability	cal Age	68.3 % c.i.	95.5 % c.i.
100 %	780 cal BC	820 BC - 740 BC	910 BC - 580 BC

Calibrated with the marine data set MARINE98 from:
M.Stuiver, P.J.Reimer, and Th.F.Braziunas; Radiocarbon 40#3 (1998) p1127

Delta R reservoir correction = -120 ± 45 years
Based on results for RC11S801A and RC11S801



ISOTRACE RADIOCARBON CALIBRATION REPORT
Output by calibration program C14CAL98
Copyright (c) R.P.Beukens

334

06-Feb-01

TO-858c RC11S802 shell frags

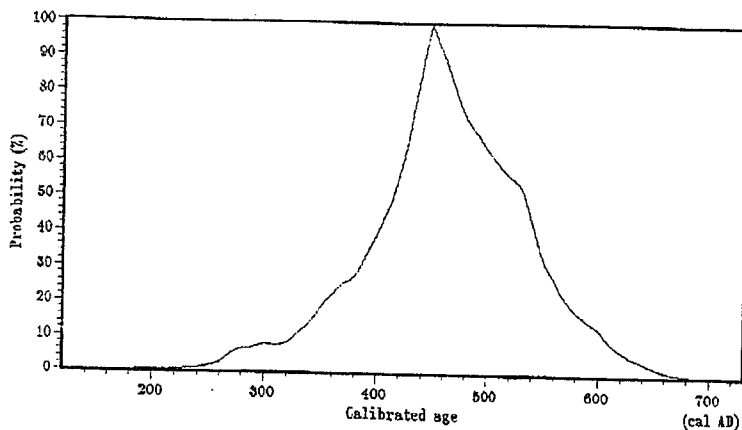
Radiocarbon date : 1620 ± 60 BP

All solutions, with a probability of 50% or greater for the calibrated age of this radiocarbon date, have been calculated from the dendro calibration data. The 68% and 95% confidence intervals, which are the 1σ and 2σ limits for a normal distribution, are also given. A probability of 100% means the radiocarbon date intersects the dendro calibration curve at this age. All results are rounded to the nearest multiple of 5 years.

Probability	cal Age	68.3 % c.i.	95.5 % c.i.
100 %	445 cal AD	385 AD - 550 AD	265 AD - 630 AD

Calibrated with the marine data set MARINE98 from:
M.Stuiver, P.J.Reimer, and Th.F.Braziunas; Radiocarbon 40#3 (1998) p1127

Delta R reservoir correction = -120 ± 45 years
Based on results for RC11S801A and RC11S801



APPENDIX C

Photographs and descriptions of inner basin core
TUL99B06

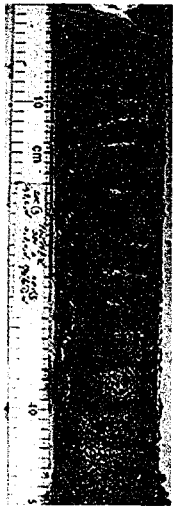
B06S1A

0-49 cm

Dk. Olive grey
3/2, to black,
2.5/2, mud,
some traces of
laminations.

After surface
scraping,
sediments
appear black.

B06 S1



B06S2A

49-73 cm

Black, 2.5/1, massive mud, many small terrigenous organic fragments, light color, up to 0.5 cm in length. Some very faint dark laminations.

73-91 cm

Black, 2.5/1, massive mud with v, faintly defined laminations, no terrigenous organics as above. Several white laminae at 82 cm.

91 cm to ...

Slight color change to dark olive grey, 3/2, no trace laminations.

B06S2B

...to...

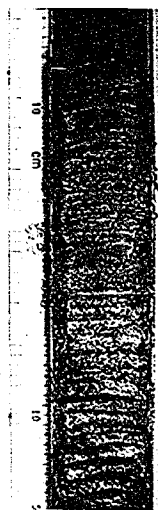
B06S2C

..to 106 cm.

106 to end of section.

Olive grey, 3/2 distinctly laminated mud, ~ 4 varves/cm.

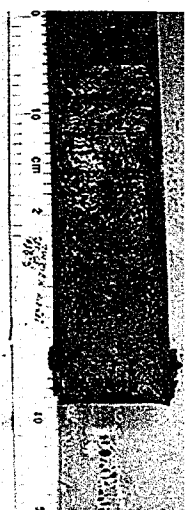
B06 S2a



B06 S2b

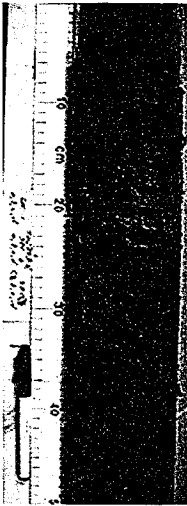


B06 S2c

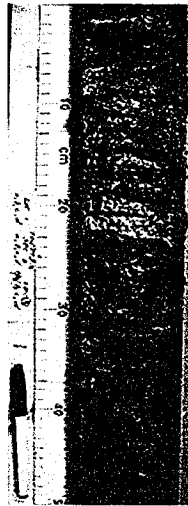


B06S3A	Mud, fining upwards defined by terrigenous organics and shell fragments.	B06S3B ...to 266 cm	B06S3C ..to 321 cm.
185 - 214 cm		Massive mud.	Massive mud.
Sediments lost on recovery		266 to 270 cm	321-329 cm
214-219 cm	230 - 261 cm. Very faintly laminated mud. ~ 4-5 varves/cm where visible.	Faintly laminated mud, ~ 12 varves.	Laminated mud, thick diatom laminae, ~ 3-4 varves/cm.
Dk. olive grey 3/2 massive mud.		270-272 cm	329-337 cm
219-223 cm.	Distinct white laminae at 28, 43, and 51 cm. Wood piece at 252 cm.	Massive mud.	Massive mud with very faint traces of laminations.
Dk. olive grey laminated mud, ~ 4-5 varves/cm		272-306 cm.	
224-227 cm Mud, fining upwards defined by small terrigenous organics.	261 cm to...	Distinctly laminated mud, ~ 6 varves/cm. Wood at 276 cm.	337-344 cm Laminated mud, some disturbance of laminae.
227-230 cm		306 cm to....	344 cm to end of core section
Laminated mud. ~ 4-5 varves/cm.			Masive mud, very faint traces of laminations.
230 - 232 cm			
Mud, fining upwards defined by terrigenous organics.			
232-235 cm.			
Laminated mud ` 3 varves/cm.			
235 - 237 cm			

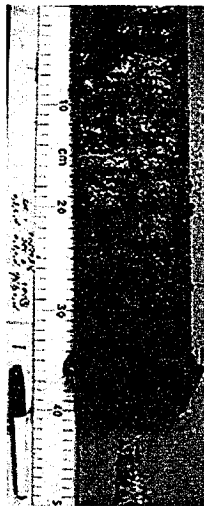
B06 S3a



B06 S3b

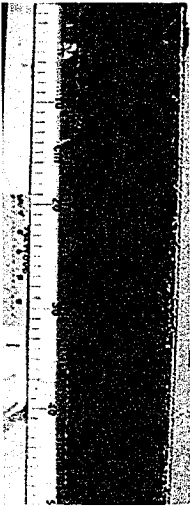


B06 S3c

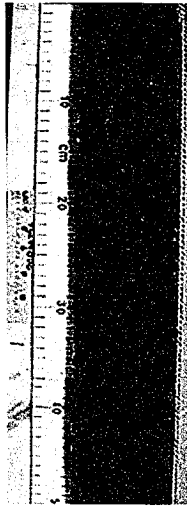


B06S4A	B06S4B	B06S4C
359 – 361 cm	...to 439 cm	...to 62 cm
Olive, 5/3 massive mud.	439- 445 cm	462 – 464 cm
361-371 cm	Black 2.5/2 massive mud with many fine terrigenous organics.	Shell fragments and and fine gravel.
Black, 2.5/2 massive mud, many fine terrigenous organics.	445-448 cm	464-480 cm
371 to ...	Indistinctly laminated mud.	Laminated mud, 1.5-5 varves/cm. Particularly thick diatom laminae.
Olive /dk. olive indistinctly laminated mud, poorly defined, diatom laminae thick.	448 to ..	480-484 cm.
	Dark olive grey massive mud, fewer terrigenous fragments than above.	Dk. Olive grey 3/2 massive mud.
		484-487 cm.
		Indistinctly laminated mud.
		487-492 cm.
		Massive mud.
		492-510
		Laminated mud.
		510-512 cm.
		Massive mud.

B06 S4a



B06 S4b



B06 S4c

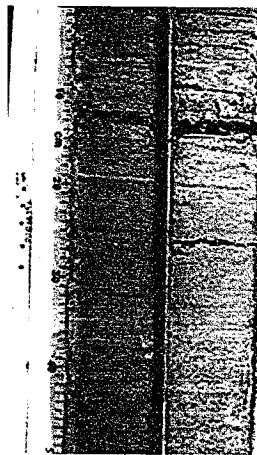


B06S5A	B06S5B	B06S5C
512-543 cm	...to 596 cm	...to 662 cm
Piece lost on recovery.	Massive mud.	662 – 673 cm
543-547 cm	596-598 cm Laminated mud.	V. dk. Grey 3/1 massive mud with terrigenous organics.
Dark olive grey 3/2 massive mud. Very indistinct traces of laminations.	598-600 cm Massive mud.	673-690 cm
547-584 cm. Laminated mud, "brecciated" disturbance to 551 cm, ~ 3-4 varves/cm. Intact fish on bedding plane at 564 cm.	600-611 cm V. dk grey 3/1 massive mud, small terrigenous organics.	Indistinctly laminated mud.
584 – 586 cm	611 to...	690-692 cm Massive mud.
Dk. olive grey massive mud.	Indistinctly laminated mud. Large twig at 629 cm. Distinctive white laminae at 116 cm.	692-696 cm. Indistinctly laminate mud.
586-592 cm		696-to end of core section Laminated mud.
"Brecciated" laminated mud.		
592 to...		

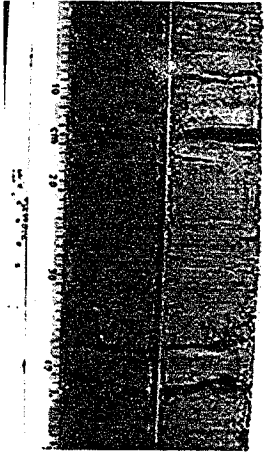
B06 S5a



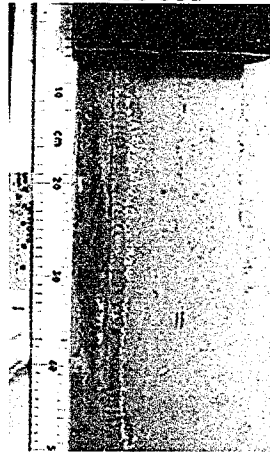
B06 S5c



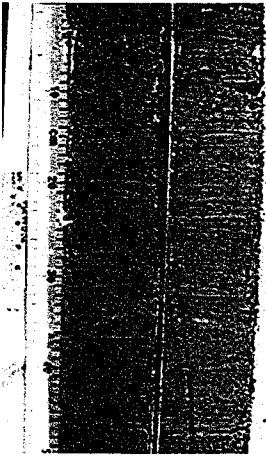
B06 S5b



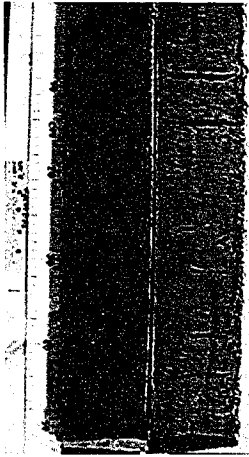
B06 S5d



B06S6A 698-705 cm	V. dk. Grey massive mud with terrigenous organics.	B06S7B ...to 751 cm	B06S7C ...to 812 cm
V. dk. Grey indistinctly laminated mud.		751-761 cm	812-816 cm
705-709 cm V. dk. grey 3/1 massive mud. Large twig at 708 cm.		"Brecciated" laminated mud.	Massive mud.
708-709 cm		761-775 cm	816-825 cm
Faintly laminated mud.		Massive mud.	Laminated mud.
709-714 cm		775-788 cm	825-832 cm
Dk. olive grey 3/2 massive mud, capped by lt grey 7/2 mud. Terrigenous organics.		Laminated mud.	Dk. olive grey massive mud.
714-736 cm		788 - 794 cm	832-844 cm
Shell fragments define fining upwards.		V. dk. grey massive mud.	Laminated mud, ~ 4 varves/cm.
736-738 cm		794 to ...	
Indistinct "brecciated" laminated mud.		Indistinctly laminated mud.	
738- 746 cm			
Indistinctly laminated mud, ~ 4 varves/cm.			
748 to...			



B06 S6a



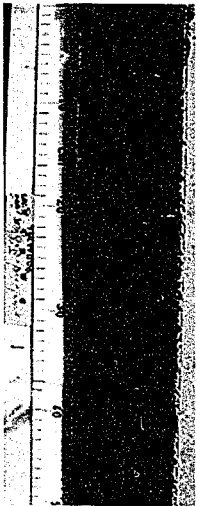
B06 S6c



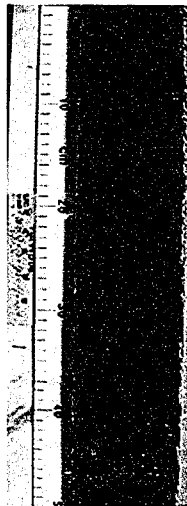
B06 S6b

B06S7A	terrigenous organics.	B06S7B	B06S7C
846-859 cm		...to 924	...to 962
Core lost on recovery.		924 - 928 cm "Brecciated" laminated mud.	Tree fragment colonized by barnacles.
860 - 864 cm		928-948 cm	962-964 cm
Laminated mud, ~ 5-6 varves/cm.		Laminated mud.	Laminated mud.
864-875 cm		948-954	964-968 cm
V. dk. grey massive mud, terrigenous organics, light grey 7/2 mud at top of interval.		Dk. olive grey 3/2 massive mud, shell fragments at top.	Massive mud.
875-900 cm		954-to...	968-974 cm
Laminated mud, distinctive olive green laminae at 885 cm.			Laminated mud.
900 - 908 cm			974-976 cm
Dk. Olive grey 3/2 mud. Light grey 7/2 mud at top, fining upwards defined by terrigenous organics.			Massive mud.
908 to..			976 - 1002 cm
Dk. olive grey massive mud, Pale olive 6/3 mud at top, fining upwards defined by			Dk. olive grey massive mud with very faint traces of laminations.

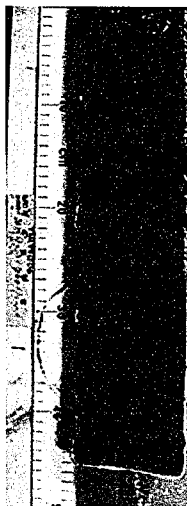
B06 S7a



B06 S7b

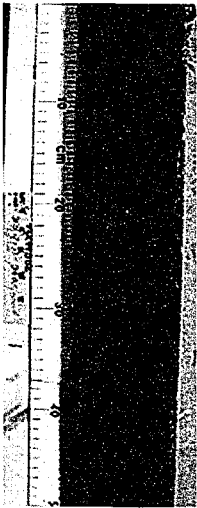


B06 S7c



B06S8A	B06S8B	B06S8C
1002 – 1025 cm	1052- 1068 cm	...to 1124 cm
Laminated mud, distinct olive green laminae at 1016 cm.~ 3-6 varves/cm.	Dk. olive grey 3/2 massive mud, some sand grains, small organics, light grey 7/2 mud at base.	1124 – 1126 cm Massive mud. 1126-1127 cm Laminated mud. 1127-1132 cm
1025-1028 cm	1068-1081 cm	1132 – 1151 cm
Dk. olive grey 3/2 massive mud, traces of laminae.	Laminated mud, ~ 3-5 varves/cm. Some thick (3mm) diatom laminae.	Massive mud, distinctive wavy basal contact defined by light grey 7/2 mud.
1028-1041 cm	1081-1083 cm	Massive mud, fine terrigenous organics.
Laminated mud, some "brecciation" 1031-36 cm.	Dk. olive grey 3/1 massive mud with terrigenous organics.	
1041- 1045 cm	1083-1090 cm	
V. dk. grey massive mud with terrigenous organics defining fining upwards.	Massive mud, faint traces of laminae.	
1045-1052 cm	1090-1096 cm	
Laminated mud, ~ 4 varves/cm, distinctive olive laminae at 48 cm.	Laminated mud, thick (3mm) diatom laminae, ~ 5 varves/cm.	
	1096 to..	
	Laminated mud, diatom laminae to 4mm.	

B06 S8a



B06 S8b



B06 S8c



APPENDIX D

Photographs and descriptions of inner basin core
TUL99B09

B09 S1A

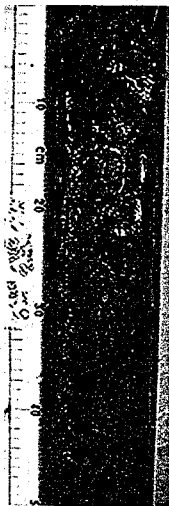
B09S1B

0 to ...

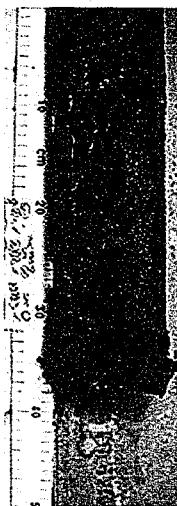
...to 87 cm.

Core section
extremely wet.
Black, 2.5/1
massive mud,
very faint traces
of laminations.

B09 S1a

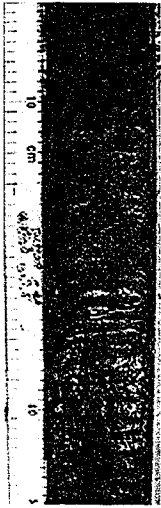


B09 S1b

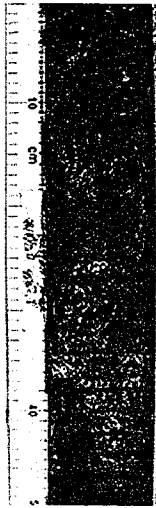


B09 S2A	B09S2B	B09S2C
Core section very wet.	...to 141 cm	...to 221 cm
87 to.....	141 -154 cm	221 - 227 cm
Dk. olive grey 3/2 faintly laminated mud.~ 3 - 5 varves/cm. White laminae 92-97 cm.	Dk olive grey 3/2 massive mud. 154-156 cm	Massive mud. 222 -231 cm
	Very faintly laminated mud. 156-164 cm.	Faintly laminated mud.
	Massive mud. 164 - to...	
	Very faintly laminated mud, ~4-5 varves/cm. Many thick diatom laminae 207-217 cm.	

B09 S2a



B09 S2b

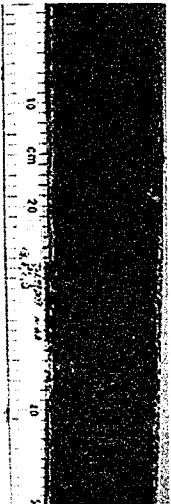


B09 S2c

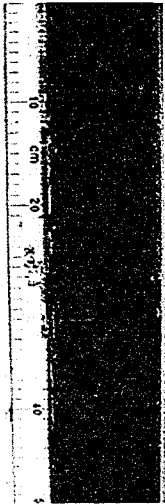


B09 S3A	B09S3B	B09S3C
231 – 248 cm	...to 298 cm.	..to 382 cm
Core lost on recovery	298 – 311 cm	
248 to...	Dk. olive grey massive mud.	
Dk. olive grey faintly to well laminated mud~ 3-8 varves/cm. Fish on bedding plane at 268 cm.	311-325 cm	
	V. faintly laminated mud, ~ 3-4 varves/cm, diatom laminae thick.	
	325 to 327 cm	
	Massive mud.	
	327 to...	
	Faintly to well laminated mud. ~ 3-7 varves/cm. Thick diatom laminae 328-331 cm. Wood piece at 340 cm.	

B09 S3a



B09 S3b



B09 S3c

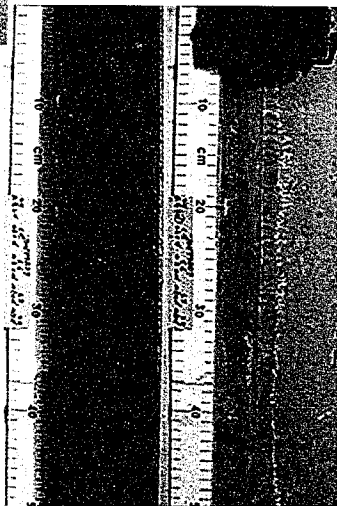


B09S4A	coarse gravel and shell fragments at base.	B09S4B	B09S4B
382-388 cm		...to 439 cm	...to 498 cm
Black 2.5/2 faintly laminated mud with terrigenous organics, ~ 5 varves/cm	423 to ...	439 - 449 cm	498 - 501 cm
	Faintly laminated mud. Thick (4mm) diatom laminae.	Massive mud with terrigenous fragments.	Massive mud.
388-94 cm		449 - 476 cm	501 to 503 cm
Black massive mud, very faint traces of laminations, terrigenous organics.		Dk. olive grey 3/2 faintly laminated mud. Thick diatom laminae 461-465 cm.	Poorly laminated mud.
394-398 cm		476 to 481 cm	503-513 cm
Dk olive grey 3/2 faintly laminated mud, ~ 4 varves/cm		Dk olive grey 3/2 massive mud, terrigenous organics. Fish on bedding plane at 487 cm.	Massive mud, paired bi-valve at 507 cm.
398 - 407 cm		481 to ...	513 - 520 cm
Massive mud, terrigenous organics lens at 405 cm.			Faintly laminated mud.
407 - 411 cm			522-523 cm
Faintly laminated mud.			Massive mud
411 -423 cm			523-526 cm
V. dk grey 3/1 mud fining upwards defined by terrigenous organics from			Faintly laminated mud.
			526-5290 cm
			Massive mud.
			529-536 cm
			Laminated mud.

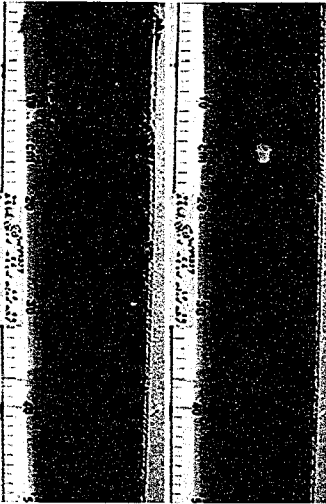


B09 S4a B09 S4b

B09 S4c B09 S4d



B09S5A	B09S5B	B09S5C
536-542 cm	...to 606 cm	..to 647 cm
V. dk grey 3/1 massive mud.	606 - 611 cm	647 - 651 cm
542-545 cm	Mud with fining upwards defined by terrigenous organics.	Dk olive grey 3/2 massive mud.
Faintly laminated mud, ~3 varves/cm	606 to...	651-673 cm
545-564 cm	Laminated mud, ~3-7 varves/cm	Laminated mud, ~3-7 varves/cm.
Dk olive grey 3/2 massive mud with faint traces of laminae.		673 -686 cm
564-567 cm		V. dl grey 3/1 massive mud.
V. dk grey 3/1 massive mud, terrigenous organics at base.		686-688 cm
567 to...		Dk olive grey 3/2 massive mud.
Laminated mud, ~5-6 varves/cm. Distinct white laminae at 592 cm.		

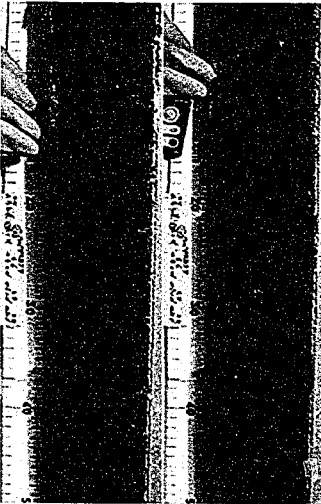


B09 S5a B09 S5b



B09 S5c B09 S5d

B09S6A	B09S6B	B09S6C	B09S6D
688-694 cm	...to 749 cm	...804 cm	...to 840 cm
Laminated mud, ~3-4 varves/cm	749 – 782 cm	804- 808 cm	840-845cm
694-697 cm	Laminated mud, ~3-5 varves/cm. Bioturbation (?) 764-768 cm.	Dk olive grey 3/2 massive mud.	Massive mud with faint traces of laminations.
V. dk grey 3/1 massive mud, fining up defined by terrigenous organics.	768 – 771 cm	808 –811 cm	
697-707 cm	Dk olive grey 3/2 massive mud, fining up defined by terrigenous organics. Lt grey 7/2mud at top.	Massive mud, fining up defined by terrigenous organics Lt. grey 7/2 mud at top.	
Laminated mud, ~3-4 varves/cm		811 – 833 cm	
707 – 721 cm	788 to...	Laminated mud, ~ 4 varves/cm .	
Dk olive grey 3/2 massive mud, large (2-3 cm) terrigenous fragments.	Laminated mud, ~ 4 varves/cm	Thick terrigenous laminae at 818 cm. Paired bi- valve at 821 cm	
721-729 cm		833-837 cm	
Laminated mud.		Massive mud, lt grey 7/2 mud at top, fining up defined by terrigenous organics.	
729-731 cm		827 to...	
V dk grey 3/1 massive mud.		Laminated mud, ~ 4 varves/cm.	
731 to ... Faintly laminated mud.			



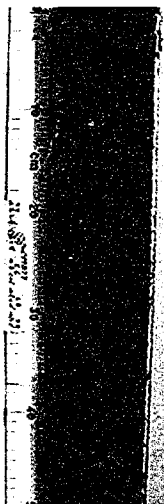
B09 S6a B09 S6b



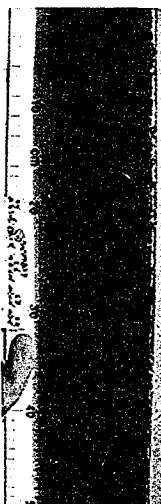
B09 S6c B09 S6d

B09S7A	mud with terrigenous fragments.	B09S7B	B09S7C
872-876 cm		922- 934 cm	972-974 cm
Olive grey 4/2 massive mud.		Laminated mud. Twig at 930 cm, ~ 8 varves/cm.	Dk olive grey 3/2 massive mud.
876-878 cm		934-936 cm	974-979 cm
Black 2S/1 mud, fining up defined by terrigenous organics.		Masive mud.	Laminated mud, ~ 6 varves/cm
878-908 cm		936-941 cm	979-994 cm
Laminated mud, thick terrigenous laminae, ~ 4- 6 varves/cm.		Laminated mud, ~ 6 varves/cm.	Mud, fining up defined by terrigenous organics. Wavy lens of lt olive (6/2) mud at 982 cm.
908-911 cm		941-943 cm	
V dk grey 3/1 massive mud with terrigenous fragments.		Massive mud.	
911-917 cm		942-948 cm	
Laminated mud, ~ 4-5 varves/cm		Laminated mud.	994- 1004 cm
917-920 cm		948-950 cm	Brecciated laminated mud.
Mud, fining up defined by terrigenous organics, lt grey 7/2 mud at top.		V dk grey 3/1 massive mud.	
920-922 cm		950 -972 cm	
Dk olive grey 3/2 massive		Laminated mud, ~ 2-6 varves/cm. Some thick (0.5cm) diatom laminae.	

B09 S7a



B09 S7b

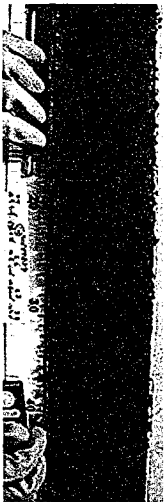


B09 S7c

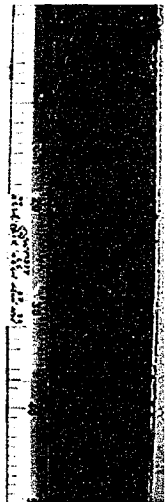


B09S8A	B09S8B	B09S8C
1008 – 1027 cm	...to 1094 cm	..to 1118 cm
Disturbed laminated mud.	1094 – 1104 cm	1118 cm – 1120 cm
1027 – 1034 cm	Dk olive grey 3/2 mud, fining up defined by terrigenous organics, lt grey 7/ mud at top. Large piece of wood at base.	Massive mud.
Undisturbed laminated mud, ~ 5 varves/cm		1120 – 1154 cm
1034-1049 cm		Laminated mud, ~ 5-7 varves/cm. Distinctive white laminae at 1140 cm. Thick (0.25-0.5 cm) diatom laminae at 1120-1122 cm.
Folded laminated mud.	1104 to ..	
1049 to ...	Laminated mud, ~ 5-7 varves/cm	
Undisturbed laminated mud, ~ 4-6 varves/cm.		

B09 S8a



B09 S8b



B09 S8c



APPENDIX E

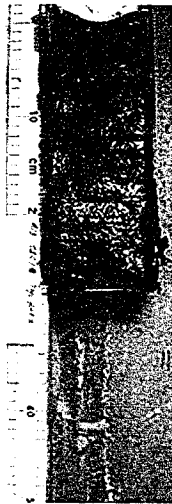
Photographs and descriptions of inner basin core
TUL99B13

B13SA

0 - 27 cm

Core is very
wet, dark olive
grey 3/2
massive mud
with faint
tracings of
laminae.

B13 S1



B13S2A

27 cm to..

Black 2.5/2
massive mud.
Wetness of core
obscures. Very
faint traces of
laminations.

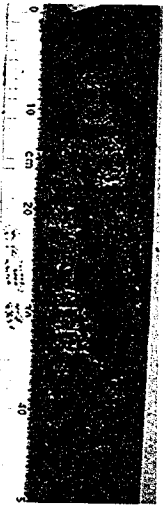
B13S2B

...to...

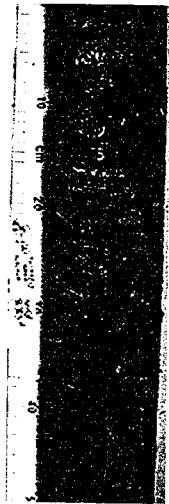
B13S2C

...to 174 cm

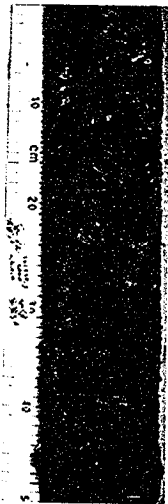
B13 S2a



B13 S2b



B13 S2c

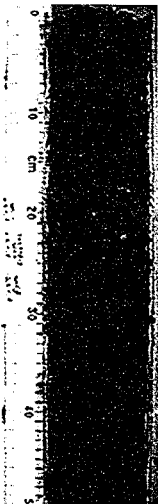


B13S3A	.. to 282 cm	...to 302 cm
174 to 200 cm	282 to ...	302 to 310 cm
Core lost on recovery.	Dk olive grey 3/2 massive mud, faint traces of laminae.	Dk olive grey 3/2 laminated mud.
200 – 206 cm		310 – 318 cm
Olive 4/3 laminated mud, ~ 3-4 varves/cm.		Massive mud.
206 – 219 cm		318 – 335 cm
Dk olive grey 3/2 massive mud, some terrigenous and shell fragments.		Poorly laminated mud.
219-221 cm		
Olive 4/3 laminated mud, ~ 6 varves/cm.		
221-224 cm		
Dk olive grey 3/2 mud, fining up defined by terrigenous organic and shell fragments.		
224 to ...		
Dk olive grey 3/2 Poorly laminated mud.		

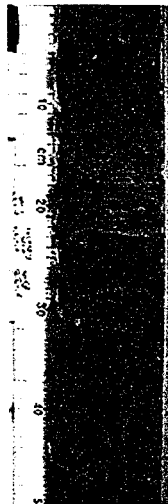
B13S3B

B13S3C

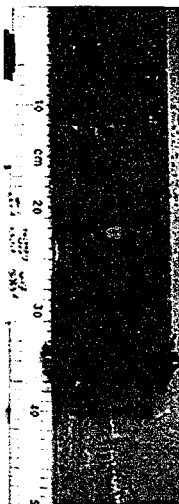
B13 S3a



B13 S3b



B13 S3c

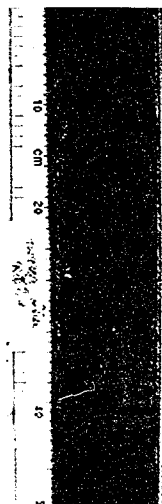


B13S4A	B13S4B	B13S4C
334 – 375 cm	...to 387 cm	...to 484 cm
Dark olive grey, 3/2 indistinctly laminated mud, ~ 4-5 varves/cm. Varves consist of terrigenous laminae thicker than diatomaceous laminae.	387 – 392 cm Dk olive grey 3/2 massive mud with terrigenous fragments.	
375 – 378 cm	392-395 cm Laminated mud.	
V. dk grey 3/1 massive mud with terrigenous fragments. Large twig at 376 cm.	395 – 412 cm	
378 to ...	Dk olive grey 3/2 mud, fining upwards defined by terrigenous organics, gravel and shell at the base. Wavy lt grey 7/2 layer at 397 cm.	
Laminated mud.	412 to ...	
	Poorly to well laminated mud. Thick (0.5 cm) diatom laminae at 438 cm. Distinctive white laminae at 458 cm.	

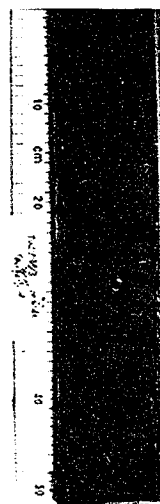
B13 S4a



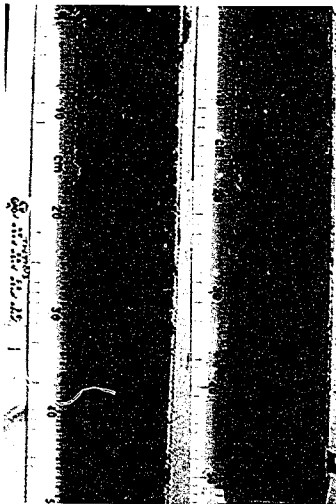
B13 S4b



B13 S4c

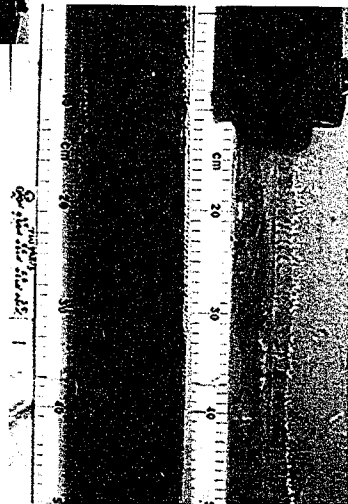


B13S5A	B13S5B	B13S5C	B13S5D
483-489 cm	...to 536 cm	..to 595 cm	...to 636 cm
Dk olive grey 3/2 massive mud, faint traces of laminae.	536-545 cm	595 to 608 cm	636 to 638 cm
489-497 cm	Poorly laminated mud.	V dk grey 3/1 massive mud with terrigenous fragments.	Laminated mud.
Faintly laminated mud.	545-552 cm	608-630 cm	638 - 640 cm
497-501 cm	V dk grey 3/1 massive mud.	Well laminated mud.	Dk olive grey 3/2 massive mud.
Poorly laminated mud.	552 to...	630 to ...	
518-522 cm	Poorly defined laminated mud. Fish bones at 569 cm. Distinctive white laminae at 581 cm to 583 cm and 584 cm.	V dk grey 3/1 massive mud with terrigenous fragments.	
Dk olive grey 3/2 massive mud.			
522-533 cm			
Poorly laminated mud.			
533 to...			



B13 S5a B13 S5b

B13 S5c B13 S5d



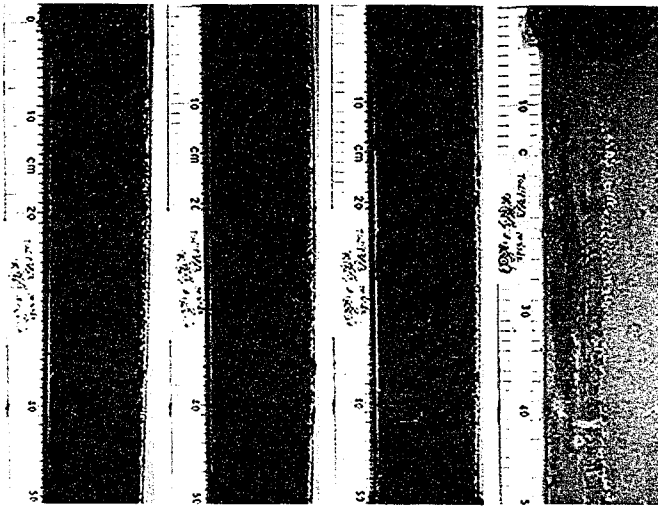
B13S6A		B13 S6B	B13 S6C
640-651 cm	with terrigenous fragments.	...to 692 cm	...to 749 cm
Faintly defined laminated mud, possible bioturbation.	681-689 cm	692 – 701 cm	749 – 752 cm
651-654 cm	Poorly laminated mud.	Laminated mud, ~ 4-5 varves/cm.	Faint laminae, ~ 5-6 varves/cm
V dk grey 3/1 massive mud.	689 to...	701 –716 cm	752-754 cm
654-655 cm	V dk grey 3/1 massive mud.	V dk grey 3/1 massive mud, terrigenous organic fragments.	Dk olive grey 3/2 massive mud. Twig at 753 cm.
Laminated mud.			754-782 cm
655-660 cm		716-727 cm	Laminated mud, ~ 6-7 varves/cm. Large twig at 777 cm.
V dk grey 3/1 massive mud with terrigenous fragments.		Poorly laminated mud, some bioturbation ?	782- 784 cm
660-678 cm		727-732 cm	Massive mud,
Poorly laminated mud. Distinctive white laminae at 675 cm. Fish skeleton on bedding plane at 680 cm.		V dk grey 3/1 massive mud with terrigenous organic fragments.	B13S6D
678-681 cm		732- ...	784-791 cm
V dk grey 3/1 massive mud with terrigenous fragments.		Poorly defined laminations, some bioturbation ?, ~ 5-6 varves/cm.	Laminated mud, ~ 6-7 cm.
V dk grey 3/1 massive mud.			

B13 S6a

B13 S6b

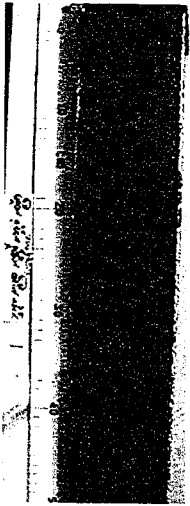
B13 S6c

B13 S6d

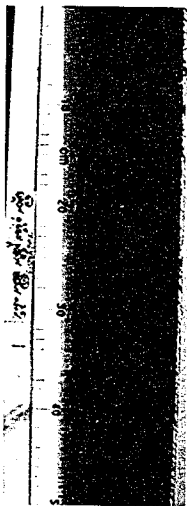


B13S7A	B13S7B	892-894 cm	B13S7C
791 – 804 cm	...to 865 cm	Poorly defined laminated mud.	...to 944 cm.
Core lost on recovery	865 – 874 cm	894 – 901 cm	
804 – 821 cm	V dk grey mud 3/1, fining up defined by terrigenous fragments.	Massive mud.	
Laminated mud, ~ 6-8 varves/cm.	Large intact bivalve shell at 872 cm.	894 to ...	
821-827 cm	874 – 877 cm	Poorly to well laminated mud, ~ 5-8 varves/cm. Bioturbation (/) at 921 cm.	
V dk grey 3/1 massive mud, fining up defined by terrigenous organics.	Poorly laminated mud. Some bioturbation (?).		
827-842 cm	877 – 880 cm		
V dk grey 3/1 massive mud. Distinctive white laminae at top. Fining up defined by terrigenous fragments.	V dk grey massive mud, terrigenous fragments.		
Large piece of wood, at 842 cm.	880-882 cm		
842 to ... laminated mud, ~ 4-8 varves/cm. Distinctive white laminae at 858 cm.	Laminated mud.		
	882- 885 cm		
	Massive mud.		
	885 – 890 cm		
	Poorly laminated mud.		
	890-892 cm		
	Laminated mud.		

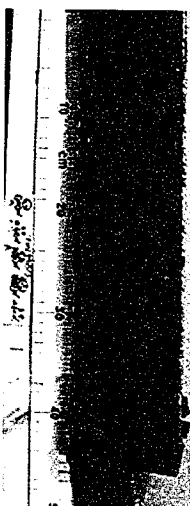
B13 S7a



B13 S7b



B13 S7c

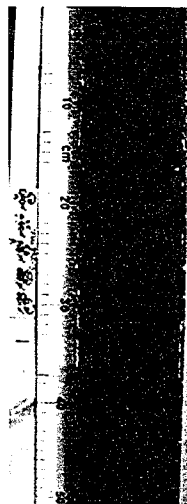


B13S8A	B13S8B	B13S8C
944 – 956 cm	...to 998 cm	...to 1074 cm
Poorly to well defined laminated mud, ~4-5 varves/cm.	998 – 999 cm	1074 – 1092
956-969 cm	V dk grey 3/1 massive mud with terrigenous organic fragments.	Laminated mud, laminations disturbed, bioturbation or brecciation ?
V dk grey 3/4 massive mud, lt olive grey 6/2 mud at top. Some terrigenous organic fragments.	999 - 1024	
969-990 cm	Laminated mud, ~4-5 varves/cm.	
Laminated mud, ~5-6 varves/cm. Thick, 1 cm diatom laminae at 976 cm.	1024-1025 cm	
990 –991 cm	Dk olive grey 3/2 massive mud.	
Dk olive grey 3/1 masive mud.	1025-1033 cm	
991 to..	Laminated mud, ~6-7 varves/cm.	
Laminated mud, ~40-5 varves/cm	1033 to...	
	V dk grey 3/1 mud. Wavy, light grey 7/2 mud layer at 1034 cm.	
	Fining up from base defined by terrigenous organics.	

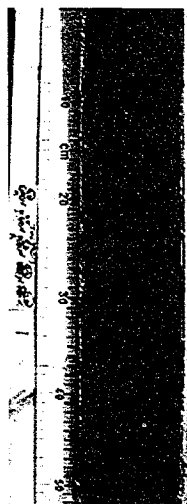
B13 S8a



B13 S8b



B13 S8c



APPENDIX F

X-rays and descriptions of inner basin core
TUL99B03

CORE DESCRIPTION TUL99B03 INNER BASIN

SECTION 1

1-12 cm

Core is very wet.

Dk olive grey 3/2 faintly laminated mud. Many terrigenous organic fragments.
Sediments on the cut face of the core have a mottled black appearance.

12 – 97 cm

Dk olive grey 3/2 to black 2.5/2 faintly laminated mud. Wetness of core obscures details.
Wood piece at 97 cm.

SECTION 2

104-154 cm

Dk olive grey 3/2 faintly laminated mud, ~ 4-6 varves/cm.

154-169 cm

Massive mud.

169-179 cm

Laminated mud, ~ 4 varves/cm.

179-183 cm

Olive 4/3 mud fining up defined by terrigenous organics.

183-185 cm

Laminated mud.

185-187 cm

Olive brown 4/3 massive mud.

187-207 cm

Dk olive grey laminated mud, ~ 4-6 varves/cm.

207-215 cm

Olive 4/3 massive mud.

215 – 237 cm

Laminated mud, ~ 4-6 varves/cm.

237-239 cm

Olive 4/3 massive mud.

SECTION 3

239 – 245 cm

Core lost on recovery.

245-255 cm

Dk olive grey 3/2 massive mud, faint traces of laminae.

255-326 cm

Dk olive grey 3/2 laminated mud, ~ 3-6 varves/cm. Large twigs at 286 and 303 cm.

326-330 cm

Massive mud.

330-337 cm

Laminated mud.

337-345 cm

Massive mud.

345-349 cm

Faintly laminated mud, ~ 5-6 varves/cm.

349-357 cm

Mud, fining up defined by terrigenous organics, sand at base.

357-387 cm

Laminated mud, ~ 3-5 varves/cm.

SECTION 4

387-410 cm

V dk grey 3/1 faintly defined laminated mud, ~ 4-5 varves/cm. Fish bones at 407 cm, stone at 390 cm.

410-414 cm

V dk grey 3/1 massive mud with terrigenous organics.

414-430 cm

Laminated mud.

430-435 cm

Dk olive grey 3/2 massive mud.

435-467 cm

Poorly defined laminated mud.

467 - 472 cm

V dk grey 3/1 massive mud.

472-481 cm

Poorly defined laminated mud. Yellow diatom laminae at 480 cm.

481-500 cm

Poorly defined laminations, bioturbation?

500-507 cm

V dk olive grey massive mud, no terrigenous fragments, some coarse grains at base, subtle fining up defined by grain size only..

507-541 cm

Poorly defined laminations, ~ 7varves/cm where countable.

SECTION 5

541-543 cm

Core lost on recovery

543- 553 cm

V dk olive grey 3/2 , massive mud.

553 – 577 cm

Laminated mud, ~ 8 varves/cm where countable, bioturbation ?

577-583 cm

Massive mud.

583 – 601 cm

Faintly laminated mud.

601-604 cm

V dk grey 3/1 massive mud.

604-610 cm

Faintly laminated mud.

610 – 614 cm.

Massive mud.

614-622 cm

Laminated mud, ~ 3-5 varves/cm, bioturbation?

622-626 cm

Black 2.5/2 mud, fining up defined by terrigenous organics.

626-631 cm

Dk olive grey 3/2 massive mud, terrigenous organic fragments. Stone at 628 cm.

631-641 cm

Poorly defined laminate mud, some distinctive white laminae, ~ 5-10 varves/cm.

641-647 cm

Dk olive grey 3/2 massive mud.

647-652 cm

Massive mud, some sand grains at base.

652 - 661 cm

Poorly defined laminations, ~ 5-6 varves/cm where countable.

661-668 cm

Dk olive grey 3/2 mud, some fining up defined by terrigenous organic fragments.

668-671 cm

Laminated mud.

671-674 cm

Massive mud.

674 -698 cm

Laminated to poorly laminated mud, ~ 4-6 varves/cm. Twig at 695 cm.

SECTION 6

698-712 cm

Dk olive grey 3/2 poorly defined laminated mud.

712 - 717 cm

V dk grey 3/1 massive mud. Lt grey 7/2 layer at 716 cm.

717 – 737 cm

Poorly defined laminated mud.

737 – 741 cm

Massive mud. Some sand at base..

741-743 cm

Laminated mud.

743 – 751 cm

Mud, some terrigenous organic fragments.

751-771 cm

Laminated mud, ~ 5-8 varves/cm, thick terrigenous (dark) laminae. Bioturbation at top of interval?

771-775 cm

V dk grey 3/1 massive mud from silt and shell fragments at base, defined by terrigenous organics, lt grey 7/2 layer at top.

775-780 cm

Laminated mud, thick diatom varves, ~ 4-6 varves/cm.

780 – 783 cm

V dk grey 3/1 massive mud, some sand grains at base.

783 – 789 cm

Laminated mud.

789 – 792 cm

Massive mud, some sand at base.

792-793 cm

Laminated mud.

793 -815 cm

Laminated to poorly laminated mud, ~ 4-6 varves/cm.

815 – 823 cm

Mud, fining up defined by faint terrigenous organics.

823-850 cm

Poorly defined laminations. Wood piece at 822 cm. Distinctive white laminae at 844 cm.

SECTION 7

850-856 cm

V dk grey 3/1 mud, fining up from defined by terrigenous organics.

856-868 cm

Poorly laminated mud, ~ 8-9 cm.

868-870 cm

Massive mud.

870-910 cm

Laminated mud, ~ 4-8 varves/cm.

910-913 cm

Massive mud.

913-920 cm

Poorly defined laminated mud.

912-970 cm

V dk grey 3/1 massive mud, thick (1 cm) lt grey 7/2 layer at 922 cm, some large terrigenous organic fragments throughout. Large wood fragments at 749 and 753 cm.

970 -981 cm

Disturbed laminated mud.

981 – 990 cm

Laminated mud, ~ 5-6 varves/cm.

SECTION 8

990 – 1030 cm

Disturbed laminae, ~ 5-10 varves/cm.

1030-1042 cm

V dk grey 3/1 massive mud, traces of disturbed laminae and some terrigenous organic fragments.

1042-1098 cm

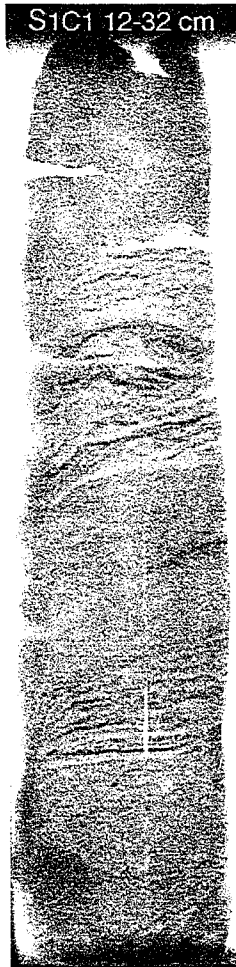
Disturbed laminated to poorly laminated mud.

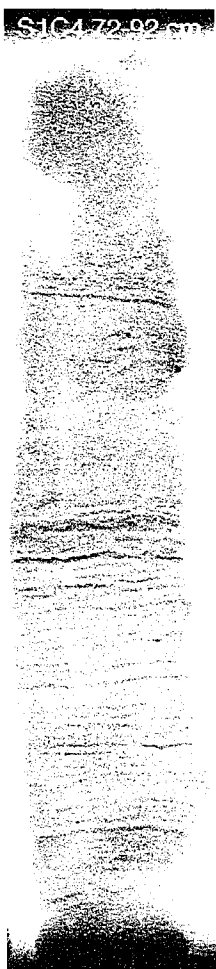
1098 -1117 cm

V dk grey 3/1 mud, fining up defined by terrigenous organic fragments, some sand at the base.

1117 to 1130 cm

Laminated mud, 5-6 varves/cm.





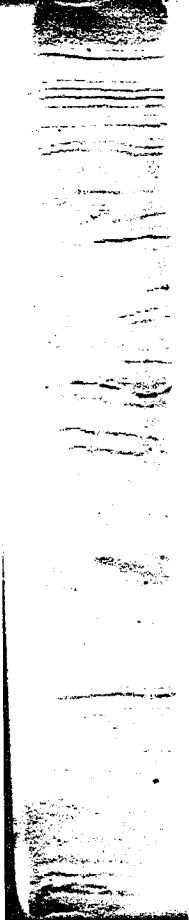
S2C3 144-164 cm



S2C3 164-



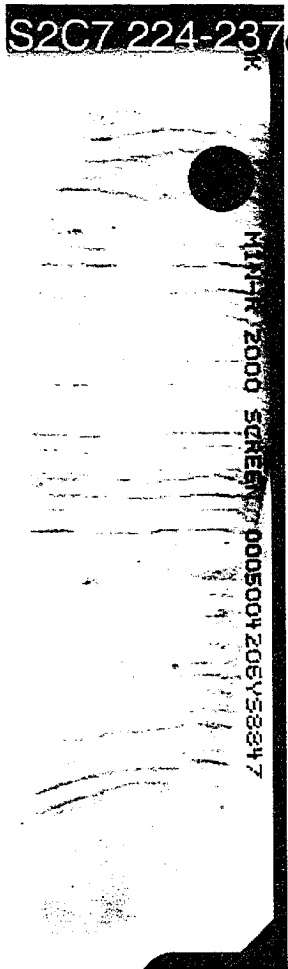
S2C5 184-204cm

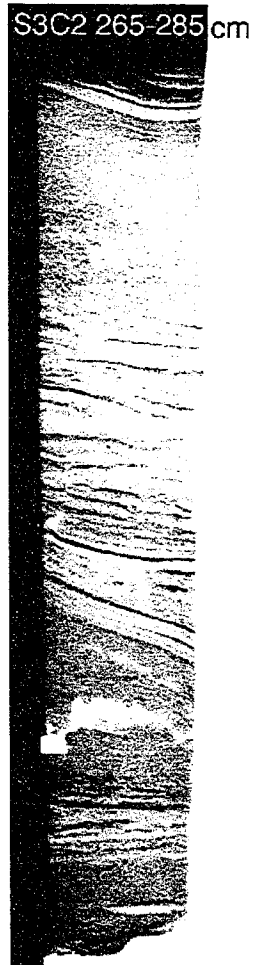


S2C6 204-24 cm



S2C7 224-237cm



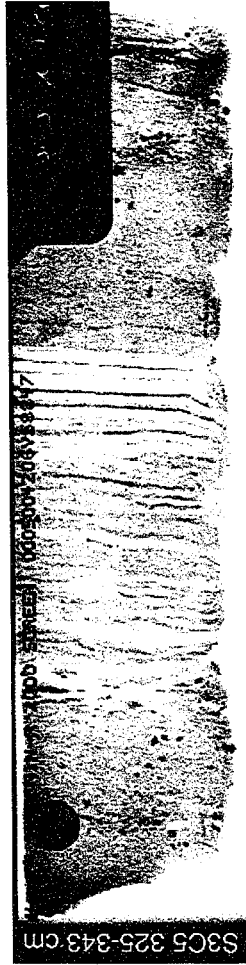
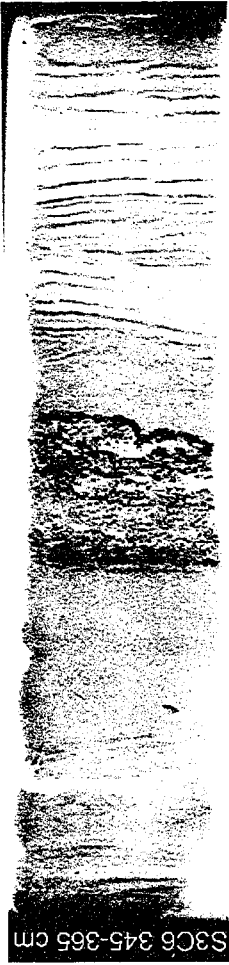


S3C3 285-305 cm

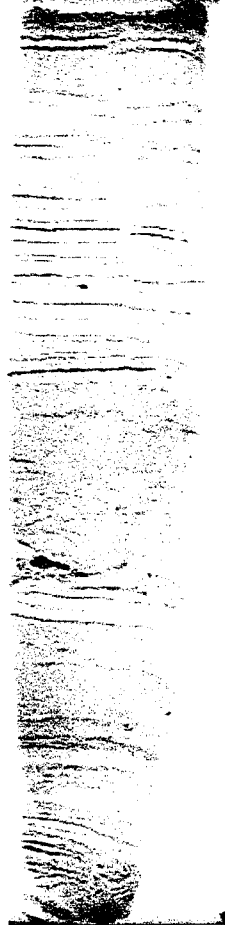


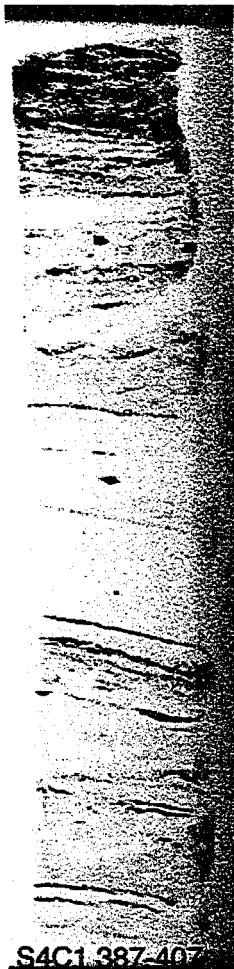
S3C4 305-325cm



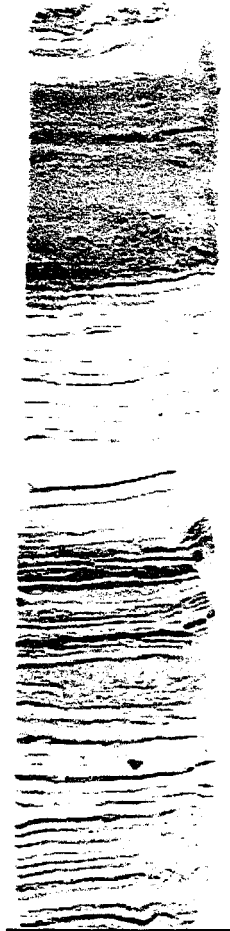


S3C7 974-990 cm

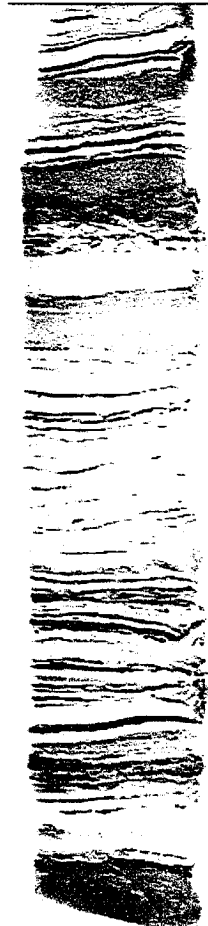
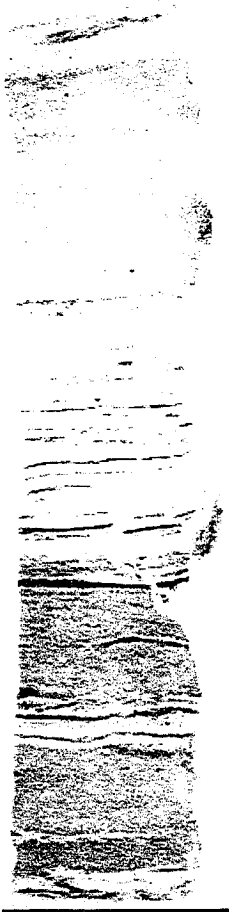




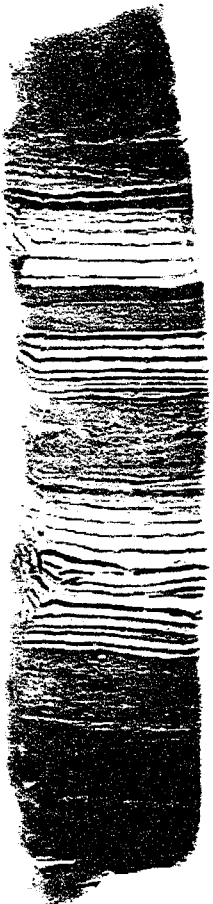
S4C2 408-428 cm



S4C3 428-449cm

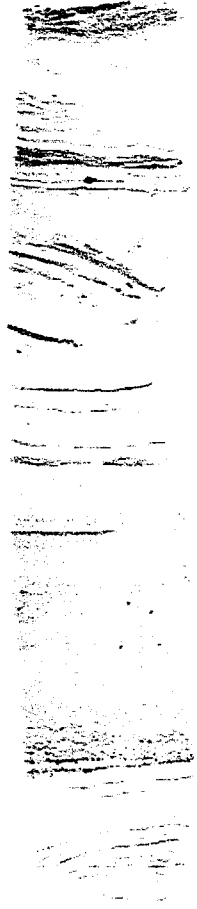


S4C4 449-469cm

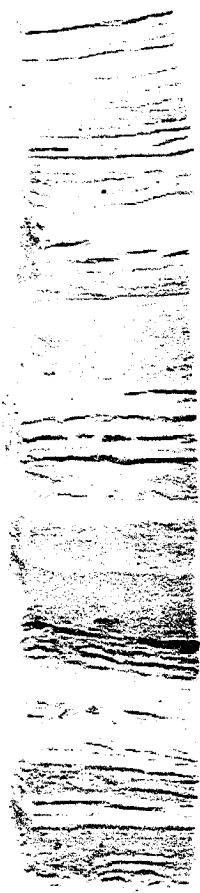


S4C5 469-489cm

S4C6 490-510cm



S4C7 510-530
cm



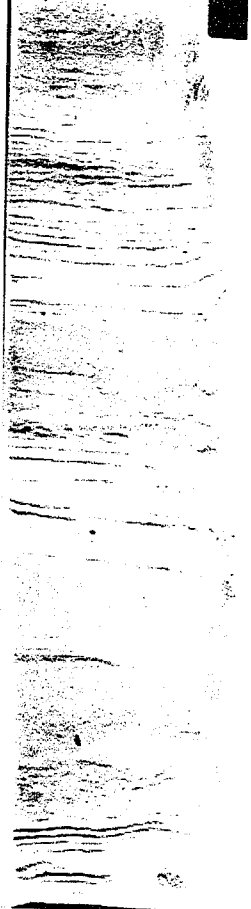
S4C8
530-
541cm



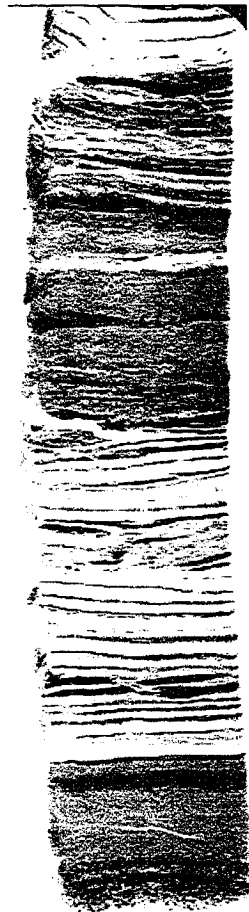
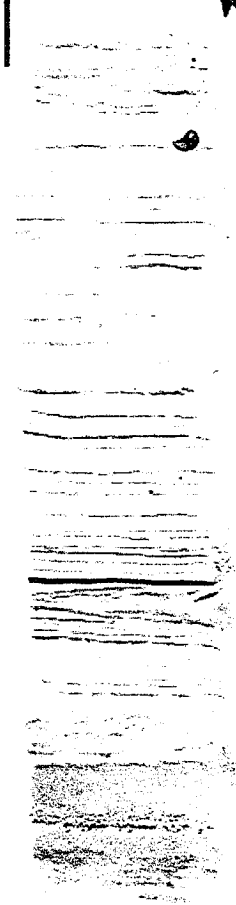
S5C1 543-564cm



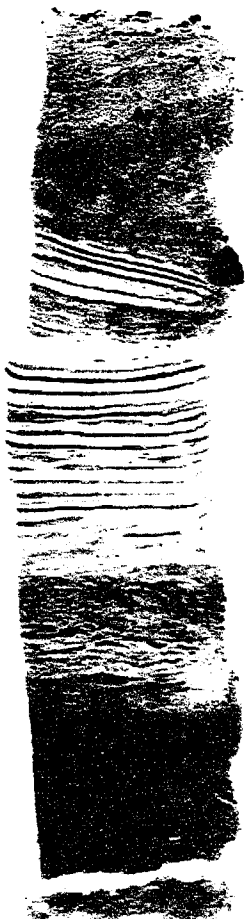
S5C2 564-584cm



S5C3 584-604 cm

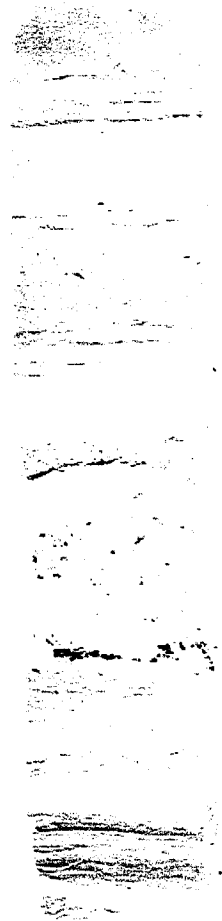


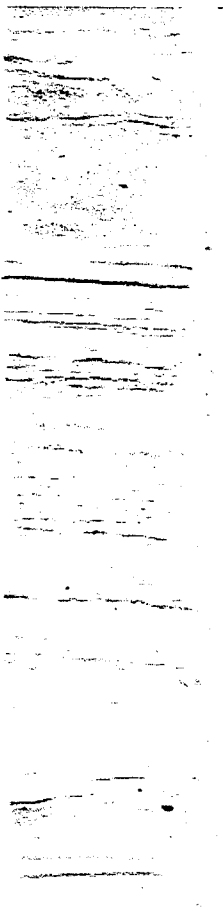
S5C4 607-627 cm



S5C5 627-645 cm

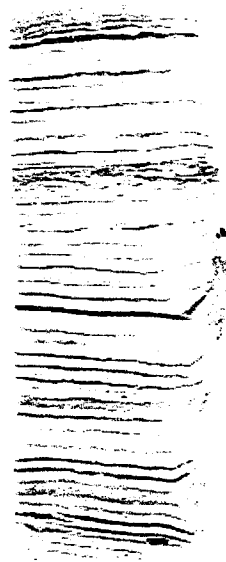
S5C6 645-664 cm



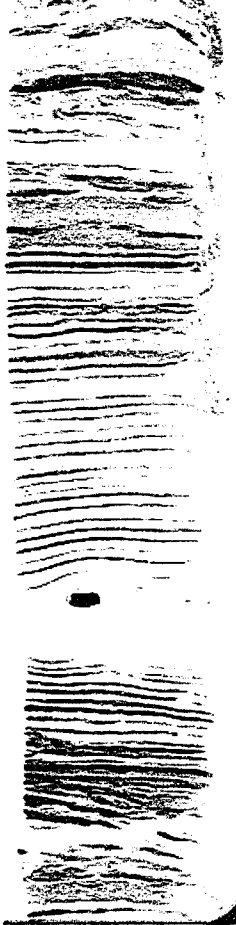


S5C7 664-684cm

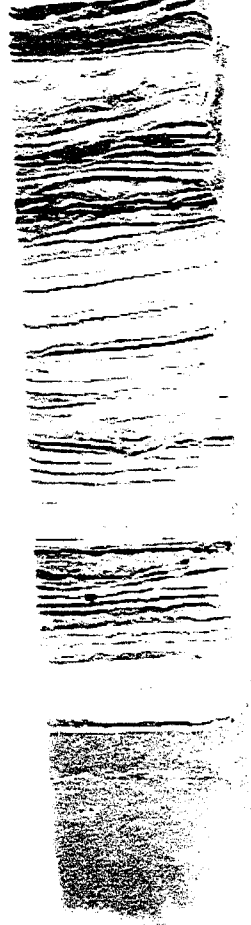
S5C8 684-695 cm



S6C1 701-721 cm



S6C2 722-742 cm



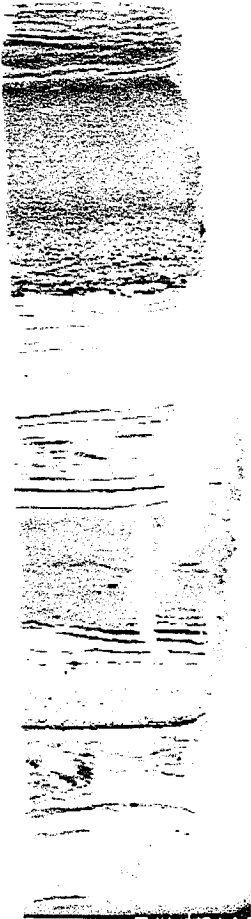


S6C3 741-759cm



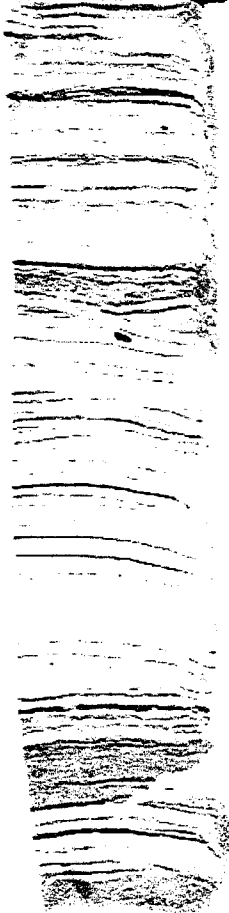
S6C4 759-778 cm

S6C5 778-798 cm



S6C6 803-819 cm

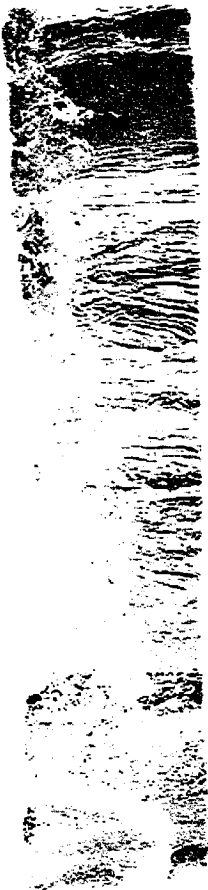
S6C7 819-840 cm



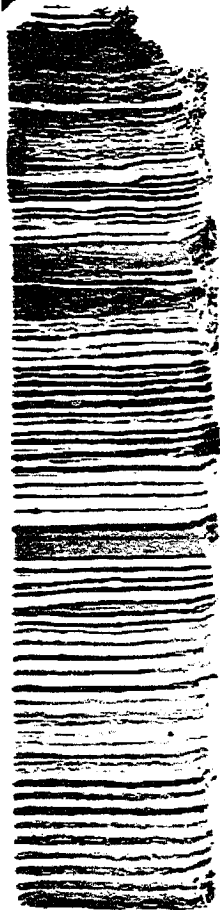
S6C8 843-851cm



S7C1 851-870 cm



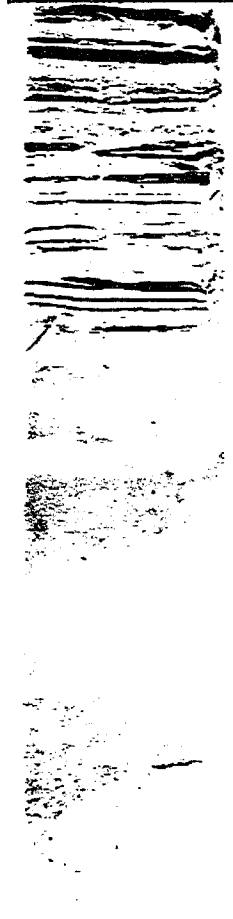
S7C2 873-893 cm



S7C3 893-913 cm



S7C4 914-933 cm



S7C5 933-954 cm



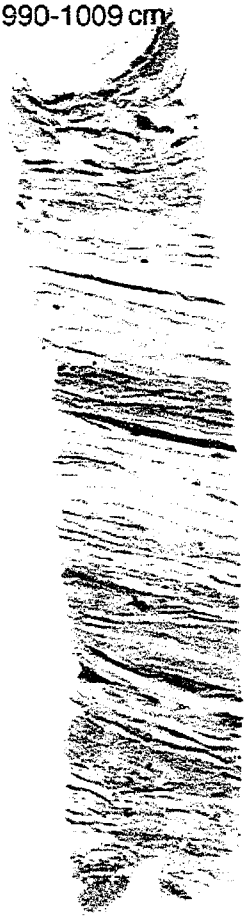
S7C6 954-972cm



S7C7 974-990 cm



S8C1
990-1009 cm



S8C2 1009-1029
cm



S8C3
1029-49cm



S8C4 1049-69 cm

APPENDIX G

X-rays and descriptions of outer basin core
TUL99B11

CORE DESCRIPTION TUL99B11, Outer basin

SECTION 1/2 (recovered together in the same core liner)

Core is very wet.

0 –3 cm

Olive 4/4 massive mud, turns to black on scraping of surface sediment with a spatula.

3 – 45 cm

Black 2.5/1 Massive mud with very faint traces of laminations especially at the base.

45- 47 cm

Pale olive 6/3 Massive mud.

47 – 112 cm.

Abrupt colour change to v. dk grey 3/1 to dk olive grey 3/2 massive mud with faint traces of laminations.

SECTION 3

112 – 141 cm

Core lost on recovery.

141 – 179 cm

Olive 5/3 to black massive mud, with faint laminations visible on scraping of top sediments.

179-184 cm

Olive 5/3 massive mud. Sand at base.

184 – 188 cm

V dk grey 3/1 mud, fining up defined by small terrigenous organics and shell fragments.

188- 195 cm

Olive 5/3 massive mud with small terrigenous organics.

195 – 265 cm

Dk olive grey 3/2 very faintly laminated mud.

SECTION 4

265 – 272 cm

Core is broken.

272 – 285 cm

Olive grey 4/2 massive mud, some very faint terrigenous (dark coloured) laminae, small terrigenous organics up to 2 cm.

Black 2.5/2 mud, fining upwards from sand at the base is defined by terrigenous organics, shell and wood fragments up to 6 cm in length.

316 – 323 cm

Olive grey 4/2 massive mud with very faint terrigenous (dark) laminations and terrigenous organics.

323 – 360cm

Olive grey 4/2 massive mud, lt olive 6/3 mud at top, some terrigenous organics.

Black 2.5/2 mud, fining up defined by terrigenous organics up to 3 cm in length, thin 2mm sand and shell at base. Wood piece at 268 cm.

360 – 405 cm

Olive grey 4/2 massive mud with faint terrigenous (dark) laminae traces.

SECTION 5

405 – 491 cm

Dk olive grey 3/2 massive mud with faintly defined terrigenous (dark) laminae. Some dark laminae up to 1 cm thick.

491–497 cm

Dark olive grey massive mud, lt olive 6/3 mud layers at top and base.

497-524 cm

Dk olive grey 3/2 massive mud, lt olive layer 6/3 at top. Large fish remains at 501 cm.

524-559 cm

Dk olive grey 3/2 laminated mud, thick terrigenous laminae, ~ 2 varves/cm where countable.

SECTION 6

559 – 642 cm

Dk olive grey 3/2 massive mud with faintly developed terrigenous (dark) laminations. Some terrigenous organics but much fewer than above sections.

642 – 645 cm

Distinct color change to olive 5/3 massive mud.

645-647 cm

Dk olive grey 3/2 laminated mud.

647 – 653 cm

Olive 5/3 mud, faint fining up from base, no terrigenous organics, grain sorting only.

653-710 cm

Olive 5/4 massive mud, lt olive 6/3, 1.5. cm thick bed at top. Very consolidated.

SECTION 7

709 – 721 cm

Olive 5/4 faintly laminated mud, no terrigenous organics.

721 – 728 cm

Olive 4/3 massive mud with sand grains and shell fragments.

728-734 cm

Black 2.5/1 mud, fining up from base defined by terrigenous organics.

734- 741 cm

Dk olive grey 3/2 mud fining up defined by terrigenous organics, from sand at base, 2 cm thick.

741-755 cm

Olive grey 4/2 massive mud, very faintly defined terrigenous (dark) laminations.

755-760 cm

Olive grey 4/2 massive mud, some faint traces of laminae.

760-851 cm

Olive 4/3 massive mud, slightly more distinctive terrigenous (dark) laminations, some sand at 786 and 801 cm.

SECTION 8

851 – 856 cm

Dk olive grey 3/2 massive mud, faint terrigenous (dark) laminations.

856-861 cm

V dk grey 3/1 mud, fining up from sand at base defined by terrigenous organics.

861-865 cm

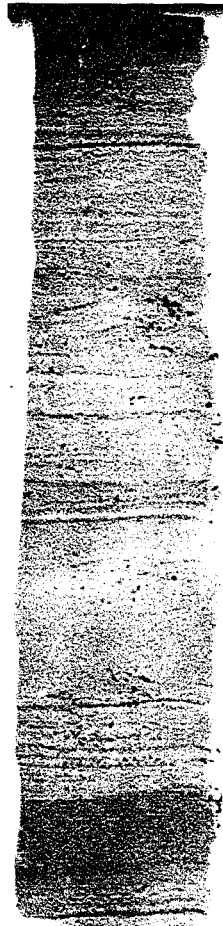
Dk olive grey mud fining up from sand at base defined by terrigenous organics.

865 – 1016 cm

Dk olive grey 3/2 faintly to distinctly laminated mud, ~ 3 varves/cm where countable. Wood piece at 907 cm. Sand at 949, 969 and 990 cm.

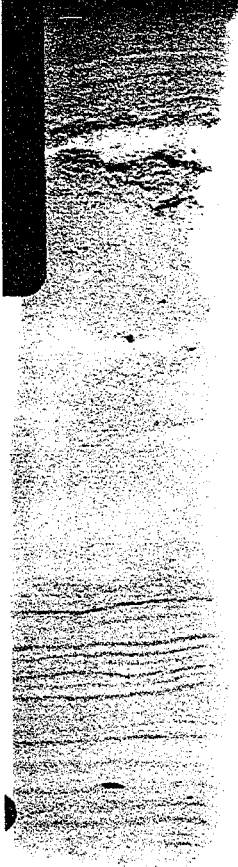


S3C1 141-161 cm

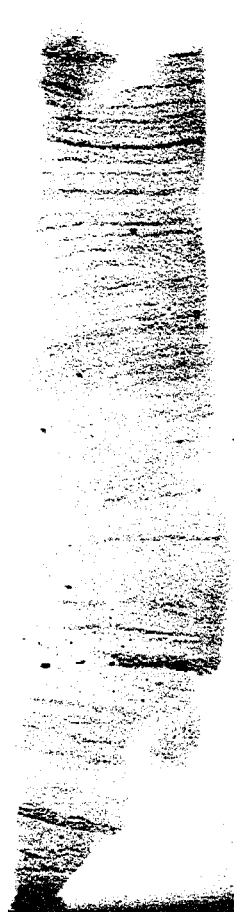


S3C2 161-181 cm

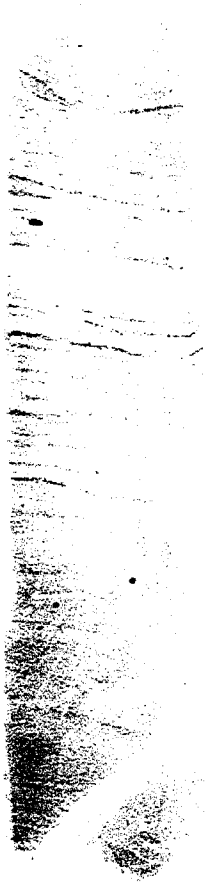
S3C3 181-201 cm



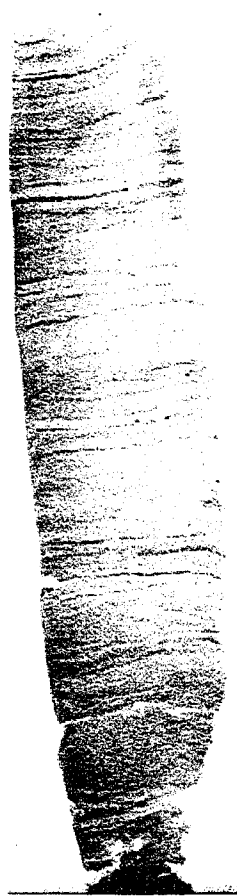
S3C4 201-219 cm



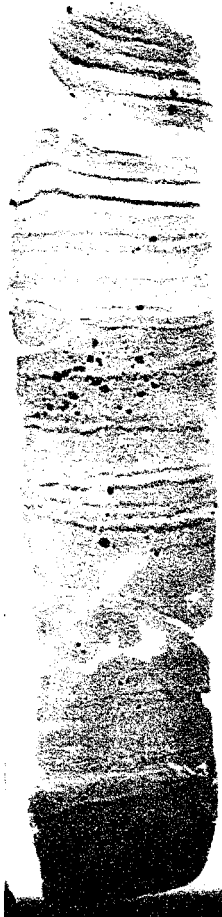
S3C5 219-236 cm



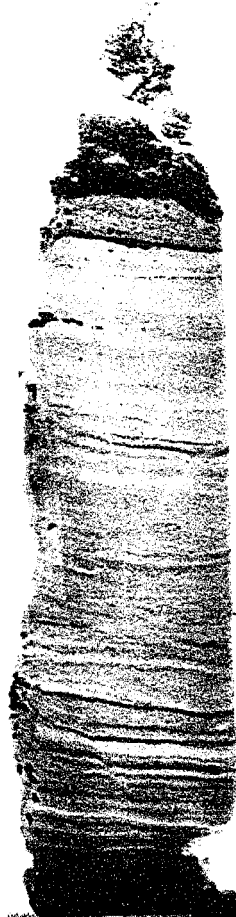
S3C6 236-255 cm



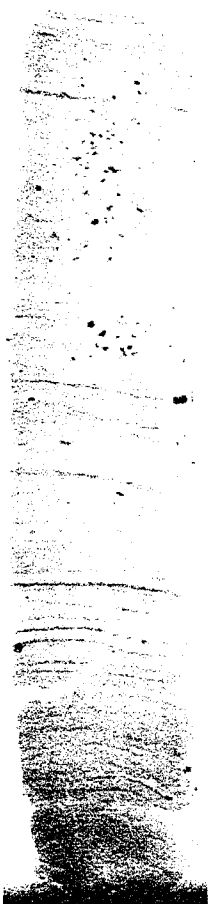
S4C1 265-283 cm



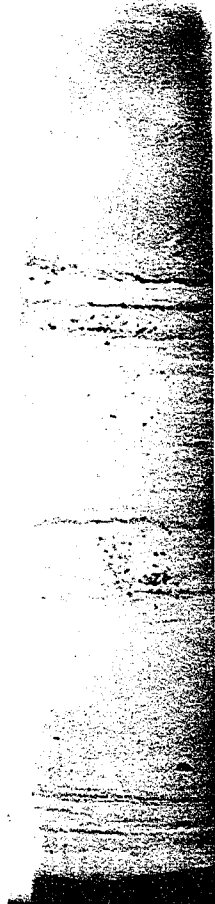
S4C2 287.5-305 cm



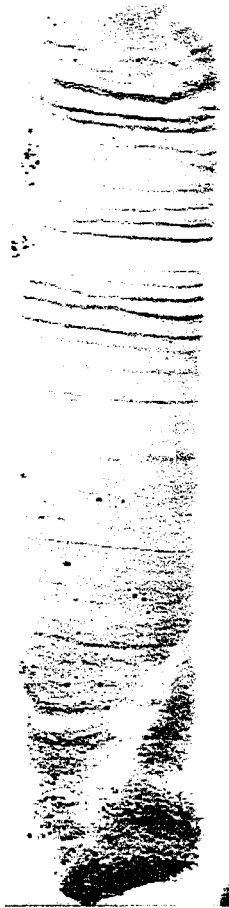
S4C3 305-324 cm



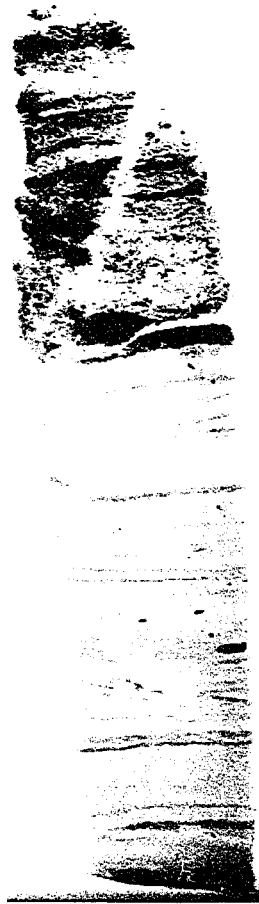
S4C4 324-341 cm



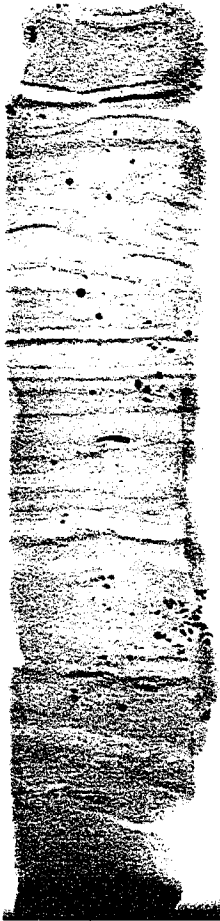
S4C5 344-362 cm



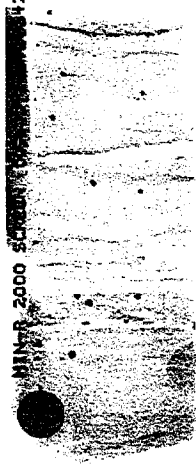
S4C6 362-378 cm



S4C7 378-398 cm



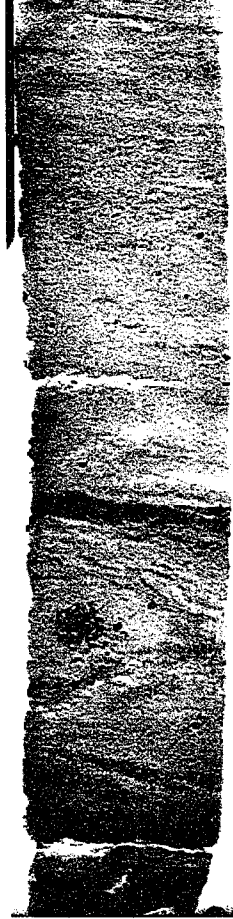
S4C8 398-405 cm



S5C1 405-424 cm



S5C2 424-444 cm



S5C3 444-464 cm

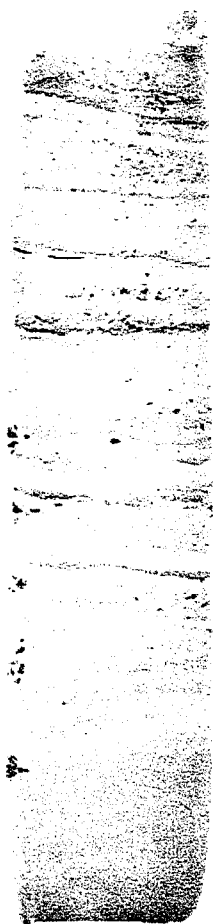


S5C4 464-483 cm



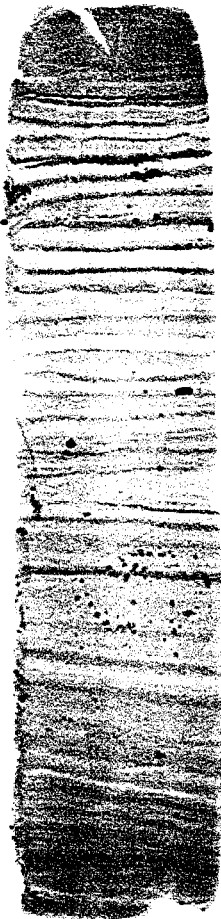


S5C5 483-503 cm



~~S5C6 509-527 cm~~

S5C7 527-548 cm



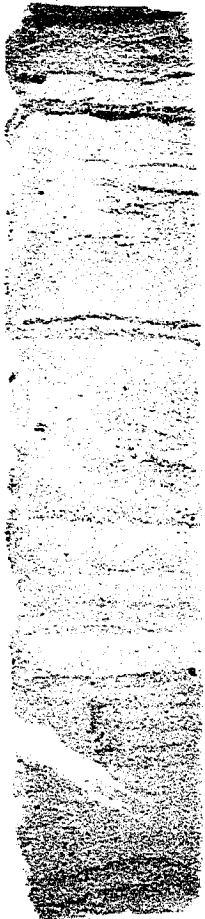
S5C8 548-559 cm



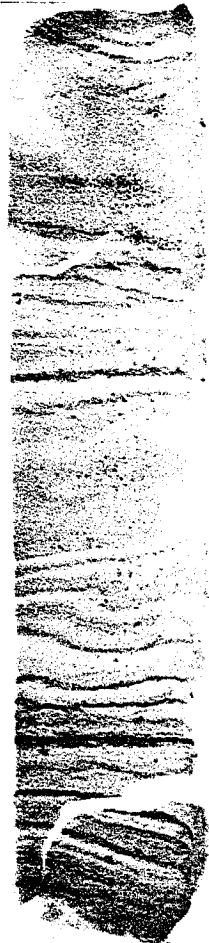
S6C1 559-579 cm



S6C2 579-600 cm



S6C3 600-620 cm



S6C4 620-640 cm



S6C6 641-661 cm



S6C7 661-681 cm

S6C7 681-701 cm



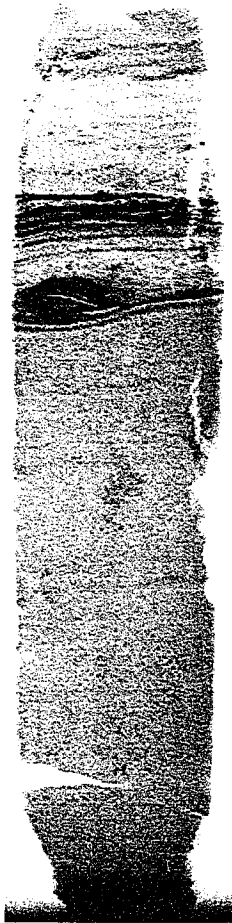
S6C8 701-709 cm



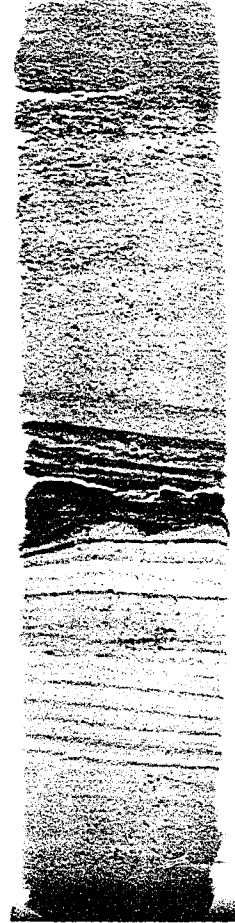
MIN-R 2000 SCREEN 660300130152247



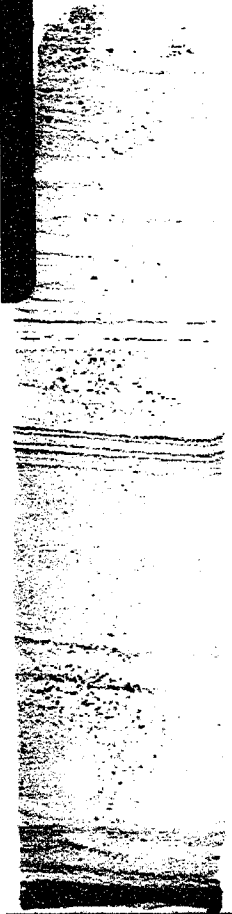
S7C1 709-729 cm



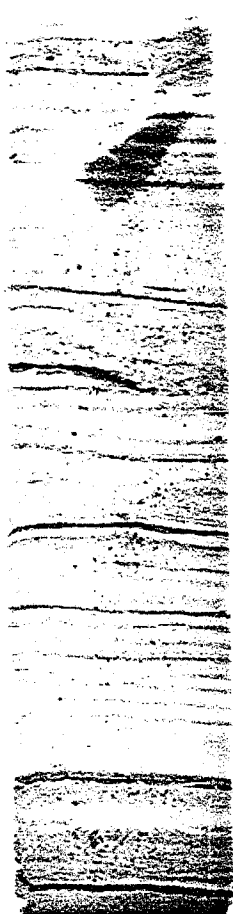
S7C2 729-749 cm



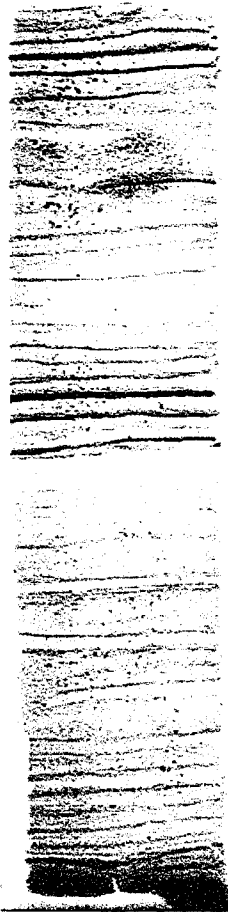
S7C3 749-769 cm



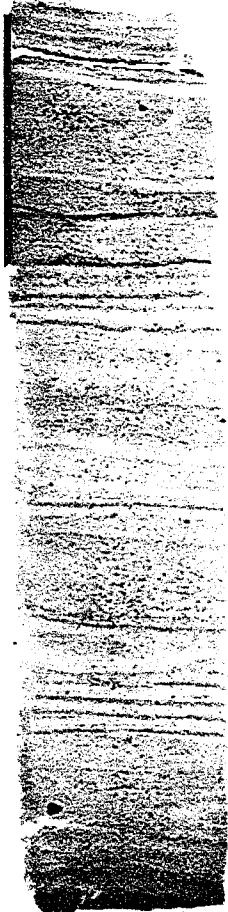
S7C4 769-789 cm



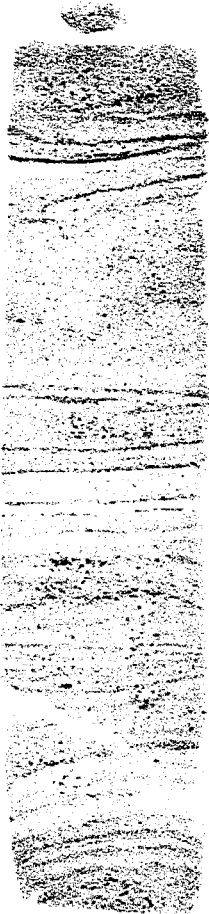
S7C5 789-808 cm



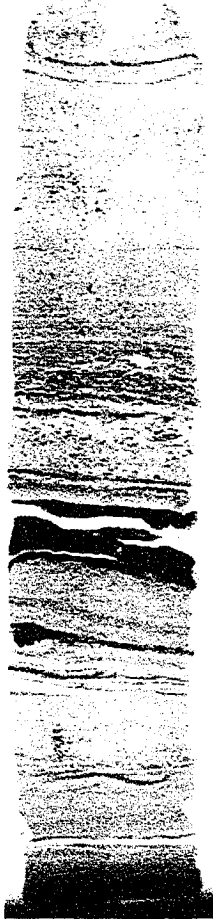
S7C6 808-828 cm



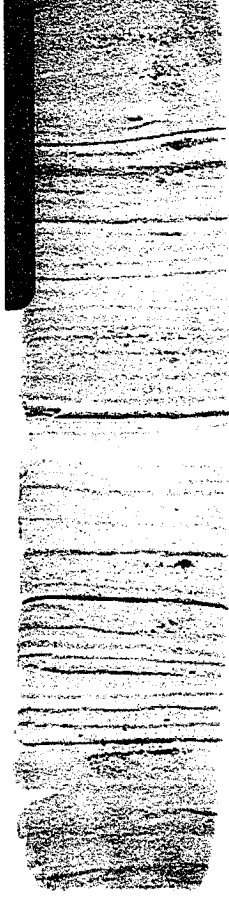
S7C7 828-845 cm



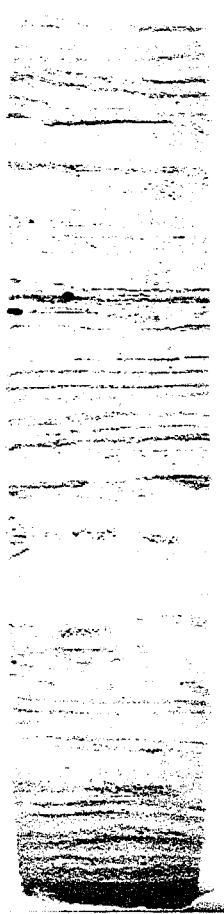
S8C1 851-871 cm



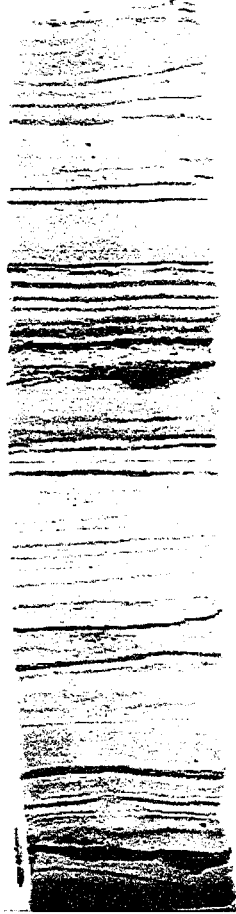
S8C2 871-891 cm

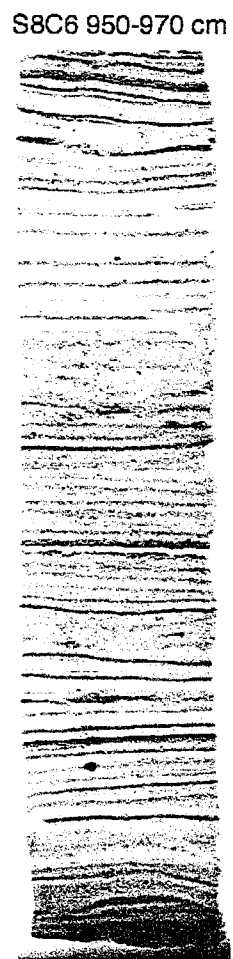
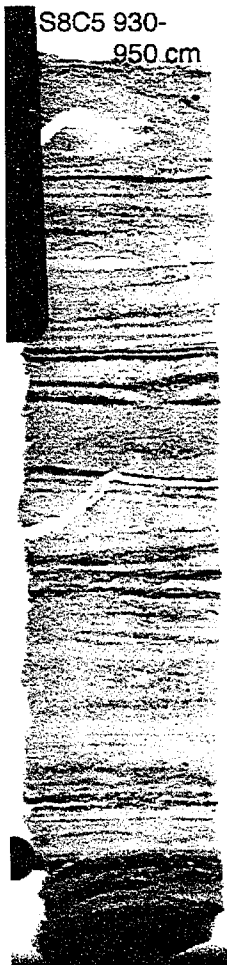


S8C3 891-910 cm

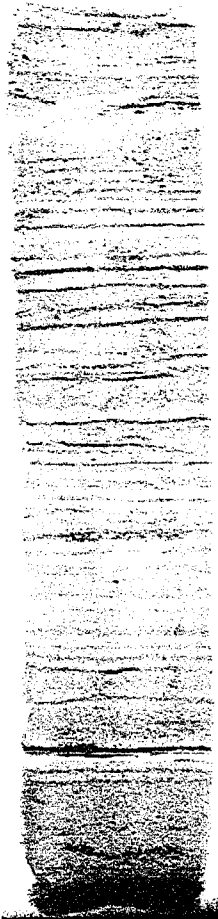


S8C4 910-930 cm

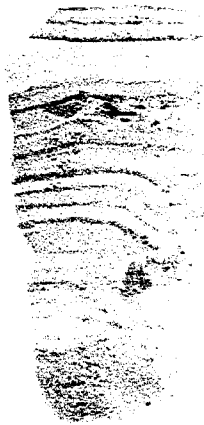




S8C7 970-990 cm



S8C8 990-999 cm



APPENDIX H

Descriptions of freeze cores

FREEZE CORE
DESCRIPTION

B04	B12	B10	B01
0 – 30 cm	0-10 cm	0- 17 cm	0 – 35 cm
Laminated mud, ~ 2-3 varves/cm	Black massive mud.	Laminated mud. 17- 90 cm	Laminated mud, disturbed on recovery.
30 cm – 118 cm	10 – 70 cm	Massive dk olive grey 3/2 massive mud, chaotic bedding, terrigenous organic fragments.	35 – 109 cm
Massive mud, chaotic bedding, terrigenous organic fragments.	Massive mud, chaotic bedding.		Massive mud, chaotic bedding, terrigenous organic fragments.
118 – 126 cm			
Laminated mud.			
			B07
			0-18 cm
			Laminated mud.
			18- 109 cm
			Massive mud.
			109 – 129 cm
			Poorly Laminated mud.

APPENDIX I

ROCK-EVAL data and grain-size analyses data

ROCK-EVAL ANALYSES

The standard ROCK-EVAL VI analysis can be performed on consolidated or unconsolidated sediments and gives an indication of whether the origin of the organic matter in the sediments is Type I (algal), Type II, (marine) or Type III, (terrestrial).

ROCK-EVAL parameters are as follows

TOC = total organic carbon

Tmax = temperature at the top of the S2 peak

S1 = hydrocarbons evolved (distilled or thermovaporized) at 300 C and 600 C

S2 = hydrocarbons evolved during heating at 25C/min between 300 C and 600 C

S3 = organic carbon dioxide evolved at 300 C and up to 390 C

PI = production index = $S1/(S1+S2)$

HI = hydrogen index = $S2/TOC$

OI = Oxygen index = $S3/TOC$

(Macauley et al., 1985; Peters, 1986)

Effingham Inlet (Sound)

Depth	TOC	PI	S1+S2	Tmax	S1	S2	S3	OI	HI
45	2.45	0.01	4.74	403	0.05	4.69	4.91	175	193
45	2.39	0.01	4.66	406	0.06	4.6	4.66	165	195
85	2.53	0.01	5.65	404	0.08	5.57	5.57	181	222
125	2.53	0.02	5.55	405	0.09	5.46	5.21	170	217
159	2.44	0.01	4.82	406	0.07	4.75	4.96	175	196
198	2.33	0.02	4.14	388	0.07	4.07	4.84	172	177
238	2.37	0.02	4.34	397	0.07	4.27	4.45	161	182
278	2.19	0.02	4.26	405	0.07	4.19	4.27	163	193
303	2.32	0.01	4.59	409	0.06	4.53	4.55	170	197
341	2.37	0.02	4.81	404	0.09	4.72	4.23	153	200
381	2.07	0.01	3.59	401	0.05	3.54	4.29	185	173
421	2.08	0.01	3.85	405	0.04	3.81	4.59	188	185
455	2.1	0.01	3.33	386	0.05	3.28	4.69	188	158
495	2.19	0.01	3.75	390	0.06	3.69	4.10	161	170
535	2.22	0.01	3.46	389	0.04	3.42	4.29	168	156
575	2.25	0.01	3.99	399	0.03	3.96	3.88	158	177
610	2.06	0.02	3.66	403	0.06	3.6	4.41	177	177
650	2.01	0.01	3.43	388	0.04	3.39	3.89	163	171
690	1.97	0.02	2.88	378	0.06	2.82	3.99	173	145
740	2.04	0.01	4.03	405	0.04	3.99	4.16	186	198
760	1.97	0.02	3.24	387	0.06	3.18	3.63	156	163
790	1.85	0.01	2.93	388	0.04	2.89	4.07	181	158
840	1.88	0.02	2.94	378	0.04	2.9	3.85	174	156
880	1.69	0.01	3.03	389	0.04	2.99	3.32	165	179

Effingham Inlet (Outer)

Depth	TOC	PI	S1+S2	Tmax	S1	S2	S3
8	5.35	0.01	11.75	415	0.14	11.61	11.87
55	4.22	0.01	9.88	417	0.14	9.74	9.82
73	4.03	0.02	9.74	415	0.16	9.58	9.2
103	4.36	0.01	10.85	424	0.13	10.72	9.79
135	4.14	0.01	9.08	414	0.09	8.99	8.82
155	5.77	0	11.5	414	0.06	11.44	12.08
203	4.17	0.01	0.11	415	0.1	0.01	9.3
263	4.18	0.02	0.17	415	0.16	0.01	9.83
323	4.72	0.01	0.13	410	0.12	0.01	9.96
373	4.23	0.01	0.11	417	0.1	0.01	9.87
419	1.7	0.02	0.09	414	0.06	0.03	4.91
443	3.76	0	0.06	407	0.04	0.02	7.98
455	5.2	0.01	0.14	414	0.13	0.01	11
503	4.16	0.01	0.12	407	0.1	0.02	8.96
563	4.04	0.01	0.11	417	0.1	0.01	9.62
583	3.7	0.02	0.15	412	0.13	0.02	8.67
605	3.45	0.01	0.1	408	0.08	0.02	7.84
623	2.26	0.01	0.04	404	0.02	0.02	5.64
653	3.95	0.02	0.16	408	0.14	0.02	8.42
683	4.3	0.01	0.15	411	0.14	0.01	8.9
723	3.54	0.01	0.11	409	0.09	0.02	7.62
733	4.07	0.01	0.11	413	0.09	0.02	9.01
753	3.49	0.01	0.1	411	0.08	0.02	7.65
793	3.38	0.01	0.08	435	0.06	0.02	7.27
873	4.91	0	0.06	442	0.05	0.01	10.31

OI	HI
189	217
193	231
191	238
190	246
181	217
176	198
188	234
194	229
173	226
197	223
243	188
175	207
181	193
184	220
198	225
196	219
190	206
209	188
181	218
176	241
180	218
182	222
182	213
180	244
176	202

Effingham Inlet (Inner)

Depth	TOC	PI	S1+S2	Tmax	S1	S2	S3
33	5.58	0.02	13.98	417	0.28	13.7	12.48
55	5.76	0.02	0.33	412	0.31	0.02	11.23
93	5.33	0.03	0.41	415	0.39	0.02	10.21
105	4.98	0.03	0.36	413	0.34	0.02	8.72
123	6.07	0.01	0.14	409	0.12	0.02	11.54
203	6.06	0.01	0.16	419	0.14	0.02	13.63
205	6.43	0.02	0.26	416	0.24	0.02	13.67
213	5.68	0.02	0.23	414	0.21	0.02	11.83
283	5.04	0.02	0.35	416	0.33	0.02	10.26
353	5.39	0.01	0.18	413	0.17	0.01	10.62
393	6.21	0.01	0.13	412	0.11	0.02	11.42
413	4.66	0.01	0.16	414	0.14	0.02	9.41
433	4.68	0.01	0.09	417	0.07	0.02	18.47
435	5.17	0.03	0.38	416	0.37	0.01	9.88
463	4.56	0.02	0.29	412	0.28	0.01	8.77
503	5.08	0.02	0.2	408	0.19	0.01	9.41
523	4.36	0.01	0.14	406	0.12	0.02	8.67
553	5.52	0.01	0.14	409	0.13	0.02	11.52
606	4.71	0.02	0.21	408	0.19	0.02	8.78
633	4.19	0.02	0.21	407	0.2	0.01	8.41
713	5.24	0.02	0.3	326	0.29	0.01	10.21
733	5.21	0.01	0.19	416	0.18	0.01	9.49
763	5.45	0.02	0.21	407	0.2	0.01	10.32
813	4.85	0.01	0.15	410	0.14	0.01	10.02
853	5.09	0.01	0.14	405	0.12	0.02	9.45
883	4.42	0.01	0.13	409	0.11	0.02	8.67

OI	HI
188	246
164	243
165	241
150	245
162	231
194	220
179	219
174	237
170	264
189	223
169	217
174	236
311	220
165	269
162	253
159	222
176	228
181	230
157	243
170	250
165	271
154	228
165	215
168	241
164	234
165	231

Terrain Sciences Division- Sedimentology Laboratory Report

Complete Grain Size Analysis - PSA

Sample # B13S6 111 113 * spilled in mixer

Name: Dallimore Date (y/m/d): 00/11/14 Report No.: 15165
 Project No.: 970017 Technician: mw/b

Sample No.	Dry Split	Weight (g)					Size Fraction (mm) (Reported as percentage of <2mm)				
		>2mm	2-0.063mm	0.063mm	0.063-0.044	0.044-0.031	0.031-0.016	0.016-0.008	0.008-0.004	0.004	
B13S1/2 011 014	3.758	0.000	0.254	3.504	6.759	21.007	18.534	30.187	15.366	7.033	1.1
B13S1/2 050 053	3.611	0.013	0.504	3.094	14.008	17.037	16.374	28.310	15.721	7.407	1.1
B13S1/2 110 113	4.822	0.000	0.126	4.696	2.613	15.258	17.488	31.457	19.630	11.116	2.4
B13S1/2 140 143	3.475	0.000	0.331	3.144	9.525	13.707	14.333	27.609	19.775	11.941	3.1
B13S3 007 010	4.171	0.000	0.265	3.906	6.353	13.782	15.599	30.473	20.179	11.303	2.3
B13S3 027 029	3.006	0.000	0.266	2.740	8.849	15.560	16.359	29.458	18.388	9.452	1.9
B13S3 031 033	3.239	0.000	0.484	2.755	14.943	15.245	14.880	27.420	16.886	8.792	1.6
B13S3 038 041	6.477	0.000	0.109	6.368	1.683	16.132	17.163	29.845	19.370	12.066	3.2
B13S3 066 069	4.470	0.000	0.048	4.422	1.074	15.452	16.600	30.882	20.348	12.222	3.4
B13S3 091 094	3.947	0.000	0.077	3.870	1.951	17.826	18.652	31.442	18.573	9.564	1.9
B13S3 121 124	4.140	0.000	0.277	3.863	6.691	14.764	16.800	30.582	18.774	10.184	2.2
B13S4 020 023	5.933	0.000	0.161	5.772	2.714	13.675	14.951	28.846	20.870	13.939	4.0
B13S4 066 069	7.161	0.000	0.133	7.028	1.857	14.876	15.826	29.730	20.386	12.954	4.3
B13S4 096 099	7.147	0.000	0.173	6.974	2.421	15.840	16.697	29.666	19.636	12.055	3.0
B13S4 141 143	4.834	0.000	0.157	4.677	3.248	15.465	17.484	31.534	18.975	10.376	2.9
B13S401260129	7.201	0.022	0.114	7.065	1.588	13.182	15.454	29.679	20.558	14.126	5.0
B13S5 020 023	4.331	0.000	0.119	4.212	2.748	14.677	16.769	30.187	20.449	11.851	3.3
B13S5 036 039	7.123	0.000	0.079	7.044	1.109	14.694	17.160	30.594	19.471	12.660	4.3
B13S5 070 073	3.598	0.000	0.088	3.510	2.446	12.867	14.766	29.564	23.016	13.456	3.0
B13S5 104 107	4.830	0.000	0.057	4.773	1.180	13.454	14.678	28.622	21.188	14.968	5.0
B13S5 117 120	6.339	0.000	0.180	6.159	2.840	16.263	17.719	30.189	18.998	10.805	3.0
B13S5 148 151	4.990	0.000	0.101	4.889	2.024	16.928	17.525	30.590	18.910	10.902	4.0
B13S6 016 019	7.203	0.016	0.088	7.099	1.224	16.448	16.910	29.186	19.784	12.423	4.0
B13S6 040 043	8.133	0.000	0.409	7.724	5.029	13.611	14.930	27.531	19.726	13.654	5.0
B13S6 063 066	4.331	0.000	0.111	4.220	2.563	14.591	15.157	28.961	21.630	13.303	3.0
B13S6 072 075	10.179	0.000	0.385	9.794	3.782	15.787	16.358	28.698	19.399	12.132	3.0
B13S6 111 113 *	6.552	0.000	0.088	6.466	1.313	14.265	15.917	30.796	20.660	13.082	3.0
B13S6 130 133	5.220	0.021	0.044	5.155	0.846	13.784	15.511	30.125	21.556	13.750	5.0
B13S7 010 013	5.627	0.000	0.041	5.586	0.729	14.265	14.991	28.485	21.503	14.611	4.0
B13S7 027 030	7.913	0.000	0.079	7.834	0.988	13.920	15.815	30.308	21.171	13.357	4.0
B13S7 032 035	6.226	0.000	0.152	6.074	2.441	14.438	15.712	29.897	20.777	12.812	3.0
B13S7 037 040	8.281	0.042	0.456	7.783	5.535	14.732	15.575	27.862	18.714	12.640	4.0
B13S7 060 063	6.146	0.000	0.135	6.011	2.197	16.686	17.532	30.302	19.289	10.846	3.0

Sedimentology Laboratory Report

Grain Size Analysis - PSA

15165

Size Fraction (mm)	Reported as percentage of < 2mm						% of Bulk Sample	wt. % Sand-Silt-Clay		
	0.075-0.150	0.150-0.300	0.300-0.600	0.600-1.250	1.250-2.000	> 2.000	% Pebbles	% Sand	% Silt	% Clay
18.534	30.187	15.366	7.033	1.114	0.000	0.000	0.000	8.759	93.241	0.000
16.374	28.310	15.721	7.407	1.143	0.000	0.000	0.360	14.008	85.992	0.000
17.488	31.457	19.630	11.116	2.437	0.000	0.000	0.000	2.613	97.387	0.000
14.333	27.609	19.775	11.941	3.111	0.000	0.000	0.000	9.525	90.475	0.000
15.599	30.473	20.179	11.303	2.311	0.000	0.000	0.000	6.353	93.647	0.000
16.359	29.458	18.388	9.452	1.934	0.000	0.000	0.000	8.849	91.151	0.000
14.880	27.420	16.886	8.792	1.833	0.000	0.000	0.000	14.943	85.057	0.000
17.163	29.845	19.370	12.066	3.742	0.000	0.000	0.000	1.683	98.317	0.000
16.600	30.882	20.348	12.222	3.421	0.000	0.000	0.000	1.074	98.926	0.000
18.652	31.442	18.573	9.564	1.992	0.000	0.000	0.000	1.951	98.049	0.000
16.800	30.582	18.774	10.184	2.206	0.000	0.000	0.000	6.691	93.309	0.000
14.951	28.846	20.870	13.939	4.676	0.330	0.000	0.000	2.714	96.956	0.330
15.826	29.730	20.386	12.954	4.370	0.000	0.000	0.000	1.857	98.143	0.000
16.697	29.666	19.636	12.055	3.685	0.000	0.000	0.000	2.421	97.579	0.000
17.484	31.534	18.975	10.376	2.918	0.000	0.000	0.000	3.248	96.752	0.000
15.454	29.679	20.558	14.126	5.038	0.373	0.000	0.306	1.588	98.039	0.373
16.769	30.187	20.449	11.851	3.319	0.000	0.000	0.000	2.748	97.252	0.000
17.160	30.594	19.471	12.660	4.312	0.000	0.000	0.000	1.109	98.891	0.000
14.766	29.564	23.016	13.456	3.885	0.000	0.000	0.000	2.446	97.554	0.000
14.678	28.622	21.188	14.968	5.486	0.423	0.000	0.000	1.180	98.397	0.423
17.719	30.189	18.998	10.805	3.186	0.000	0.000	0.000	2.840	97.160	0.000
17.525	30.590	18.910	10.902	3.120	0.000	0.000	0.000	2.024	97.976	0.000
16.910	29.186	19.784	12.423	4.025	0.000	0.000	0.222	1.224	98.776	0.000
14.930	27.531	19.726	13.654	5.115	0.404	0.000	0.000	5.029	94.567	0.404
15.157	28.981	21.630	13.303	3.775	0.000	0.000	0.000	2.563	97.437	0.000
16.358	28.698	19.399	12.132	3.843	0.000	0.000	0.000	3.782	96.218	0.000
15.917	30.796	20.660	13.082	3.938	0.000	0.000	0.000	1.313	98.687	0.000
15.511	30.125	21.556	13.750	4.428	0.000	0.000	0.402	0.846	99.154	0.000
14.991	28.485	21.503	14.611	5.049	0.369	0.000	0.000	0.729	98.903	0.369
15.815	30.308	21.171	13.357	4.430	0.000	0.000	0.000	0.998	99.002	0.000
15.712	29.897	20.777	12.812	3.923	0.000	0.000	0.000	2.441	97.559	0.000
15.575	27.862	18.714	12.640	4.590	0.352	0.000	0.507	5.535	94.113	0.352
17.532	30.302	19.289	10.846	3.148	0.000	0.000	0.000	2.197	97.803	0.000

Terrain Sciences Division- Sedimentology Laboratory Report

Complete Grain Size Analysis - PSA

Sample # B13S8 111 113 * spilled in mixer

Name: Dallimore Date (y/m/d): 00/11/14 Report No.: 15165
 Project No.: 970017 Technician: mw/jb

Sample No.	Weight (g)										Size Fraction (mm) (Reported as percentage of <2mm)
	Dry split	> 2mm	2-0.063mm	< 0.063mm	2 - 0.063	.063-.044	.044-.031	.031-.016	.016-.008	.008-.004	
13S7 118 121	5.054	0.000	0.075	4.979	1.484	12.954	15.639	30.267	21.083	14.139	4.4
13S8 006 009	4.561	0.000	0.168	4.393	3.683	12.584	14.923	29.494	21.480	13.190	4.3
13S8 015 019	6.661	0.000	0.626	6.035	9.398	14.227	14.817	26.671	18.672	11.812	4.0
13S8 054 055	1.742	0.000	0.115	1.627	6.602	13.002	14.026	28.253	21.441	12.378	3.9
13S8 070 073	3.617	0.000	0.048	3.569	1.327	10.155	13.205	29.064	23.852	15.902	6.0
13S8 087 091	6.271	0.000	0.310	5.961	4.943	13.226	13.885	27.262	20.536	14.349	5.3
13S8 103 06	7.742	0.000	0.400	7.342	5.167	16.641	16.608	28.900	18.334	10.865	3.4
13S8 125 128	9.617	0.004	0.797	8.816	8.291	15.864	15.457	27.382	18.043	11.152	3.6
13S8 142 145	4.989	0.000	0.137	4.852	2.746	14.854	15.729	29.043	20.581	12.893	4.1

Sample No.	Weight (g)										Size Fraction (mm) (Reported as a percent)
	Dry split	> 2mm	2-0.063mm	< 0.063mm	2-1/4	1/4-1	1-1/2	1/2-5/16	5/16-3/8	3/8-25/64	
B11S4014 016	8.162	0.083	3.046	5.033	0.607	0.904	1.238	1.621	2.921	4.679	8.1
B11S4091 093	8.510	0.043	2.713	5.704	0.012	0.201	0.531	1.098	0.720	2.256	4.2
B11S7032 033	9.863	0.000	6.965	2.898	0.041	0.061	0.193	0.700	2.312	5.962	18.
B13S4 074 077	17.175	3.296	9.664	4.215	11.355	13.524	14.965	13.567	8.034	3.286	1.8

Sedimentology Laboratory Report

Grain Size Analysis - PSA

15165

Size Fraction (mm) (Reported as percentage of < 2mm)							% of Bulk Sample	Wt. % Sand-Silt-Clay		
0.044-0.031	0.031-0.016	0.016-0.008	0.008-0.004	0.004-0.002	0.002-0.001	< 0.001	% Pebbles	% Sand	% Silt	% Clay
15.639	30.267	21.083	14.139	4.434	0.000	0.000	0.000	1.484	98.516	0.000
14.923	29.494	21.480	13.190	4.326	0.319	0.000	0.000	3.683	95.998	0.319
14.817	26.671	18.672	11.812	4.093	0.311	0.000	0.000	9.398	90.291	0.311
14.026	28.253	21.441	12.378	3.982	0.317	0.000	0.000	6.602	93.082	0.317
13.205	29.064	23.852	15.902	6.025	0.471	0.000	0.000	1.327	98.202	0.471
13.885	27.262	20.536	14.349	5.377	0.421	0.000	0.000	4.943	94.636	0.421
16.608	28.900	18.334	10.865	3.485	0.000	0.000	0.000	5.167	94.833	0.000
15.457	27.382	18.043	11.152	3.810	0.000	0.000	0.042	8.291	91.709	0.000
15.729	29.043	20.581	12.893	4.154	0.000	0.000	0.000	2.746	97.254	0.000

Size Fraction (mm) (Reported as a percentage < 2mm)										Size Fraction (mm)
0.75	0.75-0.50	0.50-0.35	0.35-0.25	0.25-0.18	0.18-0.12	0.12-0.088	0.088-0.063	0.063-0.044	0.044-0.031	0.031-0.016
1.238	1.621	2.921	4.679	8.107	7.934	6.375	3.317	9.742	9.298	17.875
0.531	1.098	0.720	2.256	4.275	7.476	9.448	6.023	9.923	9.460	19.286
0.193	0.700	2.312	5.962	18.666	24.749	13.566	4.370	3.808	3.433	8.008
14.965	13.567	8.034	3.286	1.808	1.239	1.102	0.749	3.797	4.688	9.218

Division- Sedimentology Laboratory Report

Grain Size Analysis - PSA

15165

Size Fraction (mm) Reported as percentage of < 2mm							% of Bulk Sample			
0.42:0.31	0.31:0.16	0.16:0.08	0.08:0.04	0.04:0.02	0.02:0.01	< 0.01	% Pebbles	% Sand	% Silt	% Clay
10.981	24.333	24.595	20.875	8.567	0.930	0.000	0.000	0.754	98.316	0.930
10.800	28.991	26.425	18.687	5.667	0.327	0.000	0.000	2.911	96.762	0.327
12.434	27.878	23.667	17.387	5.674	0.366	0.000	0.000	3.305	96.330	0.366
11.067	25.206	24.295	20.292	8.155	0.900	0.000	0.000	1.464	97.636	0.900
10.051	24.717	24.146	21.616	9.532	1.089	0.000	0.000	1.755	97.156	1.089
12.020	22.602	17.238	13.264	4.748	0.323	0.000	0.000	17.139	82.538	0.323
11.761	25.479	22.549	16.840	5.475	0.335	0.000	0.000	7.788	91.878	0.335
10.531	25.202	25.439	20.081	6.990	0.423	0.000	0.263	3.293	96.284	0.423
9.710	24.721	25.541	21.378	8.028	0.502	0.000	0.000	3.065	96.433	0.502
10.619	21.424	17.410	12.326	3.722	0.000	0.000	0.000	23.525	76.475	0.000
12.383	25.991	22.903	18.642	7.484	0.523	0.000	0.000	2.622	96.855	0.523
12.159	28.693	24.651	18.014	5.835	0.365	0.000	0.000	1.823	97.812	0.365
12.684	26.939	21.888	16.939	6.337	0.429	0.000	0.456	5.224	94.348	0.429
11.297	25.612	23.450	18.689	7.137	0.489	0.000	0.000	4.752	94.759	0.489
10.483	23.765	22.236	19.198	8.325	0.949	0.000	0.000	6.950	92.101	0.949
10.995	24.068	23.189	19.766	8.078	0.879	0.000	0.392	4.172	94.949	0.879
11.815	24.439	21.765	17.625	7.091	0.512	0.000	0.000	6.753	92.735	0.512
9.088	21.706	22.101	20.489	10.175	1.661	0.000	0.000	7.719	90.619	1.661
11.127	24.219	22.316	19.756	8.926	1.059	0.000	0.000	4.143	94.798	1.059
10.523	25.977	24.095	20.746	8.931	1.044	0.000	0.000	1.800	97.156	1.044
10.682	23.206	22.936	20.572	9.391	1.145	0.000	0.000	3.385	95.469	1.145
11.775	24.570	22.697	18.538	7.535	0.865	0.000	0.000	4.654	94.482	0.865
11.532	25.537	23.198	19.305	8.157	0.952	0.000	0.000	2.800	96.248	0.952
9.097	24.124	25.138	22.741	10.223	1.229	0.000	0.000	1.567	97.204	1.229
10.611	24.588	23.507	20.348	8.995	1.091	0.000	0.000	3.202	95.707	1.091
9.948	23.479	23.053	20.911	10.060	1.309	0.000	0.000	4.943	94.647	1.309
10.385	20.876	19.828	17.847	8.510	1.087	0.000	0.000	12.295	86.619	1.087
11.542	24.740	22.576	19.202	8.457	1.025	0.000	0.000	3.588	95.387	1.025
10.328	23.040	22.403	21.160	10.657	1.726	0.000	0.017	3.152	95.121	1.726
12.041	23.836	21.135	17.974	8.194	0.992	0.000	0.000	5.731	93.277	0.992
11.206	21.575	18.966	16.510	7.665	0.971	0.000	0.078	13.224	85.805	0.971
11.850	23.680	21.416	18.136	7.992	1.005	0.000	0.000	6.254	92.741	1.005
13.234	24.495	17.254	11.132	3.992	0.294	0.000	1.735	17.770	81.936	0.294
17.231	29.722	17.358	8.250	1.219	0.000	0.000	0.000	9.010	90.990	0.000

APPENDIX J

Fish scales data

	A	B	C	D	E	F	G	H	I	J	K
1	Sample label	Adjusted	Date	Seds	Cind	Scales	Bones	Ost.	For.	Charc.	X-tals
2		Depth	adjusted								
3	Section 1										
4											
5	2 to 7	14-19	164-169			39	N/A			X	
6	16-21	28-33	178-183			26	35	ost	X	X	
7	21-26	33-38	183-188			21	45			X	
8	26-31	38-43	188-193			27	22			X	
9	31-36	43-48	193-198			14	26			X	
10	46-51	58-63	208-213			38	67	ost		X	
11	51-56	63-68	213-218			35	29				
12	85-90	97-102	248-252			14	22				
13											
14	Section 2										
15											
16	20-25	110-115	260-265			19	28	ost			
17	25-30	115-119	265-269		X	35	142				
18	30-40	120-130	270-280			109	378				
19	55-65	145-155	295-300	P	X	47	408	ost			
20	100-110	190-200	340-350			104	201	ost			
21	110-120	200-210	350-360		X	204	615				
22	145-150	235-240	385-390			19	17		X		
23											
24	Section 3										
25											
26	42-47	287-292	437-442			52	39				
27											
28	CLIMATIC DIVISION										
29											
30	57-62	302-307	452-457			36	73				
31	62-67	307-312	457-462	P		36	55	ost			
32	67-72	312-317	462-467			53	93				
33	72-77	317-322	467-472			34	61				
34	77-82	322-327	472-477	MASSIVE		13	25		X		
35	92-97	337-342	487-492	MASSIVE		28	53	ost			
36	102-107	347-352	497-502	MASSIVE		43	57				
37	114-119	359-364	509-514	P	X	44	589	ost			
38	130-135	365-370	515-520			28	16	ost			
39	135-140	370-375	520-525	P		41	26	ost			
40	140-145	375-380	525-530	MASSIVE		68	110			X	
41	145-150	380-385	530-535		X	22	116	ost	X		
42	145-150 ?	385-390	535-540		X	34	230				
43											
44	Section 4										
45											
46	1 to 5	388-392	538-543		X	68	68				X
47	5 to 10	392-397	543-548	P		25	54	ost			X
48	10 to 15	397-402	548-553	P highest		28	108	ost			X
49	15-20	402-407	553-558	MASSIVE		65	207	ost			X
50	29-34	416-421	566-571			23	34	ost			

	A	B	C	D	E	F	G	H	I	J	K
51	34-39	421-426	571-576			38	38				
52	39-44	426-431	576-581			15	6	ost	X		
53	51-56	438-443	588-593	(no)P		29	192	ost	X		
54	63-68	450-455	600-605	MASSIVE		37	25	ost			
55	68-73	455-460	605-610	MASSIVE		32	17	ost	X		
56	73-78	460-465	610-615		X	12	35				
57	86-91	473-478	623-628	P		40	95	ost			
58	91-96	478-483	628-633	(no) P		41	40				
59	102-107	489-494	639-644			70	113	ost			
60	107-112	494-499	644-649	MASSIVE		37	217		X		
61	120-125	507-512	657-662	P		12	33	ost	X		
62	125-130	512-517	662-667			35	38			X	
63	130-135	517-522	667-672	MASSIV	X	94	533	ost	X		
64	140-145	525-532	675-682		X	149	180	ost			
65	145-150	532-537	682-687			29	54	ost			
66											
67	Section 5										
68											
69	20-25	563-568	713-718		X	230	103				X
70	25-30	568-573	718-723			27	23				X
71	30-35	573-578	723-728	P	X	21	88		X		
72	35-40	578-583	728-733	MASSIV	X	29	100				
73	40-45	583-588	733-738		X	12	14	ost	X		
74	45-50	588-593	738-743	P	X	11	18		X		
75	50-55	593-598	743-748	P		13	18				
76	55-60	598-603	748-753	MASSIVE		36	21	ost	X		
77	60-65	603-608	753-758			29	41				
78	75-80	618-623	768-773	Massive		16	48		X		
79	88-93	631-636	782-787	P		16	35				
80	93-98	636-641	787-792	MASSIVE		29	7	ost			
81	103-108	646-651	796-801	MASSIVE		25	53	ost	X		
82	108-113	651-656	801-806	Massive		25	10	ost			
83	113-118	656-661	806-811			30	37		X		
84	124-129	667-672	817-822	MASSIVE		58	165	ost			
85	137-142	680-685	830-835			17	39		X		
86	142-147	685-690	835-840	P		21	34	ost	X		
87	147-150	690-695	840-845	P		35	28				
88											
89	Section 6										
90											
91	10 to 15	704-712	854-862		X	18	20				X
92	19-24	716-721	866-871		X	34	50	ost			
93	24-29	721-726	871-876			53	44	ost			
94	29-34	726-731	876-881	P		15	23	ost			
95	34-39	731-736	881-886			8	7	ost			
96	50-55	747-752	897-902			24	28	ost	X		
97	55-60	752-757	902-907			14	3	ost	X		
98	60-65	757-762	907-912			14	5	ost			
99	65-70	762-767	912-917	P		9	12	ost	X		
100	76-81	773-778	923-928			16	10	ost	X		

	A	B	C	D	E	F	G	H	I	J	K
101	81-86	778-783	928-933	MASSIVE		21	31		X	X	
102	86-91	783-788	933-938	P		12	8				
103	91-96	788-793	938-943	MASSIVE		45	80	ost			
104	96-101	793-798	943-948			35	88				
105	101-107	798-803	948-953			54	43	ost	X		
106	127-132	824-829	974-979	P		8	12				
107											
108	CLIMATIC DIVISION										
109											
110	132-137	829-831	979-984	P		21	11	ost			
111	137-142	834-839	984-989			5	18	ost			
112	142-147	839-844	989-994			26	60				
113	147-152	844-849	994-999			41	17	ost	X		
114											
115	Section 7										
116											
117	10 to 15	860-865	1010-1015		X	94	226	ost			X
118	15-20	865-870	1015-1020	MASSIVE		59	84	ost			
119	20-25	870-875	1020-1025			8	28	ost			
120	25-60	875-880	1025-1030		X	34	78	ost			
121	30-35	880-885	1030-1035			13	15	ost			
122	35-40	885-890	1035-1040	P	X	10	23	ost	X		
123	40-45	890-895	1040-1045	P	X	3	11		X		
124	45-50	895-900	1045-1050	P		8	15		X		
125	50-55	900-905	1050-1055			13	30				
126	55-60	905-910	1055-1060		X	25	25		X		
127	60-65	910-915	1060-1065			58	146		X		
128	65-70	915-920	1065-1070			91	79	ost			
129	132-137	982-987	1132-1137		X	73	38	ost			
130											
131											
132	Section 8										
133											
134	0 to 5	990-995	1140-1145		X	12	100	ost	X		
135	5 to 10	995-1000	1145-1150		X	13	13	ost			
136	10 to 15	1000-1005	1150-1155		X	9	25	ost			
137	15-21	1005-1010	1155-1160			52	14		X		
138	20-25	1010-1015	1160-1165			33	16		X		
139	25-30	1015-1020	1165-1170			35	20		X		
140	78-83	1068-1073	1218-1223			34	402	ost	X		
141	83-88	1073-1078	1223-1228			19	72	ost			
142	88-93	1078-1083	1228-1233			26	69	ost			
143	104-109	1094-1099	1244-1249	P		16	395	ost			
144	129-134	1119-1124	1269-1274	P		46	22	ost			
145	134-139	1124-1129	1274-1279	P		21	22	ost			
146	139-144	1129-1134	1279-1284			41	43	ost	X		

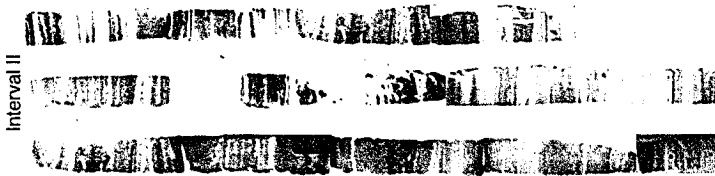
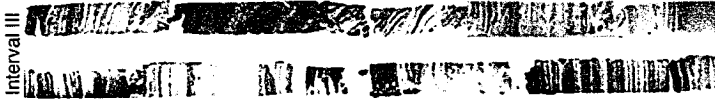
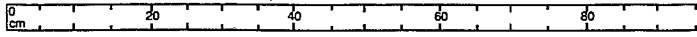
X-ray composite of inner basin freeze core
TUL99B04

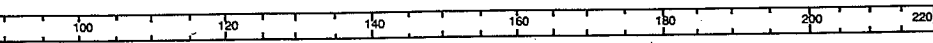
B04





X-ray composite of inner basin core
TUL99B03





5128

[Redacted text]

[Redacted text]

[Redacted text]

[Redacted text]

X-ray composite of outer basin core
TUL99B11

